MADITRACE

Artificial Fingerprinting for Mineral Traceability

Deliverable D2.6

Final Version

Authors: Omar Amri (AHK), William Hartley (AHK), Laurance Donnelly (AHK), Robert Dunn (AHK), Ian Corfe (GTK), Quentin Dehaine (GTK), Aidan Wilson (AHK)

Funded by the European Union

Funded by the European Union. Views and opinions expressed are however those of the author(s) only and do not necessarily reflect those of the European Union or HaDEA. Neither the European Union nor the granting authority can be held responsible for them.

Disclaimer

The content of this report reflects only the author's view. The European Commission is not responsible for any use that may be made of the information it contains.

Funded by
the European Union

Document Information

Grant Agreement	101091502
Project Title	Material and digital traceability for the certification of critical raw materials
Project Acronym	MaDiTraCe
Project Coordinator	Daniel Monfort (BRGM)
Project Duration	1 January 2023 – 30 June 2026 (42 months)
Related Work Package	WP2
Related Task(s)	T2.3 - Artificial Fingerprinting
Lead Organisation	Geological Survey of Finland (GTK)
Contributing Partners	Alfred H Knight (AHK), Bureau de Recherche Géologique et Minière (BRGM)
Authors	Omar Amri (AHK), William Hartley (AHK), Laurance Donnelly (AHK), Robert Dunn (AHK), Ian Corfe (GTK), Quentin Dehaine (GTK), Aidan Wilson (AHK)
Due Date	30 June 2026
Submission Date	16 July 2026
Dissemination level	Public (PU)

History

Date	Version	Submitted by	Reviewed by	Comments
29 May 2026	0.1	Omar Amri William Hartley	Laurance Donnelly Robert Dunn	Draft for review
16 June 2026	0.2	Omar Amri	Daniel Monfort (BRGM)	Draft for review
06 July 2026	0.3	Omar Amri Ian Corfe	Anne-Marie Desaulty (BRGM)	Draft for review
16 July 2026	Final	Daniel Monfort (BRGM)	Karine Lavoisier (LGI)	

Funded by the European Union

Table of Contents

Funded by the European Union

Funded by the European Union

Funded by the European Union

Funded by
the European Union

List of Figures

Funded by the European Union

List of Tables

Funded by the European Union

Funded by the European Union

Funded by
the European Union

Summary

The Material and Digital Traceability for the Certification of critical raw materials (MaDiTraCe) project was formally launched in Paris in January 2023. The aim of this 42-month European Union project was to reinforce the transparency, traceability, and sustainability of complex supply chains of critical raw materials (CRMs) including cobalt, lithium, natural graphite and rare earth elements. Deliverable 2.6 (D2.6) is part of Work Package 2 of the MaDiTraCe project. This Work Package focuses on developing material fingerprinting (MFP) and artificial fingerprinting (AFP) methods for the traceability of CRMs. The objectives of D2.6 were to produce tailor-made 3D printed tracer particles (TPs) for use with specific CRMs. As the effectiveness of AFP with CRMs remains poorly understood, proof-of-concept laboratory and small-scale transportation tests were developed to assess the behaviours of different TPs within CRMs, namely upstream mineral concentrates and chemical products. Seven CRMs (host materials) from lithium, cobalt and natural graphite supply chains were obtained to test with TPs. A total of sixteen prototype 3D printed TPs made from different materials (polymers, metal alloys and mineral-polymer composites) were produced by the Geological Survey of Finland (GTK), 3D MicroPrint GmbH and Horizon Microtechnologies GmbH. From these sixteen TPs, nine were produced in larger quantities for testing purposes. Commercially sourced ValiMark™ TPs from TraceTag International Ltd ('TraceTag') and Microtaggant® Identification Particles from Microtrace, LLC ('Microtrace') were also tested as part of this study. A preliminary financial review of AFP technology was also conducted within the scope of this work.

As standards and publicly available data for the evaluation of TPs within CRMs remain limited, this study developed several novel testing methodologies to evaluate TP behaviour within various CRMs and under various environmental conditions. Testing of TPs was conducted in two stages: 1) preliminary tests with host materials, which evaluated various application, mixing and detection methods, and 2) principal tests, which evaluated TP minimum effective dosage (MED), various ageing tests, and real-world or simulated transportation tests. As part of the principal tests, Microtrace also conducted an in-house laboratory-scale evaluation using their Molecular™ Taggant System to define the taggant abundance thresholds capable of identifying whether a host material has been diluted with non-tagged material.

Dry mixing using a riffle splitter produced the most effective, evenly distributed mixtures of TPs and commodities. Tests revealed differences between the TPs detectability and how they were held within the host materials, with TP abundance and distribution varying considerably based on TP type, host materials and application methods. Digital microscopy revealed that TP size significantly influenced detectability and surface adsorption onto host material particles: smaller TPs readily adhered to host material particles and were more detectable, whereas larger TPs occupied interstitial voids and were less detectable. Excitation light provided superior detectability for both 3D printed and commercial fluorescent TPs, under naked eye and high magnification. TPs that dispersed easily and could be identified as a result of their optical properties using high magnification were the most suitable. The MED varied, depending mainly on the TP size, and a selection of the smallest TPs were detectable at the lowest tested dosage of 0.1 ppm (0.00001%). Additionally, Microtrace's in-house evaluation of their Molecular™ Taggant System demonstrated that host-material-specific analytical thresholds could be developed to support the detection of CRM dilution or adulteration. Polymer 3D printed and

Funded by the European Union

commercially sourced TPs did not segregate from host materials, but metal-based 3D printed TPs did. Furthermore, TPs made from metal alloys were found to react with air and commodities containing sulphur, resulting in their degradation.

Overall, from the 3D printed TPs, polymer-based TPs were functionally superior and did not react with host materials. Commercially sourced TPs from TraceTag and Microtrace were also robust and did not behave negatively. A preliminary cost evaluation has determined that the economic feasibility of AFP using 3D printed TPs depends significantly on the value of the CRM to be traced. Scaling of AFP technology will require optimisation of production workflows to mitigate high labour costs, alongside tailoring TP properties according to the bulk physicochemical properties of CRMs. Additionally, implementation of AFP technology will require appropriate design of the application, blending and detection infrastructure so that TPs can be applied to CRMs successfully and without hindrance to standard operations. Further testing and refinement of 3D printed TP properties and production processes, particularly at higher technology readiness levels, is required before this technology can be utilised for the global traceability of CRMs or other mineral and metal raw materials.

Funded by
the European Union

Keywords

Artificial Fingerprinting, Artificial Taggant Particles, Cobalt, Critical Raw Materials, Lithium, Li-ion Battery REE-Magnet Traceability, Natural Graphite, Taggants, Tracer Particles, Tracers, 3D Printing.

Abbreviations and Acronyms

Acronym	Description
AFP	Artificial Fingerprinting
AHK	Alfred H Knight
ASTM	American Society for Testing and Materials
CapEx	Capital Expenditure
CIC	Combustion Ion Chromatography
CoC	Chain of Custody
CRM	Critical Raw Material
CVAAS	Cold Vapour Atomic Absorption Spectroscopy
C/SA	Carbon-Sulphur Combustion-IR Analysis
DLP	Digital Light Projection
FFF	Fused Filament Fabrication
FIBC	Flexible Intermediate Bulk Container
FMP	Flow Moisture Point
FTT	Flow Table Test
Grav	Gravimetric Analysis
GTK	Geological Survey of Finland
ICP-OES	Inductively Coupled Plasma Optical Emission Spectroscopy
IC	Ion Chromatography
IR	Infrared Radiation
IGA	Instrumental Gas Analysis
ISO	International Organisation for Standardization
ICP-MS	Inductively Coupled Plasma Mass Spectrometry
LCT	Lithium-Caesium-Tantalum
LCV	Light Commercial Vehicle
LFS	Low Force Stereolithography
LOI	Loss on Ignition
MED	Minimum Effective Dosage

MEMS	Micro-Electro-Mechanical Systems
MFP	Material Fingerprinting
µ-LPBF	Micro Laser Powder Bed Fusion
MIP	Microtaggant® Identification Particle
MHP	Mixed Hydroxide Precipitate
MLS	Micro Laser Sintering
MMA	Methyl Methacrylate
MSLA	Masked Stereolithography
ND	Not Detected
OpEx	Operational Expenditure
PLA	Polylactic Acid
PMMA	Poly(methyl methacrylate)
PµSL	Projection Micro Stereolithography
PVC	Polyvinyl Chloride
Pycno	Pycnometer Analysis
QR	Quick Response
REE	Rare Earth Element
SEM	Scanning Electron Microscopy
SEM-EDS	Scanning Electron Microscopy with Energy Dispersive Spectroscopy
SiNPs	Silicon nanoparticles
SLA	Stereolithography
TLA	Technology Licensing Agreement
TML	Transportable Moisture Limit
TP	Tracer Particle
TRL	Technology Readiness Level
TRL 3	Technology Readiness Level 3
TRL 4	Technology Readiness Level 4
T2.3	Task 2.3
UN	United Nations
UV	Ultraviolet Radiation
WP	Work Package
X-CT	X-Ray Computed Tomography
XRD	X-Ray Diffraction
XRF	X-Ray Fluorescence

Funded by
the European Union

WHO	World Health Organization

Symbols

Symbol	Description
cm	Centimetre
Eh	Redox potential
g/cm^3	Grams per cubic centimetre
g/mL	Grams per millilitre
kV	Kilovolt
max	Maximum
min	Minimum
mbar	Millibar
mL	Millilitres
mm	Millimetre
mm/s	Millimetres per second
MPa	Megapascal
mph	Miles per hour
MWh	Megawatt hour
ms	Milliseconds
m^2/g	Square metres per gram
nm	Nanometre
pH	Acidity/basicity (hydrogen ion concentration)
ppm	Parts per million
ppb	Parts per billion
% RH	Percent relative humidity
R	Range
RPM	Revolutions per minute
SD	Standard deviation
3D	Three-dimensional
™	Trademark
W	Watt
Wt. %	Weight percent
μ	Average (also known as mean)
μA	Microamp

Funded by the European Union

µg	Microgram
µm	Micrometre (also known as micron)
≥	Greater than or equal to
≤	Less than or equal to
±	Plus or minus
~	Approximately
®	Registered trademark

Funded by
the European Union

Definitions

Adulteration

Also known as 'salting', adulteration is the wilful and premeditated tampering of all, or an amount of a material or product, by adding material of a higher or lower standard, quality, or value, without the other party's knowledge or consent.

Ageing

The permanent degradation of a material's physical, mechanical or chemical properties that occurs through time.

Agglomerate

A cluster of particles that are held together by chemical or physical phenomena which is not naturally occurring.

Artificial Ageing

The change of a material's physical or chemical properties over time due to exposure to an artificially created environment where certain parameters such as temperature or humidity are set or controlled (e.g., within a climate chamber).

Blockchain

Digital technology that allows for data to be validated and subsequently stored as an immutable 'block' on a collectively owned and decentralised database, with each block being validated based on previous blocks, making it very difficult to alter. Blocks are validated either by an algorithm or a third party in the field.

Care and Maintenance

A mining industry term to describe a mine that has ceased production but is being maintained in a functional state to allow for a potential restart in the future.

Chain of Custody

The custodial sequence that occurs as ownership or control (physical or administrative) of the material supply is transferred from one custodian to another in the supply chain.

Critical Raw Materials

Raw materials that are considered essential in the modern-day economy, and often clean technologies, with however a relatively high supply risk.

Dynamic Separation

The phenomenon of forming a liquid slurry (water and fine solids) above the solid material, resulting in a free surface effect which may significantly affect the ship's stability.

Fluorescence

Materials emitting optical radiation for the duration of light energy incident on it.

Funded by
the European Union

Gramineae

A large and nearly ubiquitous family of monocotyledonous flowering plants commonly known as grasses. It includes the cereal grasses, bamboos and the grasses of natural grassland and species cultivated in lawns and pasture.

Host Materials

The materials in which tracer particles were tested.

Liquefaction

A phenomenon where cohesionless and saturated or partially saturated soil or soil-like material (e.g., tailings, ores and concentrates) behaves like a liquid under cyclic load. Wave action, currents, wind and vibrations from a vessel's engine can cause liquefaction to occur.

Micro Laser Sintering

Also known as μ-LPBF (Micro Laser Powder Bed Fusion), a powder-bed additive manufacturing technology which is used to create small and intricate metal parts/objects.

Microclimate

A distinctive climate of a localised area where atmospheric conditions differ from the surrounding area's climate. These areas can be created or influenced by natural variations in terrain and flora, as well as by man-made infrastructure.

Minimum Effective Dose

The smallest amount of a substance or input that will produce the desired outcome.

Natural Ageing

The change of a material's physical or chemical properties over time due to exposure to an ambient environment.

Natural State

The as-received physical and chemical state of a raw material as delivered to the testing facility. The material has not undergone any subsequent sample preparation or environmental conditioning prior to testing.

1.4542

Also known as 17-4PH® or AISI 630, 1.4542 is a martensitic precipitation-hardening chromium-nickel-copper alloyed stainless steel which is ferromagnetic.

Particle

A small, localized grain or fragment, which can be ascribed several physical or chemical properties, such as volume, density, or mass.

Penalty Elements

Penalty elements may change the physical properties of material and impede the proper operation of the smelting facility.

Perspex®

A premium brand of transparent thermoplastic made from poly(methyl methacrylate) (PMMA), manufactured by Perspex International Limited.

Photooxidative Ageing

The change of a material's physical or chemical properties over time due to exposure to sunlight in the presence of oxygen. Material may be exposed to visible, infrared and ultraviolet light.

Proof-of-concept

A small-scale, preliminary test used to demonstrate that a specific idea, method, or technology is feasible in the real world. Its primary goal is to mitigate risk and answer one question before significant time or money is invested: "Can this actually be built and work?"

Rare Earth Elements

A group of elements including lanthanide elements (atomic numbers from 57 to 71), scandium, and yttrium. They are divided into two groups based on their atomic weights: Light REEs (LREEs) include cerium (Ce), lanthanum (La), praseodymium (Pr), neodymium (Nd), and samarium (Sm) while Heavy REEs (HREEs) include europium (Eu), gadolinium (Gd), terbium (Tb), dysprosium (Dy), holmium (Ho), erbium (Er), thulium (Tm), ytterbium (Yb), and lutetium (Lu).

Substitution

The wilful and premeditated switching of all, or an amount of ore, mineral concentrate, refinery or smelter products, for material of a lower standard or quality, without the other party's knowledge or consent. It could also include the use of fake or counterfeit materials or products. This is illegal and considered a fraudulent practice.

Technology Readiness Levels

Technology readiness levels (TRLs) serve as a standardised metric for evaluating how developed or "mature" a specific technology is. There are nine technology readiness levels, starting from TRL 1, which is defined as basic principles of a technology have been observed and reported, to TRL 9, which is defined as actual technology that has been qualified through successful mission operations.

Technology Readiness Level 3

This is the technology readiness level which refers to a project, or a stage of a project, that is at a point where analytical and experimental tests are conducted to determine the technology's critical function or characteristic proof-of-concept.

Technology Readiness Level 4

This is the technology readiness level which refers to a project, or a stage of a project, that is at a point where basic technology validation is carried out within a laboratory environment.

Traceability

The ability to verify the history, location or application of a material or product at different stages of the value chain from the source to the market and up to the end-of-life, by documented recorded identification or other means.

Traceability Systems

Systems (digital or paper-based) that record and follow the trail as products and materials come from suppliers and are processed and ultimately distributed as end products.

Tracer Particle

Any chemical or physical marker added to materials to allow various forms of tracking, tracing and testing. Also referred to as a taggant or artificial taggant particle.

2.1293

Also known as CuCr1Zr or C18150, 2.1293 is a thermally aged copper alloy.

3D Printing

Is the construction of a three-dimensional object from a CAD model or a digital 3D model. It can be done in a variety of processes in which material is deposited, joined or solidified under computer control, with the material being added together, typically layer by layer. Also known as additive manufacturing.

1 Introduction

1.1 MaDiTraCe

The Material and Digital Traceability for the Certification of critical raw materials (MaDiTraCe) project was formally launched in Paris in January 2023. This is a 42-month (previously 36-month) European Union project funded through the Horizon Europe Programme which brings together fourteen partners from seven countries. The project aim is to reinforce the transparency, traceability, and sustainability of complex supply chains of critical raw materials (CRMs) including cobalt, lithium, natural graphite and rare earth elements. Notably, these supply chains are associated with batteries and permanent magnets, which are both necessary components for the increased adoption of sustainable technologies such as electric vehicles and wind turbines. MaDiTraCe has a principal focus on the development of integrated material and technological solutions for the traceability and certification of CRMs. Solutions were developed as part of various Work Packages (WPs) within the project, and it is anticipated these solutions may support the traceability of CRMs to comply with existing regulations and emerging European Union and international policies.

Deliverable D2.6 is part of Work Package 2 (WP2) of the MaDiTraCe project. WP2 aims to develop material fingerprinting (MFP) and artificial fingerprinting (AFP) technologies for independent control/audits of the CRM digital trail, to be included in material passports (i.e. Digital Product Passports (DPPs)) which would support compliance with developed certification schemes. WP2 is divided into five different tasks (T2.1 to T2.5), and four deliverables (D2.1 to D2.5) have been published to date (i.e. Arató et al., 2026, Desaulty, Alatalo, et al., 2026, Desaulty, Arató, et al., 2026 and Donnelly, et al., 2023) based on the results from these tasks. Of the five tasks, T2.3 specifically focuses on AFP and seeks to conduct research to prove the concept of new tracer particles (TPs), using 3D printing, for the AFP of CRMs in selected supply chains. This task is being implemented by Alfred H Knight (AHK) and the Geological Survey of Finland (GTK).

T2.3 comprises the following stages:

1. A review of existing methods for the potential use of 3D printing technologies and 3D printed tracer particles. Analysis (with MaDiTraCe industrial partner input) of mining, minerals and metals industry requirements to ensure solutions are fit-for-purpose and commercially relevant. This task has been completed and deliverable D2.1 titled "A Review of Artificial Fingerprinting and 3D Printing for the Potential Tracking of Minerals in Complex Supply Chains" is publicly available (Donnelly et al., 2023).
2. Design and manufacture of 3D printed tracer particle prototypes using appropriate materials (e.g., minerals, metals, bioplastic mineral/metal composites) based on specifications from the review of existing tracer particle technologies as part of D2.1. Subsequently, large scale tracer particle production will be carried out according to prototype results/review specifications.
3. Test and validation of 3D printed tracer particles for artificial fingerprinting of CRMs in selected supply chains, with a specific focus on mineral concentrates and black mass. This will involve the assessment of impacts from transhipment, storage times and environmental conditions on the tracer particles and a preliminary financial evaluation on the feasibility of tracer particles within CRM supply chains.

Funded by the European Union

1.2 Background

A review of current traceability systems as part of deliverable D2.1 highlighted that although existing traceability solutions are of significant importance, and in some cases critical for CRM certification, such as digital traceability solutions (e.g., blockchain) and document-based traceability systems, these solutions are vulnerable to scenarios such as 'garbage in, garbage out'. Traceability is also desirable to detect fraud such as the adulteration or substitution of CRMs.

To address these issues, artificial fingerprinting using tracer particles (TPs) is proposed as a possible verification method, which would be complementary to existing or newly developed traceability solutions. The aim would be to prove the traceability of CRMs that are traded in global supply chains.

Several existing commercial TPs were found to be largely unsuitable for CRMs for various reasons, including the presence of penalty or impurity elements or simply due to the TPs not being tested with CRMs. Furthermore, it was determined that 3D printed TPs offer potential advantages over currently available tracer particle technologies, through the ability to achieve 'mass-customisation' of tracer particle morphologies, both externally and internally, to match a commodity's properties, to optimise their dispersion within CRMs or to increase their encoding factor. Additionally, 3D printed TPs can be produced using a range of different materials which can be specifically chosen to match the commodity being traced (i.e. to meet penalty or impurity element/compound limits) or to manage industry blight.

Following the findings in deliverable D2.1, several key recommendations, in addition to continuing the development of 3D printed TPs, were proposed for further investigation as part of the MaDiTraCe project. These include:

- Experimental research on silicon from Gramineae which could be altered into silicon nanoparticles (SiNPs). These exhibit strong fluorescence under microwave radiation, potentially a source of fluorescence which could be incorporated into 3D printed TPs to improve their detectability.
- Investigations into physical unclonable functions (PUFs) which could be incorporated into 3D printed TPs.
- Further experimental work on existing TPs that have been developed for other industries.

Apart from experimental research on silicon from Gramineae plants, all the above key recommendations were taken forward to be tested and/or evaluated as part of this study. This was due to the integration of alternative sources of fluorescence into 3D printed TPs for this project. The use of silicon from Gramineae plants to produce SiNPs is still recommended as part of any future testing on 3D printed TPs. Additionally, although focus on cobalt supply chains during the research & development phase of the project was proposed as part of D2.1, other sources of CRMs from various parts of their respective supply chains have been sourced for the project since publishing deliverable D2.1, which has broadened the range of CRMs that TPs were tested against.

Funded by the European Union

1.3 Objectives

The objective of this report is based on the tasks within T2.3, which were not already satisfied as part of D2.1, as well as selected key recommendations made as part of D2.1, which includes the following:

1. Perform laboratory and field testing of 3D printed TPs and existing non-3D printed commercial tracer particles to determine their behaviour when mixed with critical raw materials. More than three types of 3D printed TPs are to be lab tested to technology readiness level 3 (TRL 3), with more than one type of 3D printed TP pilot tested to technology readiness level 4 (TRL 4).
2. Perform bias testing and variance testing to determine if TPs are homogeneously distributed and assess the impacts of transhipment, storage times and the influence of environmental conditions (e.g., oxidation and moisture content).
3. Evaluate the minimum TP concentration needed for successful identification using technologies developed in tasks T2.1 and T2.2.
4. Provide a preliminary financial evaluation of the TPs to a cost per unit (i.e. per tonne of raw material) to verify if the TPs are cost-effective and can be deployed in a commercially viable manner, considering the full artificial fingerprinting process, including the production/purchase of TPs, application and mixing, analysing and recovering/recycling costs. Clients will also be identified as part of this evaluation.

2 3D Printed Tracer Particles

2.1 Specification

Based on answers to questionnaires submitted to key stakeholders and industry participants, and an internal preliminary review, D2.1 stipulated the chemical and physical properties that TPs should abide by for industrial application.

Upon further evaluation, it was concluded that some of these properties may be acceptable based on the intended purpose of the TP, the CRM being tagged and available processing infrastructure, including the following:

- A limitation that TPs should be invisible to the naked eye: It was subsequently concluded that TPs could be visible to the naked eye if an overt traceability methodology were desired to deter fraudulent acts.
- A limitation that TPs should be non-magnetic: As part of the beneficiation of certain CRMs, such as spodumene concentrate, magnetic separation is readily carried out to refine the material and as such, magnetic TPs could be readily removed as part of existing processes to ensure the TPs do not detrimentally affect the quality of the material.

3D printed TPs have been sourced with these limitations in mind from three different sources, in-house at GTK, and through the outsourcing partners Horizon Microtechnologies GmbH and 3D Microprint GmbH.

2.2 Design and Prototyping

To tailor 3D printed TPs to the intended CRM host materials within the lithium-ion battery supply chain, a number of interlinked design parameters were considered in the design and prototyping stages. These were principally:

- Size – a range of 3D printed TP particle sizes was prototyped, between 0.3 mm and 2 mm in diameter.
- Shape – two main concepts were trialled: (a) basic geometric shapes e.g. spheres and cubes, and (b) replicating the particle morphologies of the CRM host material the TPs were intended to be used in.
- Material – three main material types were used. These were (a) polymers, (b) metal alloys, (c) mineral-polymer composites. The latter was based on the concept of using the CRM host material as a component of the TP, to minimise both the addition of materials not already present and the perception and fact of contamination or penalty element addition.
- Detection method – three detection concepts were tested: (a) incorporation of smaller, commercial, non-3D printed TPs into larger, 3D printed TPs, (b) use of 3D printing polymer materials with fluorescing properties under specific light wavelengths (e.g., 365 nm UV light), (c) magnetism of metal 3D printed TPs.
- Data encoding – data encoding was explored via external lettering of TPs, and external and internal micro QR codes were incorporated into TPs.
- Overt/covert nature of TPs themselves and of data encoding – TP size, colour and detection mode were all tested as means of making TPs either overt or covert.

Further details of each of these parameters used to tailor the design of 3D printed TPs to the CRM (host material) being tracked are discussed in the following sections. In total, sixteen prototype TPs with various combinations of the above parameters were produced in-house at GTK or by external outsourcing. Preliminary testing regarding detectability and especially manufacturability reduced this to a selection of nine that went forward to in-house and externally outsourced manufacturing in sufficient quantities for laboratory and small-scale transportation testing.

2.3 Geological Survey of Finland produced Tracer Particles

2.3.1 Materials

A range of materials were explored for the manufacture of prototype and testing TPs at the Geological Survey of Finland (GTK), according to the design parameters discussed above.

Three of these were based on the use of mineral-plastic composites of the thermoplastic biopolymer polylactic acid (PLA) with variable amounts of the CRM host material to be tracked. These were a nickel concentrate (origin B), a spodumene concentrate, and a flake graphite concentrate (see also section 4 Host Materials). PLA is a bio-based polymer material made by fermenting plant waste and is widely used in 3D printing. The blend used was Resinex PLA RXP 7502, with particle size >50 µm. The host materials were sieved, and

particle sizes between 63 µm and 125 µm were explored to determine how they responded to the compositing and printing processes.

The remaining prototype and testing TPs used Formlabs Grey Resin v4.1. This is a methacrylate polymer mix composed of 55–75% urethane dimethacrylate and 15–25% methacrylate monomers and was chosen due to its good fluorescence response in initial testing.

2.3.2 Methods

CRM-mineral/biopolymer composite filaments were produced using a 3Devo Composer 450 filament maker in 2.85 mm diameter for use with the 3D printing equipment. The Composer 450 is an all-in-one filament maker with a material input hopper, 4-piece heating system, single mixing screw extruder, cooling fans, optical filament diameter monitoring system, and filament spool winding system.

Parameters used for extruding CRM mineral/biopolymer composite filaments:

- Heating element 1: 170–180°C.
- Heating element 2: 180°C.
- Heating element 3: 190–200°C.
- Heating element 4: 180°C.
- Cooling fan: 40–100%.
- Extrusion screw speed: 3–5 RPM.

PLA and CRM host material were weighed and mixed manually. Filament was produced with nickel concentrate mineral powder at 10–30% concentration by mass; with spodumene concentrate at 5–70% by mass, and with graphite concentrate at 10–45% concentration by mass.

An Ultimaker S3 Fused Filament Fabrication (FFF) 3D printer was used to print TPs with CRM host/biopolymer composite materials from digital surface files. FFF is a form of Material Extrusion (ME) 3D printing, and operates by heating and melting a continuous thermoplastic-based filament, dispensing material onto a build platform via a movable nozzle, and building up a shape from a digital file layer by layer.

Parameters used for 3D printing TPs from CRM host/biopolymer composite filaments:

- Nozzle Ultimaker CC (hardened) 0.6 mm diameter.
- 22–120 millimetres per second (mm/s) nozzle movement speed.
- 0.1–0.2 mm layer height.
- 10–100% material infill.
- 60°C bed temperature.
- 200–210°C nozzle temperature.
- 100% cooling fans.

The freeware Ultimaker slicing program CURA v5.09 was used for converting .stl 3D digital surface files into G-code instructions for the Ultimaker S3 3D printer. A schematic for the production of CRM host/biopolymer composite TPs is presented in Figure 1.

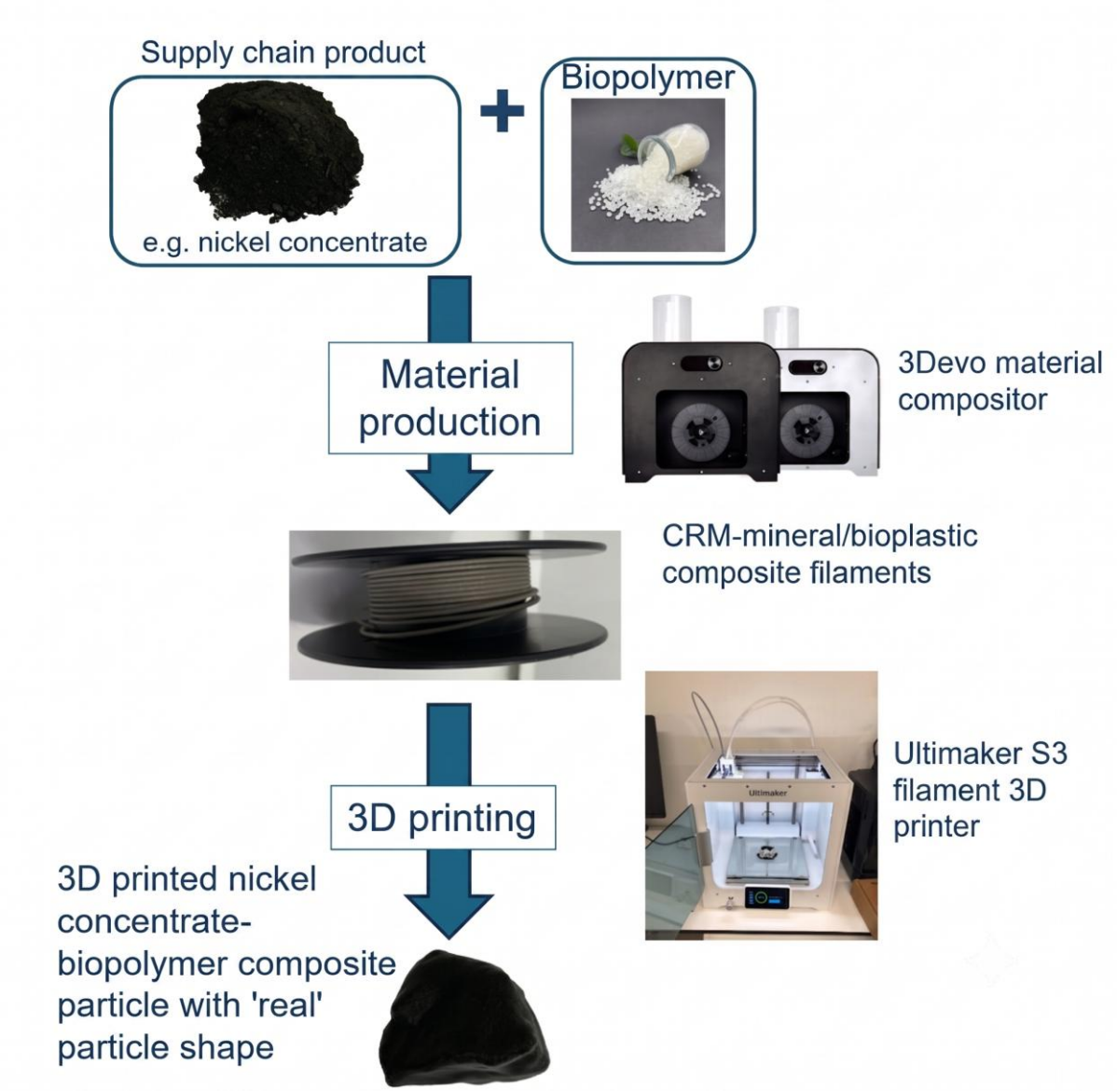

Figure 1. Schematic for production of CRM host/biopolymer composite tracer particles.

A Formlabs Form 3 stereolithography (SLA)/low force stereolithography (LFS) 3D printer was used to print TPs with Formlabs Grey Resin v4.1. Stereolithography 3D printing is also known as vat photopolymerization, and uses a vat of liquid photocurable resin and exposure to a laser light to cure/harden this liquid resin layer by layer according to a digital surface file. In low force stereolithography, the build plate is pressed down into the resin vat each layer, and the laser is below the vat and shines through a flexible layer which is gently peeled away from the most recently cured area of the object being printed.

Parameters used for 3D printing TPs from Formlabs Grey resin v4.1:

- 0.4 mm mini raft base.
- 0.5 mm height above raft of TPs.
- Touchpoint size 0.1 mm.
- 25 µm layer height.

Funded by the European Union

The Formlabs slicing program PreForm v3.5 was used for converting .stl 3D digital surface files into G-code instructions for the Formlabs Form3 3D printer.

One of the design parameters for TPs was replicating the particle morphologies of the CRM host material that the TPs were intended to be used in. To do this, digital surface files of real particles of CRM host material were required. These were acquired using X-ray Computed Tomography (X-CT) imaging.

Small vials containing approximately 1 gram of (a) nickel concentrate and (b) spodumene concentrate were imaged using a GE phoenix v|tome|x s X-ray computed microtomography device at the Geological Survey of Finland (GTK), Espoo, Finland. They were imaged using the standard tube with an accelerating voltage of 80 kV and a tube current of 38 µA, for a tube power of 3.0 W. The samples were scanned with 1,400 angle steps. At each angle the detector waited for a single exposure time and then took an average over three exposures, with a single exposure time of 1000 ms. This resulted in total scan times of 2 hours. Voxel resolution was 2.1 µm.

Data was analysed with Thermo Fisher PerGeos® 2020.2 software, and individual particles were segmented and saved as .stl surface files. These were simplified and smoothed using Meshlab 2023.12 to reduce file size to allow for multiple TPs to be produced using CURA and PreForm slicing software.

2.4 Horizon Microtechnologies produced Tracer Particles

Horizon Microtechnologies GmbH, based in Rheinstetten, Germany, is a provider of microfabrication services and products, combining microscale 3D printing with advanced coating and metallisation technologies. They use a Boston Micro Fabrication S240 Projection Micro Stereolithography (PµSL) Digital Light Projection (DLP) 3D printer to produce polymer-based parts with XYZ resolution down to 10 µm but with relatively large build volumes (100 mm x 100 mm build area) for high throughput. Coating and metallisation allow produced objects to be used in fields such as antenna structures in RF and microwave applications, alongside 3D microfluidics, 3D electrodes and contact pins, and packaging solutions for Micro-Electro-Mechanical Systems (MEMS) and miniaturised optics housings.

2.4.1 Materials

Three different materials were trialled from the Boston Micro Fabrication material portfolio, to test for printability of the planned shapes at prototype and mass production scale, and detectability in terms of their fluorescent response. The materials used were:

- HTL – a high-performance engineering grade polymer with high strength, rigidity, and heat resistance.
- BIO – a biocompatible polymer suitable for non-implantable medical applications.
- HT200 – a high temperature polymer that can withstand standard bending forces at temperatures up to 200°C.

All are methyl methacrylate (MMA) based resins with proprietary modifications and additives to give the desired material properties.

2.4.2 Methods

The particle shape chosen was one of the particles from nickel concentrate (origin B) imaged using X-ray Computed Tomography (X-CT) imaging as discussed above. The particle size of the roughly spherical particle was chosen to be 500 µm in diameter.

2.4.3 Results

Test prints to produce prototype particles showed improvements that could be made to the production method for better quality control of the prints, and easier removal from the build plate and higher yields of particles per build plate. Detection tests showed that BIO and HT200 material-based particles were visible to the naked eye within host material and showed good fluorescence, while HTL was invisible to the naked eye and showed lower fluorescence, making it difficult to detect.

2.5 3D MicroPrint produced Tracer Particles

Founded in 2013 by EOS GmbH and 3D-Micromac AG, and based in Germany, 3D MicroPrint GmbH ('3D MicroPrint') is a provider of additive manufacturing services. 3D MicroPrint utilise Micro Laser Sintering (MLS) (also known as µ-LPBF (Micro Laser Powder Bed Fusion)) technology to produce metallic micro-components for the aerospace, medical and luxury sectors (3D MicroPrint, 2019). 3D MicroPrint can produce items made from:

- Stainless steel: 1.4404 and 1.4542.
- Titanium: 3.7035 (Ti) and 3.7164 (Ti6Al4V).
- Copper: 2.0040 (CuOF) and 2.1293 (CuCr1Zr).
- Inconel® 718: 2.4668.
- Other metals including platinum, gold, cobalt, chrome and tungsten (3D MicroPrint, 2026).

2.5.1 Materials

CuCrZr alloy (2.1293) and stainless steel (1.4542) were selected to produce TPs due to their availability and suitable properties.

2.5.1.1 CuCrZr (2.1293)

Widely used in additive manufacturing, CuCrZr offers high-temperature strength, excellent tempering, and wear resistance (3D Microprint, 2025a). The alloy resists natural, industrial and maritime atmospheres, as well as non-oxidising, alkaline solutions and neutral saline solutions. However, it is susceptible to seawater, oxidising acids, ammonia, halogenide, cyanide and hydrogen sulphide solutions and atmospheres (Aurubis Stolberg, 2026).

Although the alloy's potential hydrophilicity could interfere with beneficiation processes (e.g., froth flotation), the alloy remains a suitable material for TP production if added further downstream along a supply chain to copper-containing concentrates (e.g., nickel concentrate) processed via pyrometallurgy, as these metallurgical processing steps are not strongly dependent on the surface chemistries of the raw materials. The addition of this alloy

would not detrimentally affect the quality of the material, as ≥97.8% of each TP is made from copper.

Additionally, as this material is made from at least five different elements, including ≤0.5% of "other" elements (Table 1), it is possible that the chemical signatures from these TPs could be used for traceability purposes, depending on (a) if the source material used to produce these TPs has been chemically characterised, and (b) if the chemical properties of different source materials for 3D printing are distinct enough for material fingerprinting purposes.

Table 1. CuCrZr alloy (2.1293) specifications (3D MicroPrint, 2025a).

Elements	Wt. %
Copper	≥97.8
Others	≤0.5
Zirconium	0.03–0.30
Silicon	≤0.1
Iron	≤0.08

2.5.1.2 Stainless steel (1.4542)

This is a magnetic, martensitic, precipitation-hardenable chromium-nickel-copper steel which provides high yield strength, wear resistance, corrosion resistance and biocompatibility (3D Microprint, 2025b). The alloy has various applications, including within the medical technology and aerospace sectors. While the complex composition of this alloy could impact certain methods of CRM processing (e.g., where specific elements such as carbon, iron, nickel and sulphur are regulated) (Table 2), the ferromagnetism of this alloy enables recovery via magnetic separation. Magnetic separation is a standard industrial pre-treatment step, used for example for spodumene concentrate and black mass (Khodadadmahmoudi et al., 2023; Retamal et al., 2024).

Table 2. Stainless steel (1.4542) specifications (3D MicroPrint, 2025b).

Elements	Wt. %
Iron	≥30.69
Chromium	15.00–17.00
Nickel	3.00–5.00
Copper	3.00–5.00
Carbon	0.00–0.07
Manganese	0.00–1.00
Molybdenum	0.00–0.60
Phosphorus	0.00–0.04
Sulphur	0.00–0.03
Silicon	0.00–1.00
Niobium/Tantalum	0.15–0.45

2.5.2 Methods

Quick Response (QR) codes were invented in 1994 by Denso Corporation for inventory management at manufacturing sites (Hara, 2019). Due to limitations with the volume of data

that can be included in a single one-dimensional barcode, two-dimensional QR codes were developed to increase the volume of information that can be inserted into a single printable code.

Today, QR codes are widely used within many industries, from supporting basic administrative tasks, to applications in marketing and the verification of the authenticity of documents or products. QR codes are also used within supply chains for traceability purposes, such as within food supply chains (Li et al., 2024), and they have been successfully integrated into traceability systems for conflict minerals (Hyperledger Foundation, 2019). Additionally, the use of QR codes will be particularly significant for battery supply chains within the EU, as the European Commission has mandated the marking of batteries with QR codes that link to the battery's DPP (European Parliament & Council of the European Union, 2023).

Due to 3D printing resolution limits, micro QR codes were evaluated instead of traditional QR codes. Micro QR codes are highly condensed variants of traditional QR codes which utilise only one finder pattern and a narrower quiet zone (Figure 2). Micro QR codes have also been used for traceability purposes, for example where they have been used to identify printed circuit boards (PCBs) (Vanstron Automation, 2025). For proof-of-concept evaluation, the M1 micro QR code, which is the smallest variant of a micro QR code, was utilised to encode TPs. M1 variants are made up of 121 modules, do not support error correction and have a maximum data capacity of five numeric values. As micro QR codes have a low data capacity, the numeric encoding associated with TPs for a particular consignment could be recorded in a secure database for cross-verification along the chain of custody (CoC).

Figure 2. Comparison of an M1 micro QR code (left) and a Version 1 QR code (right). The QR codes yield the numeric encoding "12345". Figure adapted from Karrach et al. (2020) and Scandit (2026).

Alongside the use of micro QR codes for encoding TPs, the use of a letter on each individual TP was also explored. Although letters provide a lower encoding factor than micro QR codes, the presence of TPs with different letters in a consignment could be evaluated, combined and used for verification purposes.

Three encoding configurations were implemented for TPs made from CuCrZr alloy (2.1293) and stainless steel (1.4542):

1. External overt: M1 micro QR code on the TP surface.
2. External overt: Lettering on TP surfaces.
3. Internal covert: M1 micro QR code within the TP structure.

2.5.3 Results

TPs with functional internal and external micro QR codes were successfully fabricated from stainless steel (1.4542) (Figure 3 and Figure 4). While internal micro QR codes were not experimented with CuCrZr alloy (2.1293), external micro QR codes were also produced for this alloy (Figure I-1). Although external micro QR codes were not directly scannable due to insufficient contrast between grooves and the face of the TP, scannable micro QR codes were successfully reproduced from TPs on an 11 x 11 grid template by third parties who had not beforehand seen the micro QR codes. The readable micro QR codes were obtained from X-CT results, where density variations between residual stainless steel 1.4542 powder within the structure of the micro QR code and the solid matrix allowed for feature identification (e.g., Figure 4c and Figure 4d).

Funded by
the European Union

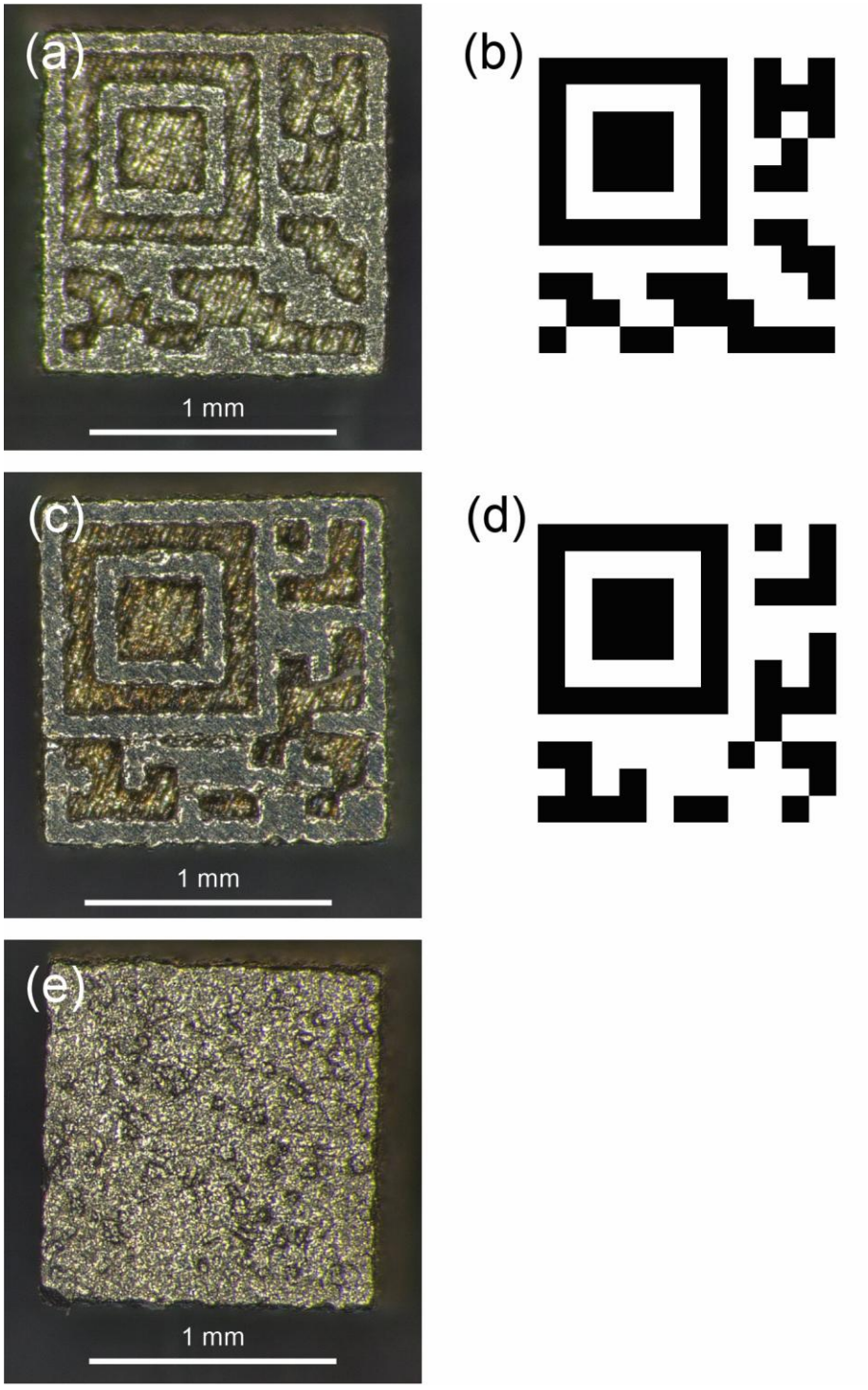

Figure 3. Stainless steel (1.4542) TPM01 and TPM05 tracer particles and associated micro QR codes used for encoding. (a) TPM01 stainless steel cube with the "24455" micro QR code, (b) M1 micro QR code which yields the numeric encoding "24455", (c) TPM01 stainless steel cube with the "48550" micro QR code, (d) M1 micro QR code which yields the numeric encoding "48550", and (e) TPM05 stainless steel cube containing an internal micro QR code.

Funded by
the European Union

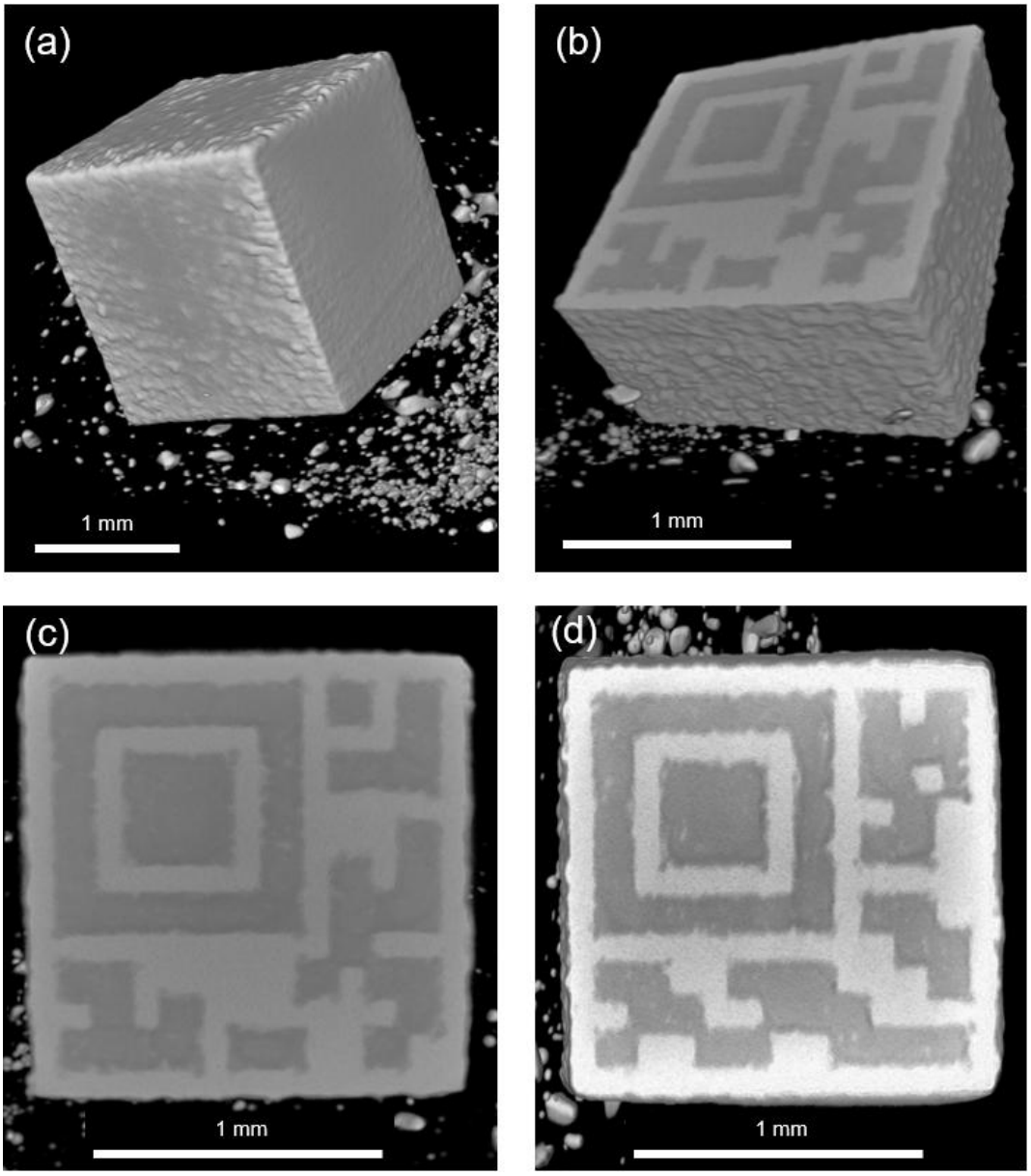

Figure 4. X-Ray Computed Tomography imagery of stainless steel (1.4542) TPM05 tracer particles showing the 3D printed internal micro QR codes. (a) Image of external surfaces of the TPM05 tracer particle, (b) cross-section slice parallel to the surface of the internal micro QR code, (c) scannable "48550" micro QR code, and (d) scannable "24455" micro QR code.

Spherical TPs with lettering were successfully produced from CuCrZr alloy (2.1293) (Figure 5) and stainless steel (1.4542) (Figure I-2). Due to the 3D printing process, the TPs were not perfect spheres but were rather truncated spheres with flat bases (Figure 5b and Figure I-2b).

Funded by the European Union

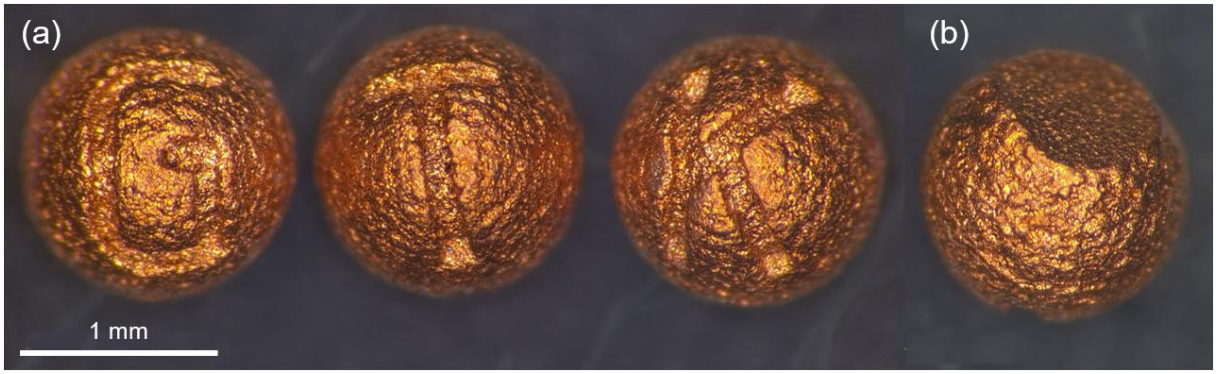

Figure 5. CuCrZr alloy (2.1293) (TPM02) tracer particles with lettering. (a) TPM02 tracer particles printed with the letters "G", "T" and "K" and (b) Flat base of TPM02, revealing its truncated sphere shape.

2.6 Summary of 3D Printed Tracer Particles

Nine different 3D printed TPs were produced in larger quantities from three different manufacturers (including GTK). A summary of these TPs and their properties is provided in Table 3.

Table 3. A summary of 3D printed tracer particles used in the project and their properties.

Producer	Name	TP Alphanumeric Code	Summarised TP Properties
GTK	GTK NiCo	TPG01	500 µm tracer particle made from 55–75% urethane dimethacrylate, 15–25% methacrylate monomers and undefined additives including photoinitiators and others. The tracer particles resemble particle morphologies of NiCo particles from nickel concentrate.
3D MicroPrint	2.1293 cubes with external micro QR code	TPM01	Cube with side lengths of 1.43 mm which are made from the CuCrZr alloy 2.1293. Micro QR codes were printed onto one side of the cube.
	2.1293 spheres with external letters	TPM02	1.41 mm (l) x 1.41 mm (w) x 1.32 mm (h) truncated spheres made from the CuCrZr alloy 2.1293. Letters "G", "T" and "K" were printed separately onto the surface of each tracer particle.
	1.4542 cubes with external micro QR code	TPM03	Cube with side lengths of 1.43 mm which are made from the alloy 1.4542. Micro QR codes were printed onto one side of the cube.
	1.4542 spheres with external letters	TPM04	1.41 mm (l) x 1.41 mm (w) x 1.32 mm (h) truncated spheres made from the alloy 1.4542. Letters "G", "T" and "K" were printed separately onto the surface of each tracer particle.
	1.4542 cubes with internal micro QR code	TPM05	Cube with side lengths of 1.43 mm which are made from the alloy 1.4542. Micro QR codes were printed within the interior of the cube.
Horizon Microtechnologies	HT200	TPH01	Irregular sphere with a diameter of up to 0.46 mm. Made from methyl methacrylate resins.
	HTL	TPH02	
	BIO	TPH03	

Funded by the European Union

3 Commercially Sourced Tracer Particles

Five types of TPs were obtained from two independent commercial sources, and the TP names have been replaced with alphanumeric codes (Table 4):

1. TraceTag International Ltd ('TraceTag'): supplied four types of TPs from their ValiMark™ range of luminescent and chemical compound tracers.
2. Microtrace, LLC ('Microtrace'), supplied Microtaggant® Identification Particles (MIPs), herein referred to as TPB01.

All TPs obtained from TraceTag (ValiMark™ range of tracers; TPA01–04) and Microtrace (Microtaggant® Identification Particles; TPB01) were part of each supplier's standard range of TPs and were not optimised for the specific host materials, application methods, or detection workflows used in this proof-of-concept study.

Table 4. Commercially sourced tracer particles obtained as part of the project.

Supplier	TP	TP Properties
TraceTag International Ltd	TPA01	PY series (yellow) mineral microspheres. 10 µm to 11 µm in size.
	TPA02	PY series (yellow) mineral microspheres. 15 µm in size.
	TPA03	PY series (yellow) mineral microspheres. 20 µm in size.
	TPA04	Organic microspheres E 580 (red; powder form). 55 µm to 65 µm in size.
Microtrace, LLC	TPB01	Microtaggant® Identification Particles. ~37 to 75 µm in size.
Note: TP = tracer particle.		

Individual TPs obtained from both suppliers ranged in size from 10 µm to 75 µm and were not visible to the naked eye under natural light. However, under specific light configurations, the TPs would fluoresce and would become visible with the use of supplier-provided or supplier-recommended detectors. Further details regarding these detectors can be found in the methodology section.

Furthermore, Microtrace conducted a proof-of-concept evaluation of Microtrace's Molecular™ Taggant System separately under confidential laboratory conditions.

4 Host Materials

The four critical raw materials included within the scope of the MaDiTraCe project are lithium, cobalt, rare earth elements (REEs) and natural graphite. For D2.6, AHK and GTK have sourced seven different critical raw materials, herein referred to as host materials. The seven different host materials represent raw material from various stages of their respective supply chains, from ore and concentrate to intermediate chemical products and secondary raw materials (Table 5). Host materials from REE supply chains were not obtained as part of this study.

A brief description of the host materials used is outlined below:

- Lithium ore: A mined rock containing economic concentrations of the element lithium (approximately 1.5% Li_2O (Table II-7)) contained within the minerals zinnwaldite and

lepidolite (Figure II-3, Table II-9 and Table II-10). The geological deposit from which the ore was obtained, which could be either a rare metal granite or a lithium-caesium-tantalum (LCT) type pegmatite, could not be verified. Although the obtained material was described as an ore by the supplier, it appears the material may have undergone comminution, as 86% by mass of the material is made up of particles that are <2 mm (Table II-2), which is atypical for an ore. This type of lithium ore would undergo processing to form a lithium concentrate, a key feedstock for the lithium-ion battery supply chain.

- Spodumene concentrate: A refined lithium intermediate material derived from LCT pegmatites, containing 5% Li_2O (Table II-19). The concentrate would subsequently undergo beneficiation to produce lithium carbonate or lithium hydroxide, which are chemicals required for cathode production.
- Lithium carbonate: A chemical product suitable for direct use as a battery-grade feedstock (e.g., in lithium iron phosphate (LFP) cathode material), or which undergoes further processing to form lithium hydroxide. The lithium carbonate obtained for this project has a lithium content of 18.5% (40% Li_2O; Table II-30).
- Nickel concentrate: A sulphide ore-derived intermediate material containing nickel and cobalt. Nickel concentrate was obtained from two different anonymised origins: (a) origin A and (b) origin B, with only nickel concentrate from origin A obtained in sufficient quantities for host material characterisation. Nickel concentrate from origin A contained approximately 9% nickel and 0.7% cobalt (Table II-39). The nickel concentrate would undergo processing to form cobalt sulphate and nickel sulphate, which are used to produce nickel-rich cathode chemistries such as nickel manganese cobalt (NMC).
- Graphite concentrate: A refined intermediate material produced from flake graphite ore. The graphite concentrate contains a minimum purity of 96.7% graphitic carbon (Table II-56). It serves as a precursor for coated spherical graphite, the primary material used in battery anodes.
- Mixed hydroxide precipitate (MHP): A chemical product containing a mixture of nickel and cobalt hydroxides. The MHP obtained for this project contains approximately 37% nickel and 3% cobalt (Table II-62). It is an intermediate hydrometallurgical product of nickel laterite ore processing. This material is a key feedstock for battery-grade cobalt sulphate and nickel sulphate.
- Black mass: An intermediate product in the recycling of spent, end-of-life batteries. Black mass comprises crushed and shredded battery cells, made up of a mixture of graphite and metals, including lithium, manganese, cobalt, copper and nickel. Metals are separated and purified, such as into battery-grade chemicals that are transformed into precursor cathode active material to produce cathode material. The black mass obtained comprised approximately 32% NMC cathode material (Figure II-26 and Table II-72).

Funded by the European Union

Table 5. Summary table of host materials obtained as part of this study, and the critical raw materials (CRMs) within the scope of the MaDiTraCe project that are economically extracted from these commodities.

Commodity	Position within the CRM supply chain	CRMs within the scope of the MaDiTraCe project
Lithium ore	Primary Raw Material	Lithium
Spodumene concentrate	Upstream (Processed/Refined Raw Material)	Lithium
Lithium carbonate	Upstream (Processed/Refined Raw Material)	Lithium
Nickel concentrate	Upstream (Processed/Refined Raw Material)	Cobalt
Graphite concentrate	Upstream (Processed/Refined Raw Material)	Natural graphite
Mixed hydroxide precipitate	Upstream (Processed/Refined Raw Material)	Cobalt
Black mass (NMC)	Downstream/ Secondary Source (Recycled Raw Material)	Cobalt Lithium

Note: NMC = nickel manganese cobalt. The list of EU-defined CRMs was obtained from Grohol & Veeh (2023).

Each host material has also been characterised based on relevant standards for the identification and classification of soil (ISO 14688-1:2017), rock (ISO 14689:2017) and using analytical techniques which are used industrially to characterise these materials, including moisture determination according to ISO 10251:2006, chemical and physical analysis (e.g., bulk density, laser particle sizing and X-ray fluorescence (XRF)), X-ray diffraction (XRD) and automated mineralogy using Scanning Electron Microscopy with Energy Dispersive Spectroscopy (SEM-EDS)). The majority of characterisation and analyses were carried out by AHK Group companies (Alfred H Knight International (UK), LMA B.V. (Netherlands) and ASMIN (Chile)). Additional analyses were carried out by Helford Geoscience and Vidence (automated mineralogy of black mass and graphite concentrate) and ProGraphite (physical/chemical analyses of graphite concentrate).

Results of the host material characterisation are provided in 13.2 Appendix II: Host Material Characterisation.

Funded by the European Union

5 Methodology

5.1 Previous Research

Despite the global use of diverse TP technologies, as evaluated by Donnelly et al. (2023), comprehensive data regarding the testing methodologies for TP technologies remains sparse in the public domain. This lack of information in the public domain is attributable to the prevalence of intellectual property protections and the retention of proprietary methodologies or industry secrets by private entities.

Furthermore, a research gap exists regarding the efficacy of TP technologies within the mining, minerals and metals industries. While artificial TPs have been implemented for specific high-value segments of the mining, minerals and metals industries, such as the laser inscription of gemstones (De Beers Group, 2026; Microtrace, 2026a), DNA and "molecular" tagging of gemstones (Haelixa, 2026; Microtrace, 2026a) and gold bullion (Zurich Cantonal Bank, 2025), TP technology is not in general use for upstream materials including ores, mineral concentrates and chemical products. Aside from preliminary investigations into Microtaggant® Identification Particles (MIPs) conducted by AHK (Donnelly et al., 2023), the published scientific literature remains devoid of research or operational investigations evaluating TP applications within this industry.

5.1.1 Alfred H Knight Preliminary Tests

From 2019 to 2022, Alfred H Knight conducted a series of preliminary research experiments using Microtrace's Microtaggant® Identification Particles (MIPs), which were applied to samples of copper concentrate. The experiments were designed to analyse and evaluate the TPs' ultraviolet (UV) intensity, infrared (IR) intensity and certain application methods. In addition to these tests, colour coding identification and verification was also performed by observing the TPs using a binocular microscope. Finally, sampling simulation and grinding/milling tests were also performed.

The results showed there to be complete coverage and good distribution of the TPs over the host copper concentrate. In addition, the application of the TPs with lacquer/water, allowed the TPs to bond with the copper concentrate and remained on top of the exposed surface of the concentrate contained as a hard lacquer coat. It was important to dilute the lacquer with water to avoid any unwanted discolouration over the tagged concentrate. It was found that a ratio of 60/40 or 70/30 percent of water to lacquer is enough to create a thick, coated layer that was transparent.

From the drying tests, it was found that the TPs could resist temperatures commonly used for the moisture determination of mineral concentrates (105°C ± 5°C). Also, it was found that the TPs mixture took 30–40 minutes to dry under laboratory conditions.

From the grinding/milling test, it was observed that the TPs do pulverise together with the copper concentrates. Therefore, it is unlikely to be able to identify the particles after a sample has been prepared for assaying.

Funded by the European Union

5.1.2 U.S. Congress Office of Technology Assessment

The 1980 assessment by the U.S. Congress Office of Technology Assessment (OTA) provides the results of an investigation outlining test methodologies for TPs. This assessment investigated the mandated integration of TPs into explosives and gunpowder, evaluating chemical, radiological, and detection TPs, as well as physical TPs such as the 3M Identification Taggant (the patent for which is currently held by Microtrace (2026b)). The scope of the OTA's research included natural ageing tests, assessments of TP post-detonation survivability, and chemical compatibility. Additionally, the economic feasibility of TP technologies was also evaluated. However, the descriptions provided of the different tests lacked the technical information required to reproduce them. Furthermore, some of the tests such as post-detonation survivability, extended beyond the scope of this study.

5.2 Preliminary and Principal Tests

There are numerous tests developed and standardised to assess the durability of polymeric materials (e.g., Chang et al., 2020; Gu & Gu, 2005; Markovičová & Zatkalíková, 2019). Given the absence of recognised standards or publicly available literature outlining testing methodologies specifically for Tracer Particles (TPs), AHK and GTK adapted several existing polymeric material tests and developed new tests for this purpose.

The developed testing method was implemented in two distinct stages:

1. First Stage (Preliminary): These tests were designed to characterise TP behaviour within host materials. The objective was to determine optimal procedures for the application, mixing, and detection of TPs in preparation for ageing tests.
2. Second Stage (Principal): These tests evaluated TP performance within host materials following various ageing or environmental stimulation methods. This stage comprised tests aligned with Technology Readiness Levels (TRLs) 3–4.

5.2.1 Preliminary Tests

The preliminary tests developed included:

1. Evaluation of dry and wet (pneumatic atomiser) application methods.
2. Evaluation of different mixing methods, including bag mixing and mixing using a riffle splitter.
3. Evaluation of different detectors to detect TPs.
4. Determination of the optimal TP dosage for principal test work through evaluation of TP distribution in the host material and TP detectability.

Evaluation of TP detectability involved a visual assessment by naked eye, supplier-provided or supplier-recommended detectors (for TPs that fluoresce under excitation light; Figure 6) or magnets (for TPM03 and TPM04; Figure 21b), and using a digital microscope (ZM0756H4K8MPA All-in-one Zoom Monocular HDMI Digital Microscope) which had a maximum magnification of x594, with and without excitation light sources (Figure 7).

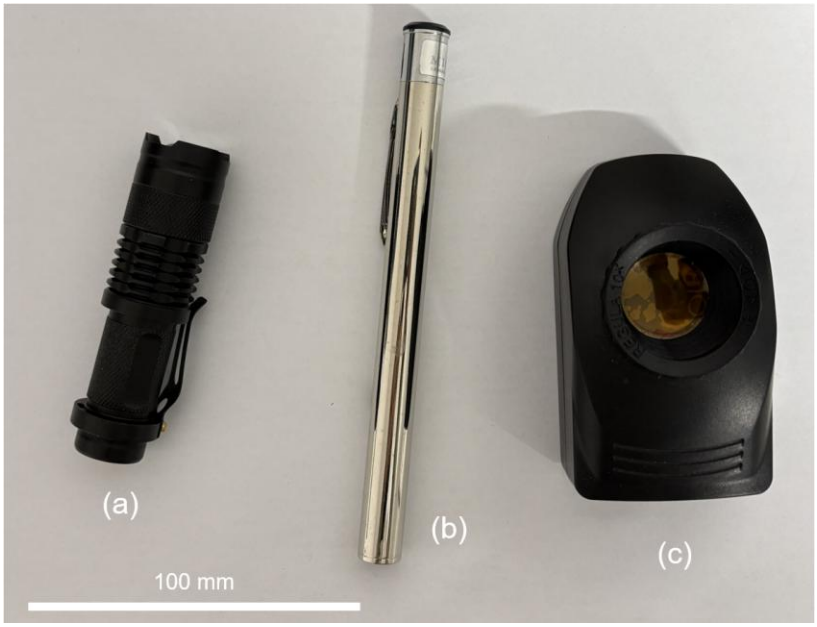

Figure 6. Supplier-provided and supplier-recommended handheld detectors. (a) Unbranded battery-powered 91 mm x 24 mm 365 nm UV torch, (b) Microtrace's handheld detector, and (c) TraceTag's ValiScan S3 detector.

Supplier-recommended detectors varied depending on the light configuration that TPs fluoresced. For TPs that fluoresced under ultraviolet (UV) light, detectors used included an unbranded battery-powered 91 mm x 24 mm 365 nm UV torch, and for use with the digital microscope, two gooseneck-type 365 nm UV-LEDs. For TPs that fluoresced under other commercially sensitive light configurations, a separate laboratory-based set-up was used.

Funded by
the European Union

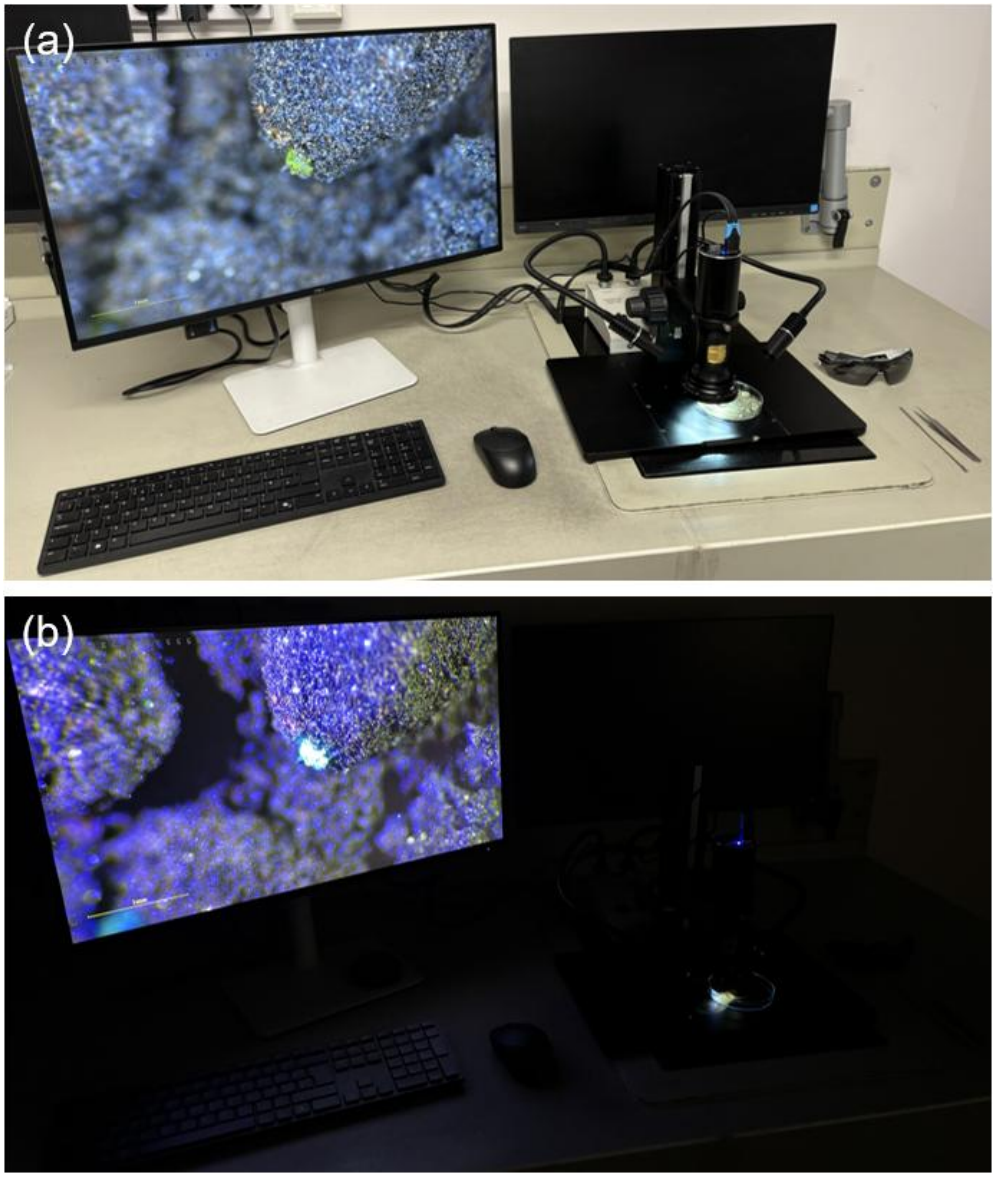

Figure 7. ZM0756H4K8MPA All-in-one Zoom Monocular HDMI Digital Microscope set up. (a) Set up in a lit room (under white light). (b) Set up in a dark room, using excitation light sources to illuminate the sample.

To assess TP distribution, an industry-accepted and ISO standard-approved method of sampling particulate material from bags or drums using spears, was adapted. ISO 12743:2021 specifies that a sampling spear (a hollow cylinder) should be inserted vertically into a bag or drum, ensuring that it penetrates the full vertical depth and a complete vertical column of concentrate is extracted. For host materials as part of the project, where ~1 kg masses of host material were handled for the evaluation of TP distribution, a 100 mm x 100 mm transparent cube made from poly(methyl methacrylate) (PMMA) (Perspex®) and five PMMA or glass spears measuring approximately 20 mm in diameter and 100 mm in length were used in a quincunx geometric pattern to obtain spatially representative samples of the full depth of material (Figure 8). Depending on the properties of the commodity being sampled and methods of TP detection (e.g., microscope or handheld device), either glass hollow cylinder spears or PMMA hollow cuboid spears were used to sample the material.

Funded by
the European Union

Once optimal methods of application, mixing and detection were established from these tests, these methods were then employed as part of the principal laboratory tests.

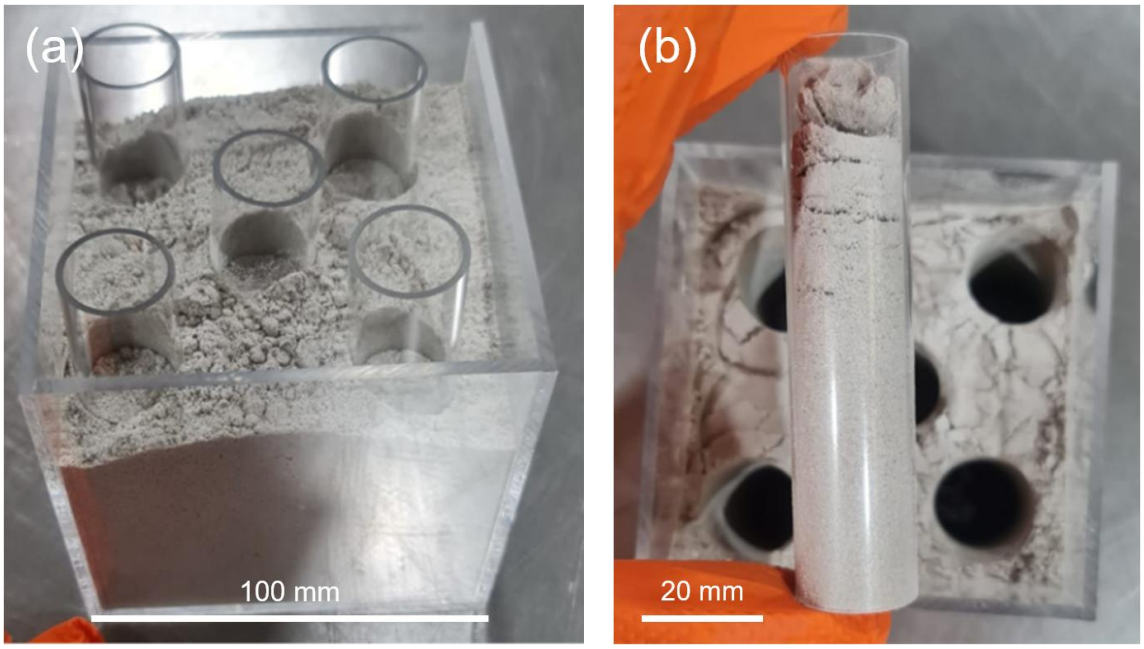

Figure 8. Spodumene concentrate within the poly(methyl methacrylate) cube. (a) Cylindrical spears inserted in a quincunx pattern. (b) A glass spear with a full vertical depth of spodumene concentrate extracted (with the empty columns remaining within the material after the removal of all spears in the background).

5.2.2 Principal Tests

5.2.2.1 Dilution

Within global metals and minerals supply chains, the blending or mixing of raw materials from disparate sources is standard industrial practice. Legitimate, large-scale blending is typically conducted to achieve specific technical, commercial and operational objectives, including:

- Feedstock homogenisation: Reducing the chemical and physical variability of a raw material through blending may take place to ensure consistent raw material properties. This may be carried out to comply with quality requirements in agreed-upon contracts or metallurgical processing requirements stipulated by smelters or refiners.
- Physical and chemical conditioning: Raw materials may undergo blending to optimise moisture content to improve material handling, mitigate dust generation and ensure compliance with transportable moisture limits for maritime transportation. Additionally, conditioning is utilised to dilute the concentration of penalty or impurity elements and compounds to meet thresholds set by regulatory bodies or end receivers.
- Adherence to chain of custody (CoC) models: Standardised responsible handling models such as segregation, controlled blending and mass balance explicitly permit the blending of CRMs from disparate sources and are widely used within the industry today (ISO 22095:2020).

Raw material manipulation also occurs illicitly through substitution or adulteration. These practices may be carried out to alter the physical or chemical properties of a consignment or to surreptitiously introduce non-certified material. Such activities can occur via wholesale or partial cargo substitution or adulteration utilising heavy machinery to mechanically mix tens of tonnes of stockpiled material from different origins, or at a laboratory sample scale, involving the addition or subtraction of gram or sub-gram quantities to distort analytical results.

Given these prevalent industrial blending and illicit manipulation practices, the utilisation of AFP for material certification purposes requires verification that the technology can accurately detect and quantify any dilution of tagged CRM. Microtrace conducted this laboratory-scale evaluation in-house using its Molecular™ Taggant System and reported the results to AHK; the methodology remains confidential. However, the primary objectives of this testing were to identify and authenticate the taggant signature once applied to a host material and define the taggant abundance thresholds capable of identifying whether a host material has been diluted with non-tagged material. Dilution of tagged material with 5%, 10%, 25%, 50% and 75% by mass of untagged material were assessed across all seven host materials (Table 5).

5.2.2.2 Minimum Effective Dosage

For traceability purposes, the minimum effective dose (MED) of TPs should be determined to ensure that TPs are added to commodities in a cost-effective, efficient and practicable manner that is also environmentally acceptable. Depending on the commodity being tagged, the recommended and existing MED of TPs range considerably from parts per billion levels for fuel (Tracerco, 2026) to several hundred parts per million for explosives (OTA, 1980).

The minimum effective dosage test was developed and applied to ensure TPs at a particular dosage (concentration) were detectable within a reasonable timeframe. Different TPs were each added to a nominal mass of host material at a specified dosage to ensure the total combined mass of TP and host material was equal to 100 g. Once added to the host material, the material was passed through a riffle splitter and recombined three times to ensure the TPs and host material were thoroughly mixed. Handheld detectors were then used to determine if TPs were detectable within samples in transparent self-seal polypropylene bags (100 mm x 140 mm).

As part of this test, host material and TP combinations were weighed in triplicate. TPs were either weighed to 10 µg (0.00001 g) or the mass of a single TP as a starting dosage, and if TPs were not detectable within all three samples at the lowest dosage, a higher TP dosage was evaluated until TPs were detectable within all three samples, which would then be taken as the MED for that particular type of TP. For smaller TPs (i.e. TPA01–04 and TPB01), if TPs were undetectable at the smallest dosage 10 µg (0.00001 g), the dosage was systematically increased to 50 µg (0.00005 g), 100 µg (0.00010 g) and 150 µg (0.00015 g) until the detection criteria were satisfied. For larger TPs (i.e. TPG01, TPH01 and TPM01–04), any dosage adjustments were scaled incrementally by adding the mass equivalent of a single TP per test until successful TP detection was achieved across all three test samples.

All TPs were tested with spodumene concentrate. TPH01, TPG01 and TPs made from CuCrZr alloy (2.1293) (TPM01 and TPM02) could not be tested with nickel concentrate due

to the host material's limited availability. A calibrated Mettler Toledo XPR6UD5 balance, with a readability of 0.5 µg, was used to measure TP masses.

5.2.2.3 Abundance and Distribution

The physical distribution of the TPs within a commodity has significant implications for detection and sampling methodologies. If TPs segregate within the host material this could have a negative impact on its potential application for traceability. For example, by surface deposition on upper layers or by gravitational segregation.

TP distribution and any associated bias or variance as a result of dry and wet application methods and the host material properties were evaluated on representatively collected 10 to 20 gram tagged samples (in triplicate per TP and host material combination) containing a TP dosage of 100 ppm (0.01%). These samples were placed in a petri dish (90 mm diameter x 15 mm depth) and the TPs were detected and counted as follows:

1. Observations of the TPs over the entire surface of the sample within a petri dish by naked eye alone.
2. The petri dish was divided into five areas (Figure 9), and the digital microscope was used to count the number of TPs within each area under natural light and under excitation light. The petri dish was positioned so that one field of view per area was evaluated using the microscope. The counting limit for TPs was also capped at 40 TPs for this part of the test.

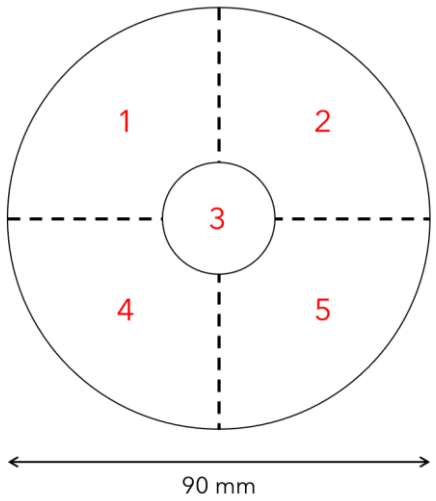

Figure 9. Plan view of petri dish split into five areas.

Additionally, as part of this test, samples were submitted for manual scanning electron microscopy (SEM) to assess external physical interactions between TPs and host materials. No reverse engineering, compositional analysis, or chemical analysis of TraceTag's or Microtrace's tracer particle technologies was performed. These tests were carried out on tagged samples prior to any ageing tests. The TPs and host materials used for this test are presented in Table 6.

Table 6. Outline of host material and the tracer particle combinations which were tested.

TP \ Host Material	Spodumene concentrate	Mixed hydroxide precipitate	Nickel concentrate (origin A)	Black mass
TPA01	✓	✓	-	✓
TPA02	✓	✓	-	✓
TPA03	✓	✓	✓	✓
TPA04	✓	✓	✓	✓
TPB01	✓	✓	✓	✓
TPG01	-	-	✓	-
TPH01	-	-	✓	-
Note: TP = tracer particle.				

5.2.2.4 Modified Flow Table Test

Critical raw materials (CRMs), such as cobalt-containing nickel ore and spodumene concentrate, are transported around the world in bulk within vessel cargo holds. When transported in bulk, some of these raw materials may be susceptible to liquefaction or dynamic separation, especially if they contain a high moisture content combined with a significant proportion of fine particles. Liquefaction and dynamic separation may cause a vessel to become unstable and in extreme circumstances, the vessel can capsize. Between 2015 and 2024, liquefaction accounted for 61.8% of the total bulk carrier loss of life (International Association of Dry Cargo Shipowners, 2025).

To avoid liquefaction and dynamic separation from occurring during maritime transportation, the completion of Flow Moisture Point (FMP) and Transportable Moisture Limit (TML) testing is a mandatory requirement for cargoes susceptible to these phenomena. The International Maritime Solid Bulk Cargoes (IMSBC) Code (2025) outlines different methods that are in general use for the determination of the FMP and TML. These are the Flow Table Test (FTT), the Penetration Test, and the Proctor/Fagerberg Test, as well as its various modifications. These laboratory tests are designed to exaggerate the conditions cargo may be exposed to during marine transportation by sea freight. As part of the MaDiTraCe project, the FTT was adapted to assess how TPs distribute themselves within host materials that are exposed to stimulated cyclic forces that represent vessel motion (e.g., caused by wave action, currents, water density variability and prevailing winds), compaction or engine vibrations.

As part of these tests, 100 mm x 100 mm PMMA cubes were filled with a host material and TP combination (at a TP dosage of 100 ppm (0.01%)) and were subsequently sealed. These cubes were then firmly secured onto the surface of a flow table and supporting apparatus which are according to ASTM Designation (C230-68), see Figure 10. The PMMA cube was then raised and dropped up to 250 times through a height of 12.5 mm at a rate of 25 times per minute for a continuous total test duration of 10 minutes. Once the test was completed, TP distribution was externally evaluated by making observations through the PMMA cube. Once these were completed, internal evaluation using spears, as outlined in section 5.2.1 Preliminary Tests, was carried out. This test was carried out in triplicate per host material and TP combination.

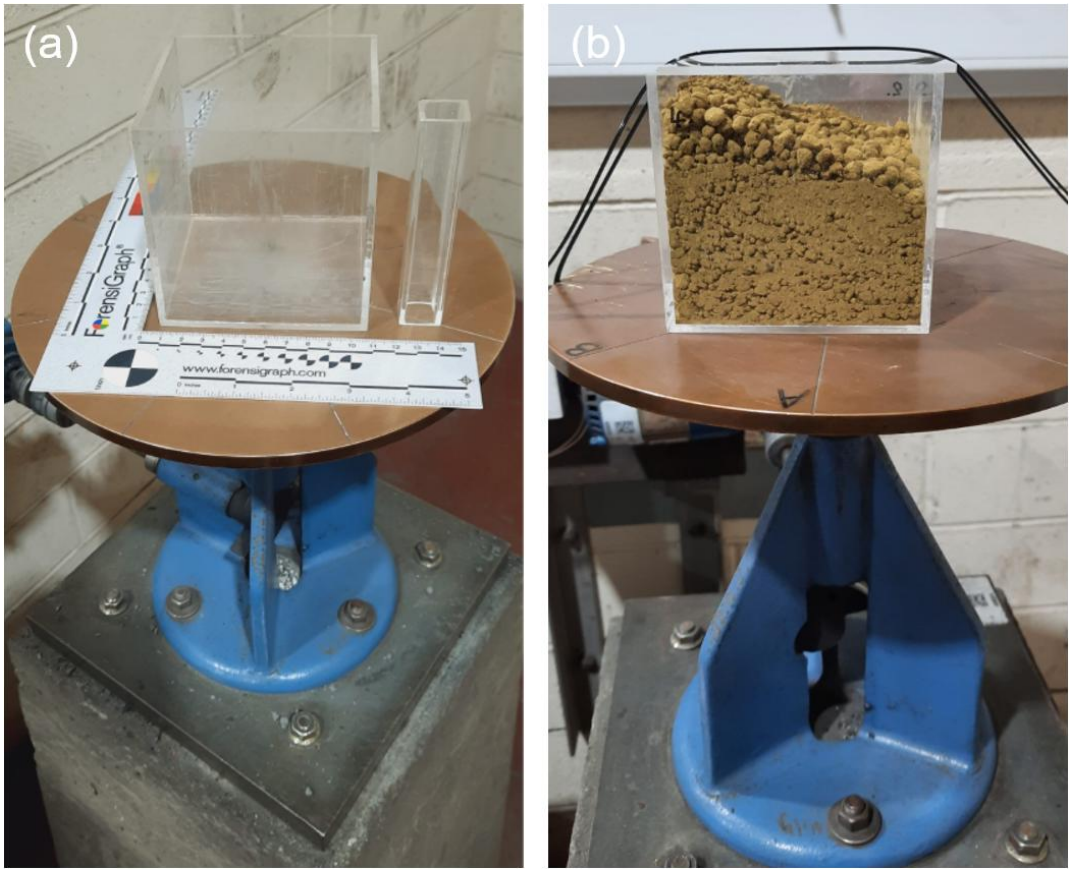

Figure 10. Flow Table Test apparatus and poly(methyl methacrylate) (PMMA) cube. (a) Apparatus used for the test including PMMA cube and cuboid spear. (b) Sealed PMMA cube for the Modified Flow Table Test.

For a selection of 3D printed TPs, which showed unique behaviours as part of this test when compared to the majority of TPs, the above outlined test method was repeated with an increased total duration of 20 minutes (up to 500 drops). The TPs and host materials used for this test are presented in Table 7. Certain material and TP combinations were not tested due to the limited availability of TPs and host material.

Table 7. Outline of host material and tracer particle combinations which were tested on the flow table.

TP \ Host Material	Spodumene concentrate	Mixed hydroxide precipitate	Nickel concentrate (origin A)	Black mass
TPA03	✓	✓	-	✓
TPA04	✓	✓	-	-
TPB01	✓	✓	-	-
TPG01	-	-	✓	-
TPM01	-	-	✓	-
TPM02	-	-	✓	-
TPM03	✓	-	-	-
TPM04	✓	-	-	-

Note: TP = tracer particle.

Funded by the European Union

5.2.2.5 Natural Ageing

The time intervals between CRM mining and mineral processing can vary, ranging from days to years. These intervals can be driven by several factors such as operational constraints, strategic stockpiling due to price volatility, supply chain logistics, a mine being placed into care and maintenance or legal issues. The exposure of the CRMs to the atmosphere during these periods also varies according to factors such as storage location (from controlled warehousing to open-air storage), diurnal and seasonal weather fluctuations, and ocean freight transit times that can range from 15 days (East Asia to Western North America) to 50 days (Europe to Australia) (WTA Group, 2026). Geopolitical tensions and conflict, which may arise suddenly, can further disrupt and extend these transit windows (United Nations Conference on Trade and Development, 2025).

Mineral commodities can be susceptible to rapid chemical and physical change during transit and/or storage via secondary processes such as oxidation (Donnelly et al., 2023). Oxidation may also pose a risk to the integrity of any TPs that have been added to a host material. It was therefore considered necessary to evaluate the behaviour of TPs under environmental conditions to determine their resilience and functionality.

A natural ageing test was devised, whereby 150 g samples of each host material containing TPs (at a TP dosage of 100 ppm (0.01%)) were collected and placed into 229 mm x 305 mm polypropylene woven sacks. These woven sacks were partially folded, and their mouths opened with the aid of coated wire. These bags were subsequently placed into Euro crates (Figure 11).

Figure 11. Natural ageing samples mid-test.

Note: Samples were placed on grated spill bunds to safely collect any rainwater containing leachate.

With the exception of the black mass samples, the crates were placed in an open and ambient environment within the courtyard of a secure AHK facility. Black mass is typically transported within United Nations (UN) certified flexible intermediate bulk containers

(FIBCs). These contain additional control and safety features such as impermeable inner liners and coated fabrics and are typically stored within a sheltered environment (e.g., a warehouse). All black mass samples used for this test were placed into polypropylene bags, which were sealed and stored in an isolated building that was naturally ventilated. Control samples of untagged host material were also included as part of the test.

These samples were left for a duration of 60 days (1,440 hours) and then taken to the laboratory for evaluation. Further information on the samples tested, the location, duration and climatic conditions experienced during the test can be found in Table 8 and section 13.3.2 Natural Ageing and Photooxidative Ageing (Appendix III).

Table 8. Outline of host material and tracer particle combinations for the natural ageing test.

Host Material / TP	Spodumene concentrate	Mixed hydroxide Precipitate	Nickel concentrate (origin A)	Black mass
TPA01	✓	✓	-	✓
TPA02	✓	✓	-	✓
TPA03	✓	✓	✓	✓
TPA04	✓	✓	✓	✓
TPB01	✓	✓	✓	✓
Note: TP = tracer particle.				

5.2.2.6 Photooxidative Ageing

In contrast to the natural ageing test, which completely exposes samples to the environment, the photooxidative ageing test prevents precipitation from contacting the in-situ samples. This test was intended to assess the effect of sunlight more selectively on samples in a ventilated environment. These conditions simulate alternative methods of the storage and transportation of CRMs (e.g., sealed UN-certified bags which may allow penetration of certain wavelengths of sunlight).

For this test, three 10 g samples of each host material and TP combination (at a TP dosage of 100 ppm (0.01%)) were placed into plastic petri dishes (90 mm diameter x 15 mm depth). These petri dishes were then covered with individual lids, which were securely taped in place, before being placed under a cloche made of corrugated polyvinyl chloride (PVC) (Figure 12). Samples were left for a duration of 35 days (840 hours) and then taken to the laboratory for evaluation. The TPs and host materials used for this test are presented in Table 9. The location of the test is outlined in section 13.3.2 Natural Ageing and Photooxidative Ageing (Appendix III).

Table 9. Outline of host material and tracer particle combinations which were tested for the photooxidative ageing test.

HM / TP	Lithium ore	Spodumene concentrate	Lithium carbonate	Mixed hydroxide precipitate	Nickel concentrate (origin A)	Black mass	Natural graphite
TPA01	✓	✓	✓	✓	✓	✓	✓
TPA02	✓	✓	✓	✓	✓	✓	✓
TPA03	✓	✓	✓	✓	✓	✓	✓
TPA04	✓	✓	✓	✓	✓	✓	✓
TPB01	✓	✓	✓	✓	✓	✓	✓

Note: HM = Host material; TP = tracer particle.

Figure 12. Photooxidative ageing samples mid-test.

Note: Samples were placed on grated spill bunds in case of spillage.

5.2.2.7 Artificial Climate Ageing

Except for Antarctica, CRMs are extracted from every continent in the world. Through the value chain, CRMs may be subject to extreme environmental conditions and fluctuations. Mining produces CRMs in regions where temperatures fall below -50°C, such as at the Talnakh and Norilsk nickel-copper-palladium-platinum-gold mines in Siberia, Russia (Reuters, 2024), and in regions where temperatures approach +50°C, such as at the Pilgangoora lithium-tantalum mine in Western Australia (Bureau of Meteorology, 2026).

Fluctuations in environmental conditions are further influenced by localised conditions (or microclimates) associated with certain methods of storage and transportation. Using shipping containers as an example, internal temperatures have been recorded to rise to approximately double external temperatures and elevated temperatures of 50–59.5°C can be sustained in these containers over several hours within a single day (The German Insurance Association, 2026; Singh et al., 2012). Temperatures within these containers have also been recorded to reach as high as 70°C (Marquez et al., 2012). Humidity extremes and fluctuations may also occur within shipping containers, which have been recorded to swing

from 32% RH to 96% RH in less than 16 hours (Leinberger, 2006). Conversely, in some locations, such as central Asia and Canada, continental climates can freeze mineral concentrates during storage and transportation.

Artificial climate ageing is a form of artificial ageing, which uses a climate chamber to control atmospheric parameters such as humidity, temperature, precipitation or wind. This is a well-established method of artificial ageing in the field of materials science (e.g., for the testing of polymers) and allows for the artificial simulation of different climatic conditions within a laboratory. With the aid of a climate chamber and considering the different environmental conditions TPs may be exposed to, various tests were developed to evaluate the resilience of TPs under different artificially induced conditions. These tests are detailed in Table 10.

- Short-term tests: Samples were subjected to an eight-day (192-hour) incremental thermal ageing test. The samples were maintained at controlled temperatures for 48 h periods; the temperature was increased by 10°C at the end of each period, starting at 45°C for the first 48 h period and increasing to 55°C, 65°C and 75°C during the second, third and fourth 48 h periods, respectively. Two variants of this test were carried out: (a) 192-hour ageing under low relative humidity (20% RH), and (b) 192-hour ageing under high relative humidity (85% RH). These tests were completed for TPG01 in nickel concentrate (from origins A and B).
- Medium-term test: Samples were subjected to a three-week (504-hour) incremental thermal ageing test. The samples were maintained at a constant low relative humidity (10% RH) and exposed to weekly temperature increases of 10°C, starting at 55°C for the first week and increasing the temperature to 65°C and 75°C during the second and third weeks, respectively.
- Long-term test: Ageing of samples at 40°C and 80% RH for three weeks (504 hours), followed by ageing at –5°C for two weeks (336 hours) to simulate the transport of CRMs from a high-humidity port (e.g., a wet tropical climate) to a cold polar climate. The total test duration was five weeks (840 hours).
- Targeted tests: (a) TPM01 were subjected to 75°C and 85% RH for five days (120 hours) in nickel concentrate, (b) TPM01 were subjected to 75°C and 85% RH for 3 weeks (504 hours) without any host material, (c) TPM01 were subjected to ageing for approximately one month (~720 hours) at temperatures ranging from 55°C to 75°C (85% RH) in nickel concentrate, (d) TPH01, TPH02 and TPH03 were subjected to 75°C and 85% RH for four days (96 hours) in nickel concentrate, and (e) TPM03 were subjected to 75°C and 85% RH over a one-month (720-hour) period in nickel concentrate.

Funded by the European Union

Table 10. Outline of host material and tracer particle combinations for artificial climate ageing tests.

Host Material / TP	Spodumene concentrate	Mixed hydroxide precipitate	Nickel concentrate (origin A)	Nickel concentrate (origin B)	Black mass
TPA01	■▲	■▲	■▲	-	■▲
TPA02	■▲	■▲	■▲	-	■▲
TPA03	■▲	■▲	■▲	-	■▲
TPA04	■▲	■▲	■▲	-	■▲
TPB01	■▲	■▲	■▲	-	■▲
TPG01	-	-	●○	●○	-
TPH01	-	-	◈	-	-
TPH02	-	-	◈	-	-
TPH03	-	-	◈	-	-
TPM01	-	-	◈	-	-
TPM02	-	-	◈	-	-
TPM03	-	-	◈	-	-

Note: TP = tracer particle. Symbols represent the following tests: Short-term low humidity (●) and high humidity (○), medium-term (■), long-term (▲), and targeted (◈) tests.

For each test, three 30 g samples of each host material and TP combination (at a TP dosage of 100 ppm (0.01%)) were collected and placed into glass vials. The vials were left open and were transferred into a Thermotron SE1000-3-3 Environmental Chamber (Figure 13) for the test duration. The climate chamber was stabilised for 24 h at the required test parameters before each test commenced. Between changes of parameters as part of a single test (e.g., change of temperature), samples were removed from the climate chamber and TPs examined. This process was carried out as swiftly as possible to ensure the timely return of samples into the climate chamber to continue the test under the new set of parameters.

Funded by the European Union

Figure 13. Thermotron SE1000-3-3 Environmental Chamber.

5.2.2.8 Transportation Test

Raw material consignments are typically transported from diverse geographical locations using flexible intermediate bulk containers (FIBCs), standard shipping containers or as bulk cargo within the holds of ocean vessels. The scale of these shipments varies significantly, ranging from several tonnes to upwards of 50,000 tonnes per consignment. Conversely, significantly smaller quantities of these materials, ranging from several grams to tens of kilograms, are frequently transported globally for purposes distinct from commercial supply, such as analytical samples.

Unlike industrial-scale transport, analytical samples are often dispatched via expedited logistical channels, including light commercial vehicles (LCVs), heavy goods vehicles (HGVs) and air freight facilitated by postal or courier networks. Consequently, the environmental conditions to which these samples are exposed during transit may differ substantially from the conditions encountered in large-scale industrial shipping environments. Samples containing TPs, especially in situations where the TPs contain covert PUFs or high encoding factors that can only be identified or deciphered using laboratory-based analytical techniques, are likely to be sent through these expedited logistical channels. Therefore, there is a requirement to assess how TPs behave in these environments.

For this transportation test, six 50 g samples of each host material and TP combination (at a TP dosage of 100 ppm (0.01%)) were prepared. Three of these samples were put into 100 mm x 140 mm polypropylene self-seal bags and three samples were placed in heat-sealed

Funded by the European Union

aluminium packets (Figure 14). Once all samples were prepared, these were dispatched from AHK's headquarters in Prescot, United Kingdom, to GTK's headquarters in Espoo, Finland. The samples were then promptly sent back to AHK's headquarters and were evaluated under laboratory conditions. During this test, samples were exposed to transportation by road and by air and associated transhipment phases. The TPs which were tested as part of these tests are given in Table 11.

Figure 14. Example of prepared samples in a self-seal polypropylene bag (left) and a heat-sealed aluminium packet (right).

Table 11. Outline of host material and tracer particle combinations which were tested as part of the transportation test.

HM / TP	Spodumene concentrate	Mixed hydroxide precipitate	Nickel concentrate (origin A)	Nickel concentrate (origin B)	Black mass
TPA01	✓	✓	-	-	✓
TPA02	✓	✓	-	-	✓
TPA03	✓	✓	-	-	✓
TPA04	✓	✓	-	-	✓
TPB01	✓	✓	-	-	✓
TPG01	-	-	✓	✓	-
TPH01	-	-	✓	✓	-
TPM01	-	-	✓	-	-
TPM02	-	-	✓	-	-
TPM03	✓	-	-	-	-
TPM04	✓	-	-	-	-

Note: TP = tracer particle; samples were dispatched in both polypropylene self-seal bags and sealed aluminium packets.

6 Results

6.1 Preliminary Tests

Preliminary test work identified two application methods: dry mixing using a riffle splitter and wet mixing using water and spraying TPs on a commodity using an atomiser. All TPs were observed to block the aperture of several different commonly available spray atomisers and therefore this technique was discontinued. Dry mixing using a riffle splitter produced evenly distributed mixtures of TPs and commodities. Using a riffle splitter had a potential negative effect whereby TPs were observed to adhere to the edges of collection trays. This was overcome by changing the rectangular trays to an oval bowl, thereby eliminating the edge effect of the trays.

The only commodity that could not be dry mixed was black mass. This was due to its hazardous properties and for health and safety reasons was discontinued. Instead, TPs for black mass applications were initially mixed with water and immediately poured evenly over the sample. The mixture was then thoroughly blended within a sealed plastic bag. Larger agglomerates formed from the addition of water were crushed within the bag and continuously mixed. These agglomerates were not weakly-bound such as those that typically appear in ores or mineral concentrates in the presence of moisture, and they required crushing by hand with the aid of metal tools (they had a "weak" unconfined compressive strength of 5 MPa to 12.5 MPa). It is possible that the different application method required for black mass had an influence on the performance of the TPs tested on this host material, by causing TPs to agglomerate within the hard agglomerates, preventing their dispersion.

Preliminary tests also revealed differences between the TPs detectability and how they were held within the host materials. The handheld supplier-provided and handheld and in-situ supplier-recommended detectors successfully detected TPs within all host materials. However, it was observed that TP size not only affected how clearly it could be observed through a microscope, but also how it was adsorbed onto the surfaces of the host materials. For example, TPA01, TPA02 and TPA03 appeared to adhere to spodumene concentrate particles, whilst TPA04 was held in the voids between the particles. TPB01 were also held between the particles, and this effect was important as it revealed that TPs may migrate through the pore spaces (Figure 15b), which may influence their detectability. MHP contained large agglomerates (up to 15 mm; Table II-58) and TPs could be observed adsorbed to their surfaces (Figure 15a). In some cases, the TP had partially settled just beneath the surface of the agglomerates, with agglomerates almost absorbing the TP.

The brownish yellow colour (10YR 6/6) of nickel concentrate was also a factor that affected detectability during the testing. The colouration of this concentrate made it difficult to observe TPA01, TPA02 and TPA03, but TPA04 was easily seen using the microscope because its red colour contrasted well against the brownish yellow colour of nickel concentrate (Figure 15d). TPB01 was easily seen within host materials due to its polychromatic design. These preliminary observations were important in helping to understand how TPs would behave during different conditions.

Funded by the European Union

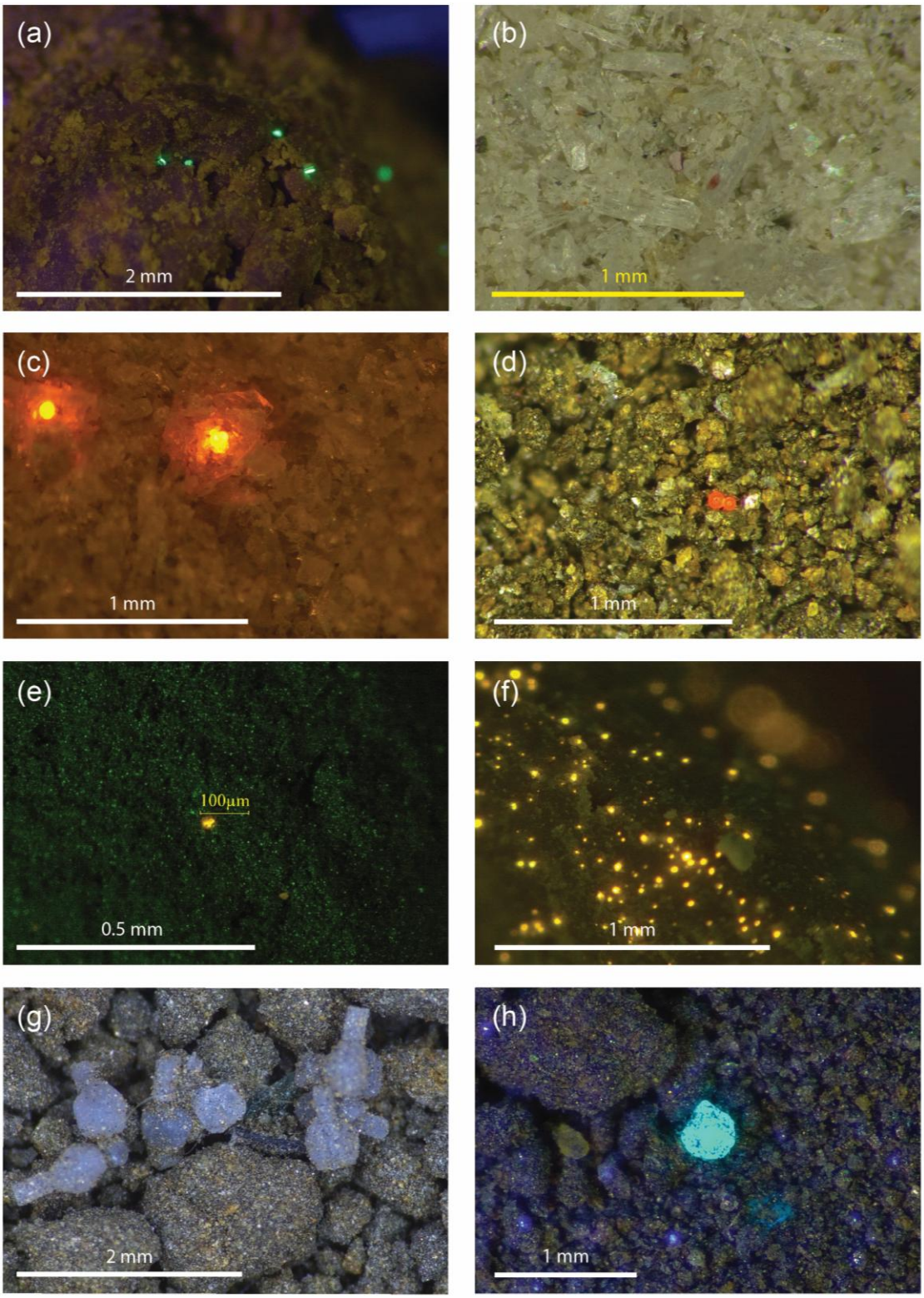

Figure 15. Selection of images of tracer particles within different host materials prior to any principal tests. (a) TPB01 within mixed hydroxide precipitate under excitation light. (b) TPB01 within spodumene concentrate under natural light. (c) TPA04 within spodumene concentrate under excitation light. (d) TPA04 within nickel concentrate (origin A) under natural light. (e) TPA02 within black mass under excitation light. (f) TPA01 within mixed hydroxide precipitate under excitation light. (g) TPG01 within nickel concentrate (origin A) under natural light. (h) TPH01 under excitation light within nickel concentrate (origin A).

Funded by
the European Union

6.2 Dilution

Due to the confidential nature of the Molecular™ Taggant System's performance results provided by Microtrace, a high-level summary of the evaluation is presented below.

The appearance of host materials was not altered following TP application (Figure 16). Microtrace reported successful authentication of its Molecular™ Taggant System across the evaluated host materials under laboratory proof-of-concept conditions. The evaluation demonstrated that host-material-specific analytical thresholds could be developed to support detection of dilution or adulteration. Performance was influenced by host material properties and sample preparation. Detailed methodology, calibration data, and quantitative thresholds remain confidential.

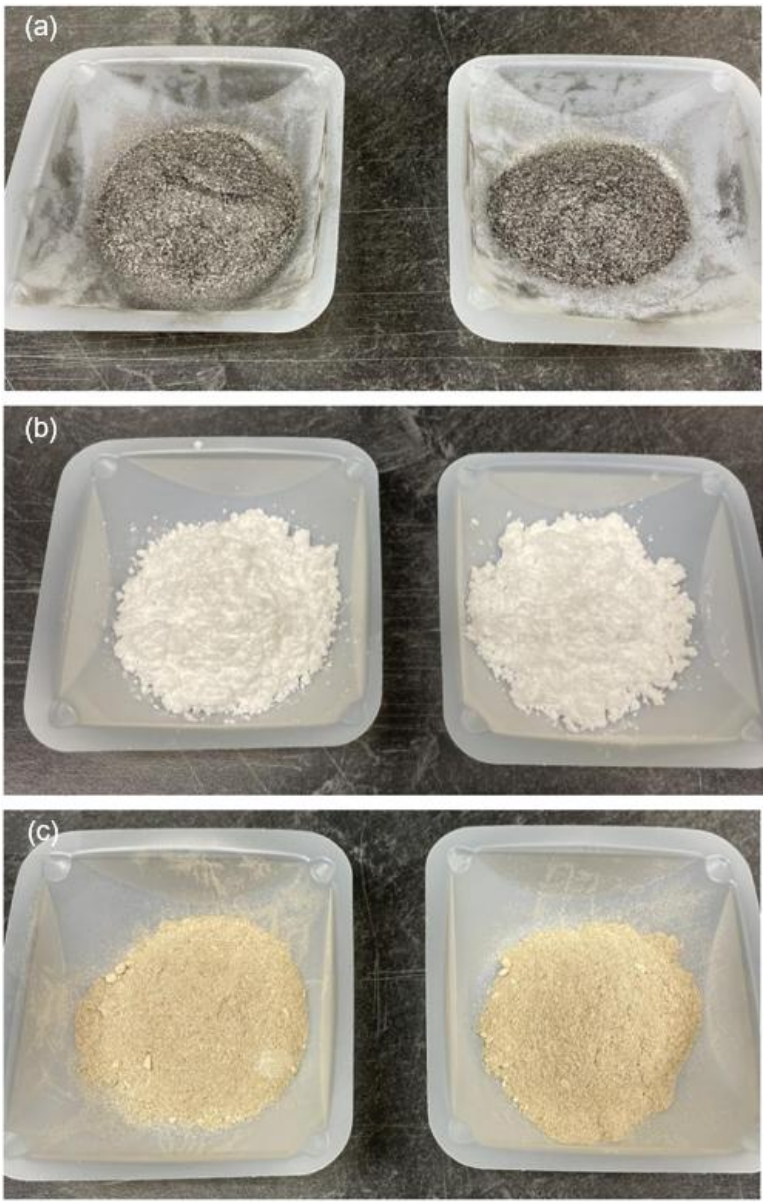

Figure 16. Photographs of a selection of host materials dispatched to Microtrace for testing with Microtrace's Molecular™ Taggant System. (a) Graphite concentrate, (b) lithium carbonate, and (c) lithium ore. The host material on the left of each image is untagged, while the host material on the right is tagged.

These results represent initial proof-of-concept indications using a standard, non-optimised formulation; in commercial deployment, the Molecular™ Taggant System is engineered and optimised for each specific material, detection objective, and budgetary requirement, and material-specific development would be expected to substantially improve detection sensitivity.

6.3 Minimum Effective Dosage

The results of the minimum effective dosage test are summarised in Table 12. The MED varied depending on the TP size and the smallest TPs were detectable to the lowest tested dosage of 0.1 ppm (0.00001%).

Table 12. Summarised results from the minimum dosage test.

TP	TP size (µm)	TP MED (ppm)	TP MED (%)
TPA01	10–11	0.1	0.00001%
TPA02	15	0.1	0.00001%
TPA03	20	0.1	0.00001%
TPA04	55–60	0.1	0.00001%
TPB01	~37–75	1.5	0.00015%
TPG01	500	5	0.0005%
TPH01	460	3	0.0003%
TPM01	1430	250	0.025%
TPM02	1410	100	0.01%
TPM03	1430	200	0.02%
TPM04	1410	100	0.01%

Note: TP = tracer particle. The TP size corresponds to the maximum length of each TP along its major axis.

6.4 Abundance and Distribution

Summarised results of the TP abundance and distribution test are presented in Table 13 and Table 14.

Apart from TPH01 and TPG01, no TPs were observed within any of the host materials by naked eye. All TPs were identified using supplier-provided or supplier-recommended handheld detectors. Using the digital microscope and under natural light, all TPs returned at least one TP from each of the five zones of the petri dish from triplicate samples containing host materials of mixed hydroxide precipitate, nickel concentrate and spodumene concentrate. Black mass was the only host material in which certain TPs (TPA01, TPA02 and TPA03) were not observed under natural light. TPA04 in MHP was the most detectable TP and the only TP detectable in black mass under natural light.

Under excitation light, all TPs returned at least one TP from each of the five zones of the petri dish from triplicate samples from all of the host materials (Table 14). The recorded taggant counts indicate that all TPs were significantly more detectable under excitation light compared to natural light. Despite the increased detection under excitation light, the host material type continued to have a significant influence on the observed TP abundance and distribution (Figure 17 and Figure 18). TPs were significantly less detectable in black mass

compared to other host materials, with a 21–43-fold difference between counts of TPs in black mass compared to counts in other host materials.

Table 13. Summarised results from counting tracer particles under natural light.

Host Material	TP	Average number of TPs per area					*min*	*max*	*R*	μ	*SD*
		1	2	3	4	5					
Black Mass	TPA01	0.00	0.00	0.00	0.00	0.00	0.00	0.00	0.00	0.00	0.00
	TPA02	0.00	0.00	0.00	0.00	0.00	0.00	0.00	0.00	0.00	0.00
	TPA03	0.00	0.00	0.00	0.00	0.00	0.00	0.00	0.00	0.00	0.00
	TPA04	2.67	1.67	2.67	3.00	2.33	1.67	3.00	1.33	2.47	0.51
	TPB01	0.67	0.00	0.00	0.67	0.67	0.00	0.67	0.67	0.40	0.37
Mixed Hydroxide Precipitate	TPA01	2.00	2.00	1.00	1.67	2.00	1.00	2.00	1.00	1.73	0.43
	TPA02	2.00	1.33	2.00	1.67	1.67	1.33	2.00	0.67	1.73	0.28
	TPA03	2.00	1.33	0.67	2.67	2.00	0.67	2.67	2.00	1.73	0.76
	TPA04	40.00	40.00	34.33	40.00	40.00	34.33	40.00	5.67	38.87	2.53
	TPB01	16.00	15.67	10.00	22.33	22.00	10.00	22.33	12.33	17.20	5.12
Nickel Concentrate (origin A)	TPA03	5.33	5.67	3.67	5.33	5.00	3.67	5.67	2.00	5.00	0.78
	TPA04	3.00	4.67	2.67	4.00	5.00	2.67	5.00	2.33	3.87	1.02
	TPB01	2.00	3.00	1.00	2.33	2.33	1.00	3.00	2.00	2.13	0.73
	TPG01	2.00	1.67	0.33	4.33	0.67	0.33	4.33	4.00	1.80	1.57
	TPH01	2.67	2.33	0.67	1.00	1.67	0.67	2.67	2.00	1.67	0.85
Spodumene Concentrate	TPA01	4.00	3.67	3.67	6.33	3.00	3.00	6.33	3.33	4.13	1.28
	TPA02	5.00	2.67	3.33	5.33	2.67	2.67	5.33	2.67	3.80	1.28
	TPA03	2.67	1.67	1.67	4.00	3.00	1.67	4.00	2.33	2.60	0.98
	TPA04	12.67	9.33	7.00	10.33	13.00	7.00	13.00	6.00	10.47	2.48
	TPB01	1.00	1.33	1.67	1.00	1.67	1.00	1.67	0.67	1.33	0.33

Note: TP = tracer particle. Each TP and host material combination was evaluated in triplicate; counting was stopped at 40, which represents the maximum possible value.

Funded by the European Union

Table 14. Summarised results from counting tracer particles under excitation light.

Host Material	TP	Average number of TPs per area					*min*	*max*	*R*	μ	*SD*
		1	2	3	4	5					
Black Mass	TPA01	5.00	3.00	3.67	4.67	4.67	3.00	5.00	2.00	4.20	0.84
	TPA02	4.33	2.33	1.33	3.67	4.67	1.33	4.67	3.33	3.27	1.40
	TPA03	1.33	1.00	0.67	1.00	0.67	0.67	1.33	0.67	0.93	0.28
	TPA04	4.67	2.67	3.33	2.67	5.00	2.67	5.00	2.33	3.67	1.11
	TPB01	1.67	1.33	0.33	0.67	1.00	0.33	1.67	1.33	1.00	0.53
Mixed Hydroxide Precipitate	TPA01	40.00	40.00	40.00	40.00	40.00	40.00	40.00	0.00	40.00	0.00
	TPA02	40.00	40.00	40.00	40.00	40.00	40.00	40.00	0.00	40.00	0.00
	TPA03	40.00	40.00	40.00	40.00	40.00	40.00	40.00	0.00	40.00	0.00
	TPA04	40.00	40.00	40.00	40.00	40.00	40.00	40.00	0.00	40.00	0.00
	TPB01	31.00	23.33	19.67	6.33	24.00	6.33	31.00	24.67	20.87	9.10
Nickel Concentrate (origin A)	TPA03	40.00	40.00	38.00	40.00	39.00	38.00	40.00	2.00	39.40	0.89
	TPA04	6.67	7.33	7.67	12.00	12.67	6.67	12.67	6.00	9.27	2.83
	TPB01	9.67	7.00	6.00	9.67	9.33	6.00	9.67	3.67	8.33	1.72
	TPG01	3.00	2.33	1.00	5.67	1.67	1.00	5.67	4.67	2.73	1.80
	TPH01	3.67	2.67	1.67	2.33	3.33	1.67	3.67	2.00	2.73	0.80
Spodumene Concentrate	TPA01	40.00	40.00	40.00	40.00	40.00	40.00	40.00	0.00	40.00	0.00
	TPA02	40.00	40.00	40.00	40.00	40.00	40.00	40.00	0.00	40.00	0.00
	TPA03	40.00	40.00	40.00	40.00	40.00	40.00	40.00	0.00	40.00	0.00
	TPA04	35.00	38.67	26.67	37.00	38.00	26.67	38.67	12.00	35.07	4.90
	TPB01	6.00	4.00	3.67	3.00	2.33	2.33	6.00	3.67	3.80	1.39

Note: TP = tracer particle. Each TP and host material combination was evaluated in triplicate; counting was stopped at 40, which represents the maximum possible value.

Funded by the European Union

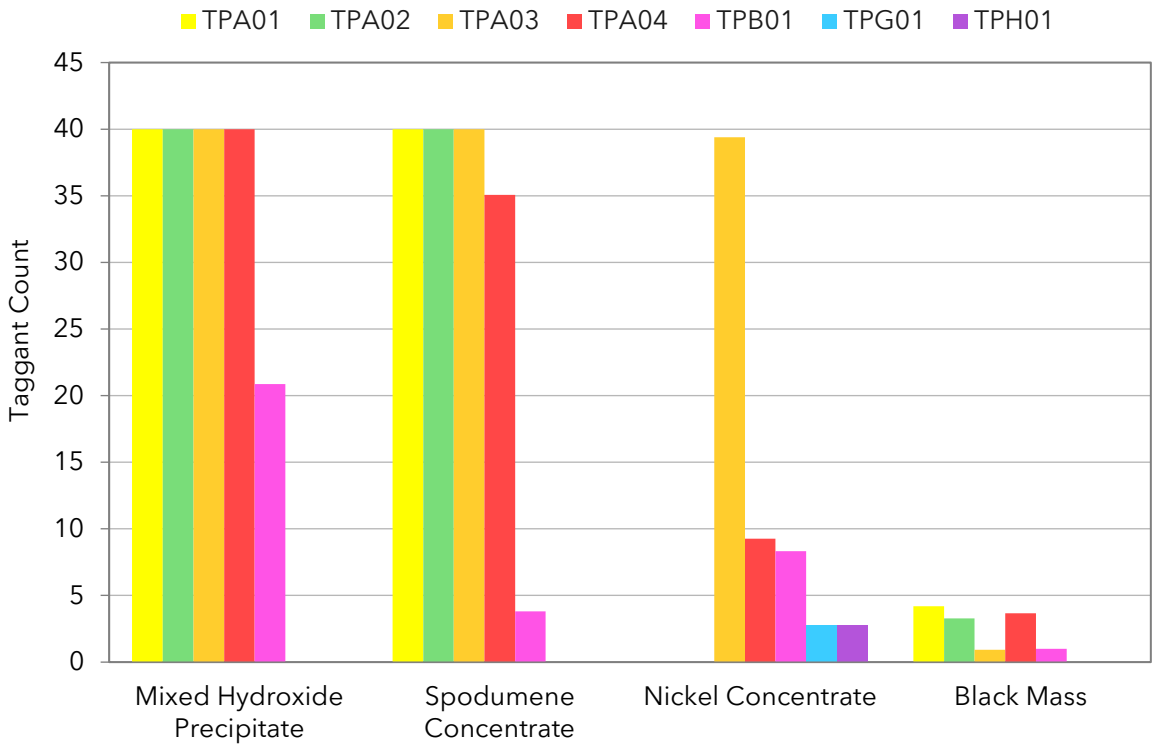

Figure 17. Average tracer particle counts under excitation light grouped by host material.

Note: TPA01 and TPA02 were not evaluated in nickel concentrate; TPG01 and TPH01 were only evaluated in nickel concentrate.

Funded by the European Union

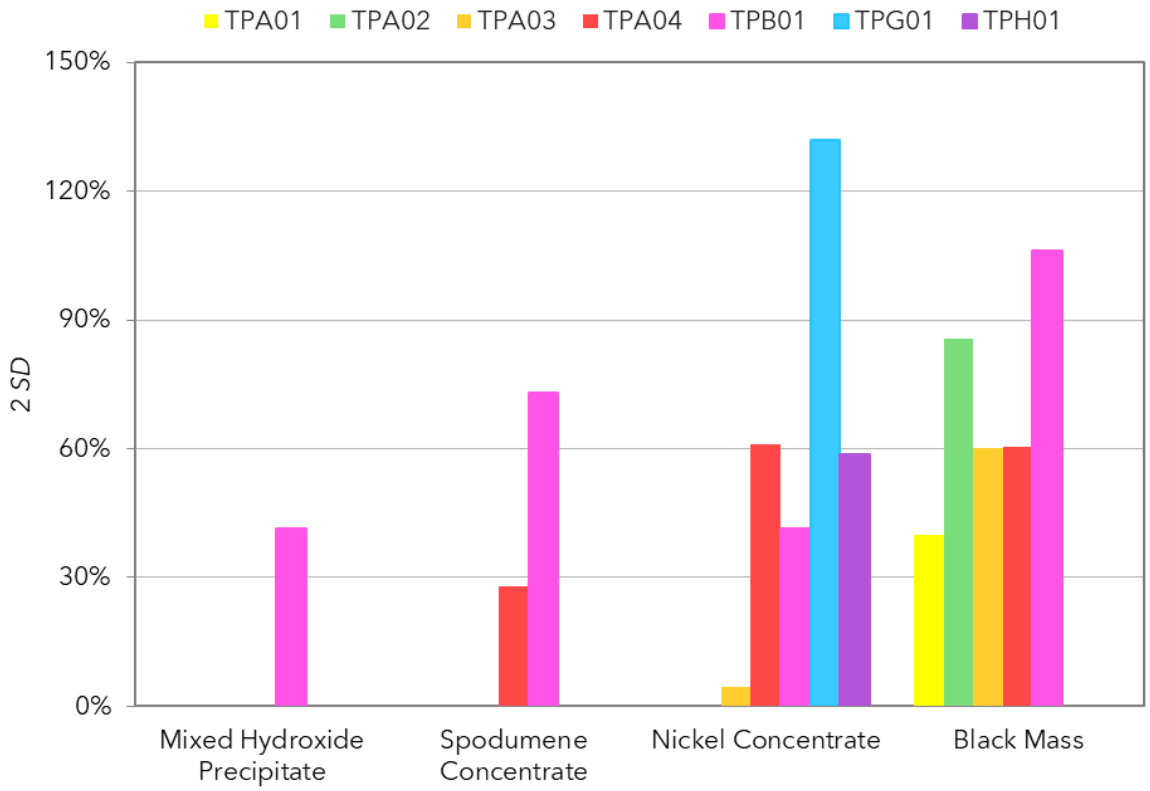

Figure 18. Two standard deviations as a percentage of the average tracer particle count from triplicate samples, grouped by host material.

Note: 2 SD = two standard deviations. TPA01–04 returned 2 *SD* (%) of zero within mixed hydroxide precipitate. TPA01 and TPA02 returned 2 *SD* (%) of zero within spodumene concentrate. TPA01 and TPA02 were not evaluated in nickel concentrate; TPG01 and TPH01 were only evaluated in nickel concentrate.

6.5 Scanning Electron Microscopy

Evaluation of TraceTag's and Microtrace's TPs by manual SEM revealed host material particles can adhere onto TP surfaces (Figure III-1). However, these interactions were superficial, and particle adhesion was localised over parts of each TP only. TPs were readily identifiable under the scanning electron microscope. No other chemical or physical interactions between the TPs and the host materials were observed.

6.6 Modified Flow Table Test

TPs obtained from TraceTag and Microtrace revealed even distribution within the commodities following 10 minutes of shock on the flow table (Figure 19). TP distribution remained homogenous and there was no evidence of redistribution or clustering/pooling at the base or top of any of the host materials within the PMMA cubes following the procedure. Although segregation of agglomerates due to the test procedure occurred (Figure 19e and h), TPs remained homogeneously distributed. A homogenous distribution was also observed within the five spears of material that were extracted from within the cube (Figure 19c, f and i). The TPs' ability to remain detectable using excitation light was also unchanged by the simulated shock (Figure 19b, e and h).

Funded by the European Union

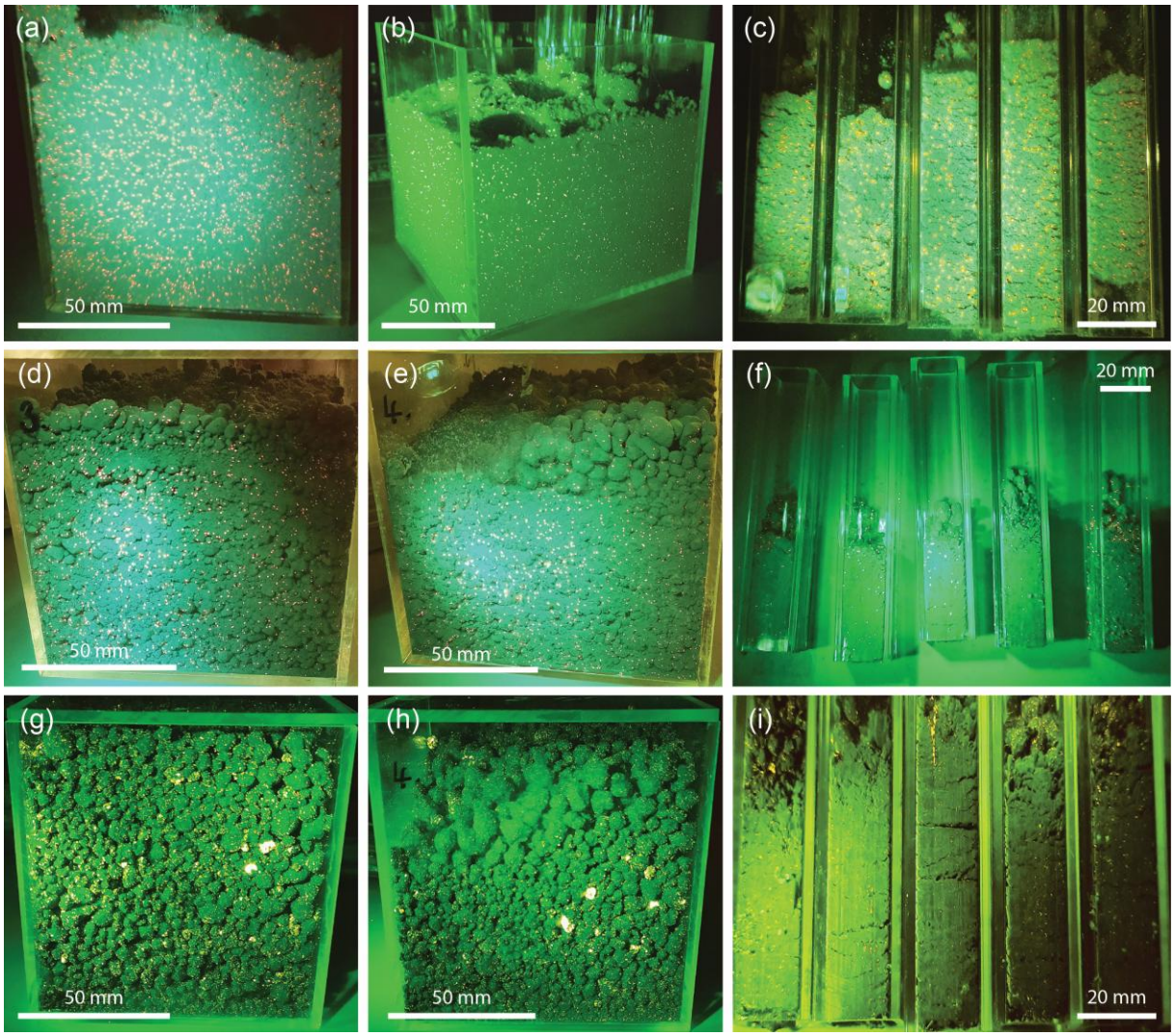

Figure 19. Tracer particle distribution in various host materials before and after the modified flow table test. (a) TPA04 in spodumene concentrate before the test, (b) TPA04 distribution in spodumene concentrate post-test, (c) TPA04 distribution in spodumene concentrate within PMMA tubes post-test; (d) TPA04 in mixed hydroxide precipitate before the test, (e) TPA04 distribution in mixed hydroxide precipitate post-test, (f) TPA04 distribution in mixed hydroxide precipitate within PMMA tubes post-test; (g) TPA03 in mixed hydroxide precipitate before the test, (h) TPA03 in mixed hydroxide precipitate post-test, and (i) TPA03 TP distribution in mixed hydroxide precipitate within PMMA tubes post-test. Note the compaction of mixed hydroxide precipitate within the tubes in (f) and (i). All images were taken using excitation light.

TPG01 were evenly distributed throughout the nickel concentrate. TPG01 were detectable with the naked eye (Figure 20). The TP's morphology and their ability to be detected by UV excitation light was not negatively impacted by the test.

Funded by
the European Union

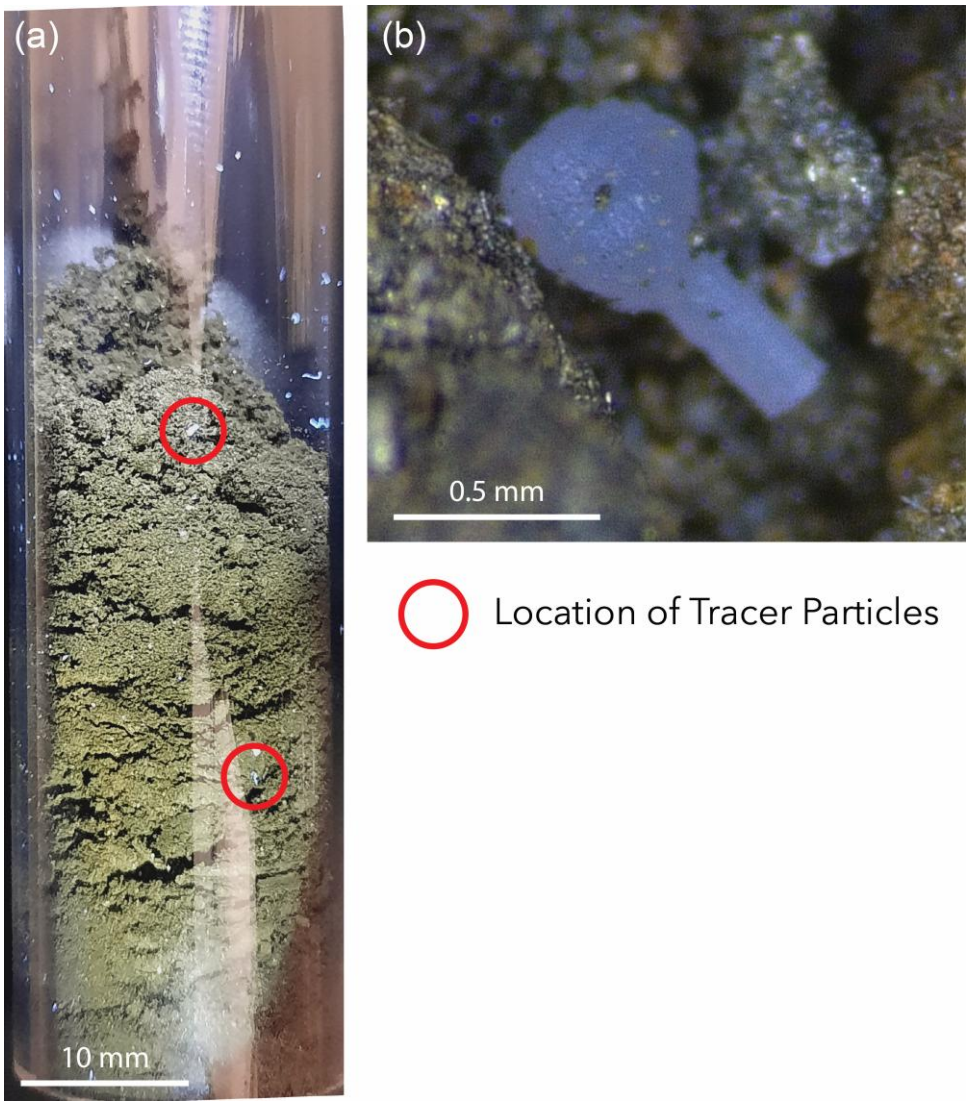

Figure 20. TPG01 within nickel concentrate (origin A) after the modified flow table test. (a) Within a glass tube extracted from material from the poly(methyl methacrylate) cube post-test. (b) TPG01 under natural light post-test.

TPM03 and TPM04 TPs underwent gravitational segregation and migrated downwards through spodumene concentrate during the test (Figure 21). A magnet was used to successfully locate and recover the TPs following the test, and it was observed that approximately half of the cube's volume of material had to be removed before the TPs were all recovered (Figure 21c). TPM01 and TPM02 also migrated downwards through the commodity during the test (Figure 22), but not to the same extent as the stainless-steel TPs (Figure 21).

Funded by
the European Union

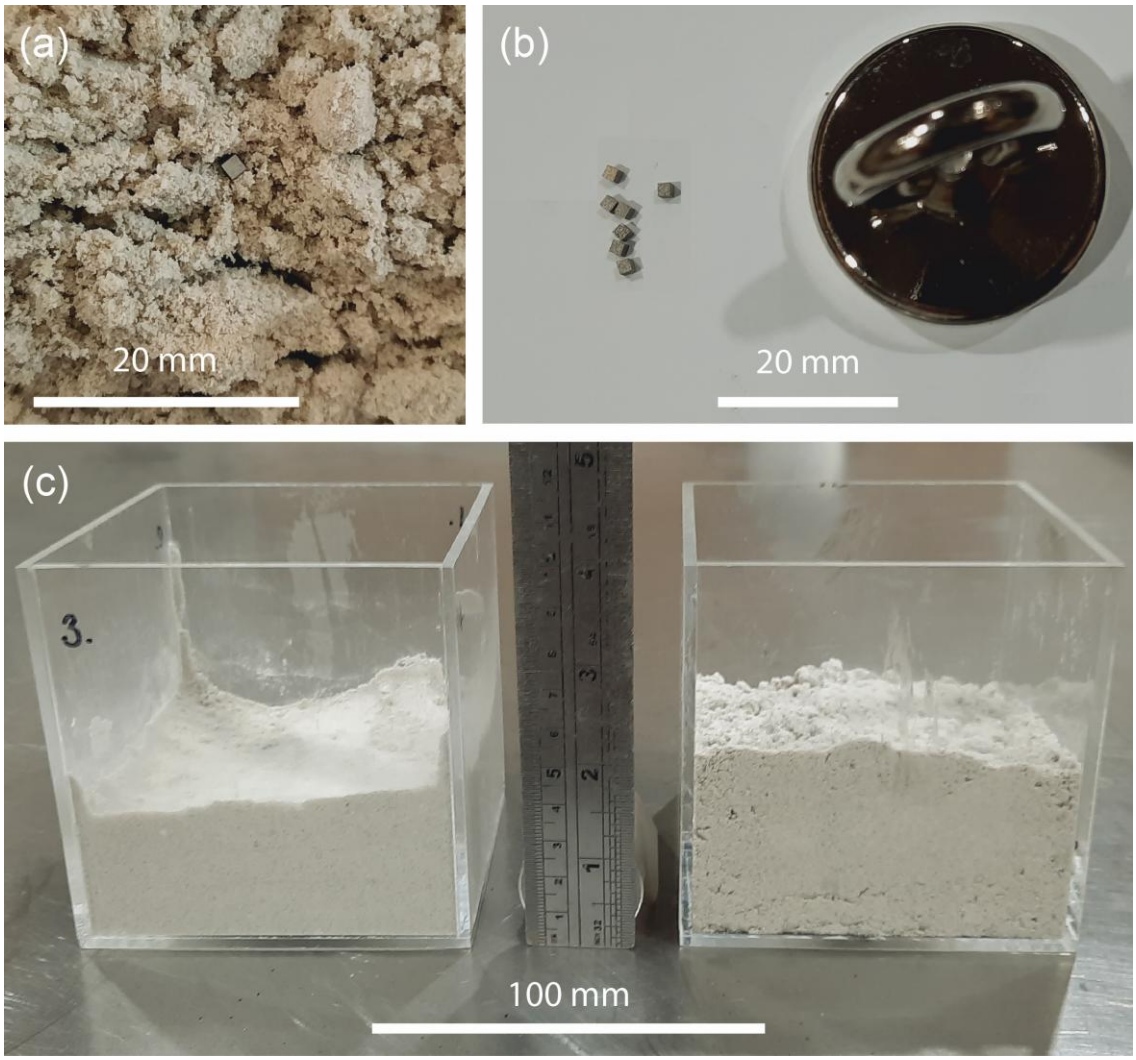

Figure 21. Modified flow table test with spodumene concentrate. (a) A single TPM03 tracer particle (TP) on the surface of the concentrate at the start of investigation, (b) TPM03 TPs and magnet, (c) left: volume of spodumene concentrate remaining once all TPM03 TPs had been recovered using the magnet, right: volume of spodumene concentrate removed to retrieve all TPM03 TPs, revealing the extent of their downward migration through the material during the test.

Funded by
the European Union

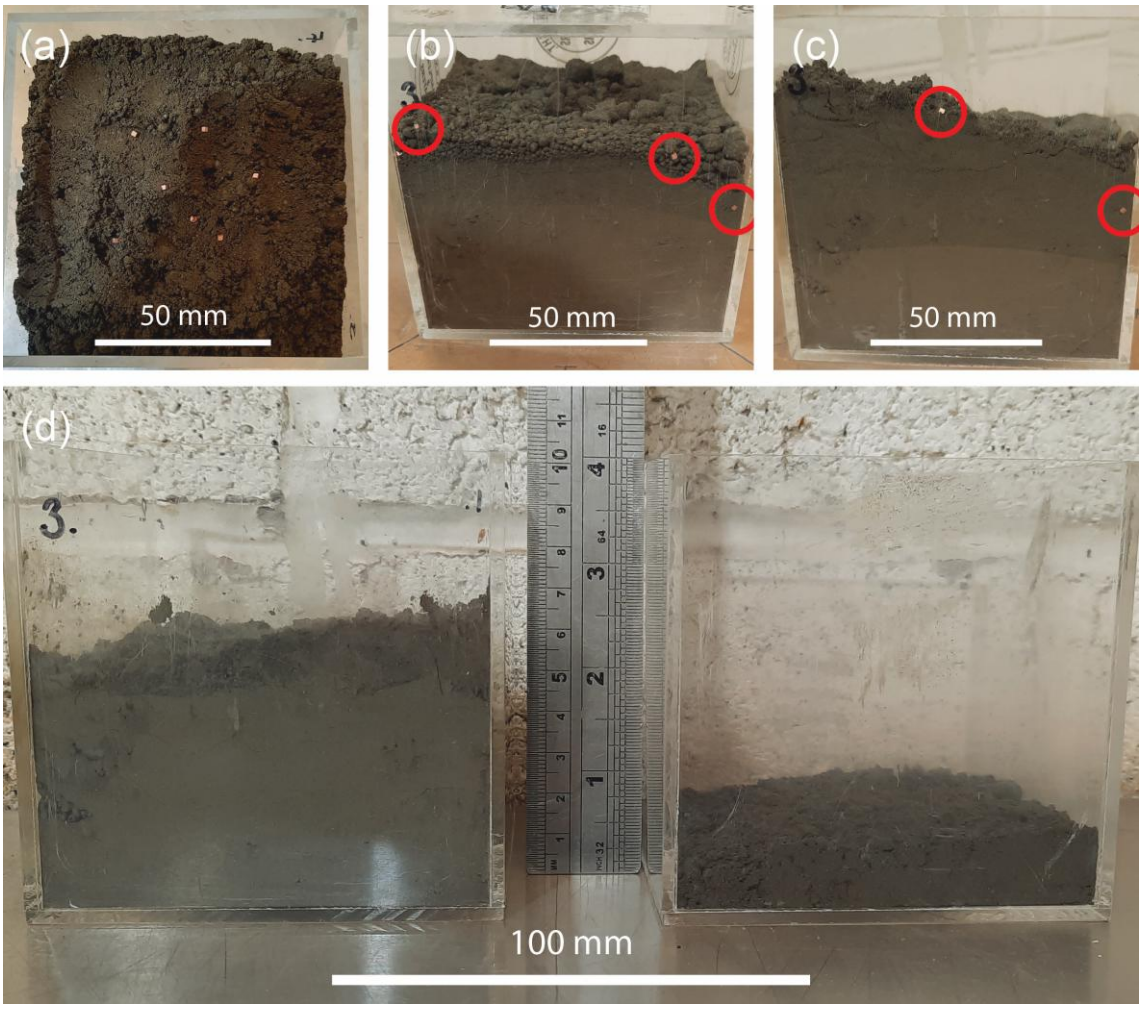

Figure 22. Modified flow table test with nickel concentrate (origin A). (a) TPM01 tracer particles (TPs) placed on the surface of the nickel concentrate at start of test, (b) position of TPM01 TPs after 10 minutes of shock, (c) position of two of the TPM01 TPs after 20 minutes, revealing the outward and downward movement of TPs, (d) left: volume of nickel concentrate at which all TPM01 TPs had been recovered; right: volume of nickel concentrate removed to retrieve all TPM01 TPs, revealing their downward migration through the material.

6.7 Natural Ageing

This natural ageing test focused on the commercial TPs from TraceTag and Microtrace. This test took place over 60 days (1,440 hours) in an outside environment. Some of the host materials provided indications of alteration or oxidation having taken place, including notable increases in the abundances of oxides and sulphates likely as a result of oxidation (e.g., in spodumene concentrate (Figure II-7 and Table II-22) and nickel concentrate (Figure II-13, Table II-41 and Table II-42)), increases in the abundance of undifferentiated phases possibly associated with secondary processes (e.g., MHP, see Figure II-22 and Table II-63), and the loss of the water-soluble minerals nickelhexahydrite and szomolnokite within nickel concentrate, due to leaching by rainwater (Figure II-13, Table II-41 and Table II-42) (Buckby et al., 2003; Karup-Møller, 1973). There were no observable differences in TP morphology or characteristics. The TPs remained homogenously dispersed throughout the host materials, and rainfall did not appear to affect their presence or distribution. All TPs remained evenly dispersed and were observed clearly using excitation light (Figure 23 and Figure 24).

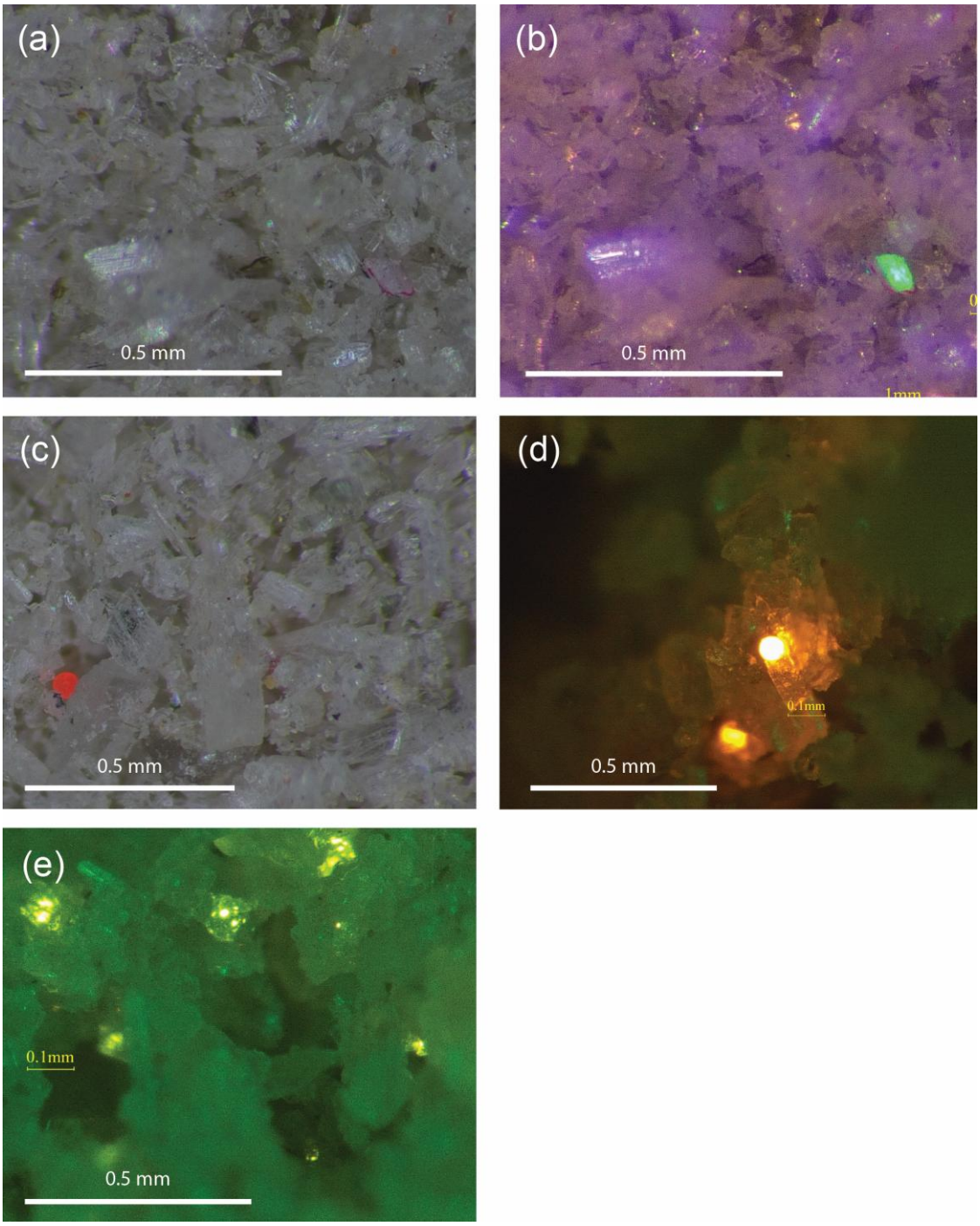

Figure 23. A selection of tracer particles observed in spodumene concentrate using a digital microscope following the natural ageing test. (a) TPB01 under natural light, (b) TPB01 under ultraviolet excitation light, (c) TPA04 under natural light, (d) TPA04 under excitation light, and (e) TPA03 under excitation light. TPA03 was not visible under natural light in the spodumene concentrate.

Funded by the European Union

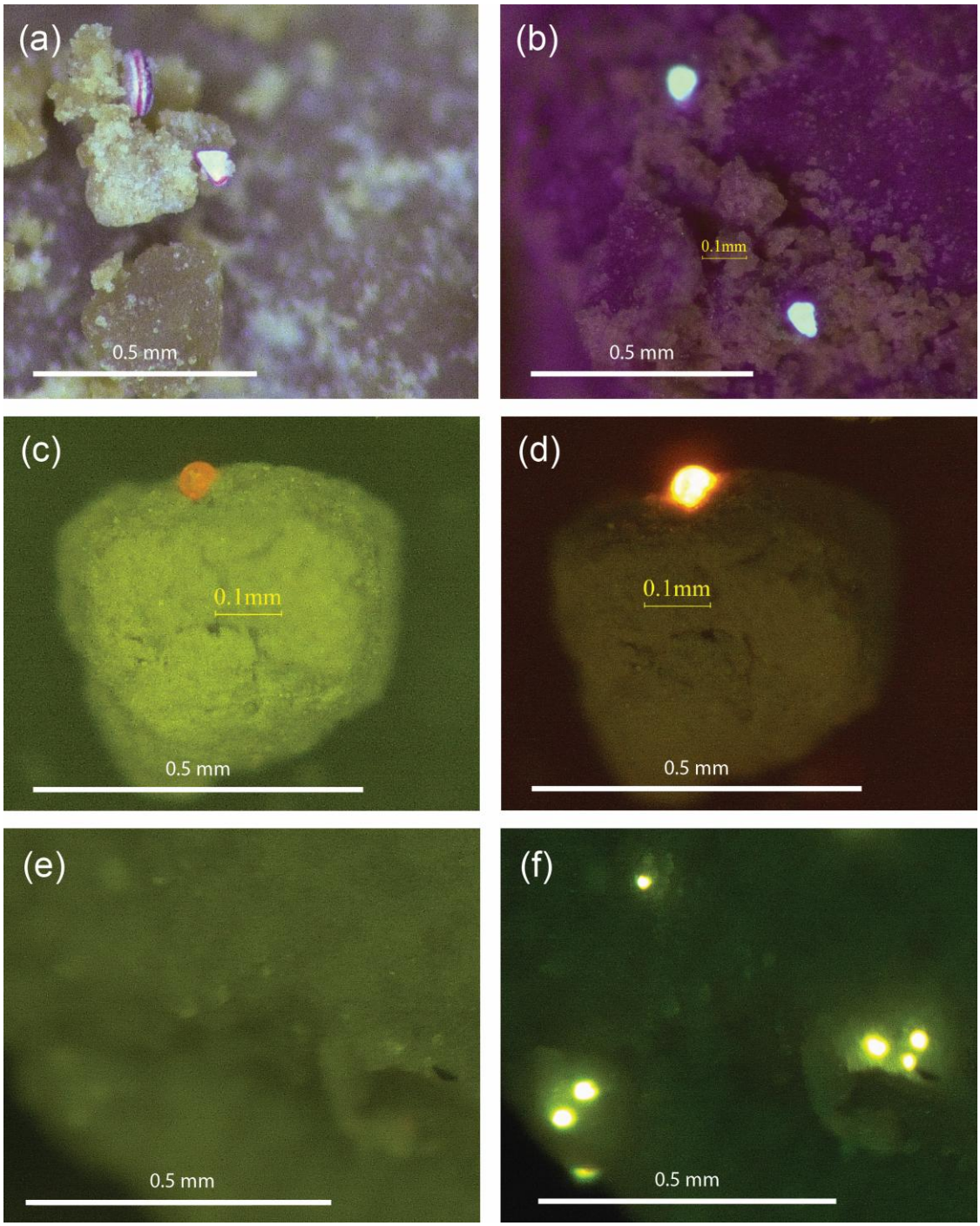

Figure 24. A selection of tracer particles observed in mixed hydroxide precipitate using a digital microscope following the natural ageing test. (a) TPB01 under natural light, (b) TPB01 under ultraviolet excitation light, (c) TPA04 under natural light, (d) TPA04 under excitation light, (e) TPA03 under natural light, and (f) TPA03 under excitation light.

6.8 Photooxidative Ageing

The photooxidative ageing investigation focused on the TPs provided by TraceTag and Microtrace. The test took place over 35 days (840 hours) and provided evidence of host material alteration or oxidation, which included observable mineral depositions and secondary recrystallisation within nickel concentrate (these were not quantified analytically). There were no observable differences in TP morphology or characteristics. TPs remained

evenly dispersed throughout the commodities and their presence was not affected by exposure to sunlight. All TPs could be viewed clearly using excitation light (Figure 25).

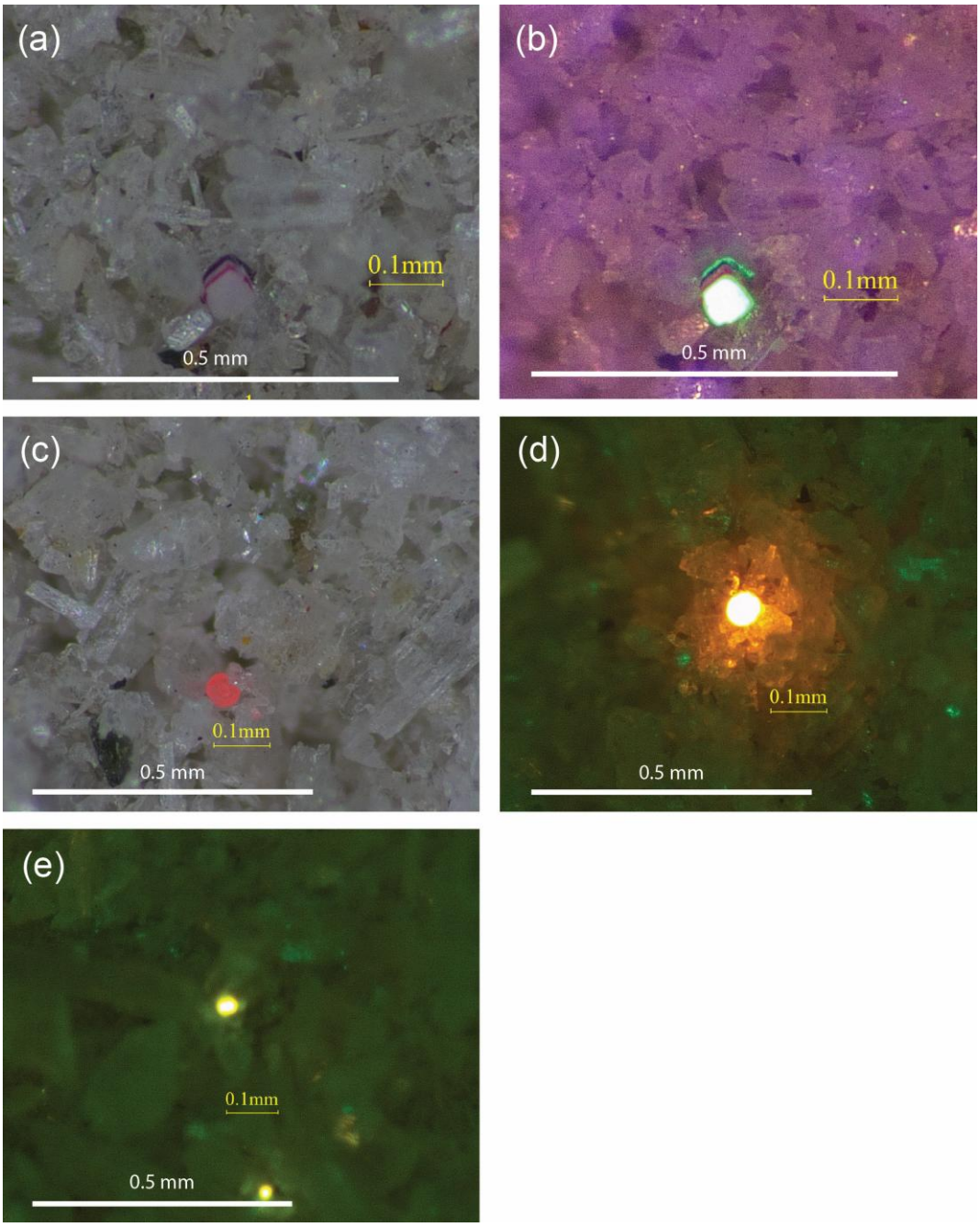

Figure 25. A selection of tracer particles observed in spodumene concentrate using the digital microscope following the photooxidative test. (a) TPB01 under natural light, (b) TPB01 under ultraviolet excitation light, (c) TPA04 under natural light, (d) TPA04 under excitation light, and (e) TPA03 under excitation light. TPA03 was not visible under natural light in spodumene concentrate.

6.9 Artificial Climate Ageing

The commercial TPs from TraceTag and Microtrace remained stable over the duration of the medium-term test (three 7-day test periods at temperatures ranging from 55°C (week one) to 75°C (week three)) (Figure 26, Figure III-3 and Figure III-4). There were no observable differences in their performance, morphology or distribution even at the highest

temperature of 75°C (Figure 26e and f). Their appearance as part of long-term ageing tests (ageing over five weeks; three weeks at 40°C and 80% RH, followed by two weeks at –5°C) also revealed no change in characteristics or morphology (Figure III-3 and Figure III-4).

The distribution and morphology of TPG01 TPs in two different nickel concentrates (origin A is shown in Figure III-6 and Figure III-7; origin B is shown in Figure 27 and Figure III-5) were observed to be stable over consecutive 48 h periods between 45°C and 75°C at low humidity (<20% RH) and at high humidity (85% RH). There was evidence of tracer particle agglomeration (Figure 27d, e and f), but the agglomerated TPs were either an artefact of the production process or observed behaviour of TPs pre-test (e.g., Figure 19g), and not because of temperature or humidity effects.

TPM01 were observed to change colour, from metallic reddish-brown to a black tarnish on their surfaces (Figure 28b and c) when in the presence of air and moisture. TPM01 attracted fine particles and contained surface agglomerates (Figure 28d), which made it difficult to locate them once they had been in the material for over five days. These TPs were only detectable after sieving and washing to remove the adhered particulates. TPM03 also revealed discolouration, presenting a black pitted surface and degradation to their surfaces following one month in contact with nickel concentrate (Figure 29). Horizon Microtechnologies' TPs (TPH) were observed to be stable over four days at 75°C and 85% RH in nickel concentrate (Figure 30). There was no observable effect to their morphology or their ability to fluoresce in the presence of UV excitation light.

Funded by the European Union

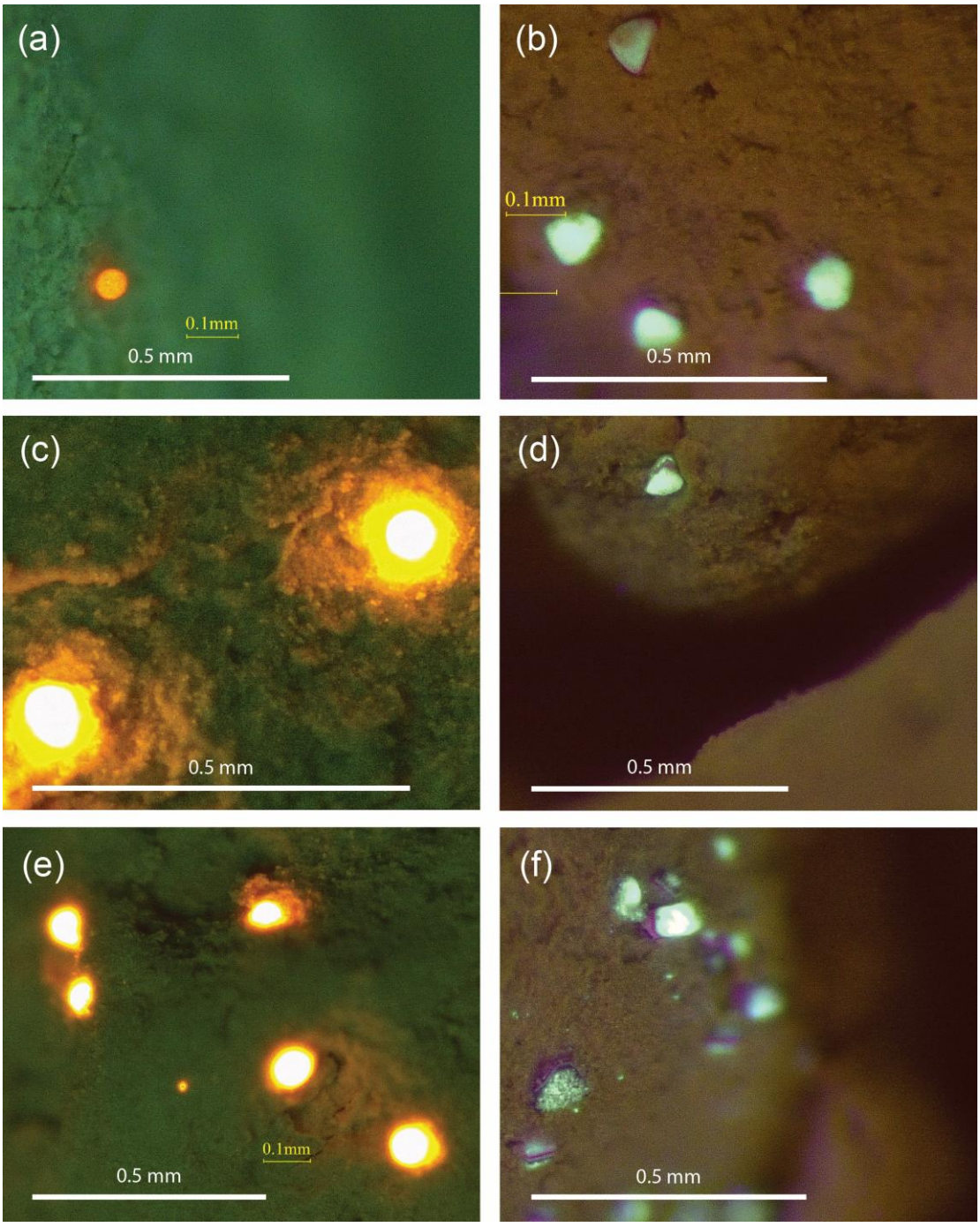

Figure 26. TPA04 and TPB01 tracer particles in mixed hydroxide precipitate using the digital microscope following the medium-term artificial climate ageing test. Images of tracer particles in mixed hydroxide precipitate following artificial climate ageing at 55°C for seven days with excitation light: (a) TPA04, (b) TPB01; subsequently at 65°C for seven days with excitation light: (c) TPA04, (d) TPB01; subsequently at 75°C for seven days with excitation light: (e) TPA04, (f) TPB01. The test was carried out at 10% RH.

Funded by the European Union

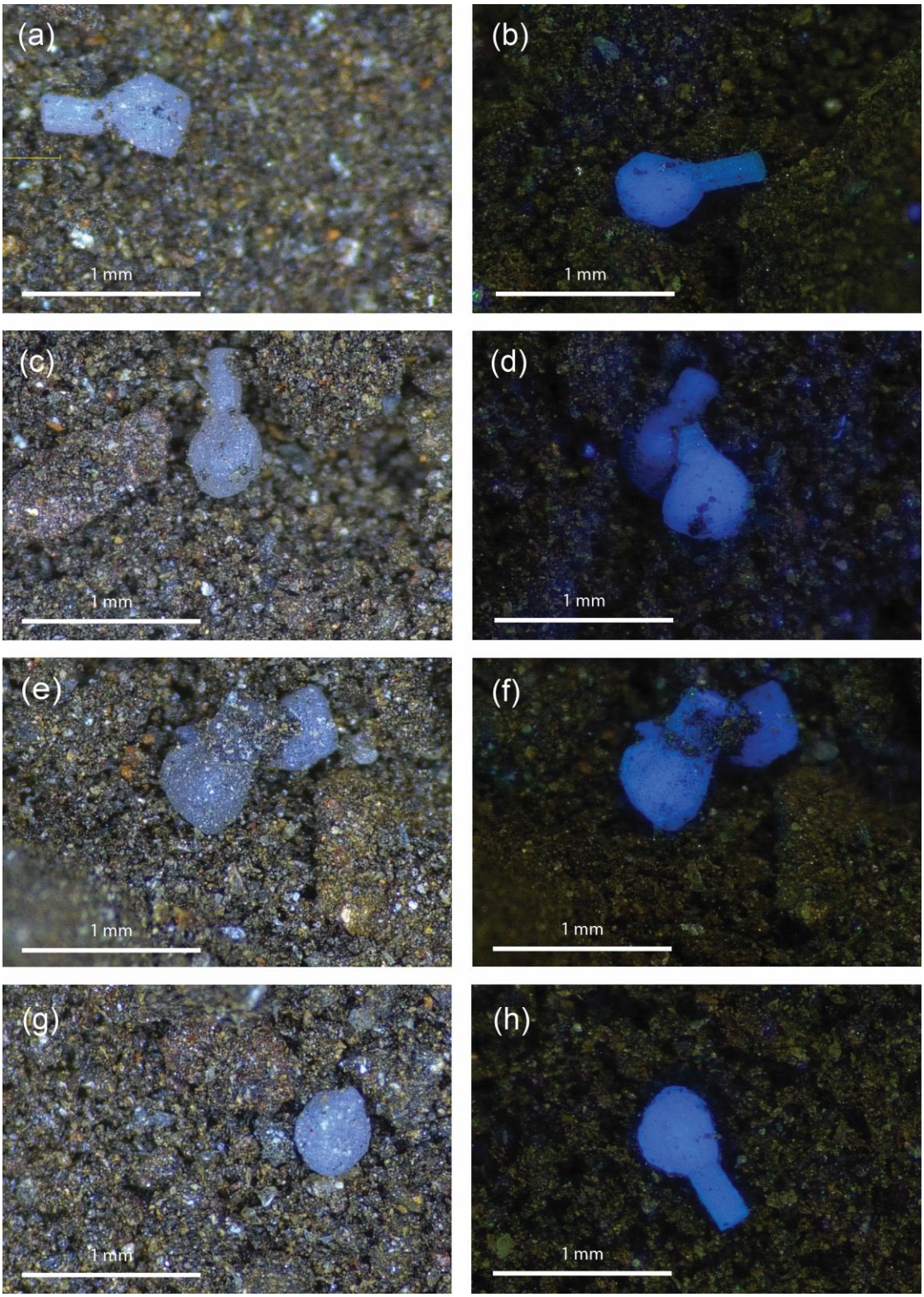

Figure 27. TPG01 tracer particles in nickel concentrate (origin B) following the short-term high humidity artificial climate ageing tests. Following ageing at 45°C over a 48-h period under (a) natural light and (b) ultraviolet (UV) excitation light; subsequently at 55°C over a 48-h period under (c) natural light and (d) UV excitation light; at 65°C over a 48-h period under (e) natural light and (f) UV excitation light; subsequently at 75°C over a 48-h period under (g) natural light and (h) UV excitation light. Tests were conducted at a humidity of 85% RH.

Funded by the European Union

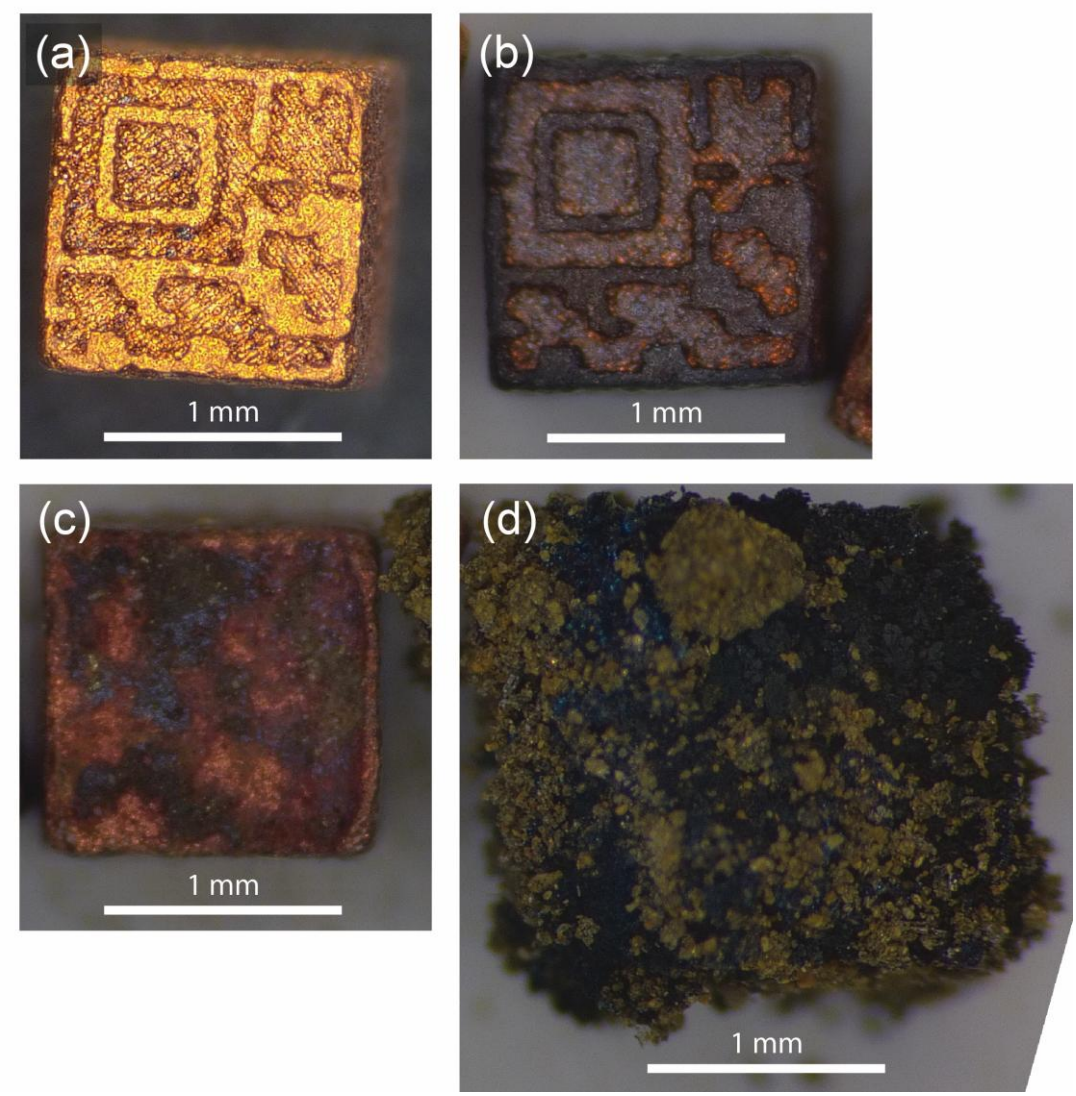

Figure 28. Changes to TPM01 following targeted artificial climate ageing and transportation tests. (a) TPM01 before experimentation, (b) TPM01 placed in a ceramic dish without any commodity and left in the test chamber for three weeks at 75°C and 85% RH (targeted test). (c) TPM01 removed from the nickel concentrate (origin A) following transport to Finland and return to the United Kingdom in self-seal polypropylene bags. The tracer particles were initially undetectable since they adhered to host material particles, but were retrieved by sieving and washing, and (d) TPM01 from the surface of the nickel concentrate (origin A) in the test chamber for approximately one month at temperatures ranging from 55°C to 75°C (85% RH) (targeted test).

Funded by
the European Union

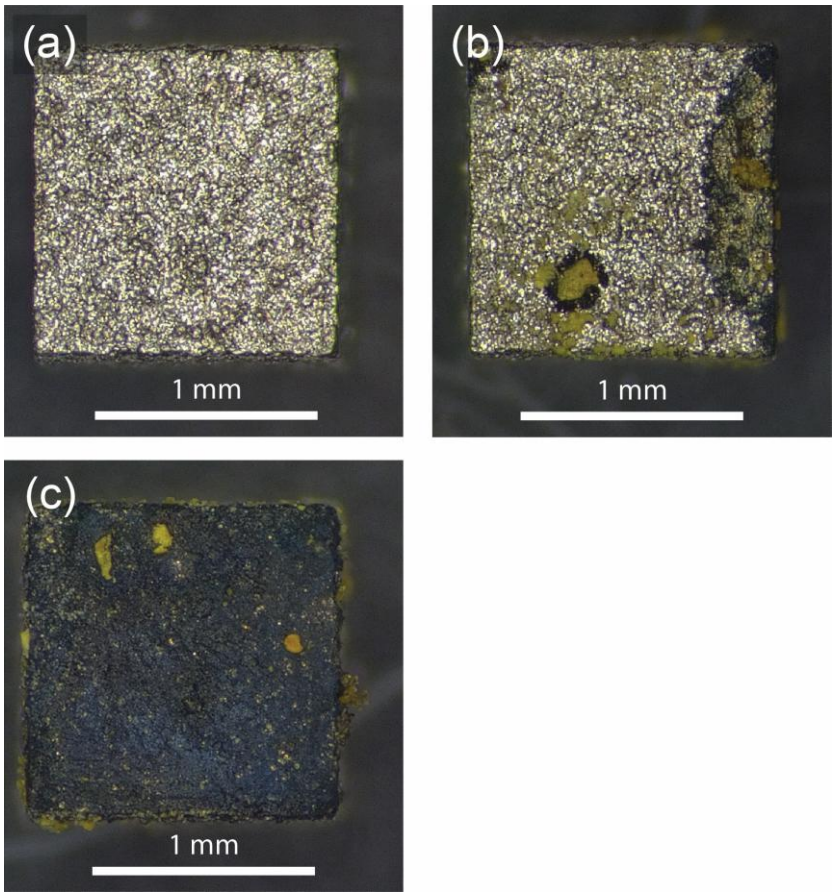

Figure 29. Changes to TPM03 following targeted artificial climate ageing at 75°C and 85% RH over a one-month period in nickel concentrate (origin A). (a) Face of TPM03 before experimentation (surface is not encoded), (b) slight degradation to a surface of TPM03 which was only in direct contact with nickel concentrate over localised areas, and (c) degradation in the form of a black pitted surface to a face of TPM03 which was entirely covered by nickel concentrate.

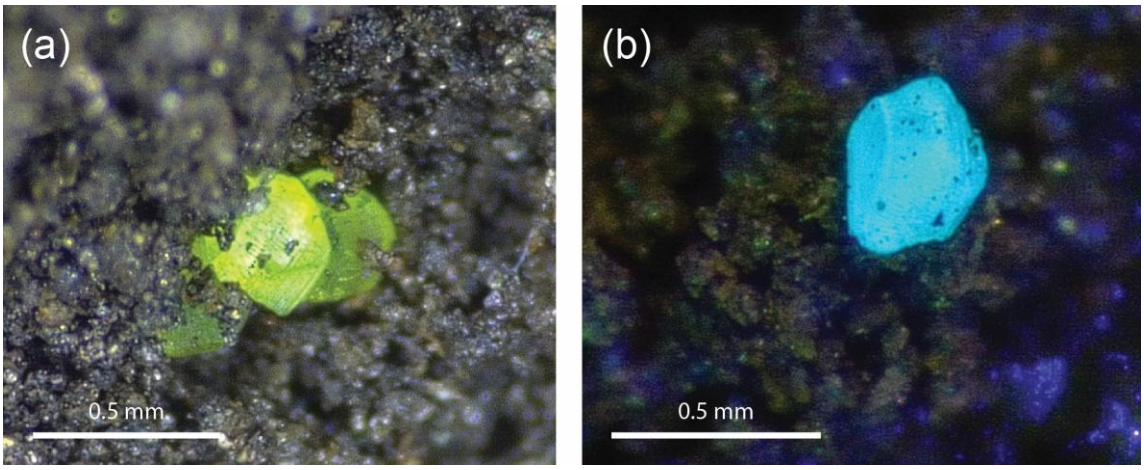

Figure 30. Horizon Microtechnologies TPH01 tracer particles in nickel concentrate after artificial climate ageing for four days at 75°C and 85% RH. (a) In natural light and (b) under ultraviolet excitation light.

Funded by
the European Union

6.10 Transportation Test

During the transportation test the distribution of the TPs provided by TraceTag and Microtrace did not show any evidence of redistribution within any host materials, even though some host materials presented particle/agglomerate segregation. The TPs were homogenously distributed throughout the host materials, and they adhered to the small and large host material particles or agglomerates and did not segregate away from these at any point (Figure 31, Figure 32, Figure 33, Figure III-8 and Figure III-9). Although certain TPs formed localised agglomerations within parts of the black mass host material, this was not due to the transportation test but was thought to be related to the initial sample mixing procedure, where water was used to mix TPs due to health and safety concerns over dust production. TPs were generally not strongly detectable within black mass, which was a broader result found with TPs mixed in this host material.

With the exception of TPM01 and TPM02, all 3D printed TPs transported within polypropylene self-seal bags and vacuum-sealed foil packs showed no evidence of redistribution or changes in morphology or detectability (Figure 34 and Figure 35). TPM01 and TPM02 changed from metallic reddish-brown (5YR 5/4) to a dark reddish black colour (5YR 3/2), showing surface degradation, and affecting the printed micro QR code on TPM01 in self-sealed plastic bags (Figure 28c). However, the micro QR code was largely unaffected when TPM01 and TPM02 were transported in vacuum-sealed packets (Figure III-10).

Funded by
the European Union

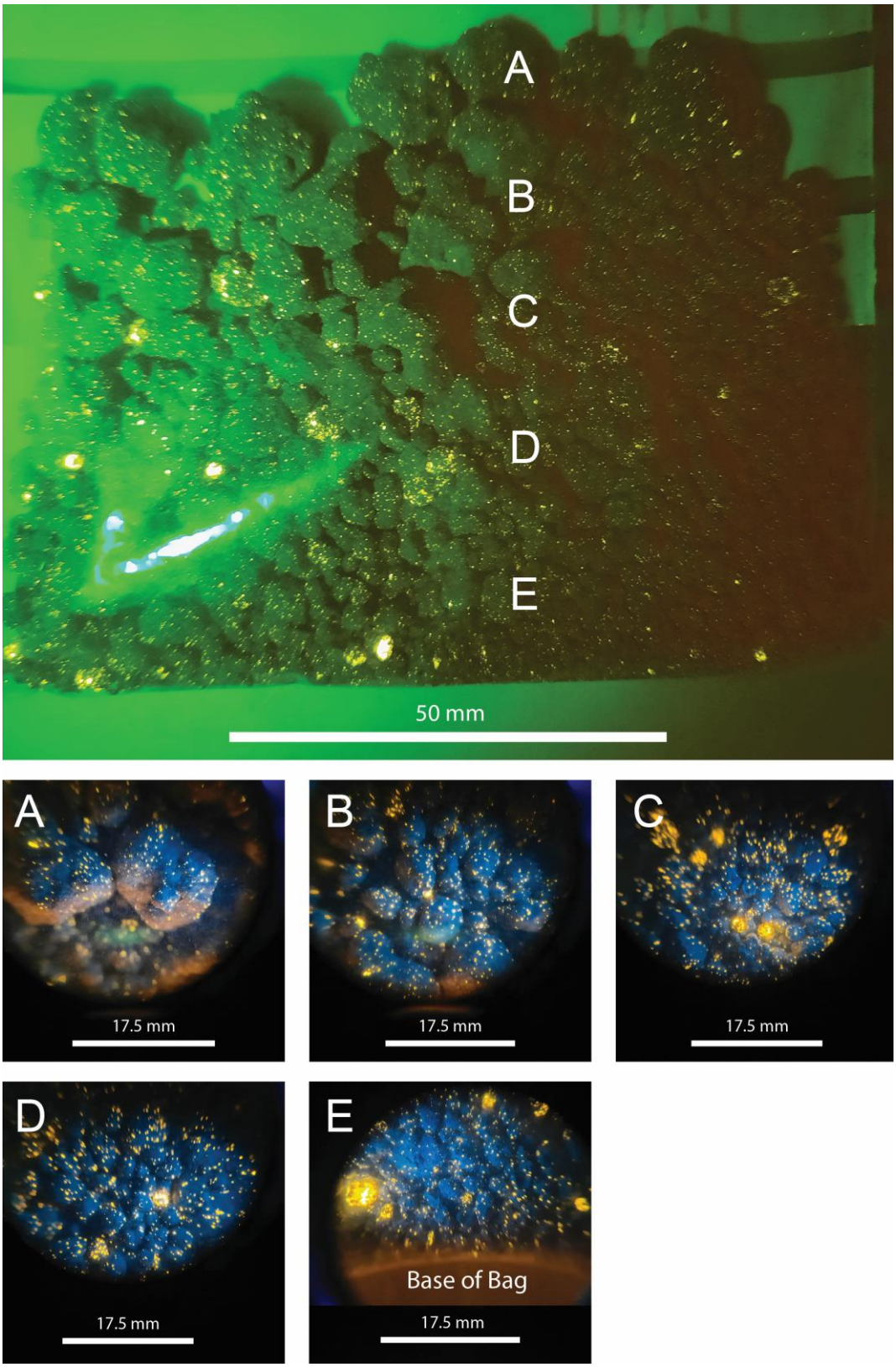

Figure 31. Distribution of TPA03 in mixed hydroxide precipitate following transportation to GTK's headquarters in Finland and return to the United Kingdom in self-seal polypropylene bags. Top: A–E: Representative photographs of tracer particle (TPA03) distribution throughout the host material (from the top to the base of the bag) as observed through TraceTag's ValiScan S3 detector.

Funded by
the European Union

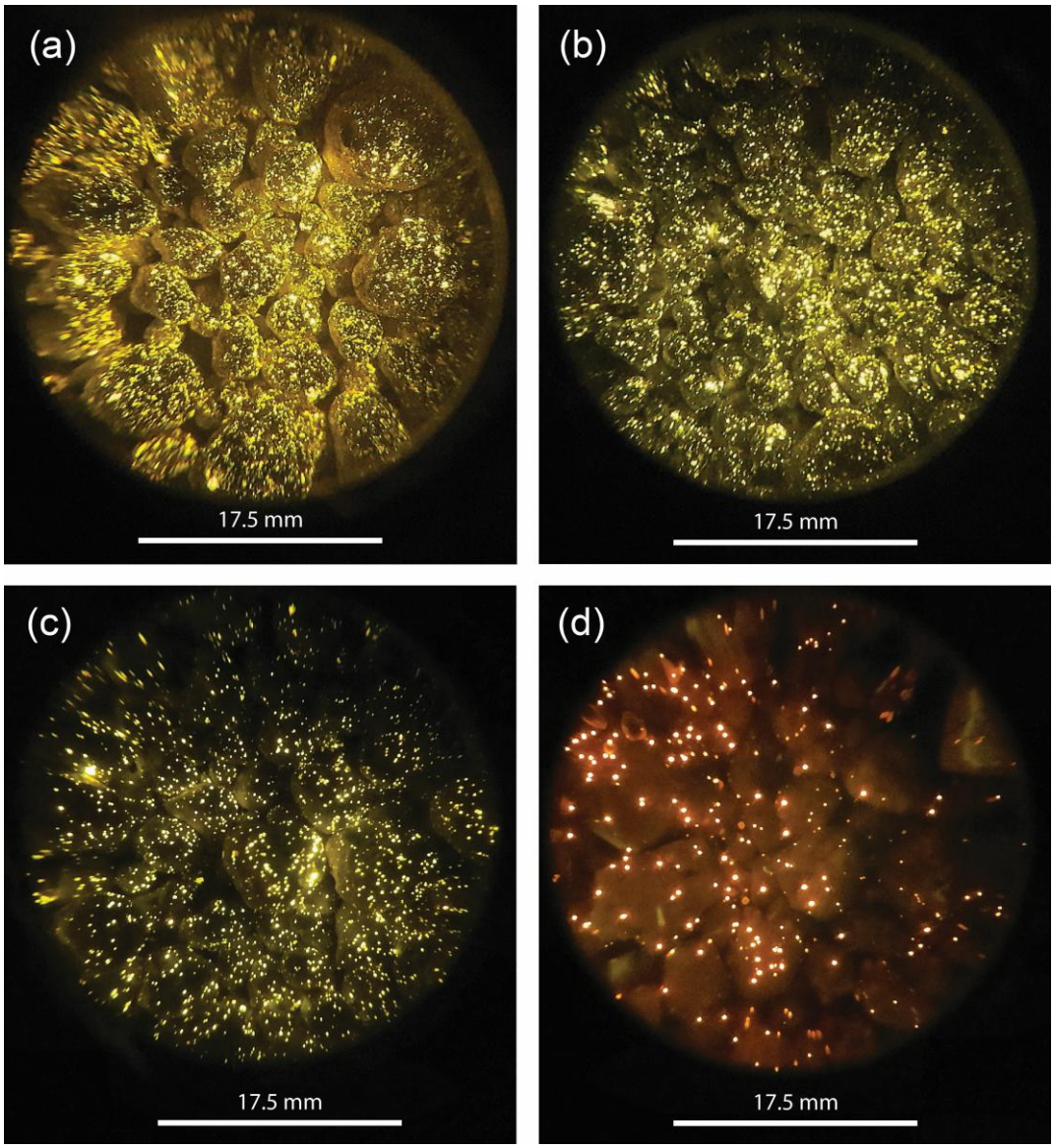

Figure 32. Distribution of (a) TPA01, (b) TPA02, (c) TPA03 and (d) TPA04 in mixed hydroxide precipitate as observed through TraceTag's ValiScan S3 detector following the transportation test.

Funded by
the European Union

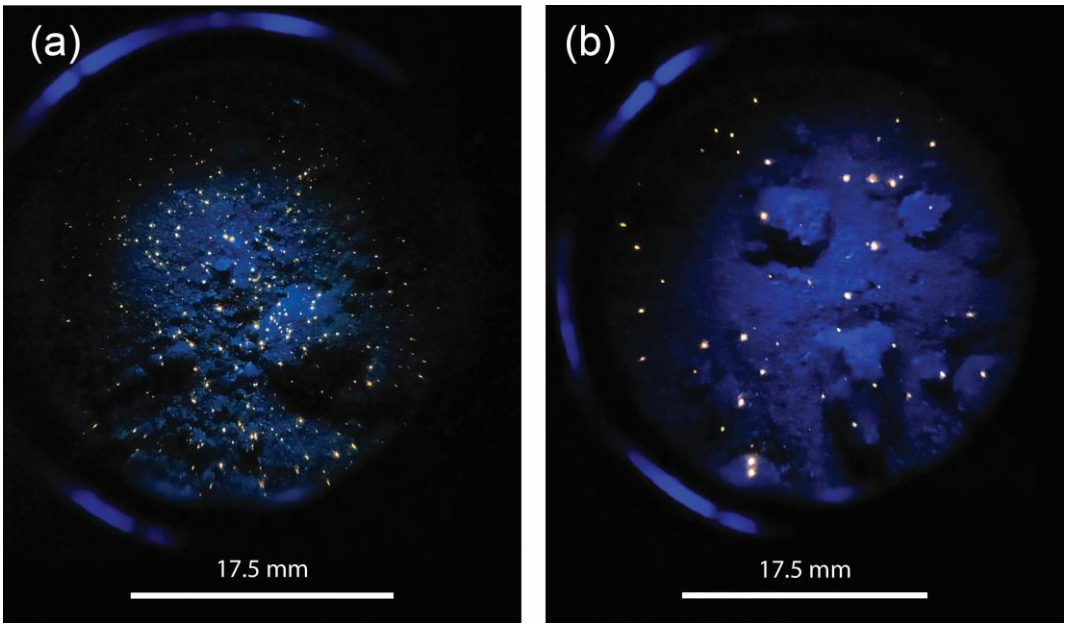

Figure 33. Distribution of (a) TPA03 and (b) TPA04 in nickel concentrate (origin A) as observed through TraceTag's ValiScan S3 detector following the transportation test.

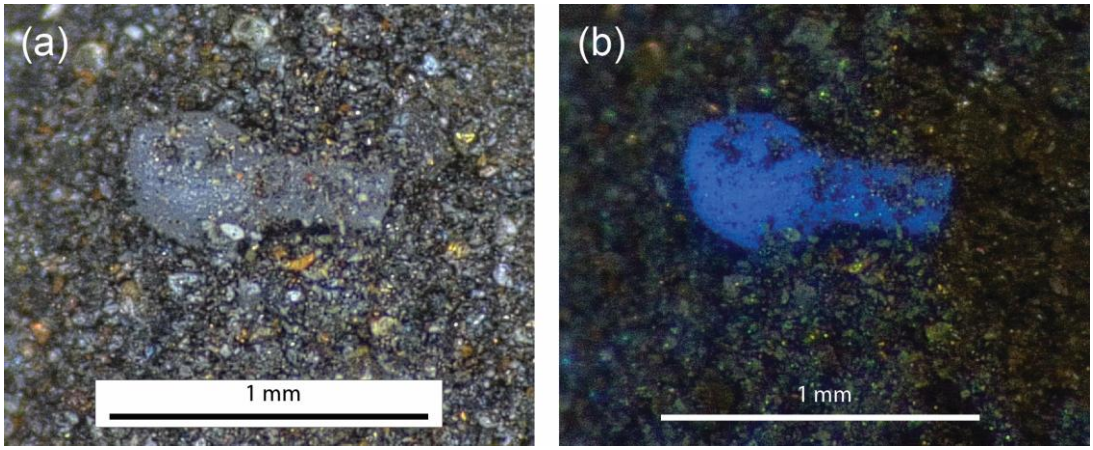

Figure 34. GTK's TPG01 following the transportation test in nickel concentrate (origin B). Under (a) natural light and (b) ultraviolet excitation light.

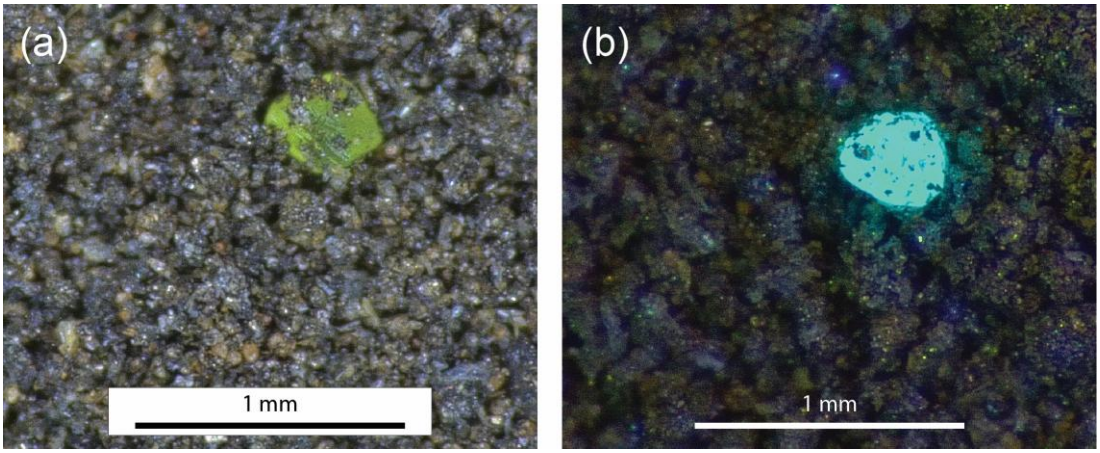

Figure 35. TPH01 in nickel concentrate (origin A) from self-seal polypropylene bags following the transportation test. Under (a) natural light and (b) ultraviolet excitation light.

Funded by
the European Union

6.11 Summary of Results

Preliminary test work established dry application and mixing as a practicable method for achieving the homogeneous distribution of TPs across most host materials. Wet mixing using a pneumatic atomiser was discontinued because of aperture blockages. Due to health and safety issues associated with black mass, a wet application method was utilised for this host material. It is possible that this different application method influenced the performance of TPs in black mass. The examination of TPs using a digital microscope revealed that the TP size significantly influenced detectability and surface adsorption onto host material particles.

Microtrace's confidential evaluation of their proprietary Molecular™ Taggant System successfully authenticated the taggant signature across all evaluated host materials and demonstrated that host-material-specific analytical thresholds could be developed to support detection of dilution or adulteration. Detailed methodology, calibration data, and quantitative thresholds remain confidential.

The MED varied by TP size, with smaller TPs detectable to lower dosages, with TP size being the largest limitation. The aid of excitation lights consistently yielded superior practicable detectability of 3D printed TPs and TPs from TraceTag and Microtrace, when compared to detectability under natural light. Under excitation light, all the TPs were detectable within each host material. TPB01 generally took longer to locate than the other commercially sourced TPs in this test configuration. Time-to-locate for Microtaggant® Identification Particles is directly related to particle size and loading level; in commercial deployments, both are tailored to the application, with loading level ultimately determined by the user as a balance between ease of location and cost of application. TraceTag's TPA01, TPA02 and TPA03 also performed well during the tests, but their detection remained elusive without excitation light, especially within spodumene concentrate and nickel concentrate. The detection of TPs within the black mass was severely inhibited.

3D MicroPrint's TPs (TPM01, TPM02, TPM03 and TPM04) were easy to detect within the host materials but were observed to be mobile which made their detection and retrieval challenging. TPM01 and TPM02 were observed to degrade in the presence of moisture and oxygen and eventually became invisible due to agglomeration of particles on their surfaces. The particles were removed by washing in a sieve (<1 mm mesh) until the TPs became visible. TPG01 performed well and was not affected by temperature or humidity, they were easy to recognise, and it did not take long to identify them within the commodity using excitation light.

Funded by
the European Union

7 Discussion

Except for TPM01, TPM02 and TPM03, the TPs demonstrated resilience when subjected to extremes of dry and wet heat, cold, high humidity, shock, and transportation. It was observed that TPs could be detected with ease in one host material whilst being concealed in another. This was most apparent for black mass, which was a more challenging host material to conduct experiments with and required a different application method for health and safety reasons. Black mass was observed to mask the luminescence of TPs and significantly reduce their detectability. Equally, the same TPs in mixed hydroxide precipitate, spodumene concentrate and nickel concentrate were more readily observed (Figure 17; Table 13 and Table 14). Therefore, the TP may reflect both host-material effects and application-method effects.

It is possible that the method of application used to mix TPs with black mass is also a cause of this difference. TPs had to be dispersed in water and then poured evenly over the black mass surface. The mixture was then mixed thoroughly within a sealed plastic bag. This was necessary to limit dust generation for health and safety purposes.

CRM texture and structure will therefore influence the ease with which a TP can be identified, as will the TP's morphology. If a CRM has an open structure which is highly porous and permeable, this may allow TPs to be mobile within it. Movement through the material during transportation may result in TP 'pooling', reducing its homogeneity within the product. Except for 3D MicroPrint's TPs (TPM), TP redistribution was not observed following the tests. This could be related to the TP particle size, TP exaggerated dosage, smaller sample masses and exposure time, all masking the effect. Longer contact times may allow gravitational settlement, for example on shipping freight transported over multiple months. This will have implications for detection during routine sampling procedures. However, sampling procedures for AFP authentication are not standardised across the minerals and metals industries, and this may have consequences for authenticating tagged CRM depending upon the behaviour of the TPs in different materials.

Discussions of results from the detectability, abundance, distribution, minimum effective dosage, and host-material performance are based on proof-of-concept testing using standard, non-optimised TPs from TraceTag and Microtrace. Additionally, TPs internally produced by GTK and TPs from outsourcing partners (3D MicroPrint and Horizon Microtechnologies) were, in some cases, prototypes and likewise not optimised for the host materials they were tested with. These results, particularly in relation to the TPs from TraceTag and Microtrace, should not be interpreted as commercial specifications or as representative of an optimised commercial deployment, where particle selection, loading level (dosage), application method, and detection workflow would be engineered around the specific use case.

7.1 Preliminary Tests

Initial test work revealed that dry application and mixing of TPs to CRMs, using a riffle splitter, was more successful than wet application using an atomiser. Numerous atomisers tested became blocked during testing, possibly due to TP agglomeration within the aperture of the atomiser. The results have clear implications for the application process to be transferred to a pilot scale. Dry application, such as through the use of a drop spreader

over a conveyor belt, may be suitable for some CRMs, however dry mixing to ensure TPs are thoroughly mixed within a CRM at an industrial scale may not be appropriate due to excessive dust creation, unless conducted in a closed system. Applying TPs through a spray system, such as existing dust suppression systems, may be more effective. However, these systems would have to be adapted to accommodate the introduction of TPs into the formulation that will be used to condition the material. Optimisation of formulation parameters such as surfactant type, dispersion stability and viscosity would need to be conducted to prevent particle agglomeration and nozzle blockage.

7.2 Dilution

Microtrace's proprietary Molecular™ Taggant System was successfully authenticated across all host materials, the quantified signature intensity threshold of the proprietary Molecular™ Taggant System for identifying adulteration depended on the physical properties of the host materials and the extent of dilution.

Environmental factors and host material characteristics heavily influenced the molecular taggant system. While the properties of the host materials did not adversely affect detection, potential long-term chemical or physical interactions between the TPs and host materials cannot be ruled out. Over durations longer than those studied, gradual degradation could occur, significantly impacting the molecular taggant system's suitability to act as a tracer.

Microtrace's Molecular™ Taggant System coats finer particles more uniformly compared to uneven or larger particles, and the collection of relatively small samples from materials with heterogeneous physical properties may result in the evaluation of an unrepresentative analytical sample, resulting in higher molecular taggant system signature variability. Furthermore, the loss of moisture between when host materials were applied with the Molecular™ Taggant System and when analysis was carried out altered the Molecular™ Taggant System to host material mass ratio, which introduced analytical variability. Although in certain circumstances this could potentially be mitigated by recording the natural moisture loss between the times of application and analysis of the Molecular™ Taggant System, this will not always be possible, particularly in situations where water is added to a CRM, for example, for dust suppression purposes.

The recorded improvement in Microtrace's Molecular™ Taggant System signature intensity variability when host materials were prepared (i.e. dried and sieved) before tagging has significant industrial implications. Controlling moisture content and particle sizing of bulk material raises significant logistical, economic and environmental challenges along many existing supply chains, in some cases requiring modifications to existing processing steps and requiring new purpose-installed infrastructure at various CoC transfer points. However, for certain CRMs where there are set moisture and particle size requirements, such as graphite, this may be achievable for specific CRMs. As this test was laboratory-based (TRL 3), scaling up the test work and a thorough evaluation of existing CRM processing steps would be required to assess the CRM supply chains that may be amenable for the application of Microtrace's molecular taggant system, considering the indications of required material preparation to optimise results.

Microtrace's Molecular™ Taggant System was evaluated as part of a "standard" formulation provided by Microtrace. Modification of the Molecular™ Taggant System based on CRM composition, integration methods, detection requirements, number of taggant signatures

required, sensitivity requirements (source identification only or dilution) would be required to advance the testing of Microtrace's Molecular™ Taggant System with CRMs. It is highly probable that adulteration probability thresholds and the quantified taggant signature intensity variability could be improved following bespoke taggant modification.

7.3 Minimum Effective Dosage

The determined MED of TPs was dependent on TP dimension and mass. Broadly, larger TPs required higher dosages for successful detection (Table 12). This trend is attributable to either the decreased spatial distribution of larger particles within the host materials, where low dosages may yield only one or two discrete TPs, or the mass limitations of individual TPs. For example, a single TP of TPM01 has a mass of 0.025 g (a concentration of 250 ppm in assessed test portions). Finer TPs demonstrated superior detectability and were successfully detected down to single-digit ppm or less than 1 ppm.

These findings carry significant industrial relevance, as they demonstrate that successful identification is achievable with low TP dosages. Minimising dosage requirements directly reduces TP procurement costs, which extends the economic viability of these TPs to both high- and low-value CRMs or CRMs with price instability. However, as these tests evaluated qualitative detectability, the operational dosages required to verify whether a CRM consignment has undergone dilution will likely need to be higher to ensure quantifiable and auditable results.

While the higher dosages required for the largest TPs (e.g., TPG01, TPH01 and TPM01–04) may be associated with higher purchase or production costs, these TPs also offer alternative functional advantages. Specifically, the larger physical dimensions of TPM allow these to be seen with the naked eye, and may serve as an overt method of traceability, providing a visible deterrent against adulteration or substitution. However, the visibility of TPs might have a profound negative impact on their use for traceability, as stakeholders such as traders and refiners may question the presence of the TPs and the perceived addition of deleterious materials. Furthermore, the increased TP size may enhance recoverability or separability. For example, the large TP sizes of the ferromagnetic TPM03 and TPM04 TPs could facilitate easier magnetic separation, enabling their recycling and reuse. Conversely, this could also increase the ease with which TPs could be illicitly removed from shipments of raw material.

Two key limitations were identified within this test. Firstly, the standardised 100 g test portions restricted the minimum concentration that could be achieved for the larger TPs. In practice, however, laboratory samples routinely range from single grams to tens of kilograms, and the 100 g mass falls well within the current range. Therefore, test portions may represent some sample sizes that would undergo collection, preparation and dispatch for laboratory analysis for certification purposes. Secondly, while the test portions were thoroughly mixed, they were not subject to artificial or natural environmental ageing. Different ageing methods could have impacted the results, for example, by improving the ability of TPs to disperse within the host material or reducing TP detectability by accelerating coating/masking effects.

Significantly, the reported MED values reflect the specific experimental design, host materials, loading strategy, search methodology, and detection workflow used in this study.

Minimum effective dosage is application-specific and should not be interpreted as a recommended commercial loading level.

7.4 Abundance and Distribution

TP abundance and distribution varied considerably based on the TP type, host materials and application methods. The identification of TPs at a dosage of 100 ppm (0.01%) was achieved across all the host materials tested, and TP detection was significantly enhanced under excitation light (Table 13 and Table 14). Their distribution and detectability appeared to be heavily influenced by the physical and potentially chemical properties of the TPs and the host material, namely the different TP sizes and morphologies. In general, the smaller TPs TPA01–03, with sizes ranging from 10–20 µm, returned higher TP counts and were more widely dispersed (Figure 17).

TPs returned the highest counts within MHP, which had a high moisture content of 52% (Table II-61). Additionally, the MHP's hydrophilic properties and the presence of large agglomerates and particles (Table II-57, Table II-58 and Table II-60), may have aided TP detectability by causing TPs to adhere onto their surfaces. Comparatively, although TP counts for smaller TPs were similar between MHP, spodumene concentrate and nickel concentrate, a moderate to significant reduction in the counts of the larger TPs TPA04 (55–65 µm) and TPB01 (37–74 µm) was observed. This may have been as a result of "coating" or "masking" effects of host material particles onto TP surfaces, which reduced the effectiveness of larger TPs to disperse within the material or caused them to become obscured.

Black mass returned the lowest TP counts of all the host materials for all TPs. It is not clear what factors may have resulted in this stark difference. However, possible reasons include previously noted segregation of TPs (concentrated into agglomerates), "coating" effects of host material particles onto TP surfaces or the strong light absorption properties of this host material, which may be particularly significant when considering that graphite is a major component of this material (TPs were similarly more difficult to detect within the graphite concentrate tested as part of the photooxidative test). In the case of black mass, a different method of application involved the mixing of TPs with water, for health and safety purposes, to reduce dust generation. The formation of agglomerates may have resulted in artefactual bias, which inadvertently prevented the dispersion of TPs, as these agglomerates could have contained TPs and were hard to break apart, requiring excessive blunt force using metal tools to crush them. Due to health and safety limitations, it was not possible to repeat the evaluation of TPs in black mass using a dry application method.

Although TP variance in relation to their abundances and distributions was similar between triplicate samples for each TP and host material combination, a sample of nickel concentrate containing TPB01 returned notably lower counts of TPs compared to the other two samples. This discrepancy may have been caused by the inherent heterogeneity associated with the nickel concentrate. The host material contained fractions of different sizes with an uneven distribution comprising loose particles (~77% of host material was <2 mm (Table II-34)) and larger agglomerates which were up to 27 mm in length (Table II-35). These may have affected the ability for TPs to become evenly dispersed throughout the host material and suggest that CRM heterogeneity can affect TP detectability. However, as the total sample count is three (N=3), this anomalous result may also be a result of random variation.

Funded by the European Union

TPH01 and TPG01 returned the lowest average TP counts from TPs tested with nickel concentrate. This was an expected result as the TP sizes were significantly larger than commercially supplied TPs and the 100 ppm (0.01%) dosages were kept constant between all TPs, meaning there would be fewer total TPs within the TPH01 and TPG01 doses. The tendency for these TPs to agglomerate in certain circumstances likely contributed or was the controlling factor for TPG01's highest recorded TP count variance between samples (i.e. the highest two standard deviations as a percentage of the average value; Figure 18).

A key limitation associated with this test is that all commercially supplied TPs were provided from a "standard" range of TPs from each supplier and were not modified according to the properties of any of the host materials used. If particle sizing, chemistry and other physical properties were considered for each host material, modified versions of the TPs could be produced to optimise TP behaviour. Furthermore, an elevated TP dosage of 100 ppm (0.01%) was utilised as a proof-of-concept dosage to ensure TPs could be qualitatively and quantitatively evaluated. While this exaggerated dosage provides a valuable indication of TP behaviour, these results may not be directly transferable to lower TP dosages which are anticipated in practice. Finally, the reliance on manual procedures, such as the transfer of TP and host material between different containers, could have resulted in material loss or modified TP distribution, which may have influenced the recorded outcomes.

7.5 Modified Flow Table Test

Samples subjected to this test were in their natural states, and as tested host materials had variable moisture contents from 0.45% (black mass) to 52% H_2O (MHP) (see section 13.2 Appendix II: Host Material Characterisation), moisture will have caused variable electrostatic forces between the host materials particles and TPs. However, apart from TPM03 and TPM04, TPs did not become segregated from the host material or present a change in their distributions post-test.

Prolonged periods of drying of host materials may affect distribution, although this will depend on the commodity's texture and structure. In this test, only vertical forces were applied to the samples to simulate wave action, ocean currents and wind, but forces created over extended rail or road transport routes may affect the TPs in different ways, such as jarring movements or horizontal forces created by a vehicle moving around a bend in a road. TPs which could be particularly affected by these conditions include TPM03 and TPM04. These TPs demonstrated vertical movement within the cubes possibly due to their larger size (> 1 mm) and mass (i.e. a single TP of TPM01 is 0.025 g and a single TP of TPM03 is 0.02 g) in comparison to the other TPs. These factors may present implications for the sampling of FIBCs for AFP authentication purposes as the TPs may settle over time towards the base of a bag or track towards the sides or middle parts of FIBCs and inevitably could be missed during sampling.

Rectangular spears were used to determine TP distribution within the cubes following this test. MHP had compacted within the spears when attempting to collect samples (Figure 19i). This may have disturbed the natural distribution of the TPs within these samples and suggests that sampling methods have the potential to change TP distribution. Therefore, in any future study, the method of sampling must be carefully selected to obtain a fully representative sample for examination. Spodumene concentrate and MHP had also compacted towards the base of the PMMA cube because of vertical vibration. However, this

appeared to have had no effect on TP distribution within the cubes or indeed the PMMA spears (which showed the compaction of host material) used to collect samples from within the cube.

7.6 Natural Ageing

The effect of rainfall on TP movement was an important consideration, as this may potentially affect their presence and distribution within a host material if they become mobilised by infiltrating water. In practice, the downward percolation of pore water may result in lower detection rates, possibly by redistributing the TPs to lower layers or the base of an FIBC or stockpile. In the host materials tested, TPs remained visible using a microscope or handheld detectors, confirming that they had not been transported by water percolation. The exposure of the host materials to fluctuating weather patterns did not have any observable detrimental effects on the distribution of the TPs within the host materials, albeit this test was relatively short in duration and further testing under more extreme weather conditions might give different results. The prevailing weather conditions during the test was typical for a temperate UK spring, with moderate to high rainfall and limited periods of prolonged dry weather (see section 13.3.2.3 Climate Data Covering Test Durations (Appendix III)). Prolonged periods of dry, cold or frozen conditions may also have an adverse effect on TP distribution, with loss of moisture reducing hydrostatic forces between TPs and the particles they are adsorbed to; this process will, however, depend on the host material, as some materials will have greater water absorption properties. A similar drying process was observed in petri dish samples (collected for observation under the microscope) of spodumene concentrate mixed with Microtrace's TPB01. Over time, the spodumene concentrate dried and it was noted that TPs disappeared from the surface of the sample, most likely having moved through pore spaces within the material towards the base of the petri dish, or they may have rested just below the surface or become held within the mass of the host material in the upper or middle layer, following drying and when the samples were disturbed. This was clearly an observation at the laboratory scale, and it is therefore unknown if the process would occur on a larger scale.

The limitations of the natural ageing test included the small sample sizes and the relatively short test period of 60 days (1440 hours). In comparison, bulk materials are potentially stored for extended periods of time, potentially for years, and the exposed surface area of FIBCs or stockpiles is considerably larger. It is likely that externally stored samples will experience greater diurnal and seasonal variations in weather over longer test durations. The small masses used in this test also limited the effects that larger volumes of material may experience, especially within the central parts of an FIBC/stockpile that could be protected from the influences of weather.

7.7 Photooxidative Ageing

Photooxidative ageing causes the breakage of polymer chains, resulting in the production of free radicals, whilst reducing the molecular weight of polymers, the consequence of which is a loss of surface gloss and significant deterioration of many material properties over time. Excessive exposure to UV radiation can rapidly accelerate degradation processes in polymeric materials, causing the effect known as photooxidative ageing (Lu et al., 2018). This study considered the effect of ultraviolet (UV) radiation, covering wavelengths between

100 nm to 400 nm from the sun (World Health Organization [WHO], 2026) on the behaviour and detectability of commercial TPs which may contain polymeric substances. This test revealed that all TPs remained evenly dispersed throughout the host materials and were not affected by prolonged exposure to sunlight. There were no observable differences in TP morphology or characteristics following the test procedure and all TPs could be viewed clearly using excitation light.

Although designed to test the effect of prolonged UV exposure, the test conditions were ultimately affected by the variability of UK weather patterns. The amount of UV radiation from the sun that hits the Earth's surface depends on several factors, including its elevation angle in the sky, latitude, altitude, ozone layer thickness, cloud cover, and ground reflection (WHO, 2026). Consequently, complete and prolonged exposure to UV during this period would have been reduced due to cloud cover in the UK. Another factor which may have reduced UV exposure rate was the use of plastic covers on the cloche and the petri dishes that the samples were contained in, which may have filtered UV rays. The combination of these factors will have reduced the desired effect on the TPs. Although not evaluated quantitatively, the cloche and petri dishes were likely to have created microclimates with humidity and temperatures above ambient conditions. However, any microclimates which were created had no observable effect on the TPs.

It is also likely that sampling in practice (e.g., with spears) will obtain TPs from within a CRM (e.g., within a stockpile), therefore collecting TPs which were not exposed to the effects of UV radiation. Abiotic processes such as photooxidation act as a preliminary degradation stage which breaks the linkages in polymeric substances and increases the surface area available for microbial colonisation (Kijchavengkul et al., 2010). This may be another route to consider, as legislation on plastic use may change with a shift towards biodegradable materials, and microbial action upon TPs before or after exposure to UV radiation, would then become an important consideration for the material selection to produce TPs.

7.8 Artificial Climate Ageing

The effects of temperature and humidity were clearly observed on TPM01 and TPM02 which resulted in a colour change from reddish brown (5YR 5/4) to dark reddish brown (5YR 3/2) (Figure 28b), whilst TPM03 changed from bluish grey (10YR 6/1) to black (N 1/) whilst also showing degradation to the edges of the TP during the targeted artificial climate ageing test (Figure 29). The surfaces of TPM01 and TPM02 became covered in host material particles and these TPs degraded and discoloured (from 5YR 5/4 to 5YR 3/2) in the presence of nickel concentrate (Figure 28d; Figure III-2). This phenomenon was also observed to degrade the micro QR code on the surface of TPM01. The nickel concentrates contained a significant amount of sulphur (sulphur-containing minerals accounted for 83% of the modal abundance of the nickel concentrate (origin A) (Figure II-13 and Table II-42)), and copper-sulphur interactions are one of the most important relationships in the environment. Copper has a thiophilic nature for sulphur, and in the presence of oxygen and moisture, secondary copper sulphides, which can be black in colour, may be generated (Ghaderi et al., 2024). These copper sulphides were possibly observed on TPM01 in this study (Figure III-2a) but chemical analysis of this material was not undertaken to confirm if this was the case. Nevertheless, this interaction has important consequences and implications for the future use and reliability of these TPs for the purposes of traceability. In the case of TPM03, corrosion resistance of stainless steel results from the presence of a thin oxide, a 'passive'

Funded by the European Union

film on the metal surface typically 1–3 nm thick (Olsson & Landolt, 2003). In the presence of sulphur (from the nickel concentrate), acidification of the local environment can occur, which acts to suppress re-passivation (formation of the film) of the steel matrix, thereby causing surface 'pitting' corrosion, creating black spots (Figure 29). Alteration of the chemistry of the stainless-steel surface in the vicinity of sulphide inclusions has also been proposed as playing an important role in localised corrosion initiation (Brossia & Kelly, 1998). Although TPM05 was not tested as part of artificial climate ageing tests, the observed surface corrosion may not penetrate to the internal micro QR code within this TP, which may mean the encoding could still be verifiable in practice.

Degradation of TPM01 and TPM03 were relatively fast (three to four weeks) revealing that these TPs could not be used for long-term traceability purposes if relying on external encoding only. TPM01 and TPM02, when transported in vacuum-sealed foil packets, did not reveal the same level of discolouration or encapsulation as observed in the plastic bags (Figure III-10). A reduction in oxygen supply may have limited the rate of oxidation and interaction between the TP and other elements, compounds or liquids.

Although the commercial TPs were not affected by temperature and humidity it is important to highlight that these studies were carried out in a test chamber using relatively small masses of material. Considerably larger one-tonne FIBCs or stockpiles of 20 tonnes may present different challenges, which were not considered here or could not be recreated in a laboratory. Laboratory studies use small volumes of material and rely on isolated variables which are constant. Larger masses of host material may be affected by redox changes over time, and small-scale experiments do not consider changeable factors in natural environments such as weather variables, ageing factors and weathering. Therefore, changes within the centre of a larger mass of raw material during transportation or when cargo is stored for an extended period may affect TP distribution in the longer term.

A study by Singh et al. (2011) concluded that temperatures in containers were greatest in dry ports (a temperature of 59.5°C was recorded in a port in New Delhi, India), when they are stationary and not at sea, whilst the highest temperature gradient between inside and outside a container was recorded at 27.5°C. Temperature changes may affect CRM moisture content, create or accelerate chemical reactions affecting elemental redistribution in host materials and promote oxidation. These changes may have an impact on TP movement, or indeed TP chemistry, possibly causing accelerated degradation. Temperature differences may be greater within sealed drums, where oxygen may also become a limiting factor, although this was not verified during this investigation. Changes in environmental conditions including pH and Eh due to oxygen levels may create anoxic conditions, thereby changing the chemistry of the commodity which may also have an impact on TPs. No adverse effects were observed in the other commercially sourced TPs or 3D printed polymer TPs used in this investigation (Figure 26, Figure 27, Figure 30, and Figure III-3 to Figure III-7), and it must be considered that their properties were resilient to the temperature and humidity settings used. Indeed, certain TPs had polymeric properties, which would not have been affected within the temperature and humidity range tested here. However, it remains evident that only observational changes in the TPs morphologies could be detected, and biological degradation, which could be accelerated under higher temperatures and humidity, could have had an influence on TP shape or functionality. During biodegradation microbes use plastic as a carbon/energy source by incorporating liberated carbon from polymers into their own structure, essentially bio-fragmenting and subsequently bio-assimilating the polymeric compounds (Bhavsar et al., 2023).

Funded by the European Union

7.9 Transportation Test

Transportation tests, which used road and air freight, revealed the TPs were generally well dispersed throughout the host materials (Figure 31 to Figure 33, Figure III-8 and Figure III-9). Undoubtedly, the texture and structure of the host materials will affect how the TPs bind and/or move within the matrix of the host materials. MHP was a hydrophilic sludge and had a high moisture content (52% H_2O), and these properties may have facilitated the binding of the TPs to particle/agglomerate surfaces, which aided even dispersion of TPs, in comparison with drier substrates (Figure 32 and Figure 33). It is also noteworthy that these samples were in self-sealing plastic bags and vacuum-sealed foil packets. In practice, transportation in one-tonne FIBCs or sealed drums may undergo chemical changes including pH and Eh within larger volumes of host material and may produce changes in elemental composition potentially affecting TPs. These changes, combined with transitions between hot and cold environments, may also form phenomena such as 'container rain' (moisture formed by condensation inside a shipping container (Yuen et al., 2022)). This phenomenon, combined with wave action, currents, wind direction, vibration and density variations over a prolonged period, may produce undesirable effects on TP distribution within FIBCs. A study by Singh et al. (2011) demonstrated a temperature shift of 33.5°C in a 24 h period and a 27.5°C gradient between the inside and outside air temperature of a container in a New Delhi dry container port. These temporal and spatial differences in temperature over 24 h were likely not covered as part of the transportation test, but long-term diurnal or spatial shifts such as these could affect TP morphology and performance during global transportation. Furthermore, Singh et al. (2011) stated that poor road conditions produced greater vibrations than those produced as part of transport by rail or ship. Although these variations in vibration were not evaluated as part of this study, they warrant future investigation.

7.10 Tracer Particle Detection Rates

From cost-effective and practicable perspectives, the time taken to detect TPs within a CRM would ideally occur in real-time or near real-time, so as not to negatively impact operations. The field detection of the TPs should be rapid, robust, low-destructive, and non-invasive and deployed at checkpoints within the CoC. Ultimately, the detection of the TPs is to support material claims if CRMs may have been adulterated or substituted, and to facilitate traceability.

A digital microscope with a maximum magnification of x594 was used to obtain images of the TPs to observe any detrimental effects from the testing programme (Figure 7). However, although the digital microscope itself is compact, an in-situ high magnification microscope which requires a 4K display to maximise the microscope's magnification would not be practicable in many operational settings where a portable, rapid and robust detection system is required. Commercially available handheld digital microscopes with built-in excitation lights may serve as a field-ready alternative.

The commercial TPs were supplied with handheld detectors that were used to effectively identify TP presence (Figure 6b and c). These were used to simply determine TP presence and distribution in a commodity. Microtrace's handheld device detected TPB01 under ambient lighting, but TPs were more readily observed in a dark room. The battery-powered UV torch had a much wider beam angle and TPB01 was much more easily detected with this

device under ambient conditions. TPG01 could be identified using the UV torch. However, they also require detection in a dark environment, limiting their operational application. Although all TPs were detectable at 100 ppm (0.01%), anticipated industrial dosages are expected to be significantly lower, and environmental conditions and industrial processes not tested as part of this study could impact their detectability.

The detectability of TraceTag's Valimark™ TPs and Microtrace's Microtaggant® Identification Particles under excitation light is directly influenced by the excitation source and test configuration. Detection performance observed in this study reflects the specific detection workflow selected by the investigators and should not be interpreted as the maximum achievable performance of TraceTag's Valimark™ TPs or of the Microtaggant® Identification Particles. Commercial deployments routinely employ application-specific optimisation of particle size, loading level, excitation source, optical filters, illumination geometry, sample presentation, and detection methodology. Light wavelength, light intensity at the sample, beam angle, working distance, ambient light conditions, host material, and particle loading all affect ease of location. Additionally, the evaluated tracer technologies differ in intended function, security level, morphology, detection method, degree of encoding, and cost structure for both the TP and detection equipment. Observed differences in detectability, and other results, should therefore be presented as specific to this proof-of-concept test configuration and should not be interpreted as a general ranking of commercial suitability.

Funded by
the European Union

8 Financial Evaluation

The industrial implementation of AFP technology is contingent upon its economic viability and scalability. Accordingly, a preliminary financial evaluation has been conducted to evaluate TP costs, specifically costs associated with acquiring TPs from external service providers and producing TPs internally at GTK. Due to commercial sensitivities associated with TP costs from existing traceability solution providers, these costs were excluded from this evaluation.

Guided by the results of MED test results, two distinct TP dosage scenarios have been evaluated as part of this financial evaluation. These were (a) a dosage of 1 g of TP per metric tonne of CRM (0.0001% or 1 ppm), and (b) a reduced dosage of 0.1 g of TP per metric tonne of CRM (0.00001% or 0.1 ppm). Although certain TPs were not tested down to these dosages, it is inferred that with a scaling up of the CRM quantities, in association with specialised industrial application and blending infrastructure, lower TP dosages will be rendered commercially practicable.

8.1 Tracer Particle Costs

8.1.1 GTK 3D Printed Tracer Particles

The calculated in-house manufacturing costs for GTK 3D printed TPs (Table 15) were estimated based on existing production workflows utilising a Formlabs Form 3 stereolithography (SLA) resin printer and post-processing kit. Capital expenditure (CapEx) for equipment procurement and specialised analytical costs for host material particle characterisation for the purposes of refining TP properties, such as laser particle sizing and X-CT, were excluded from this evaluation. The time that is required for material preparation, supervision and quality control has not been considered here.

Personnel costs represent the primary cost category, accounting for approximately 75% and 95% of total production costs for 1 g and 0.1 g of TPs, respectively. These personnel figures account for technician hours spent on the equipment preparation and cleaning, and the removal and collection of TPs. While the manufacturing costs represent batch-scale TP production (for 1 g and 0.1 g of TP), TP deployment costs per unit tonne of CRM could be reduced significantly in some situations. For example, where a TP dosage of 0.1 g per tonne of CRM may be feasible, a supplier could commission the batch production of 1 g of TP (with a manufacturing cost of €78.91) to tag a 10-tonne consignment of CRM, reducing the TP cost per tonne of CRM to €7.89.

The Formlabs Form 3 relies on a single moving laser to irradiate photosensitive resin point by point. While suitable for proof-of-concept fabrication, industrial scaling necessitates the use of high-throughput 3D printing technologies such as Masked Stereolithography (MSLA) or Projection Micro Stereolithography (PμSL), which can have significantly superior printing resolutions (down to 0.6 μm) (Ge et al., 2020; Prabhakar et al., 2021). Transitioning to industrial systems can also reduce material (resin) costs by a factor of four or more, and integrated automated cleaning and collection cycles would reduce personnel costs. Although TPs were optimised for physical performance within particular host materials, the TP designs were not optimised for cost, which could take place through the evaluation of

Funded by the European Union

alternative low-cost resins/materials and lightweighting (e.g., modelling of internal void-space).

Table 15. Running costs associated with producing GTK 3D printed tracer particles.

Cost Item	1 g of Tracer Particles	0.1 g of Tracer Particles
Material Costs[a]	€18.00	€1.80
Personnel Costs[b]	€59.31	€35.10
Utility Costs[c]	€0.08	€0.00
Consumable Costs[a]	€1.51	€0.15
Total Production Cost	€78.91	€37.05

[a]Calculated based on actual resin (material) and washing agents and resin tank (consumables) purchase costs in Euros.
[b]Calculated based on the monthly job requirement salary for a Grade 6 role (from April 1, 2026) mandated by the Collective Agreement for Salaried Employees in the Finnish Chemical Industry (Chemical Industry Federation of Finland & Trade Union Pro, 2025). Calculations assume an employee age of >25 years, include a monthly seniority bonus, and apply a divisor of 158 hours to the monthly salary to determine the hourly salary. Personnel time requirements are determined by the time required to prepare, clean, remove and collect TPs for each of the required TP masses: (a) 2 hours and 40 minutes for 1 g of TP, and (b) 1 hour and 35 minutes for 0.1 g of TP.
[c]Calculated based on electricity prices for Finnish non-household consumers within the consumption band IC (500 MWh to 2000 MWh annually) (Eurostat, 2026). Excludes taxes and levies.

8.1.2 Outsourced 3D Printed Tracer Particles

3D MicroPrint and Horizon Microtechnologies provided estimated costs to produce TPs at various quantities (Table 16). Per-gram price reductions of 29% to 91% were provided as batch masses of TPs were increased. The costs to produce 1 g and 0.1 g of TP based on these estimated costs were also evaluated (Table 17).

Operationally, 1,000 g of TPs would be sufficient to trace 1,000 to 10,000 tonnes of CRM, at TP dosages of 1 g/t (1 ppm) and 0.1 g/t (0.1 ppm), respectively. The total tonnage of a consignment will dictate how much TP is required, and 10 g, 100 g or 1,000 g of TP will not be required if consignments consist of several tonnes of CRM.

Table 16. Costs associated with producing outsourced 3D printed tracer particles.

TP	Cost to produce 1 g	Cost to produce 10 g	Cost to produce 100 g	Cost to produce 1,000 g
TPH	€1,200	€8,500	€68,000[a]	€612,000[b]
TPM01	€2,200	€5,500	€27,000	€195,000
TPM02	€2,403	€6,200	€44,000	€340,000
TPM03	€1,815	€4,200	€25,000	€205,000
TPM04	€2,100	€5,300	€41,000	€330,000

Note: TP = tracer particle; TPH = TPH01, TPH02 and TPH03; costs to produce TPH01, TPH02 and TPH03 are identical. Costs were obtained from 3D MicroPrint (personal communication, 2026) and Horizon Microtechnologies (personal communication, 2026).
[a]The cost to produce 100 g of TPH assumes a 20% discount to the 10 g retail cost.
[b]The cost to produce 1,000 g of TPH assumes a 10% discount to the 100 g cost.

Table 17. Costs associated with producing different quantities of outsourced 3D printed tracer particles.

TP	Cost based on the production of 1 g of TP		Cost based on the production of 1,000 g of TP[a]	
	1 g Cost	0.1 g Cost	1 g Cost	0.1 g Cost
TPH	€1,200	€120.00	€612.00	€61.20
TPM01	€2,200	€220.00	€195.00	€19.50
TPM02	€2,403	€240.30	€340.00	€34.00
TPM03	€1,815	€181.50	€205.00	€20.50
TPM04	€2,100	€210.00	€330.00	€33.00

Note: TP = tracer particle. TPH = TPH01, TPH02 and TPH03; costs to produce TPH01, TPH02 and TPH03 are identical. Costs were obtained from 3D MicroPrint (personal communication, 2026) and Horizon Microtechnologies (personal communication, 2026).
[a]Costs for 1,000 g of TPH are derived from the retail cost to produce 10 g of TP (€8,500), assuming a 20% discount to produce 100 g of TP and a further 10% discount to the 100 g cost (€68,000) to produce 1,000 g TP.

8.1.3 Comparison of Tracer Particle Costs

The per-gram costs to produce TPs by GTK, 3D MicroPrint and Horizon Microtechnologies are provided in Figure 36 and Figure 37. As the costs to produce the TPs by GTK are manufacturing costs, the costs on a per-gram basis are not dependent on the quantity of TPs commissioned. The costs of outsourced 3D printed TPs should be treated as indicative, as these were provided to produce TPs for the MaDiTraCe project only. Similarly, these costs are retail costs, which cover production costs and overhead expenses and include a profit margin. Strategic collaborations with these companies to produce TPs for traceability purposes may reduce per-unit costs considerably. The manufacturing costs from outsourcing partners are therefore unknown but will likely be significantly lower and potentially comparable to the manufacturing costs of the GTK TPs.

Funded by the European Union

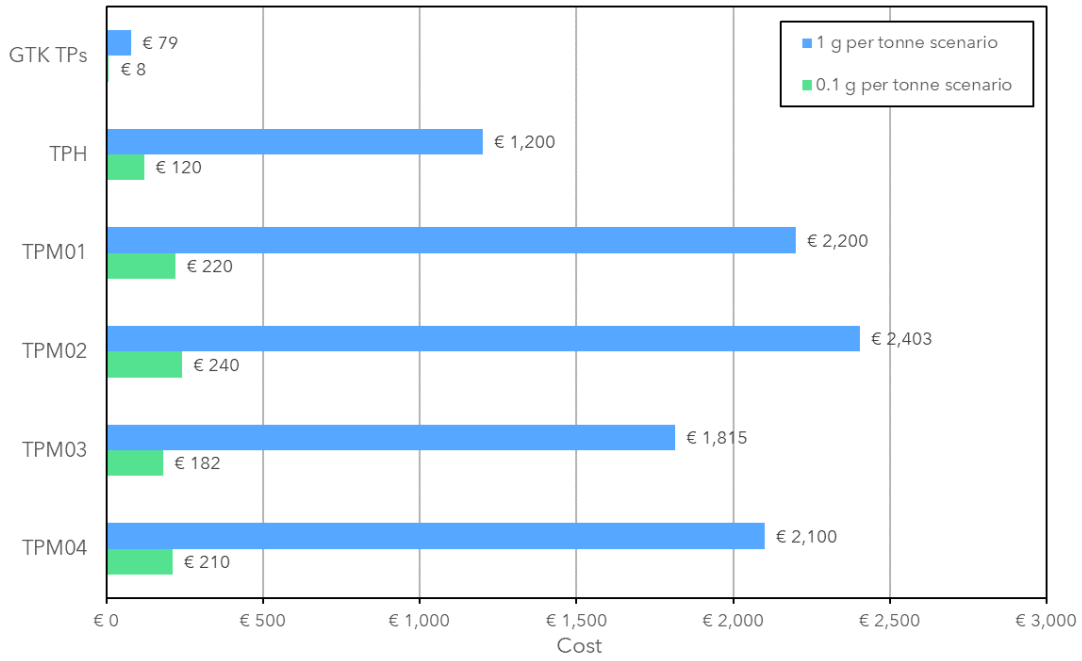

Figure 36. Per-gram GTK manufacturing cost and outsourcing partner retail costs associated with the commissioned production of 1 g of tracer particles.

Note: TP = tracer particle; TPH = TPH01, TPH02 and TPH03. Costs are rounded to the nearest Euro; only GTK costs are manufacturing costs. TPH and TPM costs were obtained from Horizon Microtechnologies (personal communication, 2026) and 3D MicroPrint (personal communication, 2026).

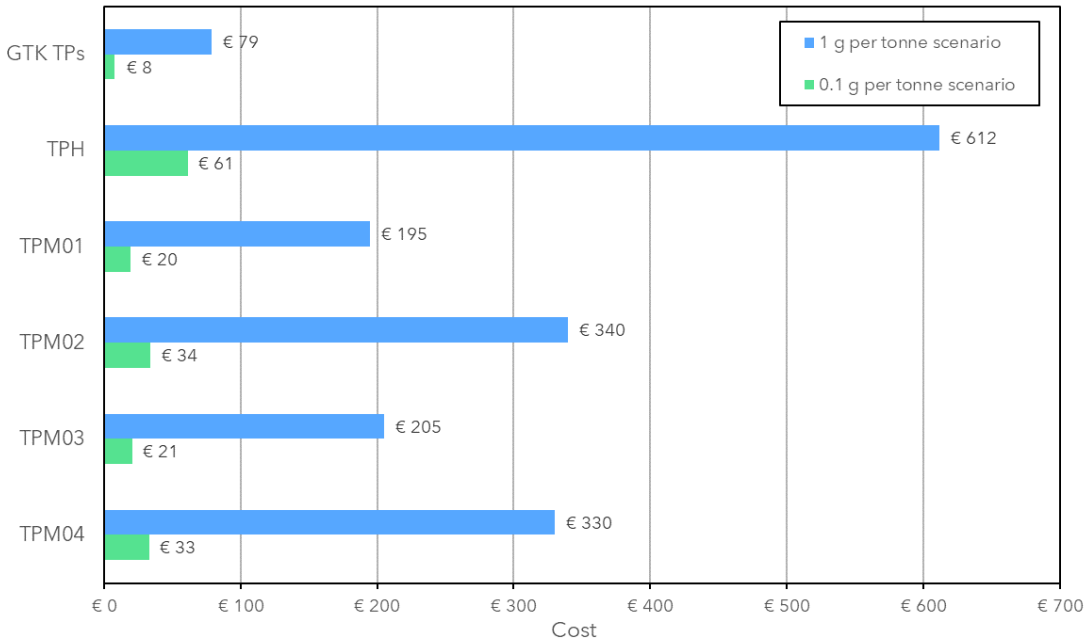

Figure 37. Per-gram GTK manufacturing cost and outsourcing partner retail costs associated with the commissioned production of 1,000 g of tracer particles.

Note: TP = tracer particle; TPH = TPH01, TPH02 and TPH03. Costs are rounded to the nearest Euro; only GTK costs are manufacturing costs; costs for 1,000 g of TPH01, TPH02 and TPH03 (TPH) were estimated from the retail cost to produce 10 g of TP (€8,500), assuming a 20% discount to produce 100 g of TPs and a further 10% discount to the 100 g cost (€68,000) to produce 1,000 g of TPs. TPH and TPM costs were obtained from Horizon Microtechnologies (personal communication, 2026) and 3D MicroPrint (personal communication, 2026).

Funded by the European Union

8.2 Comparison of Critical Raw Material Prices and Tracer Particle Costs

A preliminary assessment of the price premiums associated with AFP technology across selected CRMs was conducted (Figure 38 and Figure 39; 13.4 Appendix IV: Cost Evaluation Data). This evaluation has considered manufacturing and retail costs only and has not considered other CapEx and operational expenditure (OpEx) costs that may be associated with the implementation of AFP technology (e.g., sampling requirements, analytical verification, costs associated with integration of AFP technology with other traceability systems, auditing, etc.). Additionally, while certain TP and CRM combinations may present physicochemical behaviours that would prevent field implementation, these combinations were evaluated to illustrate the broader sensitivities of premium variances across different CRMs.

This evaluation has highlighted that the costs of TPs alone can contribute a significant price premium to CRMs depending on the MED required. Price premiums range from a nominal 0.04% (e.g., the use of 0.1 g of TPM01 per tonne of cobalt hydroxide) to an economically prohibitive 133% premium (e.g., the use of 1 g of TPH per tonne of 94–95% C natural graphite concentrate (-100 mesh)). Although companies have reported paying a price premium or "green premium" for traceable CRMs (Gagnon et al., 2026), it is unclear what premium companies would be willing to pay for the integration of new traceability methods, including AFP, and whether some of the demonstrated price premiums associated with AFP would be commercially acceptable. Furthermore, the costs of TP production have been compared to the March 2026 average commodity prices only, and CRM supply chains are susceptible to price volatility and tight profit margins, which could impact the feasibility for the long-term use of AFP technology.

Funded by the European Union

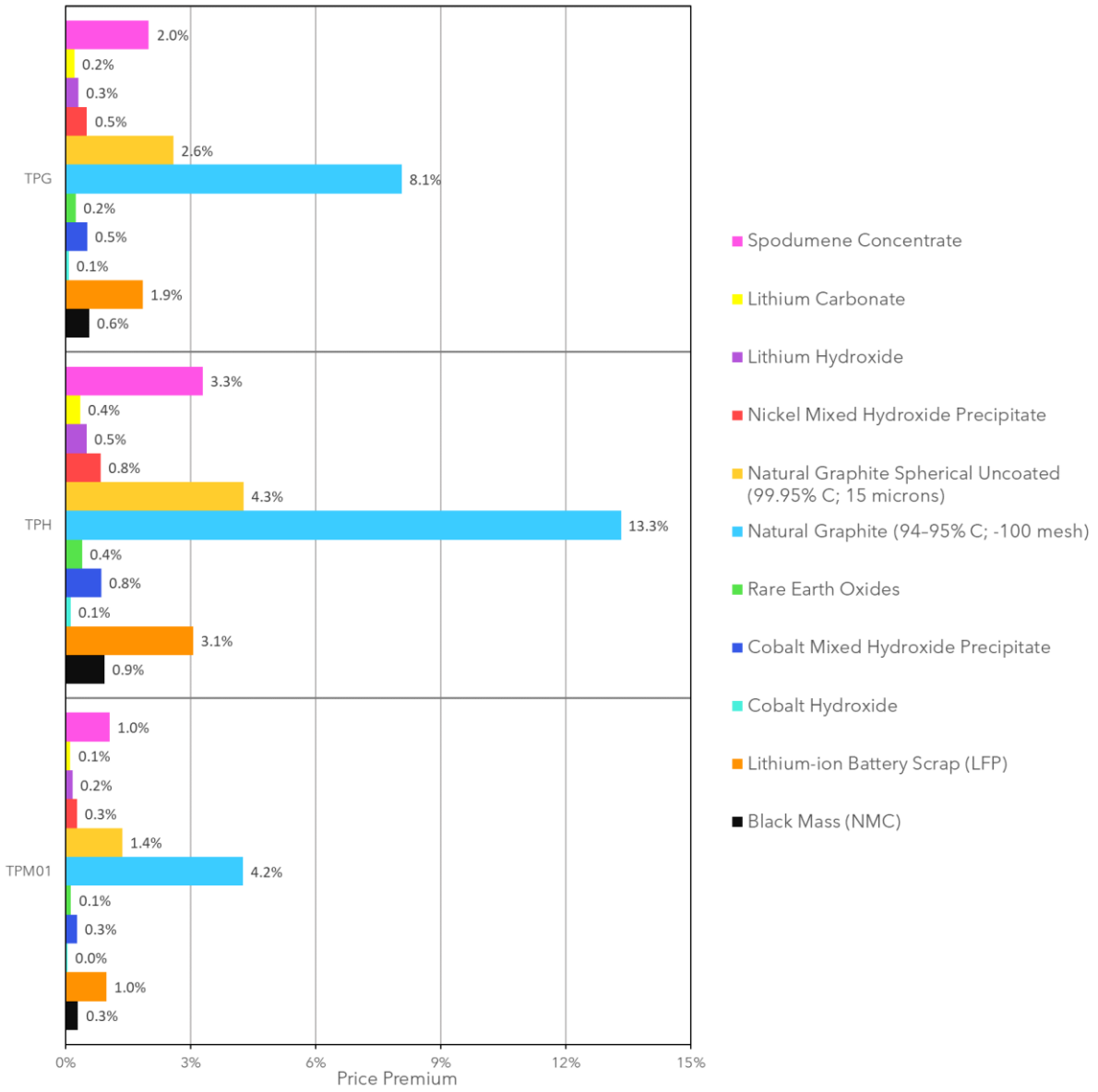

Figure 38. Price premiums on different critical raw materials determined from the costs of tagging one tonne of commodity with 0.1 g of tracer particles.

Note: NMC = nickel manganese cobalt; LFP = lithium iron phosphate; TPG = GTK tracer particles (TPs); TPH = TPH01, TPH02 and TPH03. GTK TP costs are based on the manufacturing costs of 0.1 g of TP; TPH and TPM01 costs are based on the lowest per-gram price provided by or estimated from outsourcing partner quotations (i.e. derived from the costs associated with the production of 1,000 g of each TP). The lithium-ion battery scrap (LFP) price is the commodity's gate fee. Critical raw material prices were provided by Benchmark Mineral Intelligence (2026).

Funded by the European Union

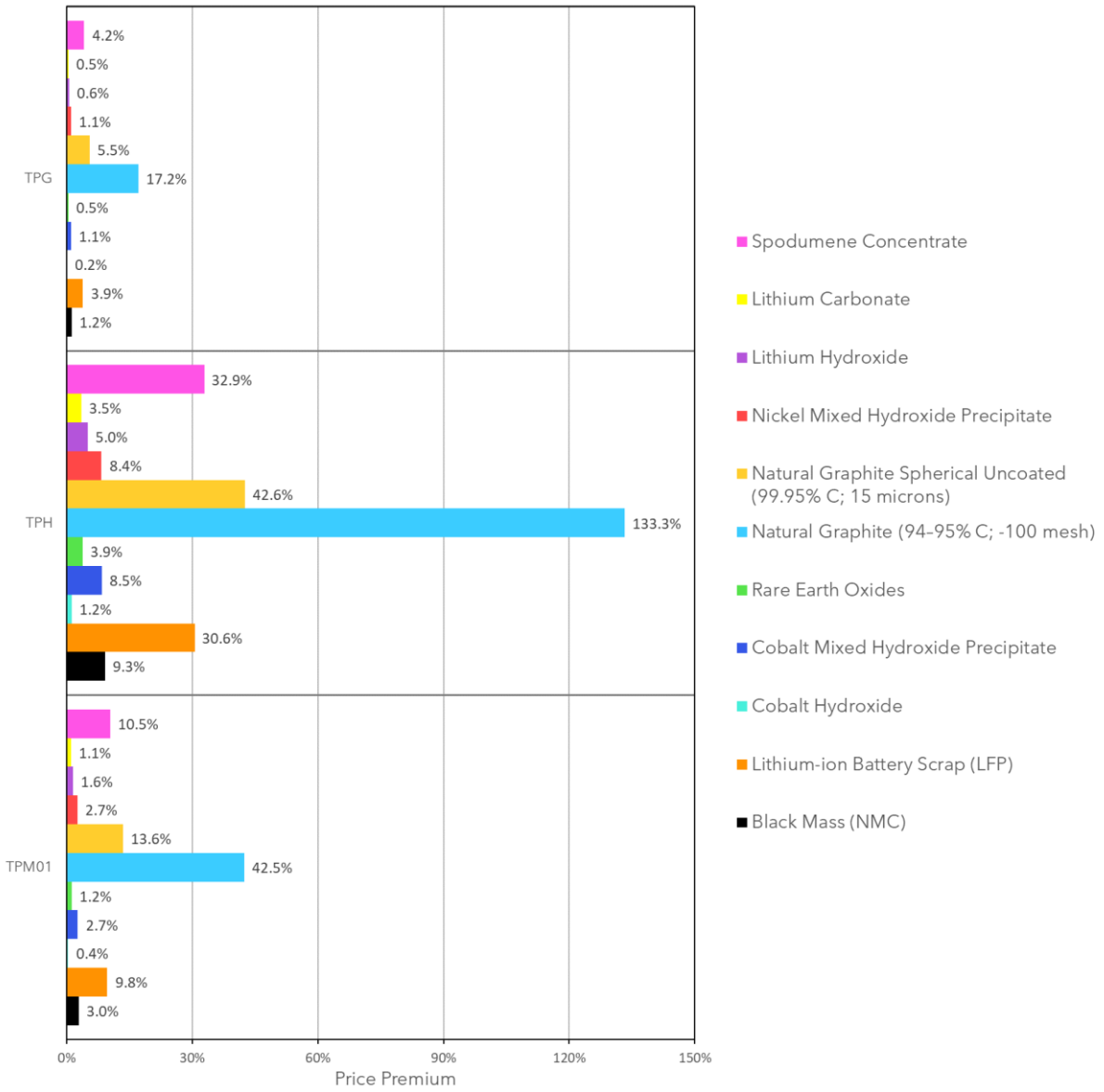

Figure 39. Price premiums on different critical raw materials determined from the costs of tagging one tonne of commodity with 1 g of tracer particles.

Note: NMC = nickel manganese cobalt; LFP = lithium iron phosphate; TP = tracer particle; TPG = GTK TPs; TPH = TPH01, TPH02 and TPH03. GTK TP costs are based on the manufacturing costs of 1 g of TP; TPH and TPM01 costs are based on the lowest per-gram price provided by or estimated from outsourcing partner quotations (i.e. derived from the costs associated with the production of 1,000 g of each TP). The lithium-ion battery scrap (LFP) price is the commodity's gate fee. Critical raw material prices were provided by Benchmark Mineral Intelligence (2026).

8.3 Other Considerations

To determine a TP price per mass of host material, there are other factors that must be considered, which considerably influence actual AFP implementation costs beyond TP production costs. For example, costs can depend on the level of required encoding within TPs and the required modifications to match TPs properties with different products, the minimum effective dosage, the application and blending workflows, sampling workflows,

Funded by the European Union

detection workflows, infrastructure requirements and the quantities of host material being traded.

Additionally, the operational methodology and sophistication of verification methods required for TPs will also have a significant impact on cost. For certain TPs with simple encoding, such as integrated fluorescence (e.g., TPG01, TPH01), external lettering (e.g., TPM02, TPM04) or external micro QR codes (e.g., TPM01, TPM04), a qualitative or low-level scale of verification such as visual confirmation only, confirmation using UV torches, or confirmation through scanning using a mobile phone would involve minimal costs. Whereas TPs which contain a higher encoding factor, such as TPs with covert encoding (e.g., the internal micro QR codes in TPM05) or TPs with intrinsic chemical fingerprints, may require formal analytical validation and certification. This higher level of verification may mandate the integration of certified and independent third-party service providers to manage field sampling, laboratory testing and CoC auditing. However, outsourcing responsibilities to these independent entities will introduce service fees. Furthermore, more sophisticated methods of verification could be associated with longer turnaround times, potentially increasing carrying or demurrage costs of tagged material pending the reception of results.

AFP implementation costs will be heavily dictated by whether the AFP technology is systemically applied across all CRM consignments or through a spot-checking methodology. Under a spot-checking methodology, stakeholders would be informed that any consignment may be selected for unannounced and covert TP integration and subsequent CoC verification. This would mitigate the costs that would otherwise be associated with the continuous tracing of every consignment under a systematic traceability system. However, this would require independent third-party intervention at critical points along the supply chain (e.g., mine-site or at processing facilities), which may inadvertently disclose which consignments have been selected for AFP integration, or may require specialised automated TP deployment and verification infrastructure at these same locations.

The commercial suppliers of TPs for this project advised that more advanced applications of TP technologies are typically implemented under a multi-year technology licensing agreement (TLA). As part of TLAs, standard royalties or fees would be included, and TPs would not be purchased on a price-per-quantity basis as part of these agreements. Similarly, 3D printed TP technologies in practice may also not be purchased on a quantity basis.

Funded by
the European Union

9 Conclusions

The traceability of complex global CRM supply chains is a critical prerequisite to ensure their sustainable supply for green technologies and to meet net-zero ambitions. To evaluate the use of AFP to trace CRM supply chains, Deliverable 2.6 of the MaDiTraCe project conducted proof-of-concept validation of 3D printed and commercially sourced TPs at TRL 3 and technologically validated the use of these TPs with CRMs in a laboratory setting at TRL 4. The results of the novel test methodologies (e.g., ageing under ambient conditions, ageing at higher temperatures and humidity of up to 75°C and 85% RH, simulated maritime transport, etc.) distinguished between TPs which had commercially enabling behaviours from those which had commercially disabling behaviours, and identified CRMs which may be particularly challenging for use with AFP technologies.

Polymer-based 3D printed TPs and commercially sourced TPs demonstrated resilience when subjected to different ageing tests and real-world or simulated transportation tests, and maintained their pre-test physical properties, detectability, distribution and fluorescence. 3D printed polymer and metal alloy, and commercially sourced TPs were all readily detectable using low-cost, laboratory and portable detection configurations, which serves as proof-of-concept that these TPs could be easily detected or authenticated in bulk CRM. TPs made from metal alloys (e.g., such as CuCrZr (TPM01 and TPM02) and stainless steel (TPM03)) reacted unfavourably as part of certain tests. Following interactions with moisture, air and sulphur-bearing host materials during artificial climate ageing and transportation tests, these metal-alloy TPs suffered from surface chemical degradation, tarnishing and pitting. Additionally, these TPs experienced significant gravity-driven segregation during simulated transportation tests, likely because of their higher densities relative to the host materials to which they were applied, which may limit their application.

The physicochemical properties of specific host materials may compromise TP implementation and performance. While polymer TPs could be more readily used within a range of commodities as they do not contain regulated elements or compounds, TPs made from metal alloys contain elements that are industrially regulated which will restrict their usage, unless suitable mechanisms to recover or remove these TPs are developed. TPs were easily identified within host materials, such as mixed hydroxide precipitate due to favourable surface adhesion, but were not easily identifiable within black mass, possibly as a result of masking effects and/or the light-absorbing properties of the host material. These varied behaviours highlight that TPs must be precisely engineered to match the physical and chemical properties of CRMs to be commercially viable.

Proof-of-concept laboratory tests conducted by Microtrace on their proprietary Molecular™ Taggant System confirmed AFP technologies can be used to support the detection of CRM dilution or adulteration. This capability is commercially significant as CRMs from disparate sources are frequently blended either legitimately under sustainable CoC models or illicitly to adulterate cargo.

Incorporating the results from minimum effective dosage tests, which determined TPs can be applied at dosages of single-digit parts per million or one-hundred parts per billion, with calculated in-house 3D printed TP production costs, indicated that the commercial feasibility of AFP technologies depends significantly on the market value of the CRM to be

Funded by the European Union

traced. Lower-purity and lower-value CRMs may yield economically discouraging or prohibitive price premiums whereas higher-purity and higher-value CRMs can more readily absorb the marginal price premiums.

Ultimately, the conclusions regarding the detectability, abundance, distribution, minimum effective dosage, and host material performance are based on proof-of-concept testing using standard, non-optimised TPs. The inherent properties of evaluated TPs varied significantly in terms of sizing, morphology, and encoding configurations, rendering direct comparison impossible. These results should not be interpreted as commercial specifications or as representative of an optimised commercial deployment, where particle selection, loading level, application method, and detection workflow would be engineered around the specific use case.

Funded by
the European Union

10 Recommendations

Following the successful laboratory validation of 3D printed and commercially sourced TPs as part of this study, the scaling of AFP technology into CRM traceability systems requires dedicated optimisation of TP properties across entire CRM supply chains and the identification or development of specialised industrial deployment technologies.

Tailored engineering of TP properties is necessary to match both the CRMs tested within this study and other CRMs. Determination of the mechanisms behind physical, chemical and biological reactions that may affect TP performance within CRMs, under conditions and durations which were not tested as part of the study, should be investigated. The tailoring of TPs must also account for specific traceability or operational goals, such as covert or overt traceability, the sophistication of encoding required for authentication and whether TPs will be used to detect dilution. Furthermore, as this study evaluated the use of AFP within predominantly upstream and entirely particulate raw materials, further work would require the evaluation of AFP with lower volume, solid or manufactured products. To ensure AFP can cover entire CRM supply chains, alternative AFP technologies, such as DNA or molecular systems, should be evaluated with these other forms of CRMs.

Optimisation of 3D printed TP properties to reduce production costs is also required. Once mechanisms which affect TP behaviours are well understood, a review of more sustainable materials for the production of TPs and the related lightweighting of TPs should be carried out. Critically, 3D printing workflows should also be scaled towards industrial, automated and higher-throughput systems. This would reduce production costs and provide the opportunity to produce 3D printed TPs at a higher resolution with higher levels of encoding and properties that more closely resemble CRM properties, such as raw material particle sizing and particle morphology. Assessment of industrial processes where AFP technology can be readily included without unreasonably increasing CapEx or OpEx is a foundational requirement for this technology to be accepted industrially.

Once feasible routes for the industrial implementation of AFP within CRM supply chains have been determined, and based on findings from this study, industrial cooperation and pilot-scale testing would be required. We believe this technology would be of interest to stakeholders throughout CRM supply chains, from suppliers and traders to original equipment manufacturers, and these parties should be engaged to develop AFP technology as part of pilot trials. These pilot trials should evaluate how AFP can be integrated with other traceability mechanisms and systems developed as part of MaDiTraCe, such as MFP, DPPs and certification schemes.

Significantly, while AFP was tested with a selection of CRMs within lithium-ion battery supply chains in this study, the scope of AFP should be widened across the broader metals and minerals sector. Future work should consider expanding the use case of AFP for other raw materials, especially as some raw materials have much higher inherent values (e.g., gold), which may make the technology more economically feasible.

Funded by
the European Union

11 References

Arató, R., Shang, Y., Pierrot, G. H., Losno, D., Moradell Casellas, A., Obbágy-Arató, G., Amri, O., Peralta, D., Perret, S., Rado, C., Suarez Criado, L., Dehaine, Q., Dèzes, M., Bordereau, N., Lohier, T., & Desaulty, A.-M. (2026). *Methodology for lab-based geoforensic supply chain due diligence audits* (Deliverable D2.4, Version No. 2.1). MaDiTraCe Project. https://www.maditrace.eu/results

Aurubis Stolberg. (2026). *Material Datasheet CuCrZr.* EN_2026_01. https://www.aurubis.com/dam/jcr:d6d50d64-69d6-4742-821d-8fb8b48c9044/cucrzr-c18160-pna-372_en.pdf

Benchmark Mineral Intelligence (2026). *Prices.* https://prices.benchmarkminerals.com/

Bhavsar P., Bhave M., & Webb, H. K. (2023). Solving the plastic dilemma: The fungal and bacterial biodegradability of polyurethanes. *World Journal of Microbiology and Biotechnology, 39*, Article 122. https://doi.org/10.1007/s11274-023-03558-8

Boston Micro Fabrication. (2026, June 16). *Materials.* https://bmf3d.com/micro-3d-printing-materials/

Boston Micro Fabrication. (2026, June 16). *microArch S240.* https://bmf3d.com/microarch-s240/

British Standards Institution. (2020). *Code of practice for ground investigations* (BS 5930:2015+A1:2020). https://knowledge.bsigroup.com/products/code-of-practice-for-ground-investigations

Brossia, C. S., & Kelly, R. G. (1998). Occluded solution chemistry control and the role of alloy sulfur on the initiation of crevice corrosion in type 304ss. *Corrosion Science, 40*(11), 1851–1871.

Buckby, T., Black, S., Coleman, M. L., & Hodson, M. E. (2003). Fe-sulphate-rich evaporative mineral precipitates from the Río Tinto, southwest Spain. *Mineralogical Magazine, 67*(2), 263–278. https://doi.org/10.1180/0026461036720104

Bureau of Meteorology. (2026, April 22). *Climate statistics for Australian locations: Monthly climate statistics for Marble Bar (Site 004106).* http://www.bom.gov.au/climate/averages/tables/cw_004106_All.shtml

Chang B. P., Mohanty, A.K., & Misra, M. (2020). Studies on the durability of sustainable biobased composites: a review. *RSC Advances, 10*(31), 17955–17999. https://doi.org/10.1039/c9ra09554c

Chemical Industry Federation of Finland, & Trade Union Pro. (2025). *Collective agreement for salaried employees in the Finnish chemical industry 2025–2027*. https://proliitto.fi/sites/default/files/2026-02/collective-agreement-for-salaried-employees-in-the-finnish-chemical-industry-2025-2027.pdf

Davison, L., & Springman, S. (2025, August 11). *Soil description and classification*. University of the West of England. https://environment.uwe.ac.uk/geocal/SoilMech/classification/default.htm

Desaulty, A.-M., Alatalo, W., Arato, R., Aupart, C., Bodereau, N., Moradell Casellas, A., Obbagy-Arato, G., Shang, Y., Soini, T., & Virokannas, D. (2026). *Methodology for on-site material flow characterization* (Deliverable D2.3, Version No. 2). MaDiTraCe Project. https://www.maditrace.eu/results

Desaulty, A.-M., Arato, R., Dehaine, Q., Dèzes, M., Pierrot, G. H., Losno, D., Moradell Casellas, A., Obbagy-Arato, G., Peralta, D., Perret, S., Rado, C., Shang, Y., & Suarez Criado, L. (2026). *Fingerprinting and tracing under controlled conditions along battery and magnet production chains* (Deliverable D2.2, Version No. 1). MaDiTraCe Project. https://www.maditrace.eu/results

De Beers Group (2026, April 24). *News from our businesses and markets.* De Beers forevermark inscribes two millionth diamond. https://www.debeersgroup.com/news-insights/business-market/archive/forevermark-inscribes-two-millionth-diamond

Donnelly, L., Dehaine, Q., Ghosh, S., Corfe, I., Dunn, R., & Pop, D. (2023). *A Review of Artificial Fingerprinting and 3D Printing for the Potential Tracking of Minerals in Complex Supply Chains* (Deliverable D2.1, Version No. 1.0). MaDiTraCe Project. https://doi.org/10.5281/zenodo.14253161

Donnelly, L., Dunn, R., Pirrie, D., Jarvis, M., & Lightfoot, C. (2023). Oxidation of copper concentrates. The Institute of Materials, Minerals and Mining, *Materials World,* December 2022/January 2023, 55–57. https://www.iom3.org/resource/investigating-the-oxidation-of-copper-concentrates.html

European Parliament, & Council of the European Union. (2023). *Regulation (EU) 2023/1542 of the European Parliament and of the Council of 12 July 2023 concerning batteries and waste batteries* (Consolidated text, 2025, July 31). EUR-Lex. https://eur-lex.europa.eu/eli/reg/2023/1542/2025-07-31

Eurostat. (2026). *Electricity prices for non-household consumers - bi-annual data (from 2007 onwards)* (Dataset nrg_pc_205; 2025-S2) [Data set]. European Commission. https://doi.org/10.2908/NRG_PC_205

Gagnon, F., Hegarty, A., & Raboca, J. (2026). *Critical Mineral Traceability for Energy and Economic Security.* https://www.iea.org/reports/critical-mineral-traceability-for-energy-and-economic-security

Ghaderi, A., Abdollahi, F., & Biglari, M. (2024). Copper-sulfur interactions leading to the formation of S-containing compounds. *Tetrahedron Letters*, *143*, Article 155112. https://doi.org/10.1016/j.tetlet.2024.155112

Ge, Q., Li, Z., Wang, Z., Kowsari, K., Zhang, W., He, X., Zhou, J., & Fang, N. X. (2020). Projection micro stereolithography based 3D printing and its applications. *International Journal of Extreme Manufacturing, 2*(2), Article 022004. https://doi.org/10.1088/2631-7990/ab8d9a

Grohol, M., & Veeh, C. (2023). *Study on the critical raw materials for the EU 2023: Final report*. Publications Office of the European Union. https://doi.org/10.2873/725585

Gu, J.-G., & Gu, J.-D. (2005). Methods currently used in testing microbiological degradation and deterioration of a wide range of polymeric materials with various degree of degradability: A review. *Journal of Polymers and the Environment, 13*(1), 65–74. https://doi.org/10.1007/s10924-004-1230-7

Haelixa. (2026, April 24). *Provenance Proof's Partnership with Haelixa to Track Emerald Origins.* https://haelixa.com/customer-story/provenance-proof-partners-with-haelixa-to-track-emerald-origin/

Hara, M. (2019). Development and popularization of QR code: Code development pursuing reading performance and market forming by open strategy. *Synthesiology English Edition, 12*(1), 19–28. https://doi.org/10.5571/syntheng.12.1_19

Horizon Microtechnologies (2026, June 16). Precision Microfabrication for Next Generation Devices. https://horizonmicrotechnologies.com/

Hyperledger Foundation. (2019). *Circulor achieves first-ever mine-to-manufacturer traceability of a conflict mineral with Hyperledger Fabric* [Case study]. LF Decentralized Trust. https://www.lfdecentralizedtrust.org/hubfs/Hyperledger/Printables/Hyperledger_CaseStudy_Tantalum_Print.pdf

International Association of Dry Cargo Shipowners. (2025). *Bulk Carrier Casualty Report; Years 2015 to 2024 and trends.* https://www.intercargo.org/wp-content/uploads/2025/03/INTERCARGO-Bulk-Carrier-Casualty-Report_2025-Pages.pdf

International Maritime Organization. (2025). *IMSBC Code: International Maritime Solid Bulk Cargoes Code and supplement* (2025 ed.). https://doi.org/10.62454/KM260E

International Organization for Standardization. (2021). *Copper, lead, zinc and nickel concentrates — Sampling procedures for determination of metal and moisture content* (ISO Standard No. 12743:2021). https://www.iso.org/standard/81126.html

International Organization for Standardization. (2020). *Chain of custody — General terminology and models* (ISO Standard No. 22095:2020). https://www.iso.org/standard/72532.html

International Organization for Standardization. (2017a). *Geotechnical investigation and testing — Identification and classification of soil — Part 1: Identification and description* (ISO Standard No. 14688-1:2017). https://www.iso.org/standard/66345.html

International Organization for Standardization. (2017b). *Geotechnical investigation and testing — Identification, description and classification of rock* (ISO Standard No. 14689:2017). https://www.iso.org/standard/66347.html

International Organization for Standardization. (2006). *Copper, lead, zinc and nickel concentrates — Determination of mass loss of bulk material on drying* (ISO Standard No. 10251:2006). https://www.iso.org/standard/41316.html

Karrach, L., Pivarčiová, E., & Bozek, P. (2020). Recognition of perspective distorted QR codes with a partially damaged finder pattern in real scene images. *Applied Sciences, 10*(21), Article 7814. https://doi.org/10.3390/app10217814

Karup-Møller, S. (1973). Nickelhexahydrite from Finland. *Bulletin of the Geological Society of Finland, 45*(2), 155–158.

Khodadadmahmoudi, G., Tabar, K. J., Homayouni, A. H., & Chelgani, S. C. (2023). Recycling spent lithium batteries – an overview of pretreatment flowsheet development based on metallurgical factors. *Environmental Technology Reviews, 12*(1), Article 2248559. https://doi.org/10.1080/21622515.2023.2248559

Kijchavengkul, T., Auras, R., Rubino, M., Alvarado, E., Montero, J. R. C., & Rosales, J. M. (2010). Atmospheric and soil degradation of aliphatic-aromatic polyester films. *Polymer Degradation Stability, 95*(2), 99–107.

Krumbein, W. C., & Sloss, L. L. (1963). *Stratigraphy and sedimentation* (2nd ed.). W. H. Freeman and Company.

Leinberger, D. A. (2006). Temperature and humidity in ocean containers. *In Proceedings of Dimensions.06*. International Safe Transit Association, USA.

Li, P., Yang, J., Jiménez-Carvelo, A. M., & Erasmus, S. W. (2024). Applications of food packaging quick response codes in information transmission toward food supply chain integrity. *Trends in Food Science & Technology, 146*, Article 104384. https://doi.org/10.1016/j.tifs.2024.104384

Lu, T., Solis-Ramos, E., Yi, Y., & Kumosa. M. (2018). UV degradation model for polymers and polymer matrix composites. *Polymer Degradation and Stability, 154*, 203–210.

Markovičová, L., & Zatkalíková, V. (2019). The effect of UV aging on structural polymers. *IOP Conference Series: Materials Science and Engineering, 465*(1), Article 012004. https://doi.org/10.1088/1757-899X/465/1/012004

Marquez, L., Dunstall, S., Bartholdi, J., & MacCawley, A. (2012). 'Cool or Hot': A Study of Container Temperatures in Australian Wine Shipments. *Australasian Journal of Regional Studies, 18*(3), 420–443.

Microtrace. (2026a, April 24). *Diamond and Gemstone Provenance*. https://www.microtracesolutions.com/industries/diamond-and-gemstone-provenance

Microtrace. (2026b, April 24). *What is a Taggant?* https://www.microtracesolutions.com/what-is-a-taggant

Munsell Color. (2009). Munsell soil color book. X-Rite.

Prabhakar, M. M., Saravanan, A. K., Lenin, A. H., Leno, I. J., Mayandi, K., & Ramalingam, P. S. (2021). A short review on 3D printing methods, process parameters and materials. *Materials Today: Proceedings*, 45, 6108–6114. https://doi.org/10.1016/j.matpr.2020.10.225

Olsson, C.-O. A., & Landolt, D. (2003). Passive films on stainless steels—Chemistry, structure and growth. *Electrochimica Acta, 48*(9), 1093–1104.

Retamal, J. I., Robles, P. A., Quezada, G. R., & Jeldres, R. I. (2024). Molecular design and spodumene flotation—A review. *International Journal of Molecular Sciences, 25*(6), Article 3227. https://doi.org/10.3390/ijms25063227

Reuters. (2024, January 12). *Ice-encrusted runners take on Siberian marathon at -52C*. Reuters Connect. https://www.reutersconnect.com/item/ice-encrusted-runners-take-on-siberian-marathon-at-52c/dGFnOnJldXRlcnMuY29tLDIwMjQ6bmV3c21sX1JDMkZHNUFLV0l3Tg

Scandit. (2026, June 17). *Micro QR code*. https://www.scandit.com/products/barcode-scanning/symbologies/micro-qr-code/

Singh, S. P., Saha, K., Singh, J., & Sandhu, A. P. S. (2011). Measurement and Analysis of Vibration and Temperature Levels in Global Intermodal Container Shipments on Truck, Rail and Ship. *Packaging Technology and Science, 25*(3), 149–160. https://doi.org/10.1002/pts.968

Time and Date. (2026, April 20). *Weather in Liverpool, England, United Kingdom*. https://www.timeanddate.com/weather/uk/liverpool

The German Insurance Association. (2026, April 22). *Container climate*. https://www.tis-gdv.de/tis_e/containe/klima/klima-htm/#klima

3D MicroPrint. (2026, March 31). *Our technology*. https://3dmicroprint.com/en/technologie/

3D Microprint. (2025a). *Material data sheet. 2.1293 | CuCr1Zr | C18150*. Rev 1. *https://3dmicroprint.com/wp-content/uploads/2025/07/Materialdatenblatt_2.1293_CuCr1Zr-1.pdf*

3D Microprint. (2025b). *Material data sheet. 1.4542 | 17-4PH*. Rev 2. *https://3dmicroprint.com/wp-content/uploads/2025/09/Materialdatenblatt_1.4542_stainless_steel_A4_rev2.pdf*

3D MicroPrint. (2019). *1 Technology*. Version 04 – 01/2019. https://3dmicroprint.com/wp-content/uploads/2025/07/Technologie_EN_v04_Download.pdf

Tracerco. (2026, May 7). *Fuel marking technology*. https://tracerco.com/fuel-marking-technology/#:~:text=Gold%20standard%20forensic%20methods%20of,nitrogen%20(CHON)%20are%20used.

U.S. Congress, Office of Technology Assessment. (1980). *Taggants in explosives* (OTA-ISC-116). U.S. Government Printing Office.

United Nations Conference on Trade and Development. (2025). *Review of maritime transport 2025: Staying the course in turbulent waters* (UNCTAD/RMT/2025). United Nations. https://unctad.org/system/files/official-document/rmt2025_en.pdf

Vanstron Automation. (2025). *Inline; Laser marker machine*. Special for PCB / FPC/ IC Chips / ceramic; traceability application [Brochure]. https://accelonix.nl/wp-content/uploads/2025-inline-laser-marking-machine.pdf

World Health Organization (2026, May 20). *Ultraviolet radiation*. www.who.int/health-topics/ultraviolet-radiation

WTA Group. (2026, April 17). *How long does sea freight take?* https://www.wtagroup.com/resources-and-insights/blogs/how-long-does-sea-freight-take#:~:text=Speed%20of%20sea%20freight%20breakdown,45%20days%20to%20West%20Australia

Yuen, P. C., Sasa, K., Kawahara, H., & Chen, C. (2022). Statistical estimation of container condensation in marine transportation between Far East Asia and Europe. *The Journal of Navigation, 75*(1), 176–199. https://doi.org/10.1017/S0373463321000746

Zurich Cantonal Bank. (2025). *Unser Traceable Gold: Dank Innovation zu mehr Transparenz im Goldhandel*. [Our Traceable Gold: Thanks to innovation for more transparency in the gold trade]. [Brochure]. https://www.zkb.ch/media/zkb/dokumente/broschueren/Traceable_Gold_Online.pdf

12 Acknowledgements

The authors gratefully acknowledge the staff at LMA B.V. (an AHK Group laboratory in the Netherlands and an affiliated entity on the project) and AHK's John Knight Laboratory (UK) for providing physical and elemental analytical results. Sincere thanks are also extended to the team at ASMIN Industrial Ltda (an AHK Group company headquartered in Santiago, Chile) for their in-kind contributions of providing XRD and automated mineralogy data. AHK's Health and Safety, FMP-TML, Market Intelligence and Facilities Departments are acknowledged for their critical assistance on the project.

Dr Duncan Pirrie at Helford Geoscience LLP and Dr Matt Power at Vidence Inc. are recognised for providing automated mineralogy results for the graphite concentrate and black mass. ProGraphite GmbH contributed additional elemental and physical data for the graphite concentrate. 3D MicroPrint and Horizon Microtechnologies are acknowledged for their assistance with the fabrication of 3D printed TPs. The authors also thank GT Vision Ltd for their guidance in selecting a digital microscope; and JB Environmental Engineering Ltd for supplying the environmental test chamber.

Finally, appreciation is extended to TraceTag and Microtrace for providing TPs for evaluation as part of this project, and for graciously permitting the public disclosure of the resulting data.

13 Appendices

13.1 Appendix I: Additional Tracer Particle Imagery

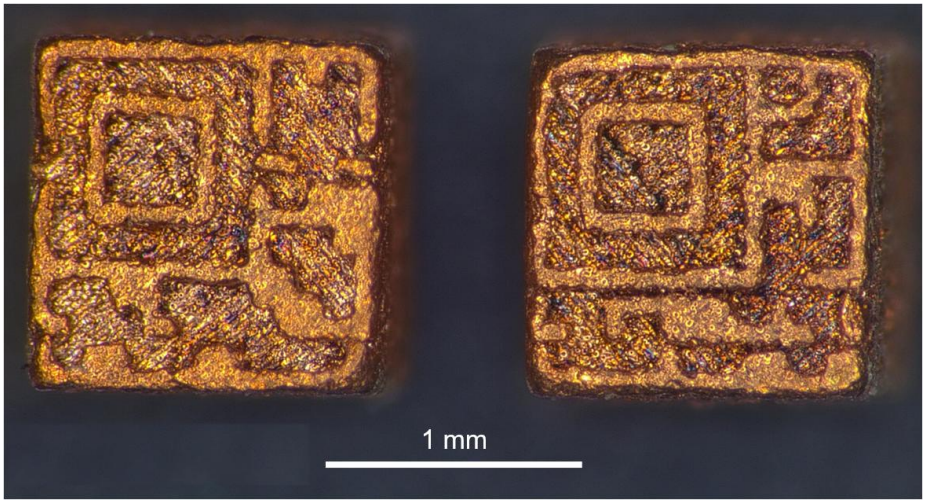

Figure I-1. TPM01 CuCrZr alloy (2.1293) tracer particles and micro QR codes used for encoding.

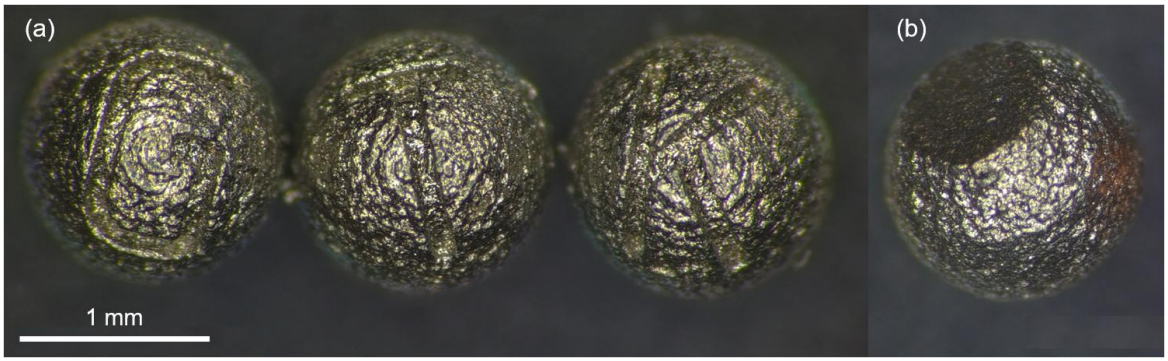

Figure I-2. Stainless steel (1.4542) (TPM04) tracer particles with lettering. (a) TPM04 tracer particles printed with the letters "G", "T" and "K", and (b) Flat base of TPM04, revealing its truncated sphere shape.

Funded by the European Union

13.2 Appendix II: Host Material Characterisation

Various analytical methods were used to determine the characteristics of the host materials. These include:

1. Material description: Determination of the properties of host materials according to ISO 14688-1:2017 and ISO 14689:2017. Certain aspects of these standards were adapted where appropriate for particular host materials (e.g., consideration of agglomerate properties).
2. Laser Particle Sizing: Laser particle size distribution analysis was undertaken using a Malvern Panalytical Mastersizer 3000 instrument. All samples submitted for laser particle sizing were sieved to <2 mm prior to analysis.
3. Physical analysis: Determination of moisture content and susceptibility to oxidation, decomposition or sublimation according to ISO 10251:2006, and determination of the host material's specific gravity, true density, bulk density and tapped density.
4. Multi-element geochemical analysis: Determination of the elemental content of the different host materials through various analytical methods, including Carbon-Sulphur Combustion-IR Analysis (C/SA), Cold Vapour Atomic Absorption Spectroscopy (CVAAS), Combustion Ion Chromatography (CIC), Ion Chromatography (IC) (H_2O solution), ICP-OES, ICP-MS, Instrumental Gas Analysis (IGA) and XRF.
5. Modal mineralogy: XRD (Rietveld method using TOPAS software) and automated SEM-EDS using either Tescan TIMA™ (Tescan Integrated Mineral Analyser) software (for lithium ore, spodumene concentrate, nickel concentrate and MHP) or Advanced Mineral Identification and Characterisation System (AMICS) software (for graphite concentrate and black mass). Unless stated otherwise, analyses were conducted on natural state samples. Compositional groups for host materials analysed using SEM-EDS with Tescan TIMA™ software are provided in Table II-1. Compositional groups for graphite concentrate and black mass, which were analysed using SEM-EDS with AMICS software, are provided in their respective sections.

Table II-1. Compositional groups for reported phases/minerals analysed using SEM-EDS with Tescan TIMA™ software.

Mineral	**Description**
Ni Mn Co and Fe Sulphate	Ni-, Mn-, Co-, Fe-, Mg-, S- and O-bearing mixed metal sulphate-hydroxide. Predominantly composed of Ni (40%), O (38%) and Mn (7%), with subordinate Co (3%) and Fe (1%). May also contain Al and Si.
Muscovite	Muscovite and illite.
Others Silicates	Silicate phases not included in other categories.
Chalcocite	Chalcocite and digentie.
Enargite	Enargite and tennantite.
Anhydrite	Anhydrite and gypsum.
Fe Oxides	Fe oxides such as magnetite and hematite.
Undifferentiated	Minerals/phases not included in other categories.
Note: Descriptions are not provided for every compositional group.	

Some host materials were not analysed or characterised to the same extent as others due to limitations associated with material availability or due to host material incompatibility with particular analytical techniques. Nickel concentrate from origin B was not characterised.

13.2.1 Lithium Ore

13.2.1.1 Description

Table II-2. Lithium ore sieving test results.

Sizing	Mass Retained (g)	Mass Retained (%)	Cumulative Mass Retained (%)	Cumulative Mass Passing (%)
≥40.00 mm	0.00	0.00	0.00	100.00
<40.00 mm to ≥31.50 mm	0.00	0.00	0.00	100.00
<31.50 mm to ≥25.00 mm	0.85	0.35	0.35	99.65
<25.00 mm to ≥20.00 mm	10.03	4.07	4.42	95.58
<20.00 mm to ≥6.30 mm	13.21	5.36	9.78	90.22
<6.30 mm to ≥2.00 mm	10.20	4.14	13.92	86.08
Pan (<2.00 mm)	211.96	86.08	100	-
Note: Mass of test sample = 246.25 g.				

Table II-3. Identification and classification of lithium ore.

Classification	Light brownish cream gravelly SAND. Composite anthropogenic soil.
Primary Fraction and Description	2.5Y 8/1. Light brownish cream. Particles are predominantly composed of fine sand (187 µm to 250 µm) with particles and agglomerates present which have a maximum length of up to 2 mm. 1–2 mm agglomerates make up 5% of the sample. The larger particles (>1 mm) are predominantly angular to rounded. 1–2 mm agglomerates were extremely weak and had an unconfined compressive strength of 0.6 MPa to 1 MPa. Particles are magnetically attracted to a magnetic pen even when it is not in contact with the sample. Upon gentle cleaning of the magnet, black particles remain strongly attracted.
Secondary Fraction and Description	Gravel comprises 14% of the total mass and consists of similar proportions of fine, medium and coarse gravel. 2.5Y 8/1. Contains flakes/books of micas (5% of sample) which can be 10YR 4/2, 5P 6/5, 5P 4/2, 5RP 6/2 and 5Y 6/1. Dark pinkish grey to dark greenish brown. Some flakes/books are translucent (almost transparent). These are flat and flat & elongate minerals that are angular, smooth along their long axis and rough on their short axis. Are up to 1 cm to 5 cm along their long axis. These have a vitreous lustre, a hardness of 2–3, a flaky or basal cleavage, have a tabular habit and are not magnetic. The unconfined compressive strength ranges from extremely weak to weak (0.6 MPa to 12.5 MPa). Rocks make up 7% of the sample and are 10YR 9.5/1, 10YR 8/1, 10Y 7/1 and 2.5Y 8/1. Rocks range from angular to sub-angular, and range from equidimensional to flat (sphericity ranges from 0.3–0.7 and roundness ranges from 0.3–0.5). Rocks range in size from 0.6 cm to 1.8 cm (average 1 cm). These are generally massive and contain fine sand sized vitreous translucent and

	black particles/crystals. Rocks >6.3 mm have a Medium strong unconfined compressive strength (25 MPa to 50 MPa). Agglomerates make up ~5% of the sample and are 10YR 8/1, 5Y 8/1 and 10Y 7/1, with rare agglomerates that are 7.5YR 9.5/1. Broadly light brownish cream. Predominantly subangular. Range from 1 mm to 12 mm. Composed of massive fine sand, some contain fine vitreous minerals and particles and dull or black minerals and particles. Agglomerates are extremely weak to very weak (0.6 MPa to 5 MPa). Difficult to segregate agglomerates from rocks in the ≥2.00 mm to <6.30 mm particle size range.
Other	No organics or artefacts were found within the sample.
Note: The host material was classified according to geotechnical investigation and testing standards for soil and rock. The soil identification naming convention is from BS 5930:2015+A1:2020. The colour notation used is based on the Munsell colour system (Munsell Color, 2009). The sphericity and roundness were determined based on the visual chart in Krumbein & Sloss (1963) (Figure 4–9). Descriptions of soil were also adapted after Davison & Springman (2025).	

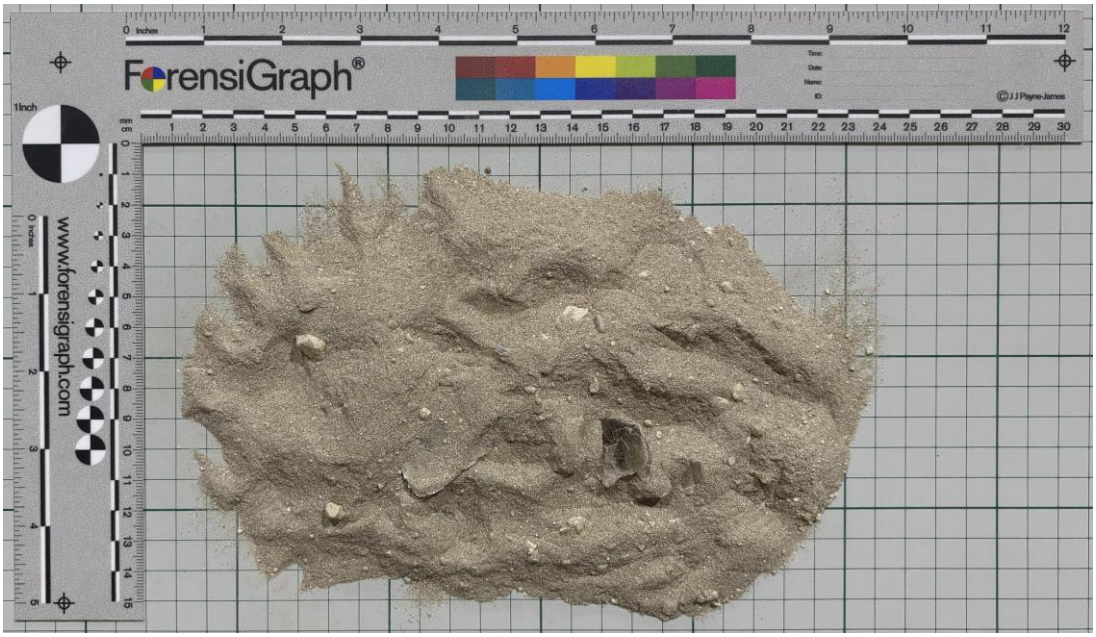

Figure II-1. Photograph of natural state lithium ore.

13.2.1.2 Laser Particle Sizing

Table II-4. Summary of lithium ore laser particle size data.

Dv(10)	Dv(50)	Dv(90)	D[4,3]
22.3 µm	104 µm	310 µm	140 µm

Table II-5. Percentage volume oversize and undersize for specific particle sizes from laser particle size analysis of lithium ore.

Size (µm)	% Volume Under	% Volume Over
0.01	0	100
0.0114	0	100
0.0129	0	100
0.0147	0	100
0.0167	0	100
0.0189	0	100
0.0215	0	100
0.0244	0	100
0.0278	0	100
0.0315	0	100
0.0358	0	100
0.0407	0	100
0.0463	0	100
0.0526	0	100
0.0597	0	100
0.0679	0	100
0.0771	0	100
0.0876	0	100
0.0995	0	100
0.113	0	100
0.128	0	100
0.146	0	100
0.166	0	100
0.188	0	100
0.214	0	100
0.243	0	100
0.276	0	100
0.314	0	100
0.357	0	100
0.405	0	100
0.46	0	100
0.523	0	100
0.594	0	100
0.675	0	100
0.767	0.07	99.93
0.872	0.13	99.87
0.991	0.21	99.79
1.13	0.28	99.72
1.28	0.36	99.64
1.45	0.44	99.56
1.65	0.53	99.47
1.88	0.63	99.37
2.13	0.74	99.26
2.42	0.86	99.14
2.75	1.01	98.99
3.12	1.18	98.82
3.55	1.39	98.61
4.03	1.63	98.37
4.58	1.91	98.09
5.21	2.22	97.78
5.92	2.56	97.44
6.72	2.95	97.05
7.64	3.37	96.63
8.68	3.84	96.16
9.86	4.37	95.63
11.2	4.96	95.04
12.7	5.63	94.37
14.5	6.40	93.60
16.4	7.27	92.73
18.7	8.27	91.73
21.2	9.44	90.56
24.1	10.81	89.19
27.4	12.43	87.57
31.1	14.34	85.66
35.3	16.6	83.4
40.1	19.23	80.77
45.6	22.27	77.73
51.8	25.71	74.29
58.9	29.55	70.45
66.9	33.73	66.27
76	38.21	61.79
86.4	42.92	57.08
98.1	47.79	52.21
111	52.78	47.22
127	57.85	42.15
144	62.93	37.07
163	67.99	32.01
186	72.96	27.04
211	77.74	22.26
240	82.23	17.77
272	86.33	13.67
310	89.94	10.06
352	93.01	6.99
400	95.50	4.50
454	97.41	2.59
516	98.75	1.25
586	99.59	0.41
666	100	0
756	100	0
859	100	0
976	100	0
1110	100	0
1260	100	0
1430	100	0
1630	100	0
1850	100	0
2100	100	0
2390	100	0
2710	100	0
3080	100	0
3500	100	0

Funded by the European Union

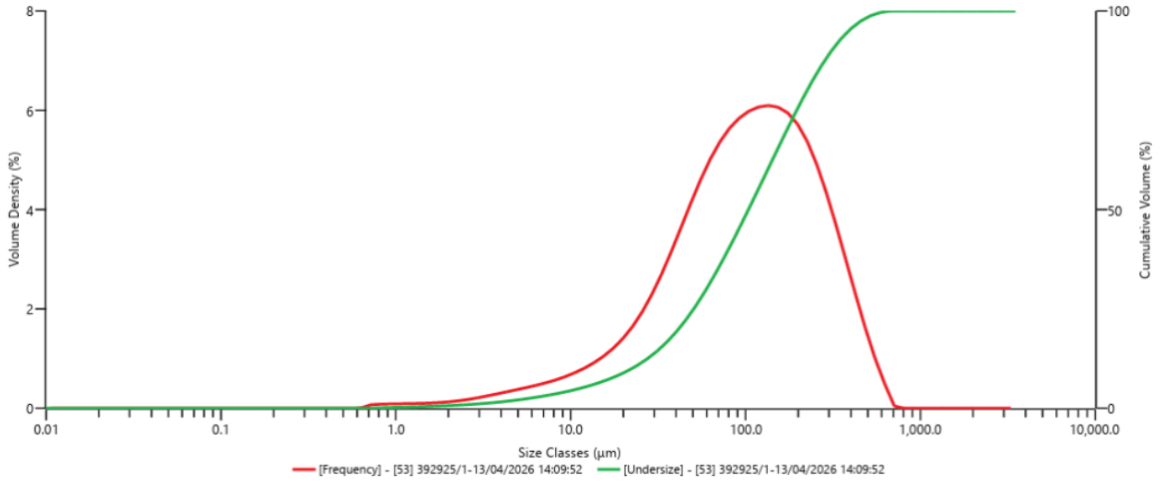

Figure II-2. Particle size analysis graph for lithium ore.

13.2.1.3 Physical Characteristics

Table II-6. Physical characteristics of lithium ore.

Test	Method	Unit	Result
Moisture Content	ISO 10251:2006	%	0.30

13.2.1.4 Multi-Element Geochemical Analysis

Table II-7. Geochemical analysis of oxides in lithium ore.

Oxide	Al_2O_3	BaO	Bi_2O_3	CaO	CeO_2	CoO	Cr_2O_3	CuO	Fe_2O_3	HfO_2
Method	XRF	XRF	XRF	XRF	XRF	XRF	XRF	XRF	XRF	XRF
Units	%	%	%	%	%	%	%	%	%	%
Result	24.2	0.04	<0.02	0.32	<0.02	<0.02	<0.02	0.03	5.53	0.08

Oxide	K_2O	La_2O_3	Li_2O	MgO	Mn_3O_4	MoO_3	Na_2O	Nb_2O_5	NiO	P_2O_5
Method	XRF	XRF	ICP-OES	XRF	XRF	XRF	XRF	XRF	XRF	XRF
Units	%	%	%	%	%	%	%	%	%	%
Result	7.80	<0.02	1.54	0.82	0.52	<0.02	1.10	<0.02	0.07	0.14

Oxide	PbO	Sb_2O_3	SiO_2	SnO_2	SrO	Ta_2O_5	ThO_2	TiO_2	U_3O_8	V_2O_5
Method	XRF	XRF	XRF	XRF	XRF	XRF	XRF	XRF	XRF	XRF
Units	%	%	%	%	%	%	%	%	%	%
Result	<0.02	0.03	52.46	0.04	<0.02	<0.02	<0.02	0.34	<0.02	<0.02

Oxide	WO_3	Y_2O_3	ZnO	ZrO_2
Method	XRF	XRF	XRF	XRF
Units	%	%	%	%
Result	0.02	<0.02	0.05	<0.02

Table II-8. Geochemical analysis of elements in lithium ore.

Element	C	S
Method	IGA	IGA
Units	%	%
Result	0.088	0.065

Funded by the European Union

13.2.1.5 X-Ray Diffraction

Table II-9. X-ray diffraction results for lithium ore.

Mineral	Mineral Formula	Wt. %
Quartz	SiO_2	7.9
Orthoclase Feldspar	$KAlSi_3O_8$	2.0
Albite	$Na_{0.95}Ca_{0.05}Al_{1.05}Si_{2.95}O_8$	7.0
Muscovite/Illite	$KAl_2(AlSi)_4O_{10}(OH,F)_2$	26.1
Biotite	$K(Mg,Fe^{2+})_3[AlSi_3O_{10}](OH,F)_2$	1.3
Zinnwaldite	$KLiFe^{2+}Al(AlSi_3)O_{10}(F,OH)_2$	42.1
Lepidolite	$K(Li,Al)_3(Si,Al)_4O_{10}(F,OH)_2$	13.4
Kaolinite	$Al_2Si_2O_5(OH)_4$	0.3
Total	-	100

13.2.1.6 Automated Mineralogy

Due to the coarse and variable particle sizing of lithium ore and the impossibility of obtaining representative subsamples from the natural state sample for automated mineralogy, the host material was milled to <500 µm to collect a representative subsample. An oversize fraction (+500 µm) of 6.17% of the original sample mass, consisting of flakes of translucent mica, could not be milled further and was not analysed.

Table II-10. Lithium ore modal abundance data (mass %) from three subsamples.

Mineral	Subsample 1	Subsample 2	Subsample 3	Average
Quartz	12.10	12.29	11.90	12.10
Feldspar	5.73	7.27	6.57	6.52
Muscovite	23.51	21.99	22.84	22.78
Biotite	1.17	0.97	0.89	1.01
Zinnwaldite	36.12	37.04	35.11	36.09
Lepidolite	19.08	18.13	20.63	19.28
Amphibole	0.16	0.16	0.15	0.16
Clays	1.68	1.51	1.22	1.47
Others Silicates	0.03	0.10	0.03	0.05
Carbonates	0.01	0.02	0.04	0.02
Pyrite	0.03	0.06	0.04	0.04
Chalcopyrite	0.01	0.02	0.03	0.02
Enargite	0.00	0.00	0.00	0.00
Cu Oxides	0.06	0.06	0.09	0.07
Sphalerite	0.00	0.00	0.00	0.00
Sulphates	0.02	0.07	0.04	0.04
Ilmenite	0.07	0.06	0.08	0.07
Fe Oxides	0.06	0.10	0.06	0.07
Apatite	0.06	0.06	0.20	0.11
Undifferentiated	0.10	0.08	0.08	0.09
Total	100.00	100.00	100.00	100.00

Funded by the European Union

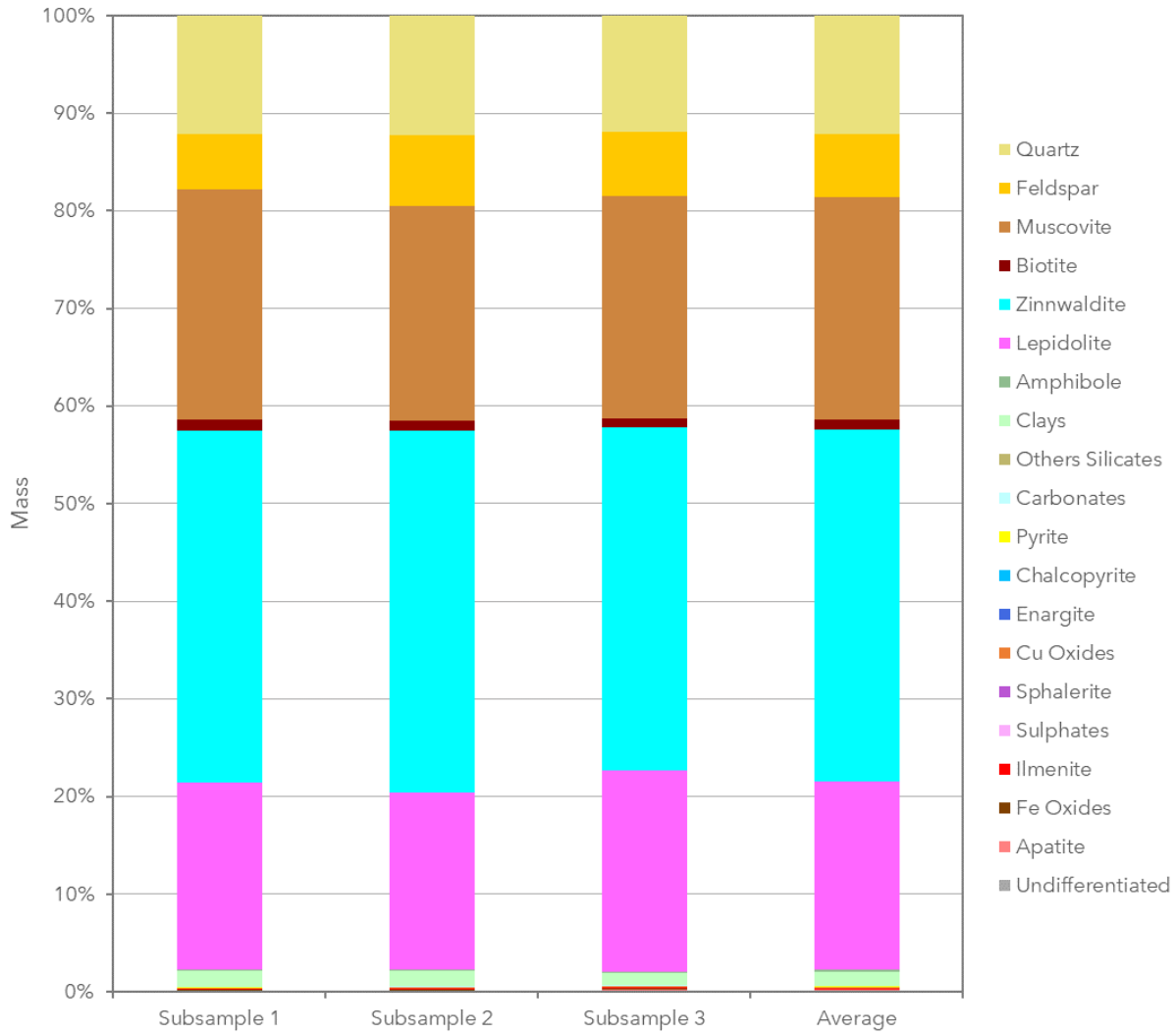

Figure II-3. Lithium ore modal abundance data (mass %) from three subsamples and the average modal abundance.

Funded by
the European Union

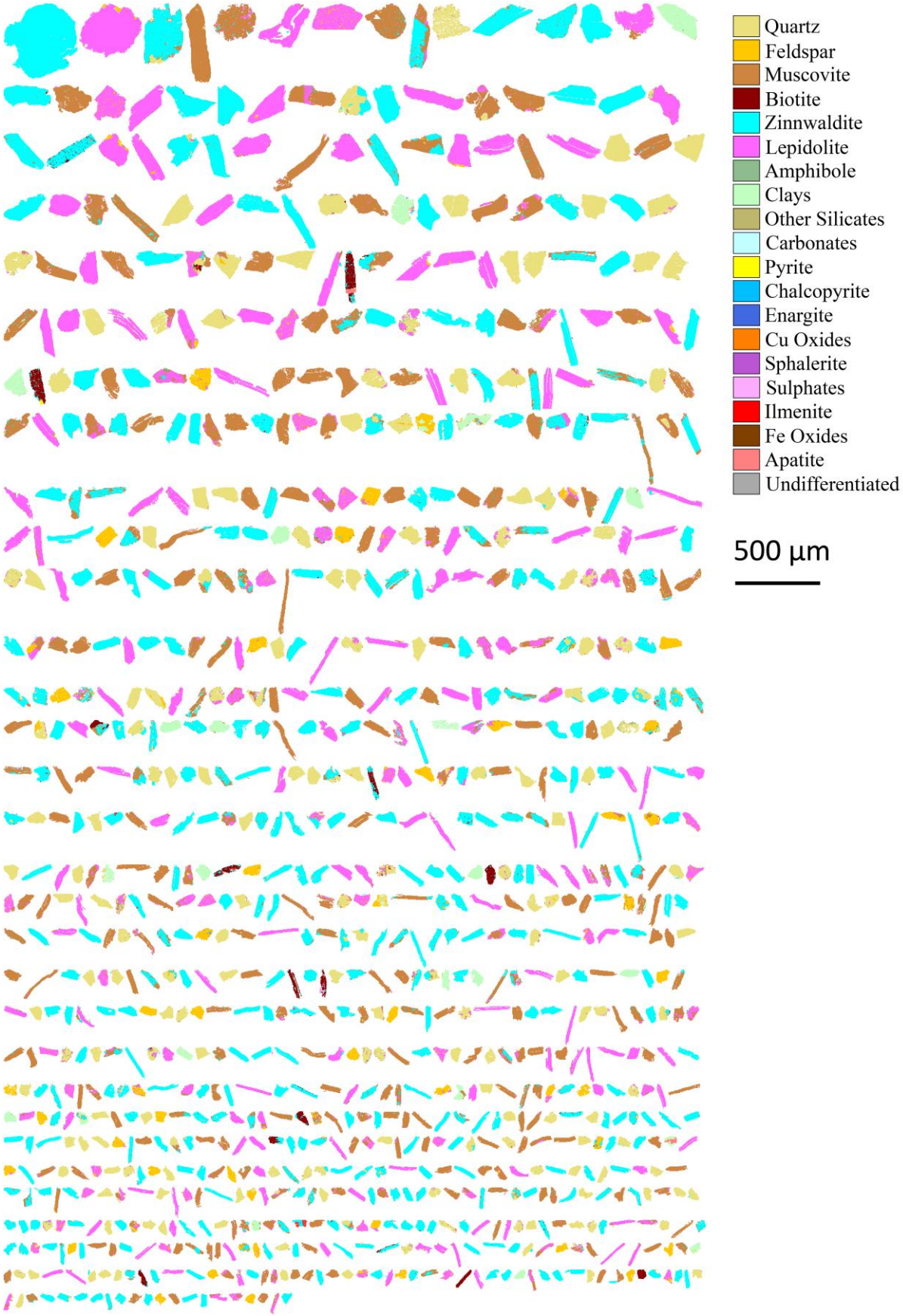

Figure II-4. Lithium ore particles arranged by area (subsample 1).

Funded by
the European Union

Table II-11. Lithium ore grain sizing from automated mineralogy.

Size (µm)	All Phases (%)	Quartz (%)	Feldspar (%)	Muscovite (%)	Biotite (%)	Zinnwaldite (%)
<0.01	0	0	0	0	0	0
<10.00	7.69	6.4	15.9	19.7	24.4	9.56
<20.00	25.42	18.4	37.7	37	44	28.81
<25.00	30.45	23	44.3	41.6	48.7	34.46
<38.00	40.79	33.8	61.5	51	61.2	45.98
<45.00	45.67	39.6	69.9	55	63.7	51.09
<53.00	50.65	44.2	76.7	59.2	67.5	56.49
<75.00	63.17	61.3	90.3	71.4	83.1	68.8
<106.00	76.74	77.3	97.6	82	86.3	81.05
<150.00	89.17	95.5	100	93.3	100	88.82
<212.00	96.97	100	100	98.7	100	96.2
All particles	100	100	100	100	100	100

Size (µm)	Lepidolite (%)	Pyrite (%)	Fe Oxides (%)
<0.01	0	0	0
<10.00	14.8	5.3	25.1
<20.00	30.5	46.6	47.4
<25.00	34.5	67.6	47.4
<38.00	41.8	100	69.9
<45.00	46.4	100	100
<53.00	50.4	100	100
<75.00	59.9	100	100
<106.00	73.3	100	100
<150.00	83.9	100	100
<212.00	97.1	100	100
All particles	100	100	100

	All Phases	Quartz	Feldspar	Muscovite	Biotite	Zinnwaldite
P50 (µm)	52	61	29	37	28	43
P80 (µm)	116	111	55	100	67	102

	Lepidolite	Pyrite	Fe Oxides
P50 (µm)	52	23	25
P80 (µm)	134	29	43
Note: Grain sizing data is from subsample 1. Grain sizing is presented in mass %.			

Table II-12. Lithium ore liberation data from automated mineralogy.

Category	Zinnwaldite	Lepidolite
Free (≥95%)	65.14	36.89
Liberated (<95% to ≥80%)	22.57	41.75
High Middlings (<80% to ≥50%)	7.93	9.88
Low Middlings (<50% to ≥20%)	2.76	5.17
Locked (<20%)	1.60	6.32
Total	100.00	100.00
Note: Liberation data has been normalised to 100%.		

13.2.1.7 Other

Table II-13. Other properties of lithium ore

Test	Method	Unit	Result
LOI	1 h @ 900°C	%	3.73

Funded by the European Union

13.2.2 Spodumene Concentrate

13.2.2.1 Description

Table II-14. Spodumene concentrate sieving test results.

Sizing	Mass Retained (g)	Mass Retained (%)	Cumulative Mass Retained (%)	Cumulative Mass Passing (%)
≥40.00 mm	0.00	0.00	0.00	100.00
<40.00 mm to ≥31.50 mm	0.00	0.00	0.00	100.00
<31.50 mm to ≥25.00 mm	0.00	0.00	0.00	100.00
<25.00 mm to ≥20.00 mm	0.00	0.00	0.00	100.00
<20.00 mm to ≥6.30 mm	3.22	0.89	0.89	99.11
<6.30 mm to ≥2.00 mm	10.30	2.85	3.74	96.26
Pan (<2.00 mm)	347.70	96.26	100.00	-
Note: Mass of test sample = 361.22 g.				

Table II-15. Identification and classification of spodumene concentrate.

Classification	Light brownish grey gravelly SAND. Composite anthropogenic soil.
Primary Fraction and Description	5Y 8/1. Fine massive particulate material, visible particles are 187 µm to 250 µm (predominantly within the medium sand (mSa) size fraction). No agglomerates. Particles are vitreous with rare black particles (1%). Minor magnetism of the fraction when a magnetic pen is passed through the sample; a few particles were magnetically attracted.
Secondary Fraction and Description	Gravel is fine and medium. Consists of agglomerates that are 5Y 8/1; light brownish grey externally, which are slightly browner within their freshly exposed centres (either not differentiable from the external colour using the Munsell colour chart or 2.5Y 8/1). Agglomerates are rounded to well-rounded with smooth surfaces. On average, agglomerates have a sphericity of 0.9 and a roundness of 0.7. When crushed, agglomerates are composed of fine vitreous, and black (1%) particles. The black particles are magnetically attracted to a magnetic pen. Agglomerates dry to N 9/. Agglomerates are extremely weak and have an unconfined compressive strength of 0.6 MPa to 1 MPa.
Other	No organics or artefacts were found within the sample.
Note: The host material was classified according to geotechnical investigation and testing standards for soil and rock. The soil identification naming convention is from BS 5930:2015+A1:2020. The colour notation used is based on the Munsell colour system (Munsell Color, 2009). The sphericity and roundness were determined based on the visual chart in Krumbein & Sloss (1963) (Figure 4–9). Descriptions of soil were also adapted after Davison & Springman (2025).	

Funded by the European Union

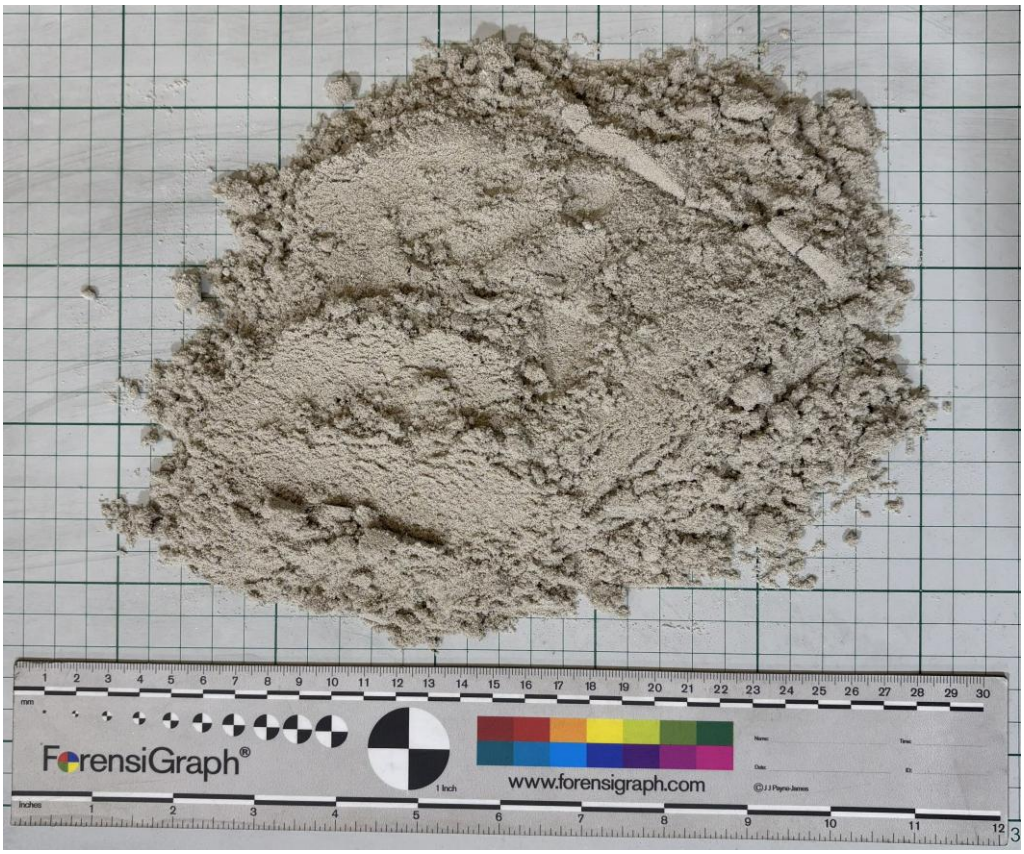

Figure II-5. Photograph of natural state spodumene concentrate.

13.2.2.2 Laser Particle Sizing

Table II-16. Summary of spodumene concentrate laser particle size data.

Dv(10)	Dv(50)	Dv(90)	D[4,3]
31.6 µm	141 µm	546 µm	233 µm

Table II-17. Percentage volume oversize and undersize for specific particle sizes from laser particle size analysis of spodumene concentrate.

Size (µm)	% Volume Under	% Volume Over
0.01	0	100
0.0114	0	100
0.0129	0	100
0.0147	0	100
0.0167	0	100
0.0189	0	100
0.0215	0	100
0.0244	0	100
0.0278	0	100
0.0315	0	100
0.0358	0	100
0.0407	0	100
0.0463	0	100
0.0526	0	100
0.0597	0	100
0.0679	0	100
0.0771	0	100
0.0876	0	100
0.0995	0	100
0.113	0	100
0.128	0	100
0.146	0	100
0.166	0	100
0.188	0	100
0.214	0	100
0.243	0	100
0.276	0	100
0.314	0	100
0.357	0	100
0.405	0	100
0.46	0	100
0.523	0	100
0.594	0	100
0.675	0	100
0.767	0	100
0.872	0	100
0.991	0	100
1.13	0	100
1.28	0	100
1.45	0	100
1.65	0	100
1.88	0	100
2.13	0	100
2.42	0	100
2.75	0.06	99.94
3.12	0.13	99.87
3.55	0.21	99.79
4.03	0.29	99.71
4.58	0.39	99.61
5.21	0.51	99.49
5.92	0.64	99.36
6.72	0.80	99.20
7.64	0.99	99.01
8.68	1.22	98.78
9.86	1.49	98.51
11.2	1.81	98.19
12.7	2.21	97.79
14.5	2.70	97.30
16.4	3.33	96.67
18.7	4.12	95.88
21.2	5.13	94.87
24.1	6.39	93.61
27.4	7.92	92.08
31.1	9.75	90.25
35.3	11.89	88.11
40.1	14.33	85.67
45.6	17.09	82.91
51.8	20.15	79.85
58.9	23.47	76.53
66.9	27.01	72.99
76	30.72	69.28
86.4	34.55	65.45
98.1	38.47	61.53
111	42.46	57.54
127	46.51	53.49
144	50.64	49.36
163	54.86	45.14
186	59.19	40.81
211	63.58	36.42
240	67.96	32.04
272	72.24	27.76
310	76.31	23.69
352	80.07	19.93
400	83.45	16.55
454	86.43	13.57
516	89.02	10.98
586	91.22	8.78
666	93.09	6.91
756	94.65	5.35
859	95.95	4.05
976	97.04	2.96
1110	97.95	2.05
1260	98.69	1.31
1430	99.27	0.73
1630	99.67	0.33
1850	99.90	0.10
2100	100	0
2390	100	0
2710	100	0
3080	100	0
3500	100	0

Funded by the European Union

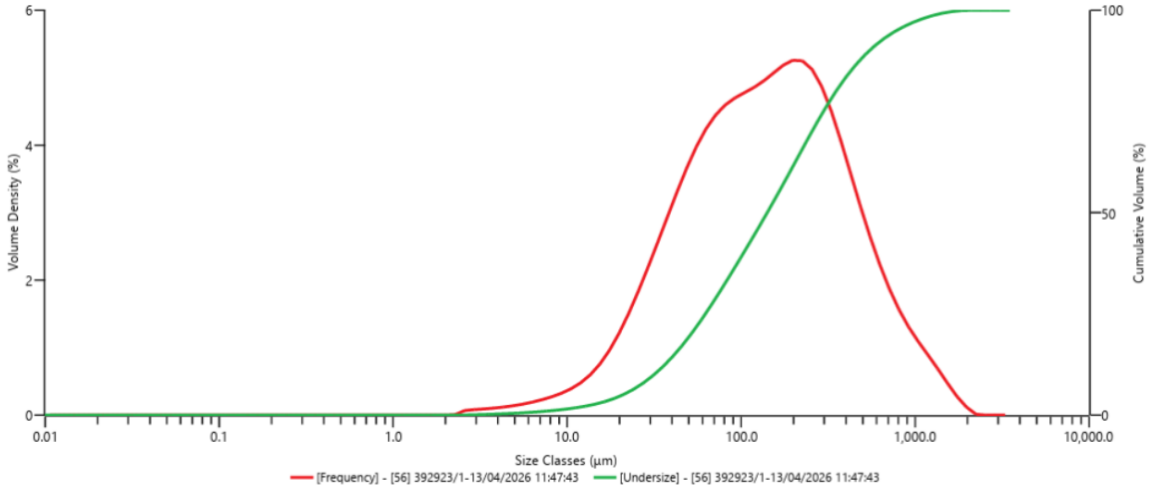

Figure II-6. Particle size analysis graph for spodumene concentrate.

13.2.2.3 Physical Characteristics

Table II-18. Physical characteristics of spodumene concentrate.

Test	Method	Unit	Result
Moisture Content	ISO 10251:2006	%	6.42
Susceptibility to oxidation, decomposition and sublimation	ISO 10251:2006	-	Not susceptible to oxidation, decomposition or sublimation
Specific Gravity	Pycno	-	3.05
True Density	Pycno	g/cm^3	3.05
Bulk Density	Grav	g/mL	0.9
Tapped Density	Grav	g/mL	1.27

13.2.2.4 Multi-Element Geochemical Analysis

Table II-19. Geochemical analysis of oxides in spodumene concentrate.

Oxide	Al_2O_3	BaO	Bi_2O_3	CaO	CeO_2	CoO	Cr_2O_3	CuO	Fe_2O_3	HfO_2
Method	XRF	XRF	XRF	XRF	XRF	XRF	XRF	XRF	XRF	XRF
Units	%	%	%	%	%	%	%	%	%	%
Result	22.44	0.02	<0.02	1.92	<0.02	<0.02	<0.02	0.02	0.95	0.07

Oxide	K_2O	La_2O_3	Li_2O	MgO	Mn_3O_4	MoO_3	Na_2O	Nb_2O_5	NiO	P_2O_5
Method	XRF	XRF	ICP-OES	XRF	XRF	XRF	XRF	XRF	XRF	XRF
Units	%	%	%	%	%	%	%	%	%	%
Result	0.72	<0.02	5.02	0.29	0.18	<0.02	0.95	<0.02	0.06	0.46

Oxide	PbO	Sb_2O_3	SiO_2	SnO_2	SrO	Ta_2O_5	ThO_2	TiO_2	U_3O_8	V_2O_5
Method	XRF	XRF	XRF	XRF	XRF	XRF	XRF	XRF	XRF	XRF
Units	%	%	%	%	%	%	%	%	%	%
Result	<0.02	0.02	65.52	0.06	<0.02	0.04	<0.02	0.18	<0.02	0.02

Oxide	WO_3	Y_2O_3	ZnO	ZrO_2
Method	XRF	XRF	XRF	XRF
Units	%	%	%	%
Result	<0.02	<0.02	<0.02	<0.02

Funded by the European Union

Table II-20. Geochemical analysis of elements in spodumene concentrate.

Element	Ag	As	Be	Br	C	Cd	Cl	Cs	Dy	Er
Method	ICP-OES	ICP-MS	ICP-OES	CIC	IGA	ICP-MS	CIC	ICP-MS	ICP-MS	ICP-MS
Units	ppm	ppm	ppm	ppm	%	ppm	ppm	ppm	ppm	ppm
Result	0.5	5	322	9	0.083	<0.5	39	265	3	0.6

Element	Eu	F	Ga	Gd	Ge	Hg	Ho	In	Lu	Nd
Method	ICP-MS	CIC	ICP-MS	ICP-MS	ICP-MS	CVAAS	ICP-MS	ICP-MS	ICP-MS	ICP-MS
Units	ppm	ppm	ppm	ppm	ppm	ppm	ppm	ppm	ppm	ppm
Result	0.2	2980	99	4	<0.1	<1	0.3	0.8	<0.1	3

Element	Pr	Rb	Re	S	Sc	Se	Sm	Tb	Te	Tl
Method	ICP-MS	ICP-MS	ICP-MS	IGA	ICP-MS	ICP-MS	ICP-MS	ICP-MS	ICP-MS	ICP-MS
Units	ppm	ppm	ppm	%	ppm	ppm	ppm	ppm	ppm	ppm
Result	1	1923	<0.5	0.097	4	<1	3	0.8	<0.5	17

Element	Tm	Yb
Method	ICP-MS	ICP-MS
Units	ppm	ppm
Result	<0.5	0.7

13.2.2.5 X-Ray Diffraction

Table II-21. X-ray diffraction results for spodumene concentrate.

Mineral	Chemical Formula	Pre-Test	Post-Test	Difference
		Wt. %	Wt. %	Wt. %
Quartz	SiO_2	13.9	10	-3.9
Orthoclase Feldspar	$KAlSi_3O_8$	6.0	8.8	2.8
Muscovite/Illite	$KAl_2(AlSi)_4O_{10}(OH,F)_2$	8.0	8.8	0.8
Clinochlore	$(MgFe^{2+})_5Al(Si_3Al)O_{10}(OH)_8$	2.1	ND	-2.1
Spodumene	$LiAlSi_2O_6$	70.0	72.4	2.4
Total	-	100	100	-

Note: ND = not detected. The results are from a representative sample pre- and post-natural ageing test.

13.2.2.6 Automated Mineralogy

Table II-22. Spodumene concentrate modal abundance data (mass %) from three pre-test subsamples and from one post-test subsample.

Mineral	Pre-Test				Post-Test	Difference
	Subsample 1	Subsample 2	Subsample 3	Average		
Quartz	7.75	7.60	8.34	7.90	8.35	0.45
Feldspar	9.46	7.93	7.89	8.43	9.25	0.82
Muscovite	4.86	4.61	5.79	5.09	5.58	0.50
Biotite	0.95	0.72	0.84	0.84	0.83	-0.01
Amphibole	1.21	1.00	1.37	1.19	1.33	0.14
Chlorite	0.19	0.12	0.25	0.19	0.26	0.07
Epidote	1.79	1.90	1.65	1.78	1.63	-0.15
Spodumene	71.36	73.24	70.20	71.60	69.13	-2.47
Clays	0.50	0.48	0.87	0.62	1.07	0.46
Others Silicates	0.47	0.56	0.81	0.61	0.64	0.03
Carbonates	0.35	0.18	0.26	0.26	0.33	0.07
Pyrite	0.02	0.02	0.04	0.03	0.02	0.00
Chalcopyrite	0.01	0.01	0.01	0.01	0.02	0.01
Chalcocite	0.00	0.00	ND	0.00	ND	0.00
Sphalerite	0.00	0.00	0.01	0.00	0.00	0.00
Sulphates	0.00	0.02	0.01	0.01	0.01	0.00
Ilmenite	0.02	0.02	0.02	0.02	0.02	-0.01
Fe Oxides	0.04	0.01	0.05	0.03	0.10	0.07
Apatite	0.95	1.47	1.48	1.30	1.27	-0.03
Undifferentiated	0.06	0.10	0.12	0.09	0.15	0.06
Total	100.00	100.00	100.00	100.00	100.00	-
Note: ND = not detected. The post-test modal abundance is from a sample of spodumene concentrate collected following the completion of the natural ageing test.						

Funded by the European Union

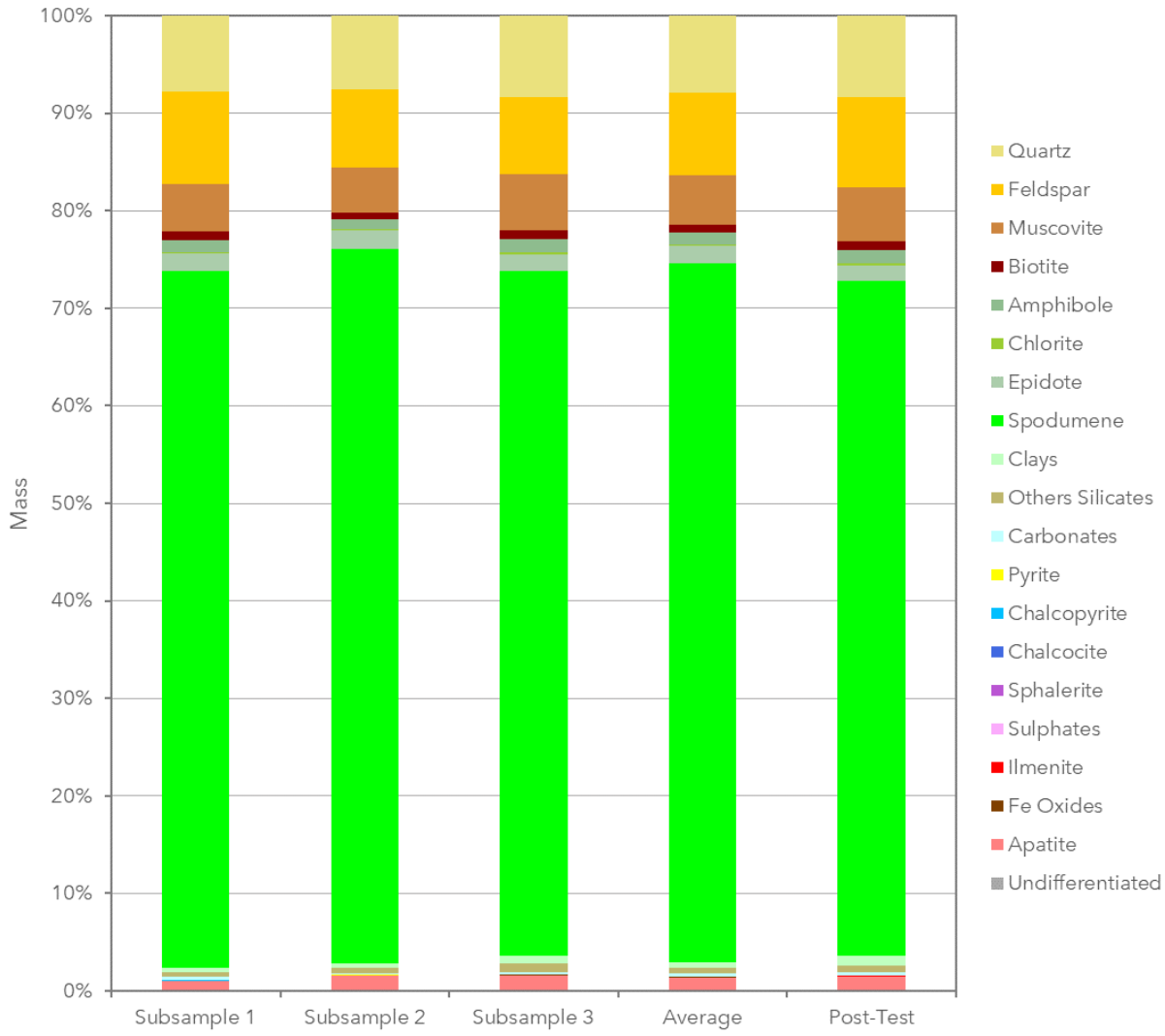

Figure II-7. Spodumene concentrate modal abundance data (mass %) from three subsamples (with average abundance) and from a post-test sample.

Note: The post-test modal abundance is from a sample of spodumene concentrate collected following the completion of the natural ageing test.

Funded by the European Union

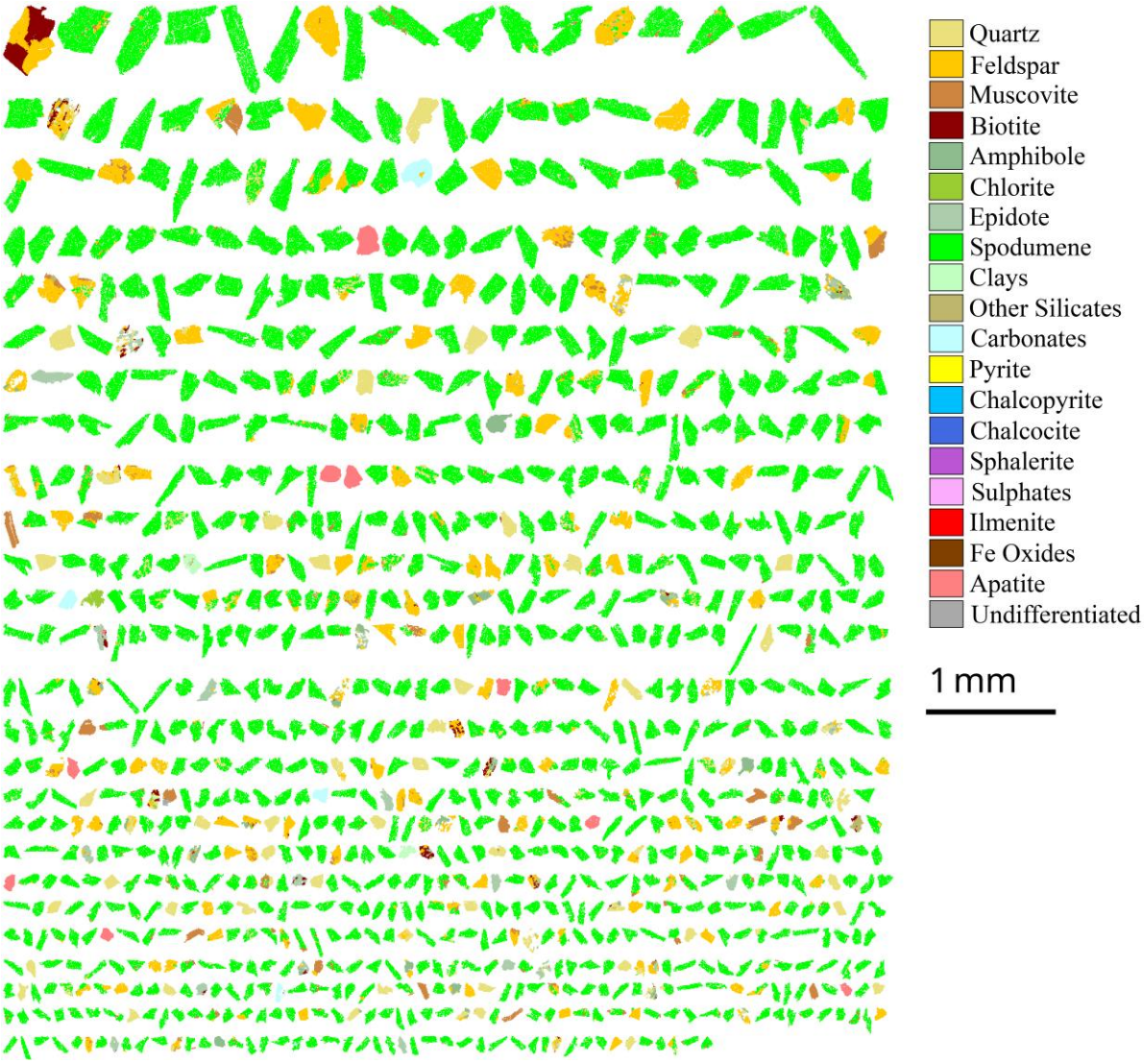

Figure II-8. Spodumene concentrate particles arranged by area (subsample 1).

Funded by
the European Union

Table II-23. Spodumene concentrate grain sizing from automated mineralogy.

Size (µm)	All Phases (%)	Quartz (%)	Feldspar (%)	Muscovite (%)	Amphibole (%)	Epidote (%)
<0.01	0.00	0.0	0.0	0.0	0.0	0.0
<10.00	3.32	5.5	3.6	14.7	5.7	3.1
<20.00	12.19	22.5	13.1	41.1	21.8	14.1
<25.00	15.86	30.5	17.4	50.9	30.4	20.3
<38.00	22.92	46.6	27.2	68.9	45.4	35.2
<45.00	26.24	53.6	32.0	74.7	52.1	39.0
<53.00	29.80	62.0	35.5	79.1	58.1	45.7
<75.00	40.12	73.8	45.8	87.6	77.7	70.0
<106.00	53.80	84.0	58.7	93.6	89.0	85.9
<150.00	72.67	93.5	76.6	98.4	92.7	94.1
<212.00	88.28	97.9	88.1	100.0	100.0	100.0
All particles	100.00	100.0	100.0	100.0	100.0	100.0

Size (µm)	Spodumene (%)	Pyrite (%)	Chalcopyrite (%)
<0.01	0.00	0.0	0.0
<10.00	2.90	4.9	0.0
<20.00	10.99	28.1	9.3
<25.00	14.08	63.6	9.3
<38.00	20.02	100.0	9.3
<45.00	23.05	100.0	9.3
<53.00	26.67	100.0	100.0
<75.00	37.59	100.0	100.0
<106.00	52.32	100.0	100.0
<150.00	72.75	100.0	100.0
<212.00	89.89	100.0	100.0
All particles	100.00	100.0	100.0

	All Phases	Quartz	Feldspar	Muscovite	Amphibole	Epidote
P50 (µm)	97	41	86	25	42	56
P80 (µm)	175	97	164	58	76	98

	Spodumene	Pyrite	Chalcopyrite
P50 (µm)	100	20	50
P80 (µm)	174	25	50
Note: Grain sizing data is from subsample 1. Grain sizing is presented in mass %.			

Table II-24. Spodumene concentrate liberation data from automated mineralogy.

Category	Spodumene	Pyrite	Chalcopyrite
Free (≥95%)	26.96	53.33	100.00
Liberated (<95% to ≥80%)	66.35	19.44	0.00
High Middlings (<80% to ≥50%)	5.41	11.00	0.00
Low Middlings (<50% to ≥20%)	1.01	0.00	0.00
Locked (<20%)	0.26	16.24	0.00
Total	100.00	100.00	100.00
Note: Liberation data has been normalised to 100%.			

Funded by the European Union

13.2.3 Lithium Carbonate

13.2.3.1 Description

Table II-25. Lithium carbonate sieving test results.

Sizing	Mass Retained (g)	Mass Retained (%)	Cumulative Mass Retained (%)	Cumulative Mass Passing (%)
≥40.00 mm	0.00	0.00	0.00	100.00
<40.00 mm to ≥31.50 mm	0.00	0.00	0.00	100.00
<31.50 mm to ≥25.00 mm	0.00	0.00	0.00	100.00
<25.00 mm to ≥20.00 mm	0.00	0.00	0.00	100.00
<20.00 mm to ≥6.30 mm	1.14	1.02	1.02	98.98
<6.30 mm to ≥2.00 mm	10.04	9.00	10.02	89.98
Pan (<2.00 mm)	100.40	89.98	100.00	-
Note: Mass of test sample = 111.58 g				

Table II-26. Identification and classification of lithium carbonate.

Classification	White gravelly CLAY. Composite anthropogenic soil.
Primary Fraction and Description	N 9.5/. Massive white particulate material. Particles were too fine to observe (<187 µm). Not magnetic.
Secondary Fraction and Description	Fine to medium gravel. Composed of white (N 9.5/) agglomerates. Agglomerates are equidimensional, rounded and have smooth surfaces, with an average sphericity of 0.7 and roundness of 0.7. Agglomerates range in size from 2 mm to 12 mm along their long axes. Agglomerates are extremely weak and have an unconfined compressive strength of 0.6 MPa to 1 MPa.
Other	No organics or artefacts were found within the sample.
Note: The host material was classified according to geotechnical investigation and testing standards for soil and rock. The soil identification naming convention is from BS 5930:2015+A1:2020. The colour notation used is based on the Munsell colour system (Munsell Color, 2009). The sphericity and roundness were determined based on the visual chart in Krumbein & Sloss (1963) (Figure 4–9). Descriptions of soil were also adapted after Davison & Springman (2025).	

Funded by the European Union

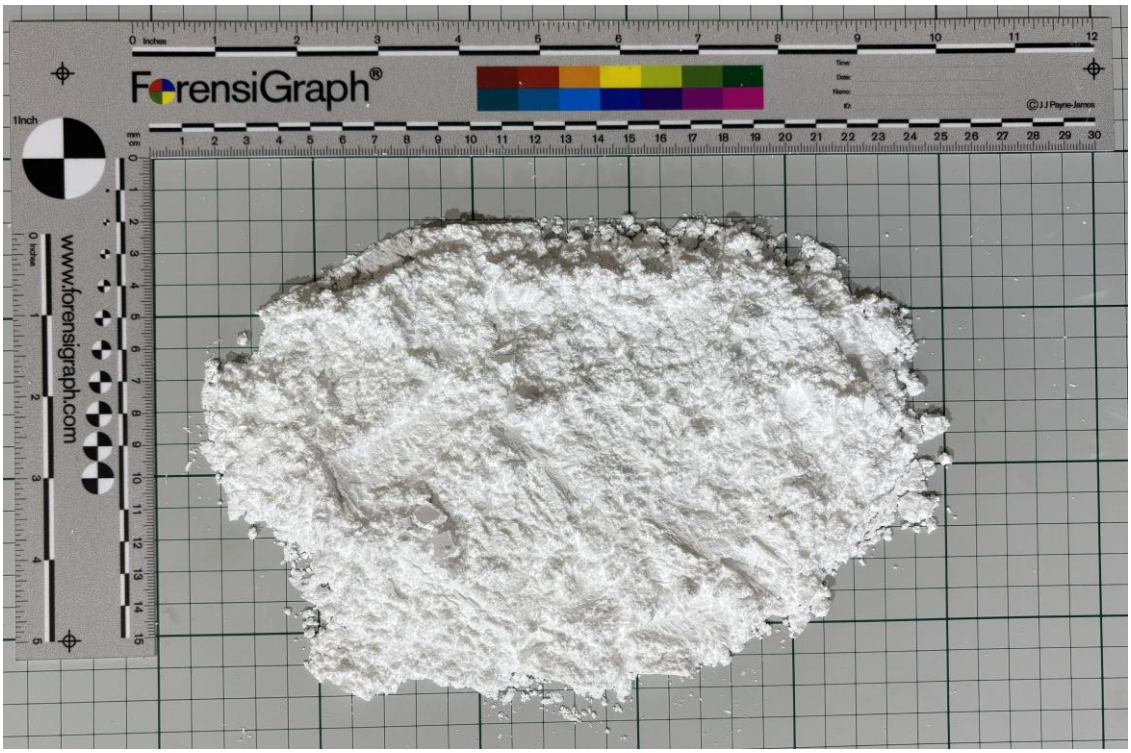

Figure II-9. Photograph of natural state lithium carbonate.

13.2.3.2 Laser Particle Sizing

Table II-27. Summary of lithium carbonate laser particle size data.

Dv(10)	Dv(50)	Dv(90)	D[4,3]
1.71 µm	6.50 µm	14.5 µm	8.13 µm

Table II-28. Percentage volume oversize and undersize for specific particle sizes from laser particle size analysis of lithium carbonate.

Size (µm)	% Volume Under	% Volume Over
0.01	0	100
0.0114	0	100
0.0129	0	100
0.0147	0	100
0.0167	0	100
0.0189	0	100
0.0215	0	100
0.0244	0	100
0.0278	0	100
0.0315	0	100
0.0358	0	100
0.0407	0	100
0.0463	0	100
0.0526	0	100
0.0597	0	100
0.0679	0	100
0.0771	0	100
0.0876	0	100
0.0995	0	100
0.113	0	100
0.128	0.06	99.94
0.146	0.19	99.81
0.166	0.37	99.63
0.188	0.61	99.39
0.214	0.90	99.10
0.243	1.24	98.76
0.276	1.63	98.37
0.314	2.05	97.95
0.357	2.50	97.50
0.405	2.98	97.02
0.46	3.48	96.52
0.523	4.00	96.00
0.594	4.52	95.48
0.675	5.05	94.95
0.767	5.59	94.41
0.872	6.14	93.86
0.991	6.72	93.28
1.13	7.33	92.67
1.28	8.00	92.00
1.45	8.77	91.23
1.65	9.69	90.31
1.88	10.82	89.18
2.13	12.24	87.76
2.42	14.05	85.95
2.75	16.35	83.65
3.12	19.25	80.75
3.55	22.84	77.16
4.03	27.18	72.82
4.58	32.32	67.68
5.21	38.22	61.78
5.92	44.80	55.20
6.72	51.88	48.12
7.64	59.24	40.76
8.68	66.58	33.42
9.86	73.59	26.41
11.2	79.96	20.04
12.7	85.45	14.55
14.5	89.91	10.09
16.4	93.30	6.70
18.7	95.69	4.31
21.2	97.24	2.76
24.1	98.14	1.86
27.4	98.62	1.38
31.1	98.83	1.17
35.3	98.91	1.09
40.1	98.92	1.08
45.6	98.92	1.08
51.8	99.00	1.00
58.9	99.13	0.87
66.9	99.28	0.72
76	99.45	0.55
86.4	99.63	0.37
98.1	99.79	0.21
111	99.91	0.09
127	100	0
144	100	0
163	100	0
186	100	0
211	100	0
240	100	0
272	100	0
310	100	0
352	100	0
400	100	0
454	100	0
516	100	0
586	100	0
666	100	0
756	100	0
859	100	0
976	100	0
1110	100	0
1260	100	0
1430	100	0
1630	100	0
1850	100	0
2100	100	0
2390	100	0
2710	100	0
3080	100	0
3500	100	0

Funded by the European Union

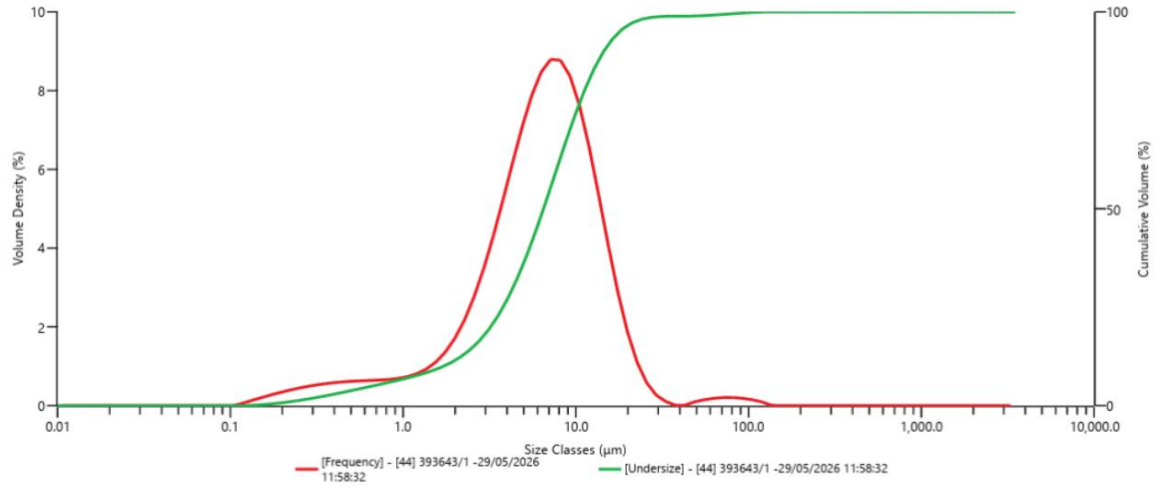

Figure II-10. Particle size analysis graph for lithium carbonate.

13.2.3.3 Physical Characteristics

Table II-29. Physical characteristics of lithium carbonate.

Test	Method	Unit	Result
Moisture Content	ISO 10251:2006	%	0.06

13.2.3.4 Multi-Element Geochemical Analysis

Table II-30. Geochemical analysis of oxides in lithium carbonate.

Oxide	Al_2O_3	BaO	Bi_2O_3	CaO	CeO_2	CoO	Cr_2O_3	CuO	Fe_2O_3	HfO_2
Method	XRF	XRF	XRF	XRF	XRF	XRF	XRF	XRF	XRF	XRF
Units	%	%	%	%	%	%	%	%	%	%
Result	<0.02	<0.02	<0.02	<0.02	<0.02	<0.02	<0.02	<0.02	0.04	<0.02

Oxide	K_2O	La_2O_3	Li_2O	MgO	Mn_3O_4	MoO_3	Na_2O	Nb_2O_5	NiO	P_2O_5
Method	XRF	XRF	ICP-OES	XRF	XRF	XRF	XRF	XRF	XRF	XRF
Units	%	%	%	%	%	%	%	%	%	%
Result	<0.02	<0.02	39.91	<0.02	<0.02	<0.02	<0.02	<0.02	<0.02	<0.02

Oxide	PbO	Sb_2O_3	SiO_2	SnO_2	SrO	Ta_2O_5	ThO_2	TiO_2	U_3O_8	V_2O_5
Method	XRF	XRF	XRF	XRF	XRF	XRF	XRF	XRF	XRF	XRF
Units	%	%	%	%	%	%	%	%	%	%
Result	<0.02	<0.02	<0.02	<0.02	<0.02	<0.02	<0.02	<0.02	<0.02	<0.02

Oxide	WO_3	Y_2O_3	ZnO	ZrO_2
Method	XRF	XRF	XRF	XRF
Units	%	%	%	%
Result	<0.02	<0.02	<0.02	<0.02

Table II-31. Geochemical analysis of elements in lithium carbonate.

Element	C	S
Method	C/SA	C/SA
Units	%	%
Result	15.70	0.01

Funded by the European Union

13.2.3.5 X-Ray Diffraction

Table II-32. X-ray diffraction results for lithium carbonate.

Mineral	Chemical Formula	Wt. %
Lithium Carbonate	Li_2CO_3	100
Total	-	100

13.2.3.6 Other

Table II-33. Other properties of lithium carbonate.

Test	Method	Unit	Result
LOI	1 h @ 900°C	%	32.44

13.2.4 Nickel Concentrate (Origin A)

13.2.4.1 Description

Table II-34. Nickel concentrate sieving test results.

Sizing	Mass Retained (g)	Mass Retained (%)	Cumulative Mass Retained (%)	Cumulative Mass Passing (%)
≥40.00 mm	0.00	0.00	0.00	100.00
<40.00 mm to ≥31.50 mm	0.00	0.00	0.00	100.00
<31.50 mm to ≥25.00 mm	0.00	0.00	0.00	100.00
<25.00 mm to ≥20.00 mm	0.00	0.00	0.00	100.00
<20.00 mm to ≥6.30 mm	30.21	8.66	8.66	91.34
<6.30 mm to ≥2.00 mm	50.17	14.37	23.03	76.97
Pan (<2.00 mm)	268.63	76.97	100.00	-
Note: Mass of test sample = 349.01 g				

Table II-35. Identification and classification of nickel concentrate.

Classification	Dark greenish brown gravelly SAND Composite anthropogenic soil.
Primary Fraction and Description	5Y 4/2. Dark greenish brown. Fine massive particulate material with particles down to <187 µm. Particles are vitreous or metallic. Contains agglomerates that are 0.5 mm to 2 mm which make up 5% of sample. Agglomerates are rounded, smooth-surfaced, equidimensional and have a sphericity of 0.8 and a roundness of 0.7. Agglomerates are extremely weak and have an unconfined compressive strength of 0.6 MPa to 1 MPa. Extremely magnetic with both agglomerates and particles magnetically attracted to the magnetic pen.
Secondary Fraction and Description	Gravel is fine and medium. 5Y 5/2 to 5Y 4/2 externally, freshly exposed centres of agglomerates are very dark grey (N 3/). Consists of agglomerates that are equidimensional, and sub-angular to sub-rounded with rough surfaces. Range in size from 2.5 mm to 27 mm along their longest axis (average 4.5 mm). On average, agglomerates have a sphericity of 0.7 and a roundness of 0.7. Agglomerates have extremely weak to very weak unconfined compressive strengths of 0.6 MPa to 5 MPa. When crushed, agglomerates are composed of fine to medium particles (187 µm to 375 µm). Vitreous particles make up 5% of agglomerates and a golden hue is visible over some particles. Particles from crushed agglomerates and smaller agglomerates (0.5 mm) are readily magnetically attracted.
Other	No organics were found within the fractions. Small pieces of unidentified plastic, potentially from FIBCs, were found as free artefacts or were incorporated into or onto agglomerates.
Note: The host material was classified according to geotechnical investigation and testing standards for soil and rock. The soil identification naming convention is from BS 5930:2015+A1:2020. The colour notation used is based on the Munsell colour system (Munsell Color, 2009). The sphericity and roundness were determined based on the visual chart in Krumbein & Sloss (1963) (Figure 4–9). Descriptions of soil were also adapted after Davison & Springman (2025).	

Funded by the European Union

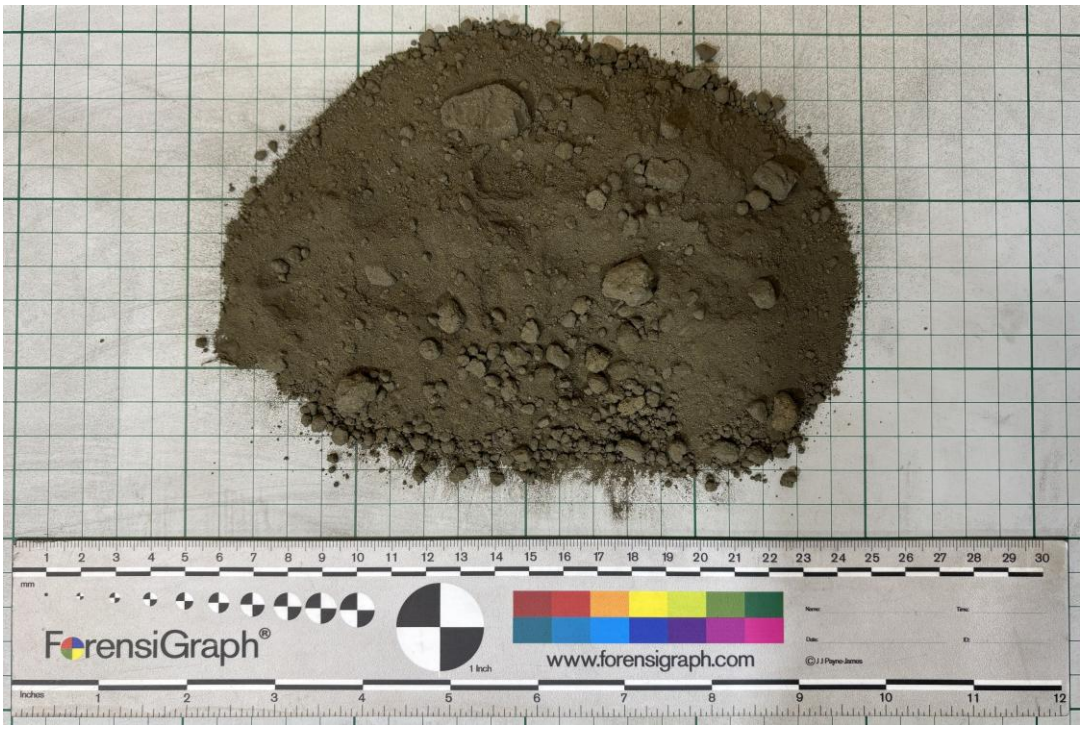

Figure II-11. Photograph of natural state nickel concentrate.

13.2.4.2 Laser Particle Sizing

Table II-36. Summary of nickel concentrate laser particle size data.

Dv(10)	Dv(50)	Dv(90)	D[4,3]
24.3 µm	78.1 µm	366 µm	137 µm

Table II-37. Percentage volume oversize and undersize for specific particle sizes from laser particle size analysis of nickel concentrate.

Size (µm)	% Volume Under	% Volume Over
0.01	0	100
0.0114	0	100
0.0129	0	100
0.0147	0	100
0.0167	0	100
0.0189	0	100
0.0215	0	100
0.0244	0	100
0.0278	0	100
0.0315	0	100
0.0358	0	100
0.0407	0	100
0.0463	0	100
0.0526	0	100
0.0597	0	100
0.0679	0	100
0.0771	0	100
0.0876	0	100
0.0995	0	100
0.113	0	100
0.128	0	100
0.146	0	100
0.166	0	100
0.188	0	100
0.214	0	100
0.243	0	100
0.276	0	100
0.314	0	100
0.357	0	100
0.405	0	100
0.46	0	100
0.523	0	100
0.594	0	100
0.675	0	100
0.767	0	100
0.872	0	100
0.991	0	100
1.13	0	100
1.28	0	100
1.45	0	100
1.65	0	100
1.88	0	100
2.13	0	100
2.42	0.06	99.94
2.75	0.13	99.87
3.12	0.22	99.78
3.55	0.32	99.68
4.03	0.44	99.56
4.58	0.59	99.41
5.21	0.77	99.23
5.92	1.00	99.00
6.72	1.27	98.73
7.64	1.61	98.39
8.68	2.03	97.97
9.86	2.53	97.47
11.2	3.12	96.88
12.7	3.82	96.18
14.5	4.64	95.36
16.4	5.61	94.39
18.7	6.76	93.24
21.2	8.15	91.85
24.1	9.85	90.15
27.4	11.93	88.07
31.1	14.51	85.49
35.3	17.65	82.35
40.1	21.44	78.56
45.6	25.88	74.12
51.8	30.95	69.05
58.9	36.56	63.44
66.9	42.55	57.45
76	48.71	51.29
86.4	54.81	45.19
98.1	60.61	39.39
111	65.93	34.07
127	70.62	29.38
144	74.62	25.38
163	77.95	22.05
186	80.66	19.34
211	82.87	17.13
240	84.73	15.27
272	86.36	13.64
310	87.91	12.09
352	89.49	10.51
400	91.17	8.83
454	92.94	7.06
516	94.76	5.24
586	96.49	3.51
666	97.98	2.02
756	99.09	0.91
859	99.76	0.24
976	100	0
1110	100	0
1260	100	0
1430	100	0
1630	100	0
1850	100	0
2100	100	0
2390	100	0
2710	100	0
3080	100	0
3500	100	0

Funded by the European Union

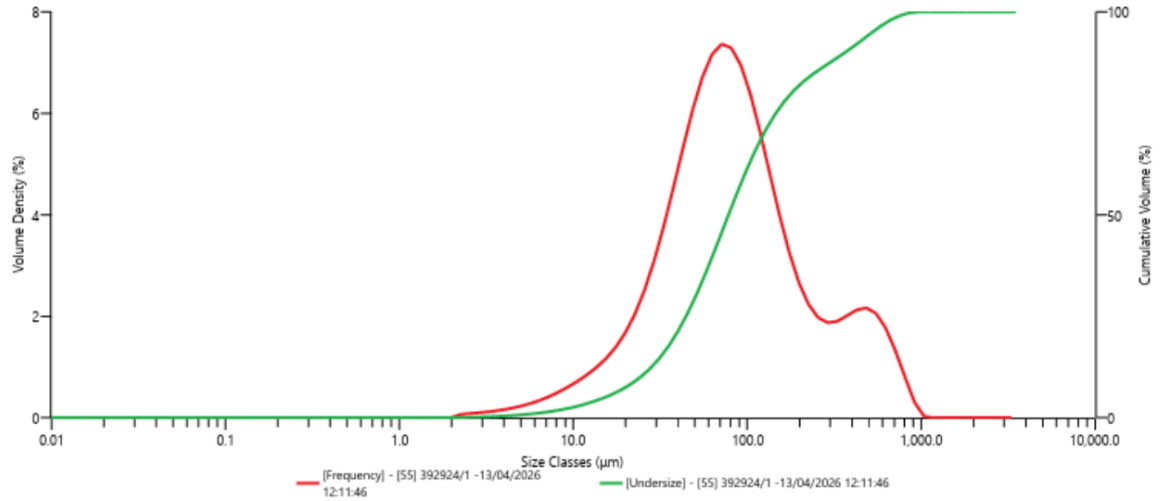

Figure II-12. Particle size analysis graph for nickel concentrate.

13.2.4.3 Physical Characteristics

Table II-38. Physical characteristics of nickel concentrate.

Test	Method	Unit	Result
Moisture Content	ISO 10251:2006	%	6.66
Specific Gravity	Pycno	-	3.74
True Density	Pycno	g/cm^3	3.74
Bulk Density	Grav	g/mL	1.32
Tapped Density	Grav	g/mL	1.61

13.2.4.4 Multi-Element Geochemical Analysis

Table II-39. Geochemical analysis of oxides in nickel concentrate.

Oxide	Al_2O_3	BaO	CaO	CoO	Cr_2O_3	CuO	Fe_2O_3	HfO_2	K_2O	MgO
Method	XRF	XRF	XRF	XRF	XRF	XRF	XRF	XRF	XRF	XRF
Units	%	%	%	%	%	%	%	%	%	%
Result	1.32	<0.02	0.90	0.86	<0.02	2.71	46.94	0.18	<0.02	6.94

Oxide	Mn_3O_4	MoO_3	Na_2O	Nb_2O_5	NiO	P_2O_5	PbO	SiO_2	SnO_2	SrO
Method	XRF	XRF	XRF	XRF	XRF	XRF	XRF	XRF	XRF	XRF
Units	%	%	%	%	%	%	%	%	%	%
Result	0.08	<0.02	<0.02	0.04	11.70	0.06	0.02	14.62	0.07	0.04

Oxide	Ta_2O_5	TiO_2	WO_3	ZnO	ZrO_2
Method	XRF	XRF	XRF	XRF	XRF
Units	%	%	%	%	%
Result	0.09	0.23	0.09	0.03	0.10

Funded by the European Union

Table II-40. Geochemical analysis of elements in nickel concentrate.

Element	Ag	As	Au	Be	Bi	Br	C	Cd	Ce	Cl
Method	ICP-OES	ICP-MS	ICP-MS	ICP-OES	ICP-MS	CIC	IGA	ICP-MS	ICP-OES	CIC
Unit	ppm	ppm	ppm	ppm	ppm	ppm	%	ppm	ppm	ppm
Result	<0.5	18.89	0.03	0.11	2.26	70.33	0.12	<0.5	3.88	129

Element	Cs	Dy	Er	Eu	F	Ga	Gd	Ge	Hg	Ho
Method	ICP-MS	ICP-MS	ICP-MS	ICP-MS	CIC	ICP-MS	ICP-MS	ICP-MS	CVAAS	ICP-MS
Unit	ppm	ppm	ppm	ppm	ppm	ppm	ppm	ppm	ppm	ppm
Result	<0.5	0.15	0.1	<0.1	56	1.59	0.17	0.97	<1	<0.1

Element	In	Ir	La	Li	Lu	Nd	Pd	Pr	Pt	Rb
Method	ICP-MS	ICP-OES	ICP-MS	ICP-OES	ICP-MS	ICP-MS	ICP-MS	ICP-MS	ICP-MS	ICP-MS
Unit	ppm	%	ppm	ppm	ppm	ppm	ppm	ppm	ppm	ppm
Result	<0.1	<0.005	<0.5	<1	<0.1	0.54	6.17	0.11	0.54	0.64

Element	Re	Rh	S	Sb	Sc	Se	Sm	Tb	Te	Th
Method	ICP-MS	ICP-OES	IGA	ICP-MS	ICP-MS	ICP-MS	ICP-MS	ICP-MS	ICP-MS	ICP-MS
Unit	ppm	%	%	ppm	ppm	ppm	ppm	ppm	ppm	ppm
Result	<0.5	<0.005	28.78	1.03	1.96	36.36	0.13	0.02	6.87	0.63

Element	Tl	Tm	U	Y	Yb
Method	ICP-MS	ICP-MS	ICP-MS	ICP-OES	ICP-MS
Unit	ppm	ppm	ppm	ppm	ppm
Result	0.77	<0.5	<0.5	1.1	<0.5

13.2.4.5 X-Ray Diffraction

Table II-41. X-ray diffraction results for nickel concentrate.

Mineral	Chemical Formula	Pre-Test	Post-Test	Difference
		Wt. %	Wt. %	Wt. %
Quartz	SiO_2	1.6	1.8	0.2
Nickelhexahydrite	$(Ni,Mg,Fe^{2+})(SO_4) \cdot 6H_2O$	9.7	ND	-9.7
Pentlandite	$(Fe,Ni)_9S_8$	18.5	19.8	1.3
Gypsum	$CaSO_4 \cdot 2H_2O$	2.7	5.2	2.5
Pyrite	FeS_2	44.8	47.9	3.1
Chalcopyrite	$CuFeS_2$	5.9	6.2	0.3
Magnetite	Fe_3O_4	0.4	0.6	0.2
Hematite	Fe_2O_3	0.3	0.5	0.2
Talc	$Mg_3Si_4O_{10}(OH)_2$	15.4	18	2.6
Szomolnokite	$Fe^{2+}SO_4 \cdot H_2O$	0.8	ND	-0.8
Total	-	100	100	-

Note: ND = not detected. The results are from a representative sample pre- and post-natural ageing test.

13.2.4.6 Automated Mineralogy

Table II-42. Nickel concentrate modal abundance data (mass %) from three pre-test subsamples and from one post-test subsample.

Mineral	Pre-Test				Post-Test	Difference
	Subsample 1	Subsample 2	Subsample 3	Average		
Quartz	0.18	0.22	0.29	0.23	0.50	0.26
Feldspar	0.09	0.09	0.09	0.09	0.22	0.13
Phyllosilicates (Mg-Fe)	0.47	0.42	0.49	0.46	0.43	-0.03
Amphibole	0.24	0.29	0.35	0.29	0.42	0.13
Talc	15.26	12.06	12.86	13.39	16.33	2.93
Clays	0.01	0.02	0.01	0.01	0.01	0.00
Others Silicates	0.14	0.15	0.19	0.16	0.20	0.04
Carbonates	0.01	0.01	0.02	0.01	0.01	0.00
Pyrite	40.39	41.05	40.50	40.65	47.42	6.77
Chalcopyrite	5.81	5.88	5.51	5.73	5.87	0.13
Bornite	0.00	0.00	0.00	0.00	ND	0.00
Chalcocite	0.00	0.00	0.00	0.00	ND	0.00
Enargite	0.00	0.01	0.00	0.00	0.00	0.00
Cu Oxides	0.08	0.22	0.25	0.18	0.32	0.14
Cu Sulphates	0.48	0.31	0.32	0.37	0.23	-0.14
Pentlandite	26.67	28.33	28.05	27.68	24.09	-3.60
Nickelhexahydrite	4.78	4.85	4.85	4.83	ND	-4.83
Sphalerite	0.02	0.06	0.01	0.03	0.00	-0.03
Anhydrite	1.59	1.47	1.61	1.56	0.79	-0.76
Szomolnokite	1.54	1.78	1.75	1.69	ND	-1.69
Other Sulphates	0.21	0.31	0.30	0.27	0.45	0.18
Ilmenite	0.08	0.14	0.09	0.10	0.08	-0.02
Fe Oxides	1.89	2.16	2.09	2.05	2.54	0.50
Apatite	0.03	0.13	0.31	0.16	0.05	-0.11
Undifferentiated	0.02	0.05	0.04	0.04	0.03	0.00
Total	100.00	100.00	100.00	100.00	100.00	-

Note: ND = not detected. The post-test modal abundance is from a sample of nickel concentrate collected following the completion of the natural ageing test.

Funded by the European Union

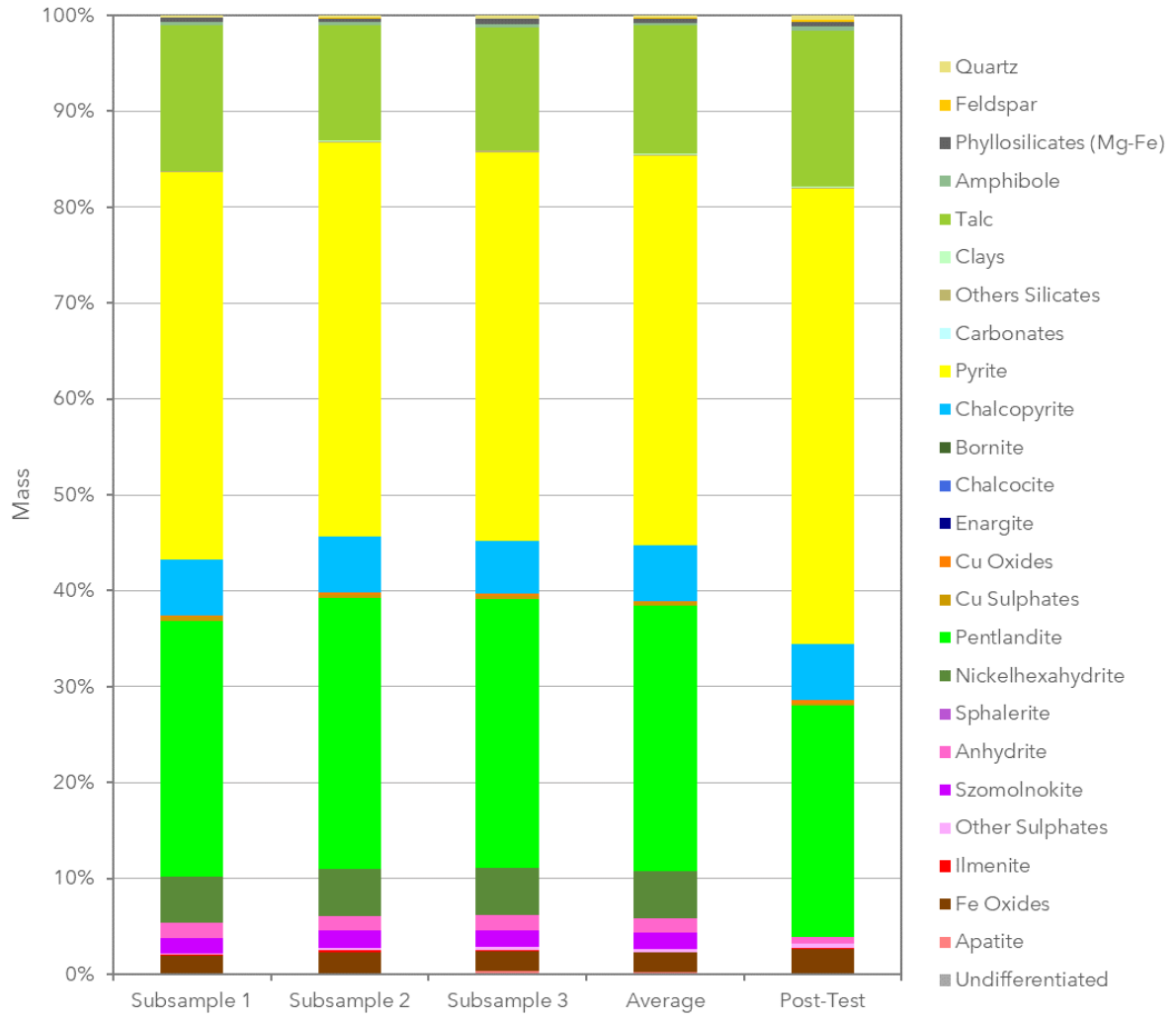

Figure II-13. Nickel concentrate modal abundance data (mass %) from three subsamples (with average abundance) and from a post-test sample.

Note: The post-test modal abundance is from a sample of nickel concentrate collected following the completion of the natural ageing test.

Funded by the European Union

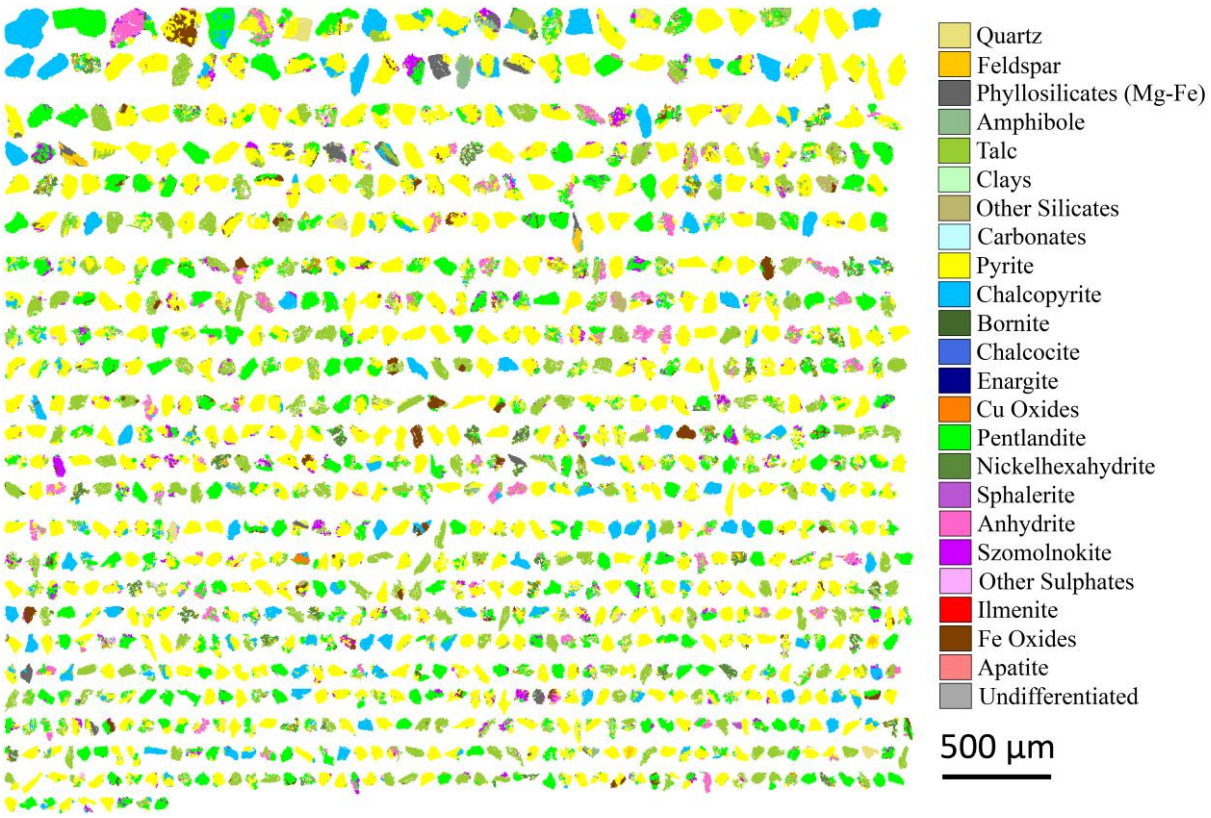

Figure II-14. Nickel concentrate particles arranged by area (subsample 1).

Funded by
the European Union

Table II-43. Nickel concentrate grain sizing from automated mineralogy.

Size (µm)	All Phases (%)	Talc (%)	Pyrite (%)	Chalcopyrite (%)	Pentlandite (%)	Nickelhexahydrite (%)
<0.01	0.00	0.0	0.0	0.0	0.00	0.0
<10.00	4.51	13.0	4.3	5.4	7.35	12.5
<20.00	17.82	41.0	18.7	20.9	28.70	43.8
<25.00	24.98	51.9	26.7	29.8	39.10	56.6
<38.00	43.56	72.9	45.9	50.1	63.65	82.1
<45.00	52.83	80.1	54.8	57.5	72.64	89.7
<53.00	62.98	86.8	64.8	64.3	81.69	95.5
<75.00	82.90	96.3	84.5	83.1	93.38	99.2
<106.00	95.81	99.7	97.8	89.0	98.31	100.0
<150.00	99.07	100.0	100.0	97.0	99.28	100.0
<212.00	100.00	100.0	100.0	100.0	100.00	100.0
All particles	100.00	100.0	100.0	100.0	100.00	100.0

Size (µm)	Anhydrite (%)	Szomolnokite (%)	Fe Oxides (%)
<0.01	0.0	0.0	0.0
<10.00	6.1	17.3	10.3
<20.00	29.8	56.6	35.6
<25.00	40.9	72.1	46.8
<38.00	62.5	89.1	72.0
<45.00	72.1	92.2	79.9
<53.00	81.0	95.6	86.9
<75.00	96.0	100.0	93.1
<106.00	96.0	100.0	95.3
<150.00	100.0	100.0	100.0
<212.00	100.0	100.0	100.0
All particles	100.0	100.0	100.0

	All Phases	Talc	Pyrite	Chalcopyrite	Pentlandite	Nickelhexahydrite
P50 (µm)	43	24	41	38	30	22
P80 (µm)	71	45	69	68	51	36

	Anhydrite	Szomolnokite	Fe Oxides
P50 (µm)	30	18	26
P80 (µm)	51	29	47
Note: Grain sizing data is from subsample 1. Grain sizing is presented in mass %.			

Table II-44. Nickel concentrate liberation data from automated mineralogy.

Category	Pyrite	Chalcopyrite	Pentlandite	Nickelhexahydrite
Free (≥95%)	52.77	54.74	45.55	38.32
Liberated (<95% to ≥80%)	20.35	14.95	19.62	16.01
High Middlings (<80% to ≥50%)	14.61	11.93	16.17	29.30
Low Middlings (<50% to ≥20%)	8.80	10.53	12.77	13.19
Locked (<20%)	3.46	7.84	5.89	3.18
Total	100.00	100.00	100.00	100.00
Note: Liberation data has been normalised to 100%.				

Funded by the European Union

13.2.5 Graphite Concentrate

13.2.5.1 Description

Table II-45. Graphite concentrate sieving test results.

Sizing	Mass Retained (g)	Mass Retained (%)	Cumulative Mass Retained (%)	Cumulative Mass Passing (%)
≥40.00 mm	0.00	0.00	0.00	100.00
<40.00 mm to ≥31.50 mm	0.00	0.00	0.00	100.00
<31.50 mm to ≥25.00 mm	0.00	0.00	0.00	100.00
<25.00 mm to ≥20.00 mm	0.00	0.00	0.00	100.00
<20.00 mm to ≥6.30 mm	0.32	0.16	0.16	99.84
<6.30 mm to ≥2.00 mm	0.10	0.05	0.21	99.79
Pan (<2.00 mm)	200.42	99.79	100.00	-
Note: Mass of test sample = 200.84 g				

Table II-46. Identification and classification of graphite concentrate.

Classification	Dark greyish black SAND. Basic anthropogenic soil.
Description	Dark greyish black massive material. Composed of metallic or metallic-like, bright silvery grey particles, which are up to 500 µm in size.
Other	No organics were found within the fractions. Artefacts consisting of a single metallic fragment (silvery grey on one surface and rusted on the rear) (18 mm in length, 11 mm in width and 1 mm thick) and an angular and equidimensional silver-grey particle (5 mm in long axis)
Note: The ≥2.00 mm and ≥6.00 mm fractions were not classed as secondary or tertiary fractions as (a) they are interpreted not to modify the engineering properties of the material, and (b) they were not deemed important for assisting in the identification of the origin of the material and thus indirectly its possible characteristics. These fractions make up 0.21% of the host material's mass. The host material was classified according to geotechnical investigation and testing standards for soil and rock. The soil identification naming convention is from BS 5930:2015+A1:2020. The colour notation used is based on the Munsell colour system (Munsell Color, 2009).	

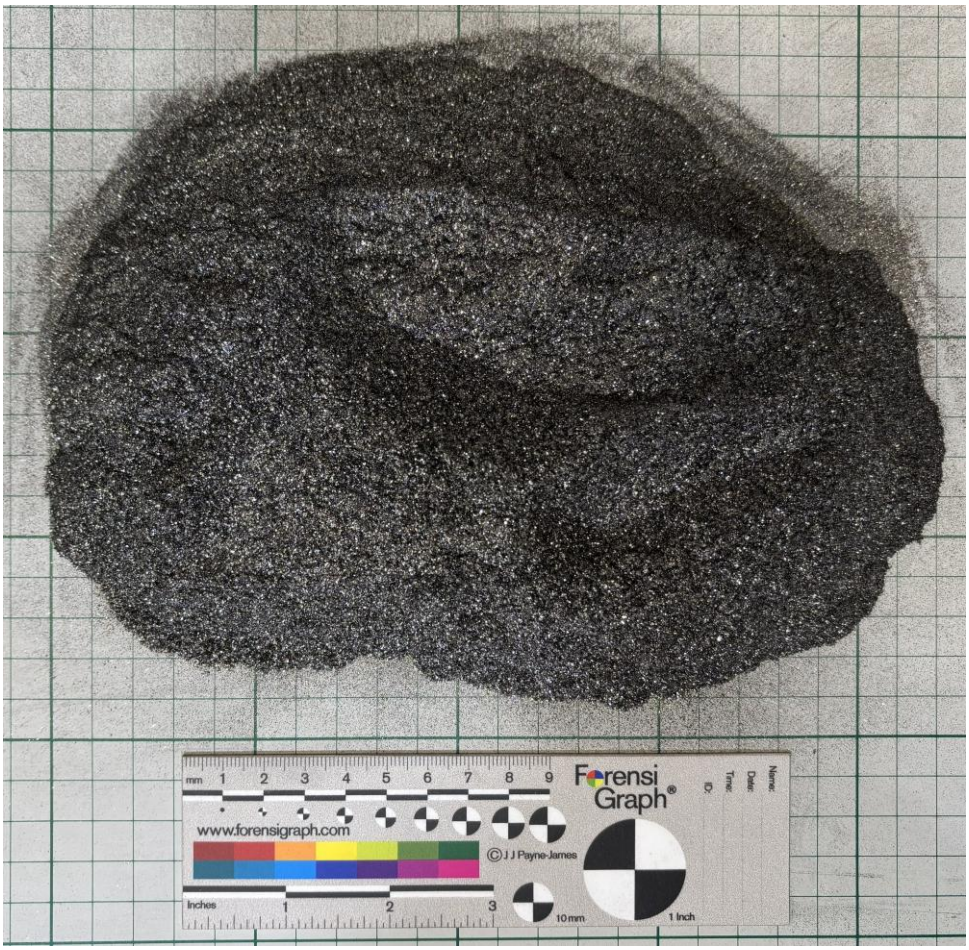

Figure II-15. Photograph of natural state graphite concentrate.

13.2.5.2 Laser Particle Sizing

Table II-47. Summary of graphite concentrate laser particle size data.

Dv(10)	Dv(50)	Dv(90)	D[4,3]
55.6 µm	242 µm	490 µm	260 µm

Table II-48. Percentage volume oversize and undersize for specific particle sizes from laser particle size analysis of graphite concentrate.

Size (µm)	% Volume Under	% Volume Over
0.01	0	100
0.0114	0	100
0.0129	0	100
0.0147	0	100
0.0167	0	100
0.0189	0	100
0.0215	0	100
0.0244	0	100
0.0278	0	100
0.0315	0	100
0.0358	0	100
0.0407	0	100
0.0463	0	100
0.0526	0	100
0.0597	0	100
0.0679	0	100
0.0771	0	100
0.0876	0	100
0.0995	0	100
0.113	0	100
0.128	0	100
0.146	0	100
0.166	0	100
0.188	0	100
0.214	0	100
0.243	0	100
0.276	0	100
0.314	0	100
0.357	0	100
0.405	0	100
0.46	0	100
0.523	0	100
0.594	0	100
0.675	0	100
0.767	0	100
0.872	0	100
0.991	0	100
1.13	0	100
1.28	0	100
1.45	0	100
1.65	0	100
1.88	0	100
2.13	0	100
2.42	0	100
2.75	0	100
3.12	0.06	99.94
3.55	0.13	99.87
4.03	0.19	99.81
4.58	0.26	99.74
5.21	0.32	99.68
5.92	0.40	99.60
6.72	0.49	99.51
7.64	0.60	99.40
8.68	0.73	99.27
9.86	0.89	99.11
11.2	1.09	98.91
12.7	1.32	98.68
14.5	1.61	98.39
16.4	1.94	98.06
18.7	2.33	97.67
21.2	2.79	97.21
24.1	3.31	96.69
27.4	3.93	96.07
31.1	4.66	95.34
35.3	5.52	94.48
40.1	6.54	93.46
45.6	7.74	92.26
51.8	9.13	90.87
58.9	10.72	89.28
66.9	12.51	87.49
76	14.46	85.54
86.4	16.57	83.43
98.1	18.87	81.13
111	21.40	78.60
127	24.29	75.71
144	27.69	72.31
163	31.78	68.22
186	36.74	63.26
211	42.66	57.34
240	49.51	50.49
272	57.10	42.90
310	65.09	34.91
352	73.03	26.97
400	80.44	19.56
454	86.89	13.11
516	92.09	7.91
586	95.90	4.10
666	98.38	1.62
756	99.75	0.25
859	100	0
976	100	0
1110	100	0
1260	100	0
1430	100	0
1630	100	0
1850	100	0
2100	100	0
2390	100	0
2710	100	0
3080	100	0
3500	100	0

Funded by the European Union

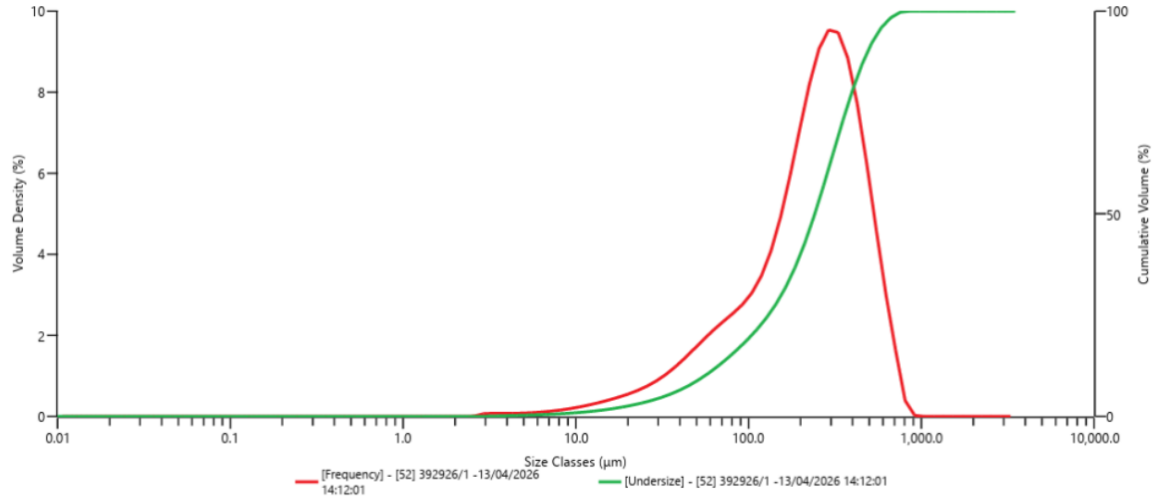

Figure II-16. Particle size analysis graph for graphite concentrate.

13.2.5.3 Physical Characteristics

Table II-49. Physical characteristics of graphite concentrate.

Test	Method	Unit	Result
Moisture Content	ISO 10251:2006	%	0.24
Susceptibility to oxidation, decomposition and sublimation	ISO 10251:2006	-	Not susceptible to oxidation, decomposition or sublimation
Specific Gravity	Pycno	-	2.25
True Density	Pycno	g/cm^3	2.25
Bulk Density	Grav	g/mL	0.48
Tapped Density	Grav	g/mL	0.68
Specific Surface Area (BET)	PA	m^2/g	1.65
Note: BET = Brunauer-Emmett-Teller theory; PA = Physical Gas Adsorption.			

Funded by the European Union

13.2.5.4 Multi-Element Geochemical Analysis

Table II-50. Geochemical analysis of elements in graphite concentrate.

Element	Ag	Al	As	Ba	Be	Bi	C	Ca	Cd	Ce
Method	ICP-OES	ICP-OES	ICP-MS	ICP-OES	ICP-OES	ICP-MS	CIC	ICP-OES	ICP-MS	ICP-OES
Unit	ppm	%	ppm	ppm	ppm	ppm	%	%	ppm	ppm
Result	3.4	0.42	3	7	0.1	0.4	96.14	0.26	0.5	77

Element	Cl	Co	Cr	Cs	Cu	Dy	Er	Eu	Fe	Ga
Method	CIC	ICP-OES	ICP-MS	ICP-MS	ICP-OES	ICP-MS	ICP-MS	ICP-MS	ICP-OES	ICP-MS
Unit	ppm	ppm	ppm	ppm	ppm	ppm	ppm	ppm	%	ppm
Result	1263	11	7	<0.5	88	0.4	0.1	0.3	0.24	2

Element	Gd	Ge	Hf	Ho	In	K	La	Li	Lu	Mg
Method	ICP-MS	ICP-MS	ICP-MS	ICP-MS	ICP-MS	ICP-OES	ICP-MS	ICP-OES	ICP-MS	ICP-OES
Unit	ppm	ppm	ppm	ppm	ppm	ppm	ppm	ppm	ppm	%
Result	1	<0.1	<0.5	0.1	<0.1	216	43	9	<0.1	0.06

Element	Mn	Mo	Na	Nb	Nd	Ni	P	Pb	Pr	Rb
Method	ICP-OES	ICP-MS	ICP-OES	ICP-MS	ICP-MS	ICP-OES	ICP-OES	ICP-MS	ICP-MS	ICP-MS
Unit	ppm	ppm	%	ppm	ppm	ppm	ppm	ppm	ppm	ppm
Result	46	24	0.01	<1	24	39	29	91	8	1

Element	Re	S	Sb	Sc	Se	Si	Sm	Sn	Sr	Ta
Method	ICP-MS	C/SA	ICP-MS	ICP-MS	ICP-MS	ICP-OES	ICP-MS	ICP-MS	ICP-OES	ICP-MS
Unit	ppm	%	ppm	ppm	ppm	%	ppm	ppm	ppm	ppm
Result	<0.5	0.06	2	0.6	<1	0.09	2	2	4	0.5

Element	Tb	Te	Th	Ti	Tl	Tm	U	V	W	Y
Method	ICP-MS	ICP-MS	ICP-MS	ICP-OES	ICP-MS	ICP-MS	ICP-MS	ICP-OES	ICP-MS	ICP-OES
Unit	ppm	ppm	ppm	ppm	ppm	ppm	ppm	ppm	ppm	ppm
Result	0.1	<0.5	6	49	<0.1	<0.5	<0.5	44	135	1

Element	Yb	Zn	Zr
Method	ICP-MS	ICP-MS	ICP-OES
Unit	ppm	ppm	ppm
Result	<0.5	31	9

13.2.5.5 X-Ray Diffraction

Table II-51. X-ray diffraction results for graphite concentrate.

Mineral	Chemical Formula	Wt. %
Muscovite/Illite	$KAl_2(AlSi)_4O_{10}(OH,F)_2$	0.4
Kaolinite	$Al_2Si_2O_5(OH)_4$	0.5
Clinochlore	$(MgFe^{2+})_5Al(Si_3Al)O_{10}(OH)_8$	0.9
Graphite	C	98.2
Total	-	100

Funded by the European Union

13.2.5.6 Automated Mineralogy

Table II-52. Modal abundance data (mass %) from three subsamples of graphite concentrate.

Mineral	Subsample 1	Subsample 2	Subsample 3	Average
Graphite	97.14	97.56	96.68	97.13
Quartz	0.42	0.08	0.10	0.20
K Feldspar	0.02	0.02	0.57	0.20
Plagioclase	0.18	0.04	0.04	0.09
Muscovite	0.03	0.03	0.03	0.03
Biotite	0.03	0.06	0.02	0.04
Illitic Clays	0.03	0.03	0.03	0.03
Kaolinite	1.16	1.06	1.33	1.18
Chlorite	0.37	0.37	0.42	0.38
Epidote	0.05	0.07	0.05	0.06
Pyroxene	0.04	0.06	0.06	0.06
Mg Silicates	0.02	0.01	0.01	0.01
Titanite	0.01	0.01	0.01	0.01
Other Silicates	0.18	0.18	0.21	0.19
Calcite	0.12	0.14	0.15	0.14
Dolomite	0.00	0.00	0.00	0.00
Fe Oxides	0.06	0.06	0.08	0.07
Ti Oxides	0.00	0.00	0.01	0.00
Fe Sulphides	0.08	0.11	0.11	0.10
Chalcopyrite	0.01	0.01	0.02	0.02
Apatite	ND	0.00	ND	0.00
Zircon	0.01	0.01	0.00	0.01
Ca Sulphates	0.01	0.06	0.02	0.03
Undifferentiated	0.03	0.03	0.03	0.03
Total	100.00	100.00	100.00	100.00
Note: ND = not detected.				

Funded by the European Union

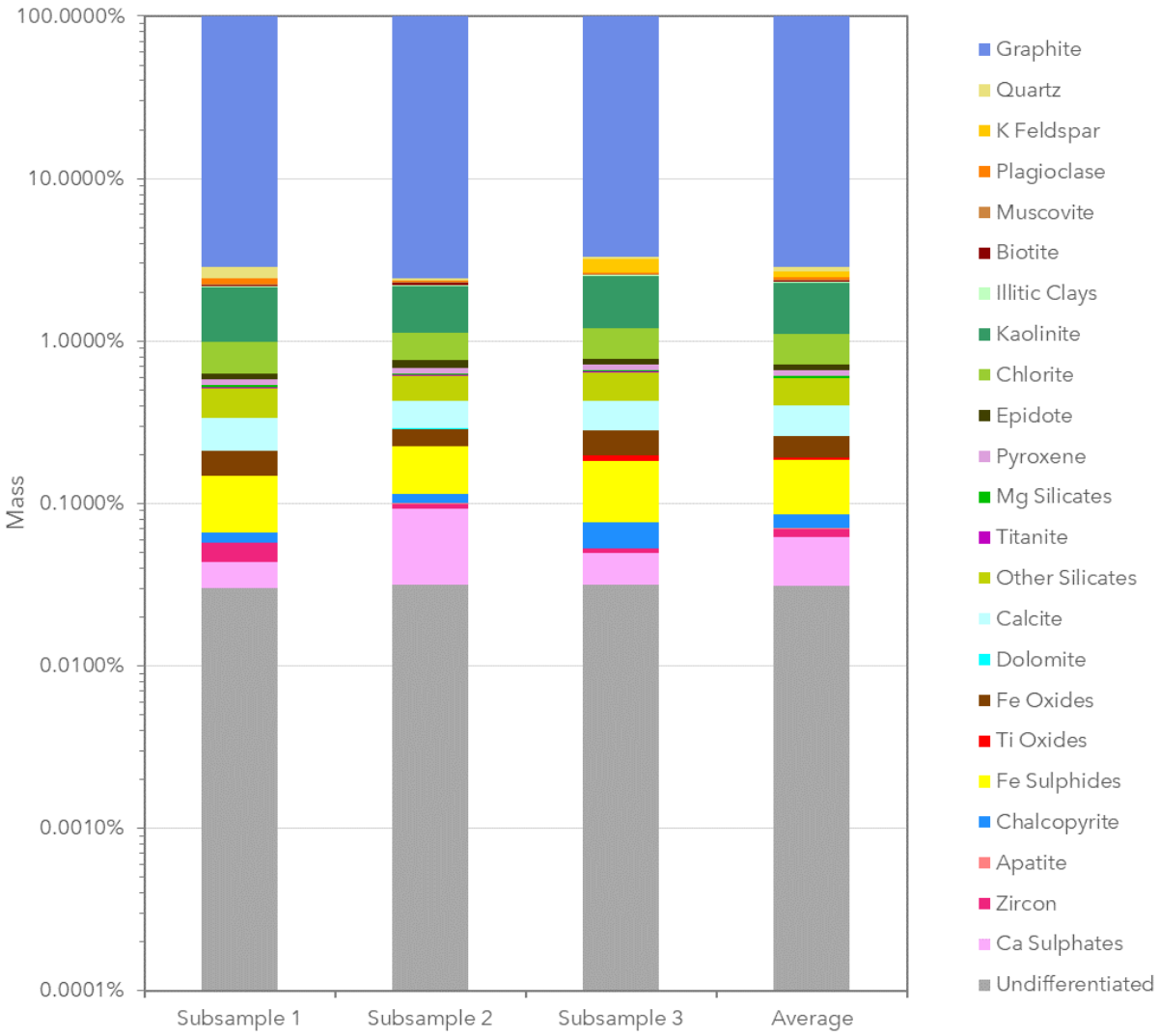

Figure II-17. Graphite concentrate modal abundance data (mass %) from three subsamples and the average abundance.

Funded by the European Union

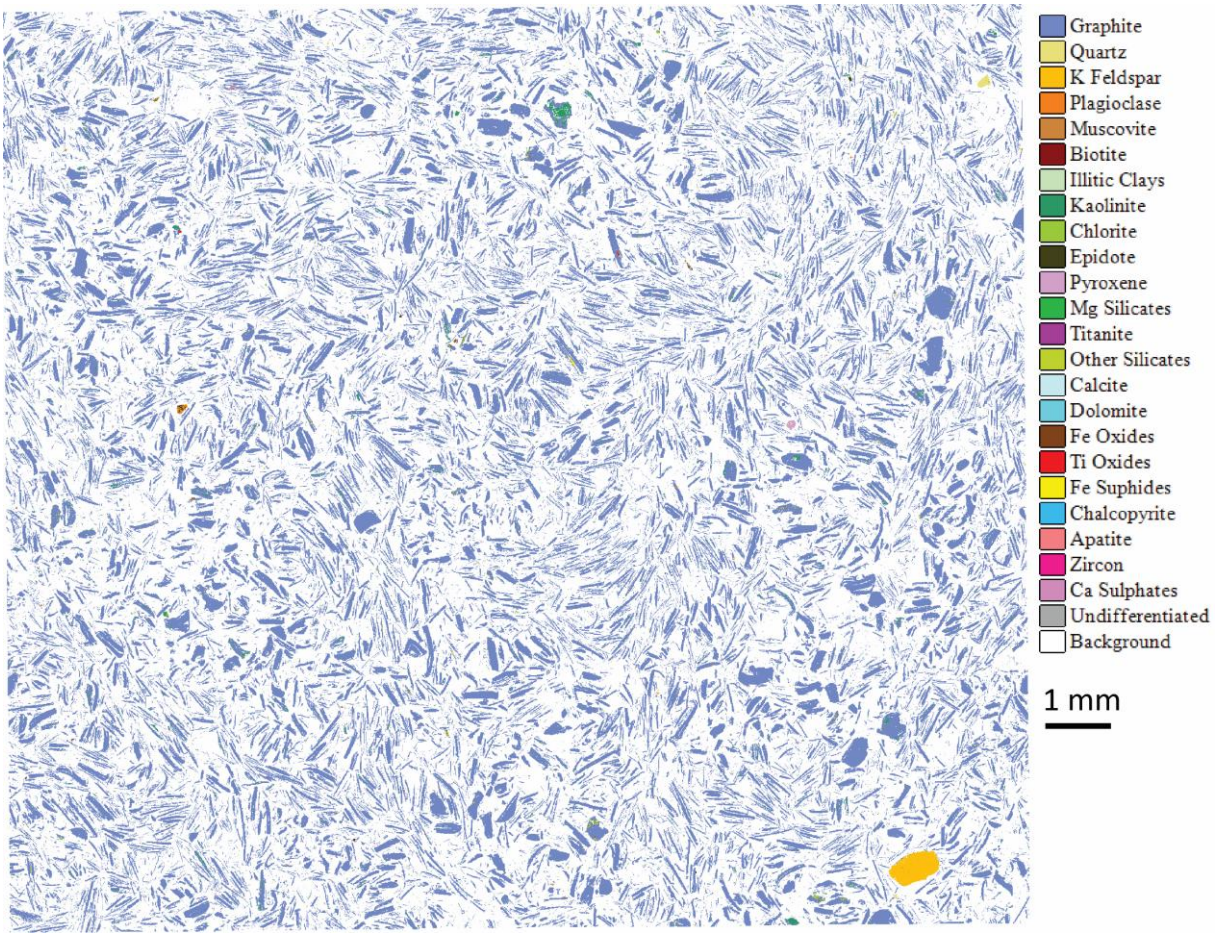

Figure II-18. Graphite concentrate particles (subsample 3).

Table II-53. Graphite concentrate grain sizing from automated mineralogy.

Size (µm)	Graphite (%)
<2.00	0.00
<9.40	0.01
<22.30	8.95
<26.50	10.02
<37.50	12.68
<44.60	14.14
<53.00	15.67
<75.00	18.76
<106.10	22.56
<150.00	28.61
<178.40	32.87
<212.10	38.20
<252.30	45.10
<300.00	54.21
<356.80	66.02
<424.30	78.16

Size (µm)	Graphite (%)
<504.50	87.53
<600.00	93.10
<713.50	96.79
<848.50	98.76
<1009.10	99.91
<1200.00	100.00
All particles	100.00

Graphite	
P50 (µm)	278
P80 (µm)	440

Note: Grain sizing data is from subsample 1. Grain sizing is presented in mass % and is based on the maximum length of each grain.

Funded by the European Union

Table II-54. Graphite concentrate liberation data from automated mineralogy.

Category	Graphite
Free (≥95%)	88.28
Liberated (<95% to ≥80%)	10.41
High Middlings (<80% to ≥50%)	1.19
Low Middlings (<50% to ≥20%)	0.11
Locked (<20%)	0.01
Total	100.00
Note: Liberation data has been normalised to 100%.	

Table II-55. Compositional groups for graphite concentrate.

Mineral	Description
Graphite	Graphite and other carbonaceous materials.
Quartz	Silica group of minerals (e.g. quartz, cristobalite, etc). Includes opal and chert.
K Feldspar	K-rich alkali feldspar including orthoclase and microcline.
Plagioclase	Plagioclase feldspar compositions from albite to anorthite.
Muscovite	Muscovite and Al-rich white mica such as sericite.
Biotite	Biotite mica. For brevity also includes Mg-rich micas such as phlogopite if present.
Illitic Clays	Illite and illite-dominant illite-smectite. May include specific mixtures of kaolinite and illite.
Kaolinite	Kaolinite and dickite.
Chlorite	Fe-rich chlorite (e.g. chamosite and intermediate Mg- and Fe-bearing compositions).
Epidote	Ca Al silicates such as epidote, zoisite, and certain zeolite compositions.
Pyroxene	Pyroxene and amphibole such as augite and hornblende.
Mg Silicates	Mg silicates such as orthopyroxene and talc.
Titanite	Titanite and perovskite.
Other Silicates	Silicate phases not included in the above categories.
Calcite	Calcite and ferroan calcite.
Dolomite	Non-ferroan dolomite.
Fe Oxides	Fe oxides such as magnetite and hematite.
Ti Oxides	Ti oxides such as rutile and anatase.
Fe Sulphides	Pyrite and marcasite. Also include pyrrhotite.
Chalcopyrite	Chalcopyrite and other Cu sulphides.
Apatite	Ca phosphates such as apatite and francolite.
Zircon	Zircon and xenotime.
Ca Sulphates	Ca Sulphates such as anhydrite and gypsum.
Undifferentiated	Phases not included in the above categories.

13.2.5.7 Other

Table II-56. Other properties of graphite concentrate.

Test	Method	Unit	Result
LOI	5 h @ 920°C	%	96.66
Volatiles	1 h @ 400°C	%	0.33
Ash Content	-	%	3.01
Fixed Carbon	-	%	96.66
Total Graphitic Carbon (TGC)	-	%	96.7

Funded by the European Union

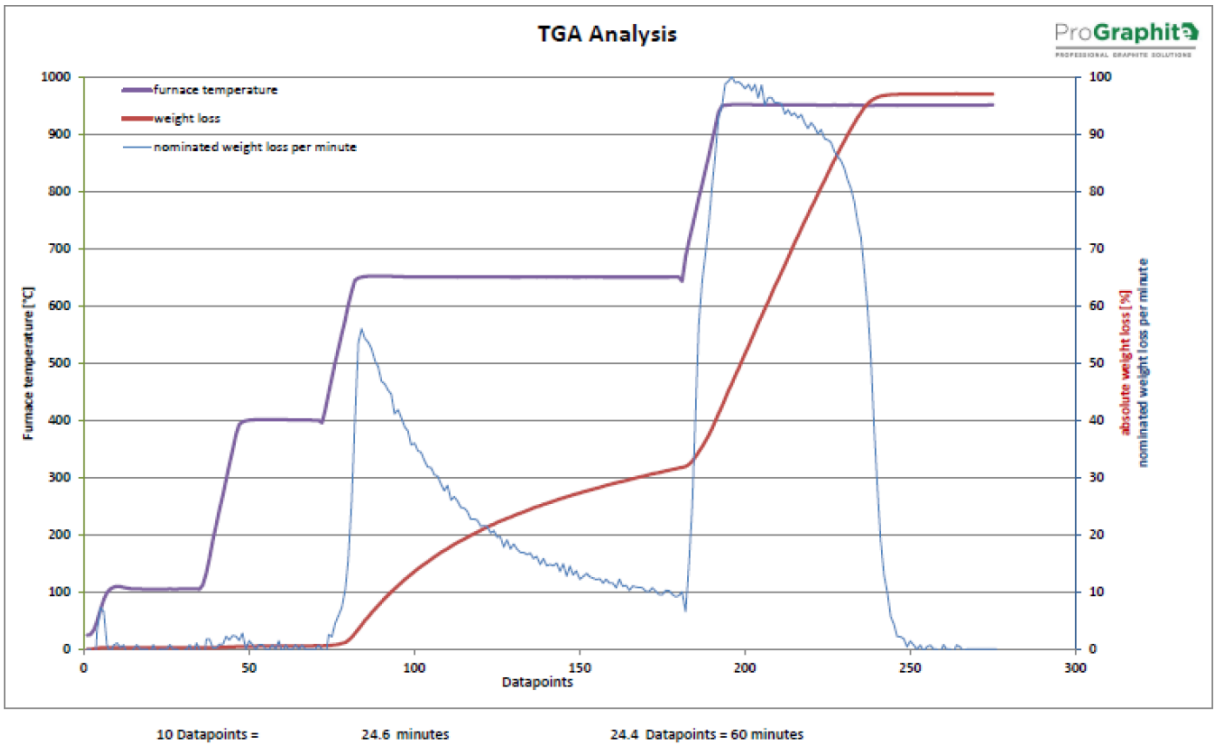

Figure II-19. Results of thermogravimetric analysis (TGA) on graphite concentrate.

Note: TGA temperature ramp: 1 h @ 105°C + 1 h @ 400°C + 4 h @ 650°C + 4 h @ 950°C.

13.2.6 Mixed Hydroxide Precipitate

Broad and low-intensity peaks returned from the XRD analysis of MHP indicated the host material had a poorly crystalline or partially amorphous nature, and semi-quantification of this material by XRD was not possible.

13.2.6.1 Description

Table II-57. Mixed hydroxide precipitate sieving test results.

Sizing	Mass Retained (g)	Mass Retained (%)	Cumulative Mass Retained (%)	Cumulative Mass Passing (%)
≥40.00 mm	0.00	0.00	0.00	100.00
<40.00 mm to ≥31.50 mm	0.00	0.00	0.00	100.00
<31.50 mm to ≥25.00 mm	0.00	0.00	0.00	100.00
<25.00 mm to ≥20.00 mm	0.00	0.00	0.00	100.00
<20.00 mm to ≥6.30 mm	68.16	19.92	19.92	80.08
<6.30 mm to ≥2.00 mm	204.36	59.71	79.63	20.37
Pan (<2.00 mm)	69.73	20.37	100.00	-
Note: Mass of test sample = 342.25 g				

Table II-58. Identification and classification of mixed hydroxide precipitate.

Classification	Dark brownish green sandy GRAVEL. Composite anthropogenic soil.
Primary Fraction and Description	Gravel is fine and medium. Consists of agglomerates that are 5Y 4/4. Dark brownish green. Agglomerates fracture conchoidally, and freshly exposed centres are 10Y 4/2 (dark greyish olive). When dried, agglomerates change colour to 5Y 7/6. Agglomerates are sub-rounded to rounded, equidimensional and have smooth surfaces. Agglomerates range in size from 2 mm to 15 mm along their longest axis (average 5.5 mm). On average, agglomerates have a sphericity of 0.8 and a roundness of 0.8. Smallest agglomerates (2 mm) are weakly magnetically attracted. Agglomerates are extremely weak and have an unconfined compressive strength of 0.6 MPa to 1 MPa. There are no visible particles within the agglomerates (material is amorphous).
Secondary Fraction and Description	Consists of agglomerates that are 5Y 4/4. Agglomerates are rounded and equidimensional. Agglomerates are fine sand (187 µm) to granule (2000 µm) sized. On average, agglomerates have a sphericity of 0.8 and a roundness of 0.9. Agglomerates are extremely weak and have an unconfined compressive strength of 0.6 MPa to 1 MPa. Agglomerates, especially the smallest agglomerates, are magnetically attracted to a magnetic pen.
Other	No organics were found within the fractions. Rare and small pieces of unidentified plastic, potentially from FIBCs, were found as free artefacts or were incorporated within agglomerates.
Note: Although this host material displays characteristics which are in line with a soil with a primary fine fraction of CLAY, the host material was classified based on the presence of gravel-sized agglomerates. The host material was classified according to geotechnical investigation and testing standards for soil and rock. The soil identification naming convention is from BS 5930:2015+A1:2020. The colour notation used is based on the Munsell colour system (Munsell Color, 2009). The sphericity and roundness were determined based on the visual chart in Krumbein & Sloss (1963) (Figure 4–9). Descriptions of soil were also adapted after Davison & Springman (2025).	

Figure II-20. Photograph of natural state mixed hydroxide precipitate.

13.2.6.2 Laser Particle Sizing

Table II-59. Summary of mixed hydroxide precipitate laser particle size data.

Dv(10)	Dv(50)	Dv(90)	D[4,3]
181 µm	641 µm	1110 µm	654 µm

Table II-60. Percentage volume oversize and undersize for specific particle sizes from laser particle size analysis of mixed hydroxide precipitate.

Size (µm)	% Volume Under	% Volume Over
0.01	0	100
0.0114	0	100
0.0129	0	100
0.0147	0	100
0.0167	0	100
0.0189	0	100
0.0215	0	100
0.0244	0	100
0.0278	0	100
0.0315	0	100
0.0358	0	100
0.0407	0	100
0.0463	0	100
0.0526	0	100
0.0597	0	100
0.0679	0	100
0.0771	0	100
0.0876	0	100
0.0995	0	100
0.113	0	100
0.128	0	100
0.146	0	100
0.166	0	100
0.188	0	100
0.214	0	100
0.243	0	100
0.276	0	100
0.314	0	100
0.357	0	100
0.405	0	100
0.46	0	100
0.523	0	100
0.594	0	100
0.675	0	100
0.767	0	100
0.872	0	100
0.991	0	100
1.13	0	100
1.28	0	100
1.45	0	100
1.65	0	100
1.88	0	100
2.13	0.07	99.93
2.42	0.14	99.86
2.75	0.21	99.79
3.12	0.29	99.71
3.55	0.36	99.64
4.03	0.45	99.55
4.58	0.56	99.44
5.21	0.67	99.33
5.92	0.80	99.20
6.72	0.93	99.07
7.64	1.06	98.94
8.68	1.20	98.80
9.86	1.32	98.68
11.2	1.45	98.55
12.7	1.57	98.43
14.5	1.69	98.31
16.4	1.80	98.20
18.7	1.92	98.08
21.2	2.05	97.95
24.1	2.18	97.82
27.4	2.31	97.69
31.1	2.46	97.54
35.3	2.61	97.39
40.1	2.78	97.22
45.6	2.97	97.03
51.8	3.17	96.83
58.9	3.42	96.58
66.9	3.72	96.28
76	4.11	95.89
86.4	4.60	95.40
98.1	5.22	94.78
111	5.98	94.02
127	6.89	93.11
144	7.92	92.08
163	9.05	90.95
186	10.25	89.75
211	11.51	88.49
240	12.88	87.12
272	14.47	85.53
310	16.49	83.51
352	19.25	80.75
400	23.08	76.92
454	28.27	71.73
516	35.04	64.96
586	43.33	56.67
666	52.86	47.14
756	63.06	36.94
859	73.14	26.86
976	82.30	17.70
1110	89.82	10.18
1260	95.29	4.71
1430	98.68	1.32
1630	99.99	0.01
1850	100	0
2100	100	0
2390	100	0
2710	100	0
3080	100	0
3500	100	0

Funded by the European Union

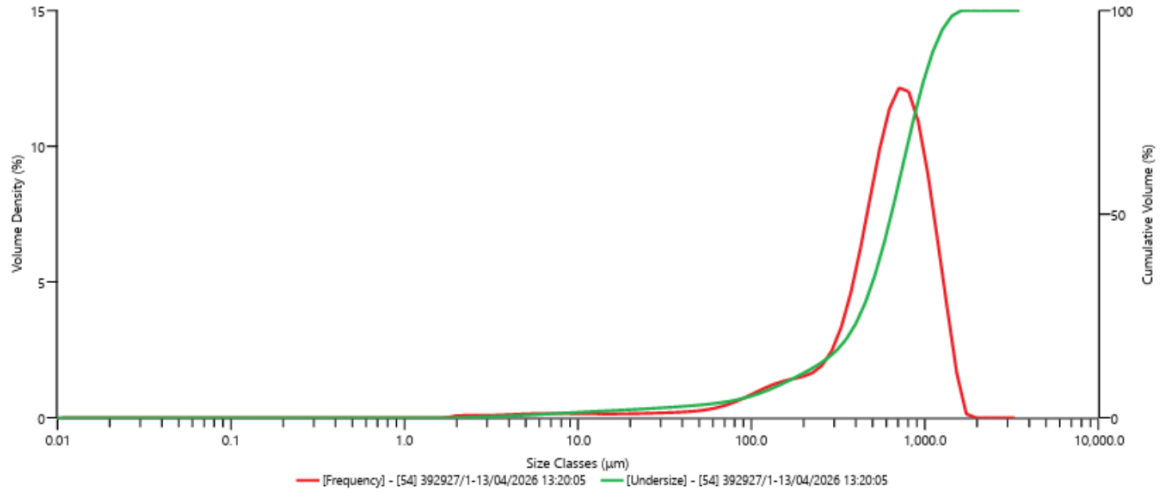

Figure II-21. Particle size analysis graph for mixed hydroxide precipitate.

13.2.6.3 Physical Characteristics

Table II-61. Physical characteristics of mixed hydroxide precipitate.

Test	Method	Unit	Result
Moisture Content	ISO 10251:2006	%	52.26
Specific Gravity	Pycno	-	2.70
True Density	Pycno	g/cm^3	2.70
Bulk Density	Grav	g/mL	0.84
Tapped Density	Grav	g/mL	0.93

Funded by the European Union

13.2.6.4 Multi-Element Geochemical Analysis

Table II-62. Geochemical analysis of elements in mixed hydroxide precipitate.

Element	Ag	Al	As	Ba	Be	Bi	Br	Ca	Cd	Ce
Method	ICP-OES	ICP-OES	ICP-MS	ICP-OES	ICP-OES	ICP-MS	CIC	ICP-OES	ICP-MS	ICP-OES
Unit	ppm	%	ppm	ppm	ppm	ppm	ppm	%	ppm	ppm
Result	5.93	0.07	1	2.66	2.42	<0.5	52.66	0.06	2.71	12.15

Element	Cl	Co	Cr	Cs	Cu	Dy	Er	Eu	F	Fe
Method	CIC	XRF	ICP-MS	ICP-MS	ICP-OES	ICP-MS	ICP-MS	ICP-MS	CIC	XRF
Unit	ppm	%	ppm	ppm	ppm	ppm	ppm	ppm	ppm	%
Result	78	3.23	14.3	<0.5	483.23	42.83	34.85	4.68	57.67	0.22

Element	Ga	Gd	Ge	Hf	Hg	Ho	In	K	La	Li
Method	ICP-MS	ICP-MS	ICP-MS	ICP-MS	CV-AAS	ICP-MS	ICP-MS	ICP-OES	ICP-MS	ICP-OES
Unit	ppm	ppm	ppm	ppm	ppm	ppm	ppm	ppm	ppm	ppm
Result	<0.5	26.82	<0.1	<0.5	<1	10.27	0.04	<10	4.06	2.82

Element	Lu	Mg	Mn	Mo	Na	Nb	Nd	Ni	P	Pb
Method	ICP-MS	ICP-OES	XRF	ICP-MS	ICP-OES	ICP-MS	ICP-MS	ICP-OES	ICP-OES	ICP-MS
Unit	ppm	%	%	ppm	%	ppm	ppm	%	ppm	ppm
Result	6.87	1.57	7.27	<5	0.18	<1	8.81	36.67	4.02	12.37

Element	Pr	Rb	Re	S	Sb	Sc	Se	Si	Sm	Sn
Method	ICP-MS	ICP-MS	ICP-MS	IGA	ICP-MS	ICP-MS	ICP-MS	ICP-OES	ICP-MS	ICP-MS
Unit	ppm	ppm	ppm	%	ppm	ppm	ppm	%	ppm	ppm
Result	1.6	<0.5	<0.5	4.4	<1	280	1.83	2.16	10.2	3.87

Element	Sr	Ta	Tb	Te	Th	Ti	Tl	Tm	U	V
Method	ICP-OES	ICP-MS	ICP-MS	ICP-MS	ICP-MS	ICP-OES	ICP-MS	ICP-MS	ICP-MS	ICP-OES
Unit	ppm	ppm	ppm	ppm	ppm	ppm	ppm	ppm	ppm	ppm
Result	3.51	0.46	5.6	<0.5	<0.5	6	<0.1	5.79	9.36	0.91

Element	W	Y	Yb	Zn	Zr
Method	ICP-MS	ICP-OES	ICP-MS	ICP-MS	ICP-OES
Unit	ppm	ppm	ppm	ppm	ppm
Result	<1	278.63	40.16	5056.3	<5

Funded by the European Union

13.2.6.5 Automated Mineralogy

Table II-63. Mixed hydroxide precipitate modal abundance data (mass %) from three pre-test subsamples and from one post-test subsample.

Mineral	Pre-Test				Post-Test	Difference
	Subsample 1	Subsample 2	Subsample 3	Average		
Ni Mn Co and Fe Sulphate	99.86	99.59	99.88	99.78	99.36	-0.42
Quartz	0.02	0.13	0.01	0.06	0.03	-0.02
Feldspar	0.03	0.01	0.00	0.01	0.02	0.00
Phyllosilicates (Mg-Fe)	0.01	0.10	0.01	0.04	0.04	0.00
Iron Silicate	0.01	0.00	0.00	0.00	0.00	0.00
Talc	0.00	0.05	0.01	0.02	0.00	-0.02
Others Silicates	0.01	0.02	0.01	0.01	0.06	0.05
Carbonates	0.00	0.00	0.00	0.00	0.00	0.00
Pyrite	0.00	0.00	0.00	0.00	0.00	0.00
Pentlandite	0.01	0.01	0.00	0.01	ND	-0.01
Anhydrite	0.05	0.01	0.00	0.02	ND	-0.02
Fe Oxides	0.00	0.00	0.05	0.02	0.08	0.06
Apatite	0.00	ND	0.00	0.00	ND	0.00
Undifferentiated	0.00	0.06	0.02	0.03	0.40	0.37
Total	100.00	100.00	100.00	100.00	100.00	-

Note: ND = not detected. The post-test modal abundance is from a sample of mixed hydroxide precipitate collected following the completion of the natural ageing test.

Funded by the European Union

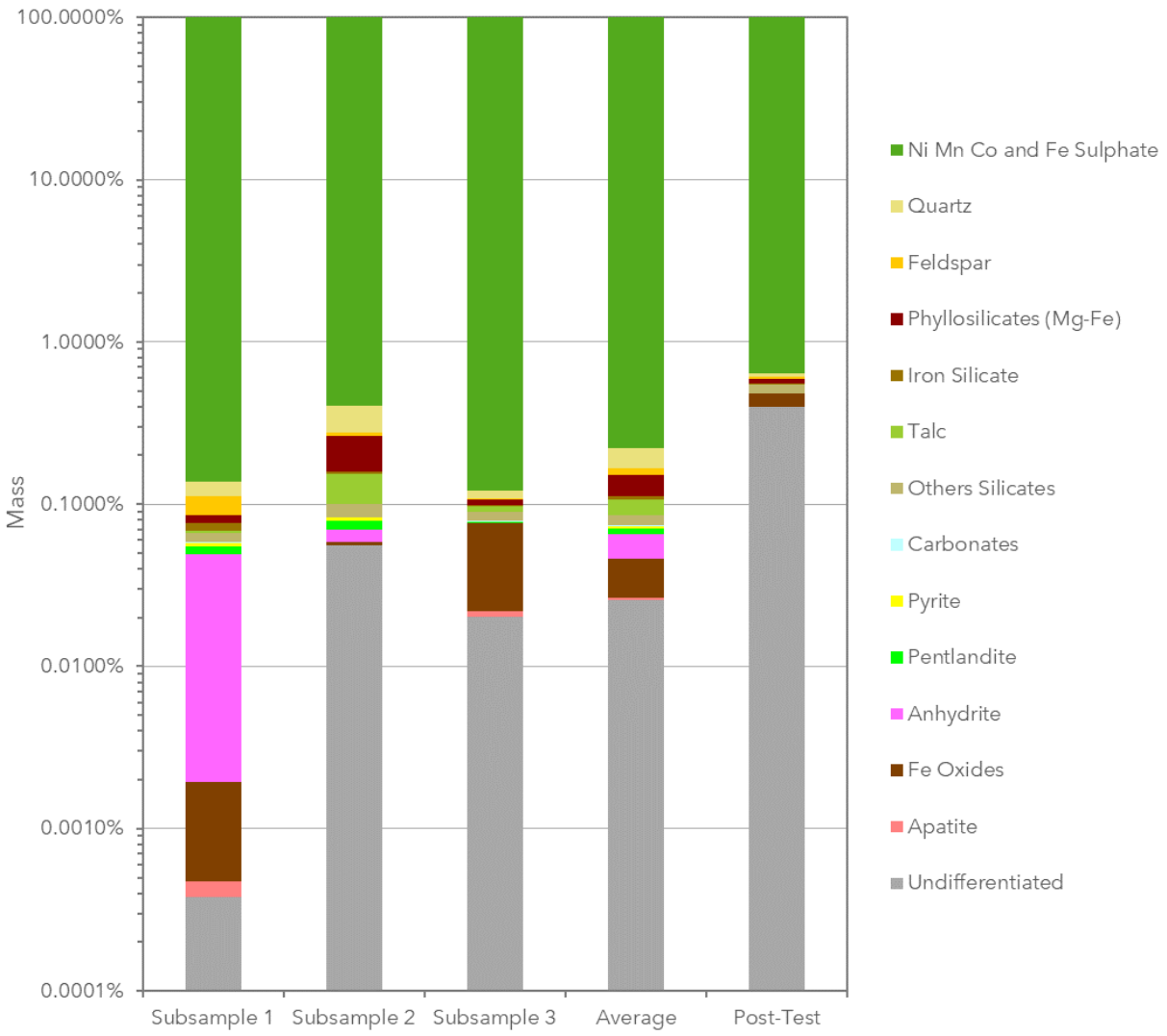

Figure II-22. Mixed hydroxide precipitate modal abundance data (mass %) from three subsamples (with average abundance) and from a post-test sample.

Note: The post-test modal abundance is from a sample of mixed hydroxide precipitate collected following the completion of the natural ageing test.

Funded by the European Union

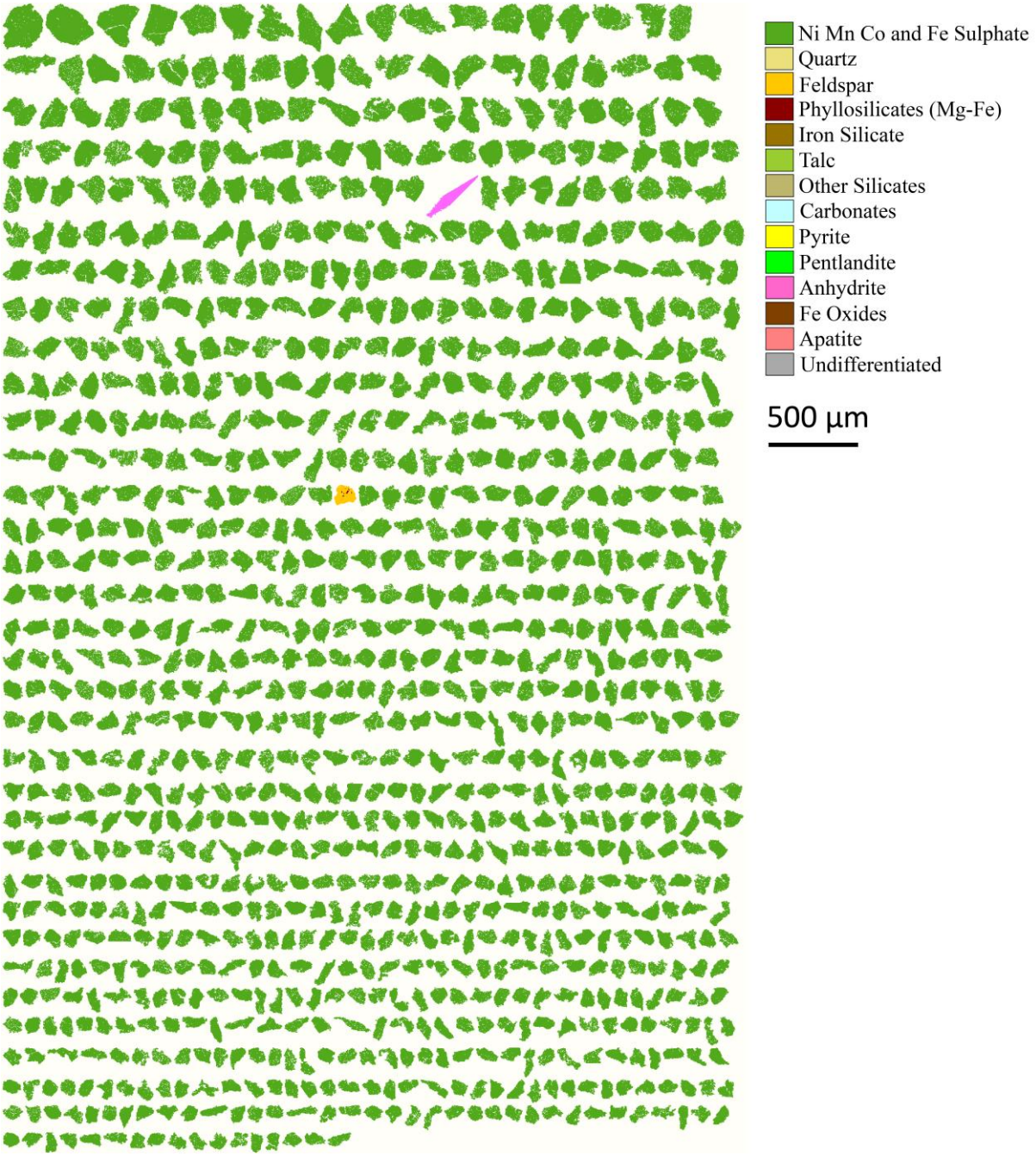

Figure II-23. Mixed hydroxide precipitate image arranged by area (subsample 1).

Funded by
the European Union

Table II-64. Mixed hydroxide precipitate grain sizing from automated mineralogy.

Size (µm)	All phases (%)	Ni Mn Co and Fe Sulphate (%)	Quartz (%)	Feldspar (%)	Phyllosilicates (Mg-Fe) (%)	Iron Silicate (%)
<0.01	0.00	0.00	0.0	0.0	0.0	0.0
<10.00	3.98	3.99	2.9	2.5	29.1	0.9
<20.00	10.93	10.99	11.9	8.3	65.5	8.4
<25.00	13.98	14.11	16.0	8.3	65.5	8.4
<38.00	23.48	23.82	23.1	8.3	100.0	8.4
<45.00	29.01	29.50	23.1	8.3	100.0	8.4
<53.00	36.13	36.88	23.1	8.3	100.0	8.4
<75.00	56.36	57.31	100.0	8.3	100.0	100.0
<106.00	80.25	81.25	100.0	8.3	100.0	100.0
<150.00	96.80	97.28	100.0	100.0	100.0	100.0
<212.00	99.67	99.67	100.0	100.0	100.0	100.0
All particles	100.00	100.00	100.0	100.0	100.0	100.0

Size (µm)	Pyrite (%)	Pentlandite (%)	Anhydrite (%)
<0.01	0.0	0.0	0.0
<10.00	0.0	10.7	0.0
<20.00	34.7	100.0	0.0
<25.00	100.0	100.0	0.0
<38.00	100.0	100.0	0.0
<45.00	100.0	100.0	7.6
<53.00	100.0	100.0	7.6
<75.00	100.0	100.0	7.6
<106.00	100.0	100.0	7.6
<150.00	100.0	100.0	100.0
<212.00	100.0	100.0	100.0
All particles	100.0	100.0	100.0

	All phases	Ni Mn Co and Fe Sulphate	Quartz	Feldspar	Phyllosilicates (Mg-Fe)	Iron Silicate
P50 (µm)	69	67	61	109	14	58
P80 (µm)	106	104	71	109	34	58

	Pyrite	Pentlandite	Anhydrite
P50 (µm)	22	14	134
P80 (µm)	22	19	134
Note: Grain sizing data is from subsample 1. Grain sizing is presented in mass %.			

Table II-65. Mixed hydroxide precipitate liberation data from automated mineralogy.

Category	Ni Mn Co and Fe Sulphate	Pentlandite	Pyrite
Free (≥95%)	85.91	83.47	79.62
Liberated (<95% to ≥80%)	14.08	0	0
High Middlings (<80% to ≥50%)	0.00	16.53	0
Low Middlings (<50% to ≥20%)	0.00	0	20.38
Locked (<20%)	0.00	0	0
Total	100.00	100.00	100.00
Note: Liberation data has been normalised to 100%.			

Funded by the European Union

13.2.7 Black Mass

13.2.7.1 Description

Table II-66. Black mass sieving test results.

Sizing	Mass Retained (g)	Mass Retained (%)	Cumulative Mass Retained (%)	Cumulative Mass Passing (%)
≥40.00 mm	0.00	0.00	0.00	100.00
<40.00 mm to ≥31.50 mm	0.00	0.00	0.00	100.00
<31.50 mm to ≥25.00 mm	0.00	0.00	0.00	100.00
<25.00 mm to ≥20.00 mm	0.00	0.00	0.00	100.00
<20.00 mm to ≥6.30 mm	0.00	0.00	0.00	100.00
<6.30 mm to ≥2.00 mm	0.00	0.00	0.00	100.00
Pan (<2.00 mm)	316.95	100.00	100.00	-
Note: Mass of test sample = 316.95 g.				

Table II-67. Identification and classification of black mass.

Classification	Dark bluish black SAND. Basic anthropogenic soil.
Description	5PB 3/1. Massive black powder; too fine to define individual particles. Contains rare (<1%) fine vitreous and metallic (silver/copper brown) particles. The material was strongly attracted to a magnetic pen.
Other	No organics were found within the fractions. Small rare pieces of burnt plastic (~1 mm) were observed within the material.
Note: The host material was classified according to geotechnical investigation and testing standards for soil and rock. The soil identification naming convention is from BS 5930:2015+A1:2020. The colour notation used is based on the Munsell colour system (Munsell Color, 2009).	

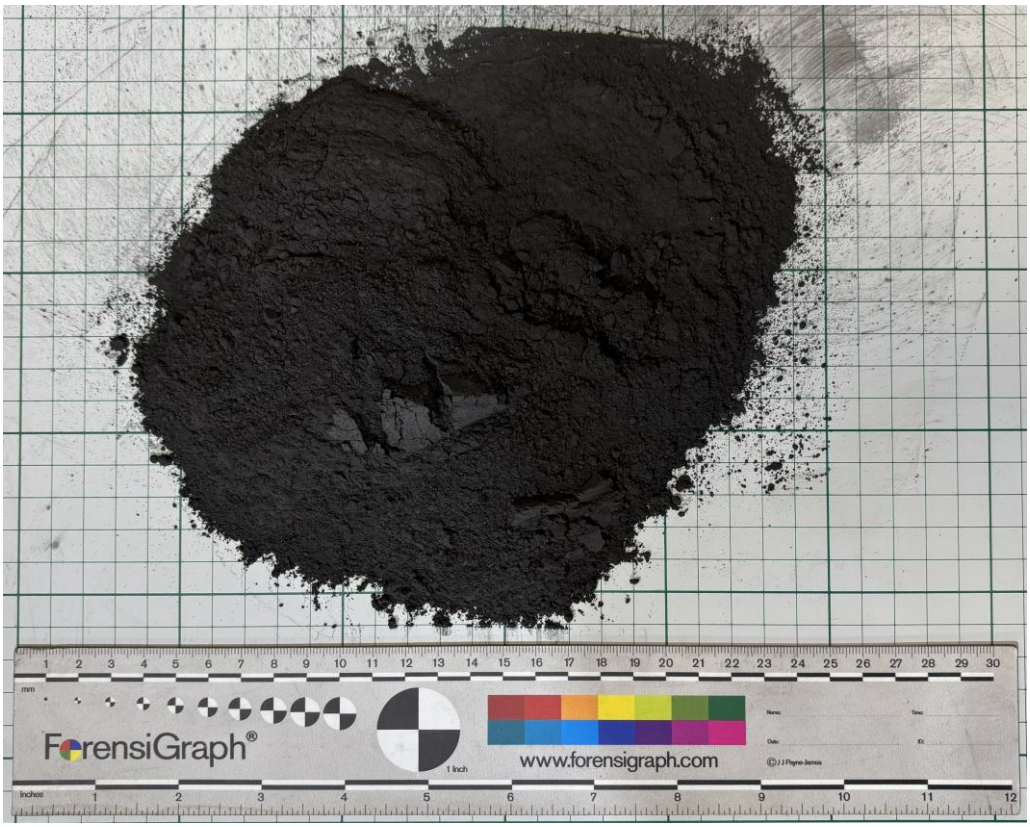

Figure II-24. Photograph of natural state black mass.

13.2.7.2 Laser Particle Sizing

Table II-68. Summary of black mass laser particle size data.

Dv(10)	Dv(50)	Dv(90)	D[4,3]
1.59 µm	10.2 µm	27.2 µm	13.7 µm

Table II-69. Percentage volume oversize and undersize for specific particle sizes from laser particle size analysis of black mass.

Size (µm)	% Volume Under	% Volume Over
0.0114	0	100
0.0129	0	100
0.0147	0	100
0.0167	0	100
0.0189	0	100
0.0215	0	100
0.0244	0	100
0.0278	0	100
0.0315	0	100
0.0358	0	100
0.0407	0	100
0.0463	0	100
0.0526	0	100
0.0597	0	100
0.0679	0	100
0.0771	0	100
0.0876	0	100
0.0995	0	100
0.113	0	100
0.128	0	100
0.146	0	100
0.166	0	100
0.188	0	100
0.214	0	100
0.243	0	100
0.276	0.09	99.91
0.314	0.23	99.77
0.357	0.43	99.57
0.405	0.71	99.29
0.46	1.07	98.93
0.523	1.54	98.46
0.594	2.10	97.90
0.675	2.78	97.22
0.767	3.57	96.43
0.872	4.47	95.53
0.991	5.47	94.53
1.13	6.57	93.43
1.28	7.76	92.24
1.45	9.03	90.97
1.65	10.38	89.62
1.88	11.81	88.19
2.13	13.32	86.68
2.42	14.94	85.06
2.75	16.69	83.31
3.12	18.59	81.41
3.55	20.66	79.34
4.03	22.95	77.05
4.58	25.48	74.52
5.21	28.29	71.71
5.92	31.44	68.56
6.72	34.99	65.01
7.64	39.04	60.96
8.68	43.61	56.39
9.86	48.71	51.29
11.2	54.27	45.73
12.7	60.15	39.85
14.5	66.14	33.86
16.4	72.02	27.98
18.7	77.54	22.46
21.2	82.51	17.49
24.1	86.76	13.24
27.4	90.22	9.78
31.1	92.88	7.12
35.3	94.82	5.18
40.1	96.13	3.87
45.6	96.99	3.01
51.8	97.53	2.47
58.9	97.92	2.08
66.9	98.26	1.74
76	98.61	1.39
86.4	98.98	1.02
98.1	99.33	0.67
111	99.64	0.36
127	99.87	0.13
144	100	0
163	100	0
186	100	0
211	100	0
240	100	0
272	100	0
310	100	0
352	100	0
400	100	0
454	100	0
516	100	0
586	100	0
666	100	0
756	100	0
859	100	0
976	100	0
1110	100	0
1260	100	0
1430	100	0
1630	100	0
1850	100	0
2100	100	0
2390	100	0
2710	100	0
3080	100	0
3500	100	0
3500	100	0

Funded by the European Union

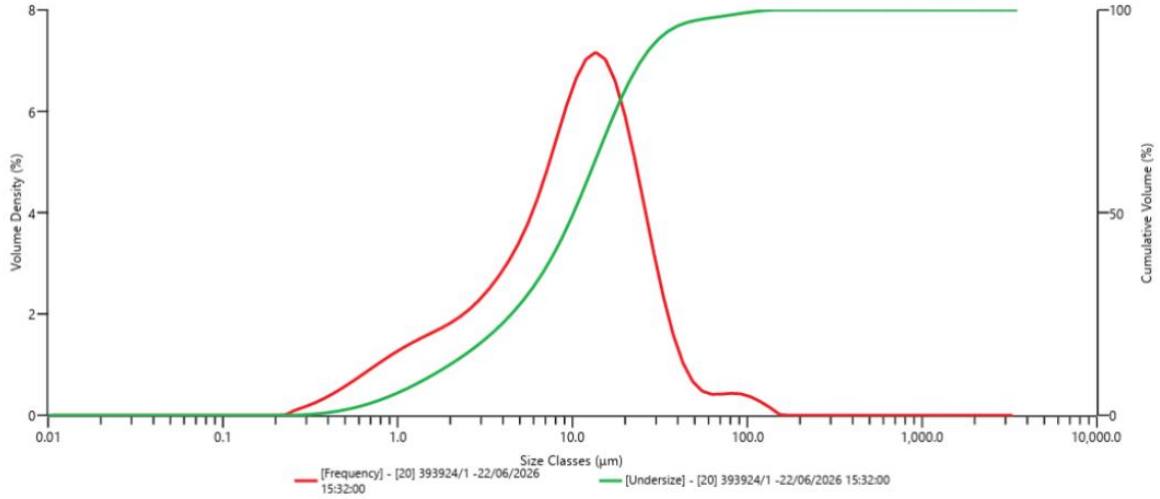

Figure II-25. Particle size analysis graph for black mass.

13.2.7.3 Physical Characteristics

Table II-70. Physical characteristics of black mass.

Test	Method	Unit	Result
Moisture Content	ISO 10251:2006	%	0.45
Specific Gravity	Pycno	-	3.24
True Density	Pycno	g/cm^3	3.24
Bulk Density	Grav	g/mL	0.81
Tapped Density	Grav	g/mL	0.98

13.2.7.4 Multi-Element Geochemical Analysis

Table II-71. Geochemical analysis of elements in black mass.

Element	Ag	Al	As	Au	Ba	Be	Bi	Br	C	Ca
Method	ICP-OES	ICP-OES	ICP-MS	ICP-MS	ICP-OES	ICP-OES	ICP-MS	CIC	C/SA	ICP-OES
Unit	ppm	%	ppm	ppm	ppm	ppm	ppm	ppm	%	%
Result	21.5	4.87	6	3.37	494	0.2	10	645	26.07	0.57

Element	Cd	Ce	Cl	Co	Cr	Cs	Cu	Dy	Er	Eu
Method	ICP-MS	ICP-OES	CIC	ICP-OES	ICP-MS	ICP-MS	ICP-OES	ICP-MS	ICP-MS	ICP-MS
Unit	ppm	ppm	ppm	%	ppm	ppm	%	ppm	ppm	ppm
Result	488	176	697	8.00	112	<0.5	7.77	2	1	0.3

Element	F	Fe	Ga	Gd	Ge	Hf	Hg	Ho	In	K
Method	IC	ICP-OES	ICP-MS	ICP-MS	ICP-MS	ICP-MS	CVAAS	ICP-MS	ICP-MS	ICP-OES
Unit	ppm	%	ppm	ppm	ppm	ppm	ppm	ppm	ppm	ppm
Result	22531	0.73	10	4	<0.1	6	<1	0.4	4	588

Element	La	Li	Lu	Mg	Mn	Mo	Na	Nb	Nd	Ni
Method	ICP-MS	ICP-OES	ICP-MS	ICP-OES	ICP-OES	ICP-MS	ICP-OES	ICP-MS	ICP-MS	ICP-OES
Unit	ppm	%	ppm	%	%	ppm	%	ppm	ppm	%
Result	289	3.40	<0.1	0.09	6.47	7	0.08	55	98	13.69

Element	P	Pb	Pd	Pr	Pt	Rb	Re	S	Sb	Sc
Method	ICP-OES	ICP-MS	ICP-MS	ICP-MS	ICP-MS	ICP-MS	ICP-MS	C/SA	ICP-MS	ICP-MS
Unit	ppm	ppm	ppm	ppm	ppm	ppm	ppm	%	ppm	ppm
Result	9024	292	0.29	26	0.13	<0.5	<0.5	0.09	547	1

Element	Se	Si	Sm	Sn	Sr	Ta	Tb	Te	Th	Ti
Method	ICP-MS	ICP-OES	ICP-MS	ICP-MS	ICP-OES	ICP-MS	ICP-MS	ICP-MS	ICP-MS	ICP-OES
Unit	ppm	%	ppm	ppm	ppm	ppm	ppm	ppm	ppm	ppm
Result	1	5.17	9	863	62	13	0.3	0.5	30	1483

Element	Tl	Tm	U	V	W	Y	Yb	Zn	Zr
Method	ICP-MS	ICP-MS	ICP-MS	ICP-OES	ICP-MS	ICP-OES	ICP-MS	ICP-MS	ICP-OES
Unit	ppm	ppm	ppm	ppm	ppm	ppm	ppm	ppm	ppm
Result	<0.1	<0.5	<0.5	25	338	12	2	980	253

Funded by the European Union

13.2.7.5 Automated Mineralogy

Table II-72. Modal abundance data (area %) from three subsamples of black mass.

Phase	Subsample 1	Subsample 2	Subsample 3	Average
Quartz	1.27	1.30	1.43	1.33
Mg Silicates	0.53	0.40	0.40	0.45
Na and Ca Glass	3.17	3.70	3.48	3.45
Other Silicates	1.66	2.13	2.00	1.93
Ca and Mg Oxides	0.41	0.35	0.53	0.43
Ca P Phases	0.26	0.36	0.32	0.31
LCO	2.84	3.09	2.75	2.89
Co Mn Oxides	0.86	0.65	0.87	0.79
Mn Oxides	5.25	5.51	5.29	5.35
Mn Al Oxides	0.47	0.44	0.48	0.46
Mn Phosphates	0.24	0.23	0.26	0.24
Fe Phosphates (LFP)	5.71	5.92	5.70	5.77
NMC 333	12.81	12.45	12.52	12.59
NMC 532	0.87	0.79	0.93	0.86
NMC 622	10.54	10.95	11.13	10.87
NMC 811	2.95	2.51	2.65	2.70
NMC (Al-Rich)	0.52	0.51	0.56	0.53
NMC (Low Co)	1.04	1.20	0.83	1.02
NMC (High Mn)	2.80	2.59	2.75	2.71
Ni Co Oxides	6.47	7.24	6.97	6.90
NMC (S-Rich)	0.07	0.05	0.03	0.05
Other Ni Phases	1.04	1.37	1.10	1.17
Al Metal	7.56	7.36	7.54	7.49
Al Oxide	18.62	18.90	17.37	18.30
Al Fluorides	0.16	0.12	0.13	0.14
Al Phosphates	0.54	0.53	0.70	0.59
Fe and Cr Oxides	0.72	0.62	1.06	0.80
Cu Metal	7.29	5.61	6.92	6.61
Other Cu Phases	1.63	1.30	1.43	1.46
Pb and Zn Phases	0.17	0.17	0.37	0.23
Sn Sb Sr Ag and W Phases	0.14	0.14	0.19	0.16
REE	0.01	0.02	0.00	0.01
Ti Phases	0.36	0.36	0.33	0.35
Cd Phases	0.02	0.01	0.02	0.02
S Phases	0.08	0.27	0.14	0.16
F Phases	0.09	0.09	0.09	0.09
Cl and P Phases	0.51	0.52	0.44	0.49
Undifferentiated	0.30	0.24	0.26	0.27
Total	100.00	100.00	100.00	100.00

Funded by the European Union

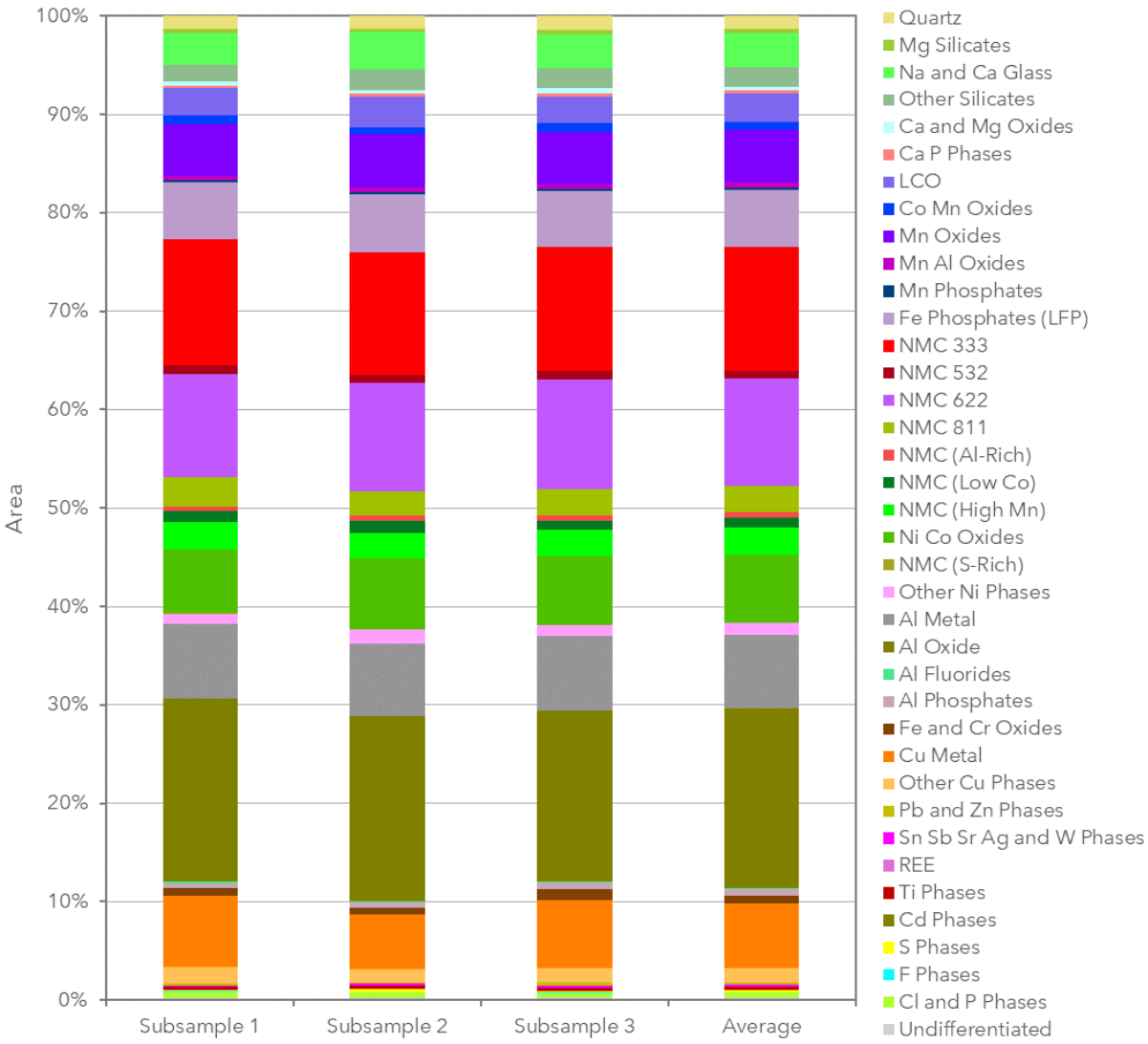

Figure II-26. Modal abundance data (area %) from three subsamples and the average modal abundance of black mass.

Funded by
the European Union

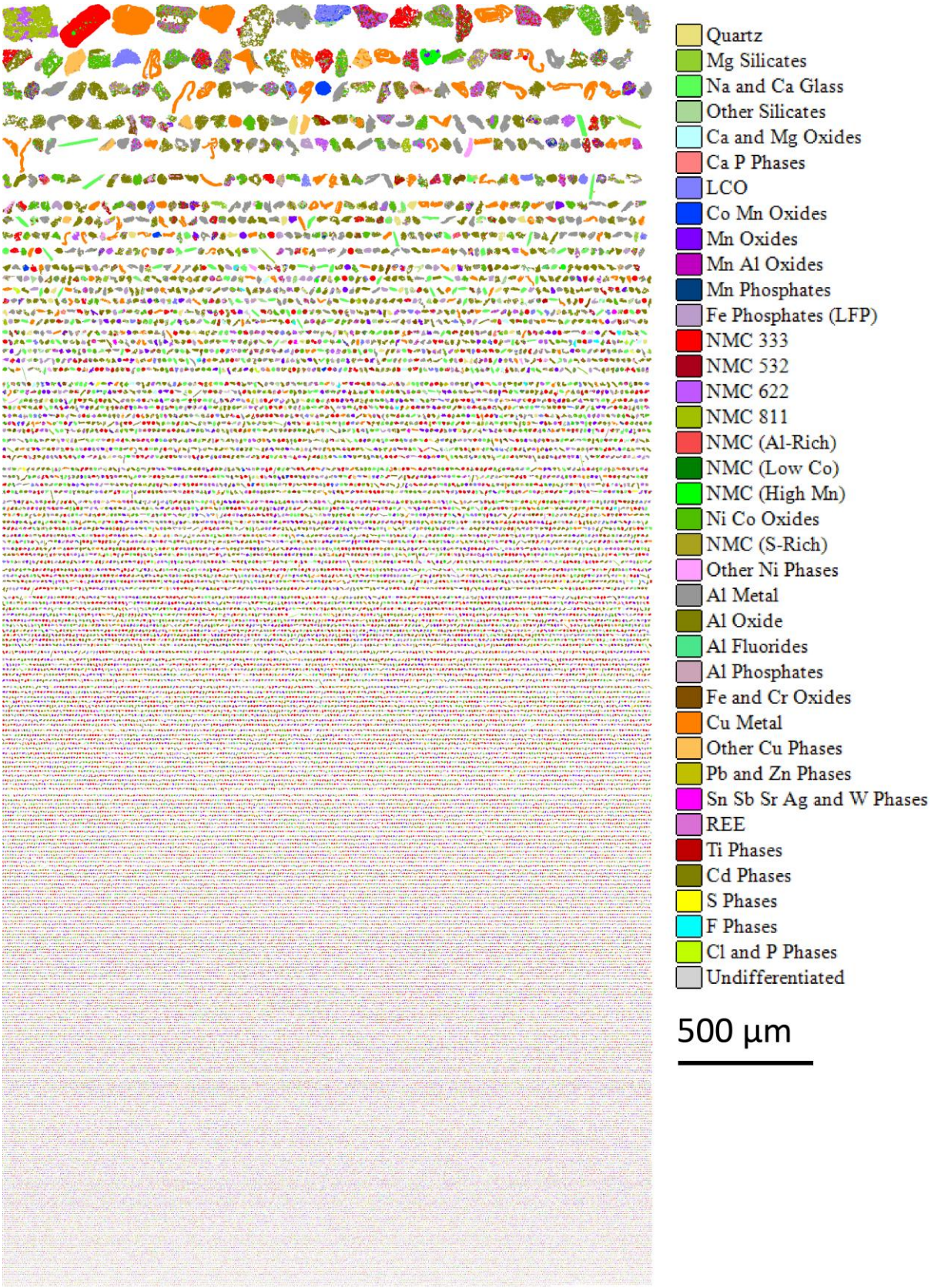

Figure II-27. Black mass particles arranged by area (subsample 1).

Funded by the European Union

Table II-73. Black mass grain sizing from automated mineralogy.

Size (µm)	All Phases (%)	LCO (%)	Mn Oxides (%)	Fe Phosphates (LFP) (%)	NMC 333 (%)	NMC 622 (%)
<0.7	0.00	0.00	0.00	0.00	0.00	0.00
<9.40	42.72	54.80	72.30	68.27	64.80	76.09
<22.30	72.41	78.82	97.75	95.77	88.35	91.79
<26.50	75.70	79.38	98.45	97.32	89.81	92.12
<37.50	80.73	83.61	100.00	98.91	91.54	96.09
<44.60	84.22	83.61	100.00	98.91	91.87	98.48
<53.00	87.06	86.05	100.00	100.00	92.38	99.15
<75.00	92.47	86.05	100.00	100.00	93.27	100.00
<106.10	97.20	100.00	100.00	100.00	95.30	100.00
<150.00	99.18	100.00	100.00	100.00	100.00	100.00
<178.40	100.00	100.00	100.00	100.00	100.00	100.00
All particles	100.00	100.00	100.00	100.00	100.00	100.00

Size (µm)	NMC 811 (%)	NMC (Low Co) (%)	NMC (High Mn) (%)	Ni Co Oxides (%)	Other Ni Phases (%)	Al Metal (%)
<0.7	0.00	0.00	0.00	0.00	0.00	0.00
<9.40	60.99	99.32	91.87	48.03	78.11	34.23
<22.30	77.94	100.00	95.80	73.95	89.83	55.17
<26.50	77.94	100.00	95.80	76.43	95.22	59.70
<37.50	79.13	100.00	95.80	85.94	95.22	65.29
<44.60	80.66	100.00	95.80	87.42	100.00	72.05
<53.00	80.66	100.00	95.80	88.50	100.00	79.05
<75.00	80.66	100.00	100.00	93.90	100.00	92.01
<106.10	80.66	100.00	100.00	100.00	100.00	95.03
<150.00	100.00	100.00	100.00	100.00	100.00	100.00
<178.40	100.00	100.00	100.00	100.00	100.00	100.00
All particles	100.00	100.00	100.00	100.00	100.00	100.00

Size (µm)	Al Oxide (%)	Cu Metal (%)	Other Cu Phases (%)
<0.7	0.00	0.00	0.00
<9.40	42.85	27.72	61.94
<22.30	75.27	41.31	68.02
<26.50	79.38	43.80	68.02
<37.50	86.11	54.01	69.75
<44.60	89.27	59.12	72.46
<53.00	93.97	62.42	80.99
<75.00	97.90	79.00	87.87
<106.10	100.00	87.39	100.00
<150.00	100.00	100.00	100.00
<178.40	100.00	100.00	100.00
All particles	100.00	100.00	100.00

	All Phases	LCO	Mn Oxides	Fe Phosphates (LFP)	NMC 333	NMC 622
P50 (µm)	11	8	5	6	7	5
P80 (µm)	36	32	12	13	13	10

	NMC 811	NMC (Low Co)	NMC (High Mn)	Ni Co Oxides	Other Ni Phases	Al Metal
P50 (µm)	7	4	4	10	4	18
P80 (µm)	42	5	6	32	10	54

	Al Oxide	Cu Metal	Other Cu Phases
P50 (µm)	11	33	5
P80 (µm)	27	77	52

Note: Grain sizing data is from subsample 1. Grain sizing is presented in mass %.

Funded by the European Union

Table II-74. Black mass liberation data from automated mineralogy.

Category	LCO	Mn Oxides	LFP	NMC 333	NMC 622	NMC 811
Free (≥95%)	60.63	62.79	75.41	33.81	25.84	16.31
Liberated (<95% to ≥80%)	12.59	13.69	6.34	20.39	11.82	32.05
High Middlings (<80% to ≥50%)	17.73	12.10	6.42	23.60	21.44	18.47
Low Middlings (<50% to ≥20%)	5.73	6.02	6.23	15.92	25.93	23.18
Locked (<20%)	3.32	5.41	5.61	6.28	14.97	9.98
Total	100.00	100.00	100.00	100.00	100.00	100.00

Category	NMC (Low Co)	NMC (High Mn)	Ni Co Oxides	Other Ni Phases	Al Metal	Al Oxides
Free (≥95%)	7.54	10.14	25.57	26.96	38.93	41.68
Liberated (<95% to ≥80%)	2.88	10.89	24.26	9.93	32.76	26.02
High Middlings (<80% to ≥50%)	14.76	15.27	26.67	12.24	13.88	18.73
Low Middlings (<50% to ≥20%)	26.23	32.33	15.61	23.20	8.00	8.60
Locked (<20%)	48.59	31.37	7.90	27.67	6.43	4.96
Total	100.00	100.00	100.00	100.00	100.00	100.00

Category	Cu Metal	Other Cu Phases
Free (≥95%)	83.06	40.76
Liberated (<95% to ≥80%)	10.98	8.17
High Middlings (<80% to ≥50%)	3.84	21.21
Low Middlings (<50% to ≥20%)	1.65	13.00
Locked (<20%)	0.46	16.87
Total	100.00	100.00
Note: Liberation data has been normalised to 100%.		

Funded by the European Union

Table II-75. Compositional groups for black mass.

Mineral	Description
Quartz	Silica and quartz.
Mg Silicates	Mg silicates such as talc and serpentine.
Na and Ca Glass	Na-bearing glass compositions. Often occurs as small prills and elongate rod-like particles. May also include other glass compositions (e.g. Ca-bearing glasses, etc).
Other Silicates	Feldspar and other silicates. May include both naturally occurring mineral matter or anthropogenic material.
Ca and Mg Oxides	Includes Ca and Mg-bearing oxides and carbonates such as calcite, dolomite, magnesite and brucite, etc.
Ca P Phases	Ca phosphates.
LCO	Co oxides interpreted to represent Li Co oxides (LCO).
Co Mn Oxides	Mn-bearing Co oxides. Likely contains Li.
Mn Oxides	Mn oxides.
Mn Al Oxides	Al-bearing Mn oxides.
Mn Phosphates	Mn phosphates and other P-bearing Mn compounds.
Fe Phosphates (LFP)	Fe phosphates interpreted to represent Li Fe phosphates (LFP).
NMC 333	Ni-, Mn-, and Co-bearing oxides with a proportion of elements consistent with NMC 333.
NMC 532	Ni-rich, Mn- and Co-bearing oxides. The proportion of elements is consistent with NMC 532.
NMC 622	Ni-rich, Mn- and Co-bearing oxides. The proportion of elements is consistent with NMC 622.
NMC 811	Ni-rich oxides with a low Mn and Co content. The proportion of elements is consistent with NMC 811.
NMC (Al-Rich)	Ni- and Co-bearing oxides. Likely contain Li.
NMC (Low Co)	Al-rich Ni-, Mn-, and Co-bearing oxides. May include binders and fillers.
NMC (High Mn)	NMC compositions with a high Mn content.
Ni Co Oxides	Ni- and Mn-rich oxides with a low Co content. Composition is similar to NMC 532 but with a low Co content and slightly higher Mn content.
NMC (S-Rich)	S-bearing NMC compositions. May include binders and fillers.
Other Ni Phases	Other Ni-bearing particles.
Al Metal	Al metal.
Al Oxide	Al oxides. Often contains F. Note that some of this material may be Br.
Al Fluorides	F-rich Al oxides. May also include F-rich Br-bearing phases such as some plastics (Al and Br lines overlap).
Al Phosphates	Al phosphates. May also include Br phosphates.
Fe and Cr Oxides	Fe and Cr-bearing oxides.
Cu Metal	Cu metal.
Other Cu Phases	Other Cu-bearing phases such as Cu oxides etc.
Pb and Zn Phases	Pb and Zn-bearing phases.
Sn Sb Sr Ag and W Phases	Metallic particles containing Sn, Sb, Ag, or W.
REE	REE-bearing phases. Also includes Zr oxides and phosphates if present.
Ti Phases	Ti-rich phases. May include pigment and filler materials.
Cd Phases	Cd-bearing phases such as Cd sulphide, Cd oxide etc.
S Phases	S-bearing phases.
F Phases	F-rich phases such as PTFE etc.
Cl and P Phases	Chlorine and/or phosphorus-bearing materials. Likely organic material or plastics. May contain Br.
Undifferentiated	Particles not reporting to the above categories. May include alloys and hydroxides containing Fe, Co, Ni and Mn in varying amounts.

Funded by the European Union

13.2.7.6 Other

Table II-76. Other properties of black mass.

Test	Method	Unit	Result
LOI	2 h @ 900°C	%	25.13

13.3 Appendix III: Additional Principal Test Data

13.3.1 Scanning Electron Microscope Micrographs

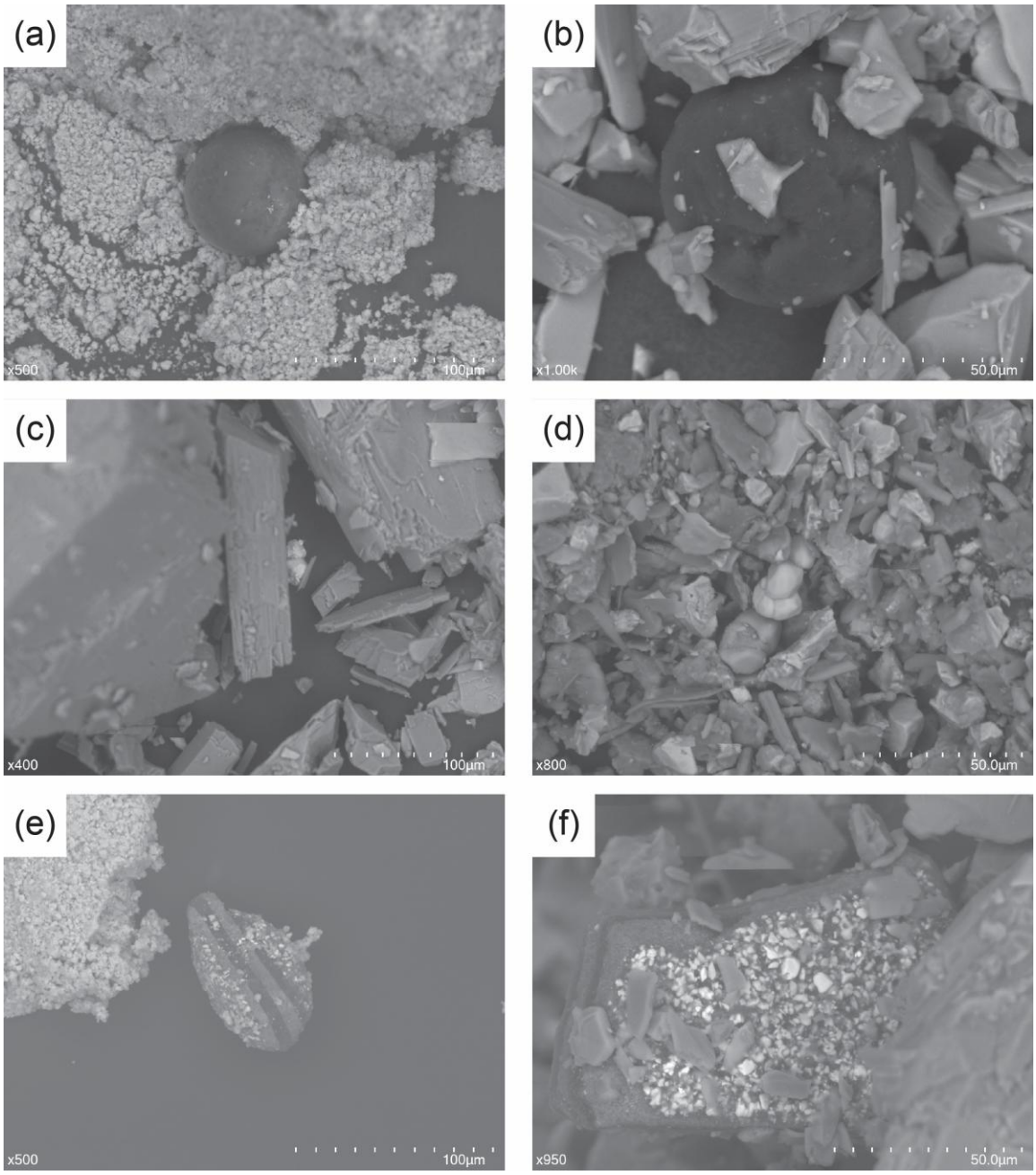

Figure III-1. Scanning Electron Microscope micrographs of tracer particles within different host materials. (a) TPA04 within mixed hydroxide precipitate, (b) TPA04 within spodumene concentrate, (c) TPA02 (centre) within spodumene concentrate, (d) TPA03 (centre) within nickel concentrate (origin A), (e) TPB01 within mixed hydroxide precipitate and (f) TPB01 within spodumene concentrate.

Funded by
the European Union

13.3.2 Natural Ageing and Photooxidative Ageing

13.3.2.1 Test Location

- WGS84: 53.424968, -2.821637
- OSGB36: 345499, 392334

13.3.2.2 Test Start and End Dates

- Natural Ageing: 9 February 2026 until 9 April 2026.
- Photooxidative Ageing: 13 March 2026 until 16 April 2026.

13.3.2.3 Climate Data Covering Test Durations

Table III-1. Climate data covering the natural ageing and photooxidative ageing test durations.

Date	Max Temp (°C)	Min Temp (°C)	Cloud Cover (%)	Wind Speed (mph)	Barometer (mbar)	Humidity (%)	Summary
09/02/2026	9	6	80	14	1015.2	88	Mostly Cloudy
10/02/2026	8	5	90	12	1016.3	85	Mostly Cloudy
11/02/2026	9	7	100	15	1013.2	92	Overcast
12/02/2026	7	4	75	11	1010.8	82	Partly Cloudy
13/02/2026	5	2	40	9	1020	78	Scattered Clouds
14/02/2026	4	2	60	8	1021	80	Partly Cloudy
15/02/2026	7	4	90	13	1014.2	86	Mostly Cloudy
16/02/2026	8	5	100	16	1008.5	90	Light Rain / Overcast
17/02/2026	5	2	70	14	1009.8	84	Passing Clouds
18/02/2026	6	3	50	10	1017.6	77	Partly Cloudy
19/02/2026	7	4	85	12	1015.2	81	Mostly Cloudy
20/02/2026	9	7	95	18	1006.4	89	Mostly Cloudy
21/02/2026	12	8	100	22	1001.7	93	Rain / Overcast
22/02/2026	11	9	100	20	1003	91	Overcast
23/02/2026	10	7	80	15	1010.8	85	Mostly Cloudy
24/02/2026	13	9	40	12	1018.6	76	Partly Cloudy
25/02/2026	12	8	65	14	1016.6	79	Partly Cloudy
26/02/2026	13	9	80	16	1011.9	84	Mostly Cloudy
27/02/2026	10	6	90	11	1016.3	82	Mostly Cloudy
28/02/2026	8	5	50	9	1020	75	Partly Cloudy
01/03/2026	10	7	85	12	1017.6	80	Mostly Cloudy
02/03/2026	12	9	75	14	1014.2	78	Passing Clouds
03/03/2026	10	6	90	10	1021	83	Mostly Cloudy
04/03/2026	11	8	95	11	1020	85	Mostly Cloudy
05/03/2026	10	7	100	13	1018.6	88	Overcast
06/03/2026	8	5	100	15	1021	93	Light Rain / Overcast
07/03/2026	9	4	40	8	1023.4	74	Clear / Passing Clouds
08/03/2026	11	6	30	9	1022	70	Sunny Intervals
09/03/2026	12	8	60	11	1017.6	76	Partly Cloudy
10/03/2026	11	7	80	14	1015.2	82	Mostly Cloudy
11/03/2026	12	8	90	16	1010.8	85	Mostly Cloudy
12/03/2026	13	9	100	18	1007.5	90	Overcast
13/03/2026	8	3	95	20	1003	84	Rain / Breezy
14/03/2026	7	2	40	12	1013.2	72	Scattered Clouds
15/03/2026	8	4	70	10	1016.3	78	Partly Cloudy
16/03/2026	10	5	85	11	1017.6	81	Mostly Cloudy
17/03/2026	13	9	100	14	1011.9	87	Drizzle / Overcast

18/03/2026	13	10	95	15	1009.8	89	Mostly Cloudy
19/03/2026	14	9	60	12	1016.3	79	Partly Cloudy
20/03/2026	10	6	80	13	1020	82	Mostly Cloudy
21/03/2026	11	7	90	10	1022	84	Mostly Cloudy
22/03/2026	9	5	100	12	1018.6	88	Overcast
23/03/2026	10	6	75	14	1015.2	80	Passing Clouds
24/03/2026	12	8	40	11	1017.6	74	Partly Cloudy
25/03/2026	7	3	30	9	1023.4	68	Clear
26/03/2026	8	4	60	10	1022	72	Scattered Clouds
27/03/2026	10	7	85	13	1017.6	81	Mostly Cloudy
28/03/2026	9	5	90	15	1014.2	85	Mostly Cloudy
29/03/2026	11	6	40	11	1018.6	76	Partly Cloudy
30/03/2026	11	7	70	12	1016.6	80	Partly Cloudy
31/03/2026	13	9	95	14	1011.9	88	Mostly Cloudy
01/04/2026	11	4	40	8	1020	70	Mostly Sunny
02/04/2026	12	5	60	10	1017.6	74	Partly Cloudy
03/04/2026	13	6	75	11	1016.3	78	Partly Cloudy
04/04/2026	12	7	90	12	1015.2	82	Mostly Cloudy
05/04/2026	11	6	100	14	1010.8	87	Overcast
06/04/2026	12	8	90	15	1011.9	85	Mostly Cloudy
07/04/2026	13	7	40	9	1017.6	72	Partly Cloudy
08/04/2026	14	8	50	10	1016.6	75	Partly Cloudy
09/04/2026	13	9	80	12	1014.2	81	Mostly Cloudy
10/04/2026	12	8	100	16	1007.5	90	Rain / Overcast
11/04/2026	12	5	40	13	1013.2	74	Partly Cloudy
12/04/2026	13	6	30	10	1021	68	Sunny
13/04/2026	14	8	65	11	1020	72	Passing Clouds
14/04/2026	15	9	75	12	1018.6	76	Partly Cloudy
15/04/2026	14	8	85	10	1017.6	79	Mostly Cloudy
16/04/2026	13	7	90	13	1015.2	83	Mostly Cloudy

Note: Data is obtained from the weather station located at the Liverpool John Lennon Airport (located within 1 km of WGS84: 53.3400, -2.8500) (Time and Date, 2026). This weather station is approximately 10.45 km south-southwest of the location of the natural ageing and photooxidative ageing tests. Minimum and maximum daily temperatures were taken from the hourly temperature records. Daily cloud cover, wind speed, barometer and humidity data are averaged from hourly data.

13.3.3 Artificial Climate Ageing

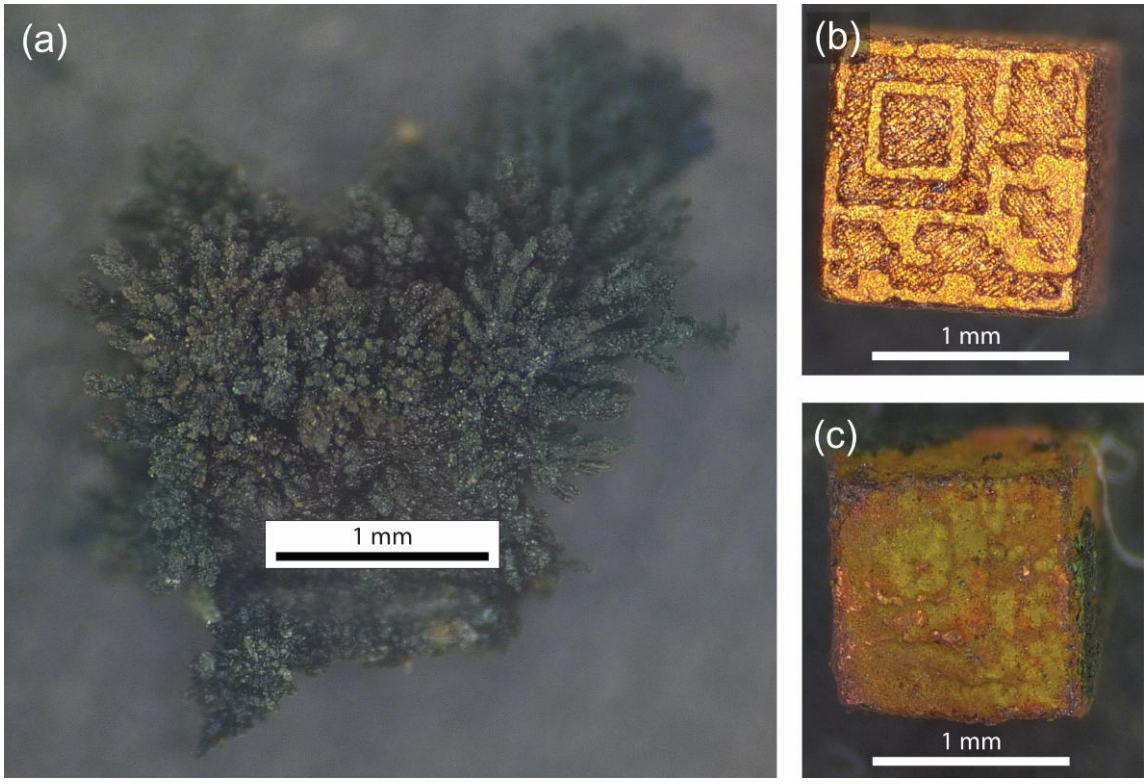

Figure III-2. TPM01 subjected to 75°C and 85% RH for five days in nickel concentrate (origin A) (targeted test). (a) TPM01 entirely covered in greenish black mineral(s), (b) TPM01 pre-test, and (c) TPM01 from (a) after washing with water, revealing the degraded micro QR code.

Funded by
the European Union

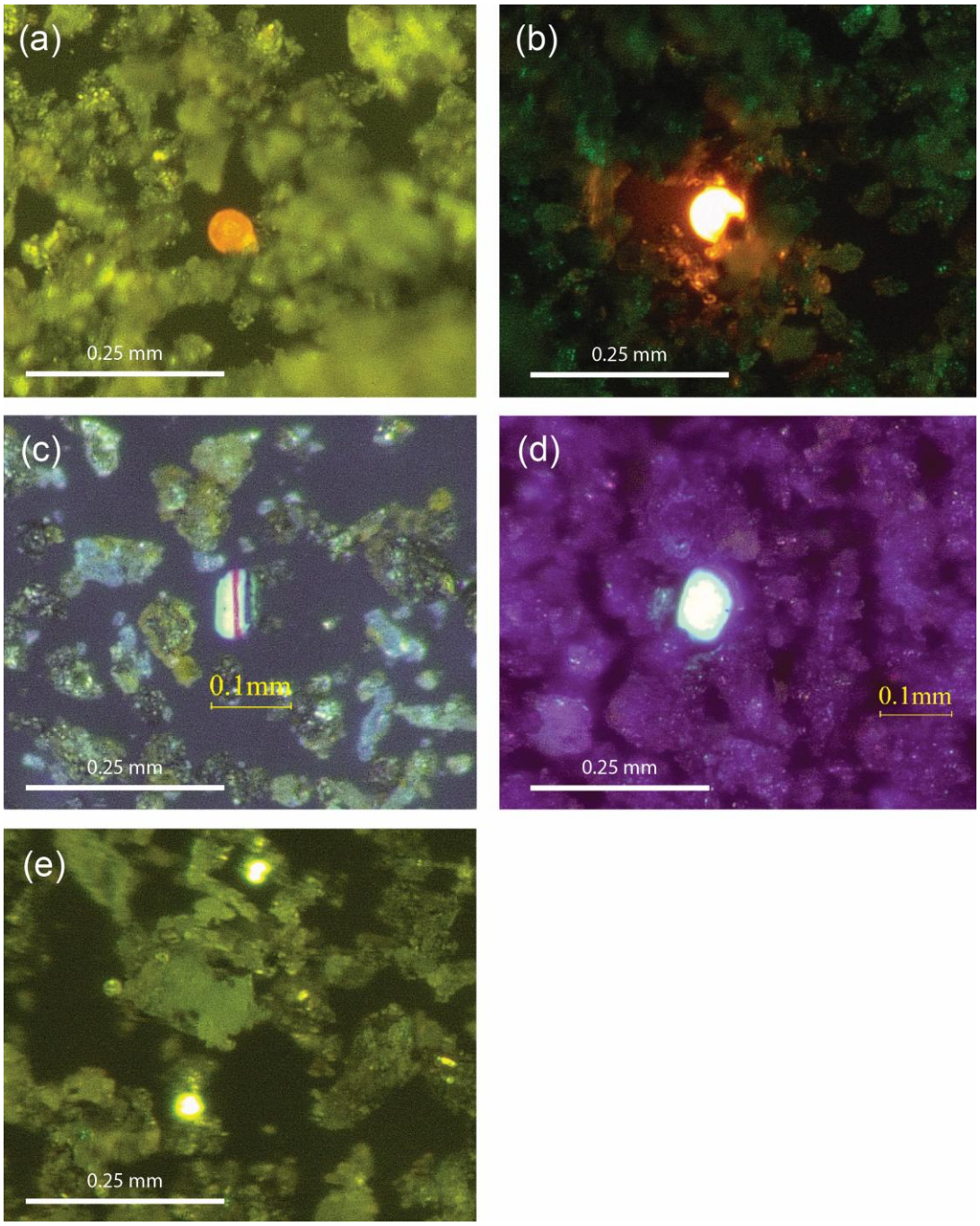

Figure III-3. Effect of temperature and humidity (40°C and 80% RH) in nickel concentrate (origin A) over three weeks (as part of the artificial climate ageing long-term test). (a) TPA04 in natural light, (b) TPA04 with excitation light, (c) TPB01 in natural light, (d) TPB01 with excitation light and (e) TPA03 with excitation light.

Funded by the European Union

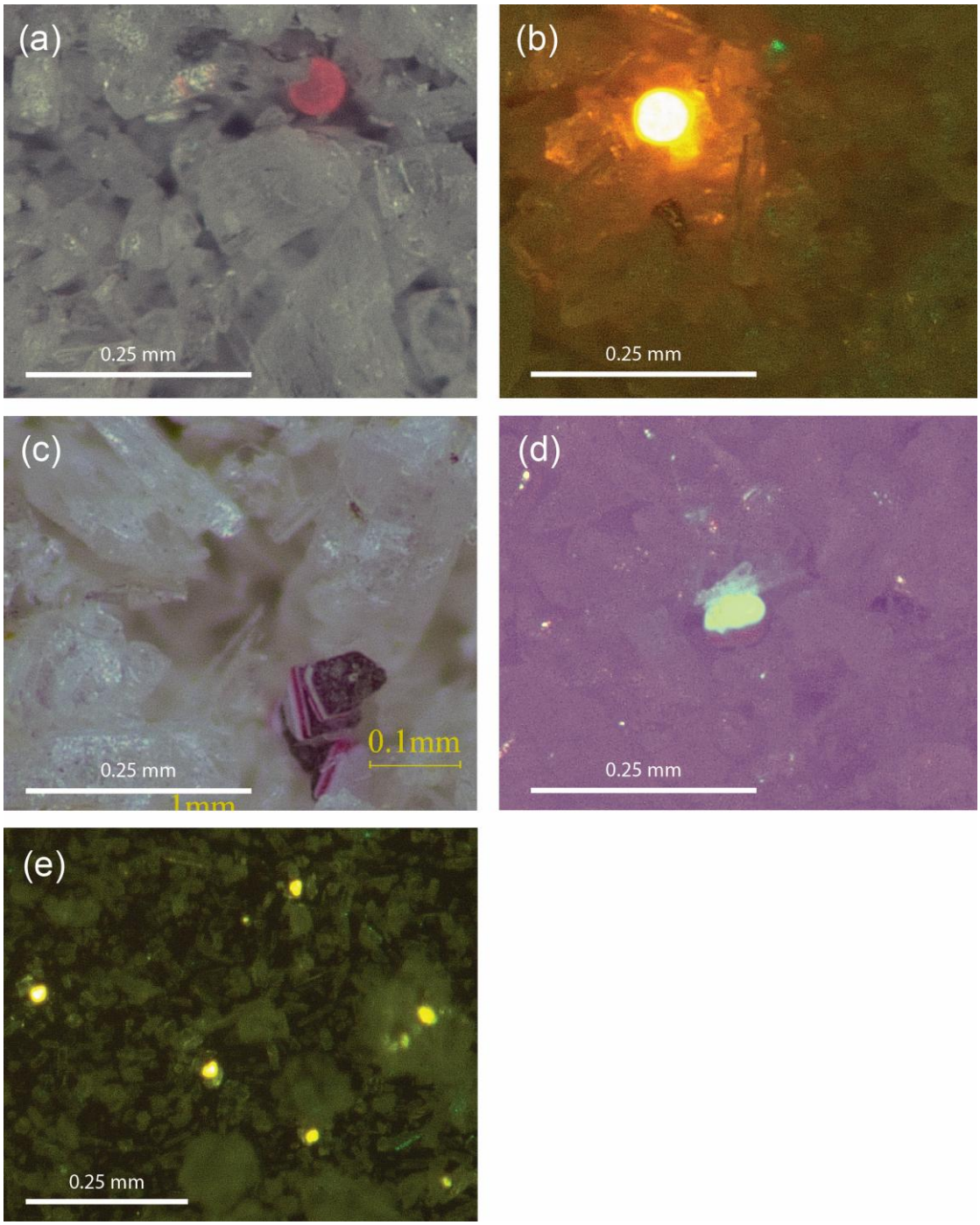

Figure III-4. Effect of temperature on tracer particle performance in spodumene concentrate at –5°C over a two-week period following ageing at 40°C and 80% RH over three weeks (as part of the artificial climate ageing long-term test). (a) TPA04 under natural light, (b) TPA04 under excitation light, (c) TPB01 under natural light, (d) TPB01 under ultraviolet excitation light, and (e) TPA02 under excitation light. TPA02 was not visible under natural light in the spodumene concentrate.

Funded by
the European Union

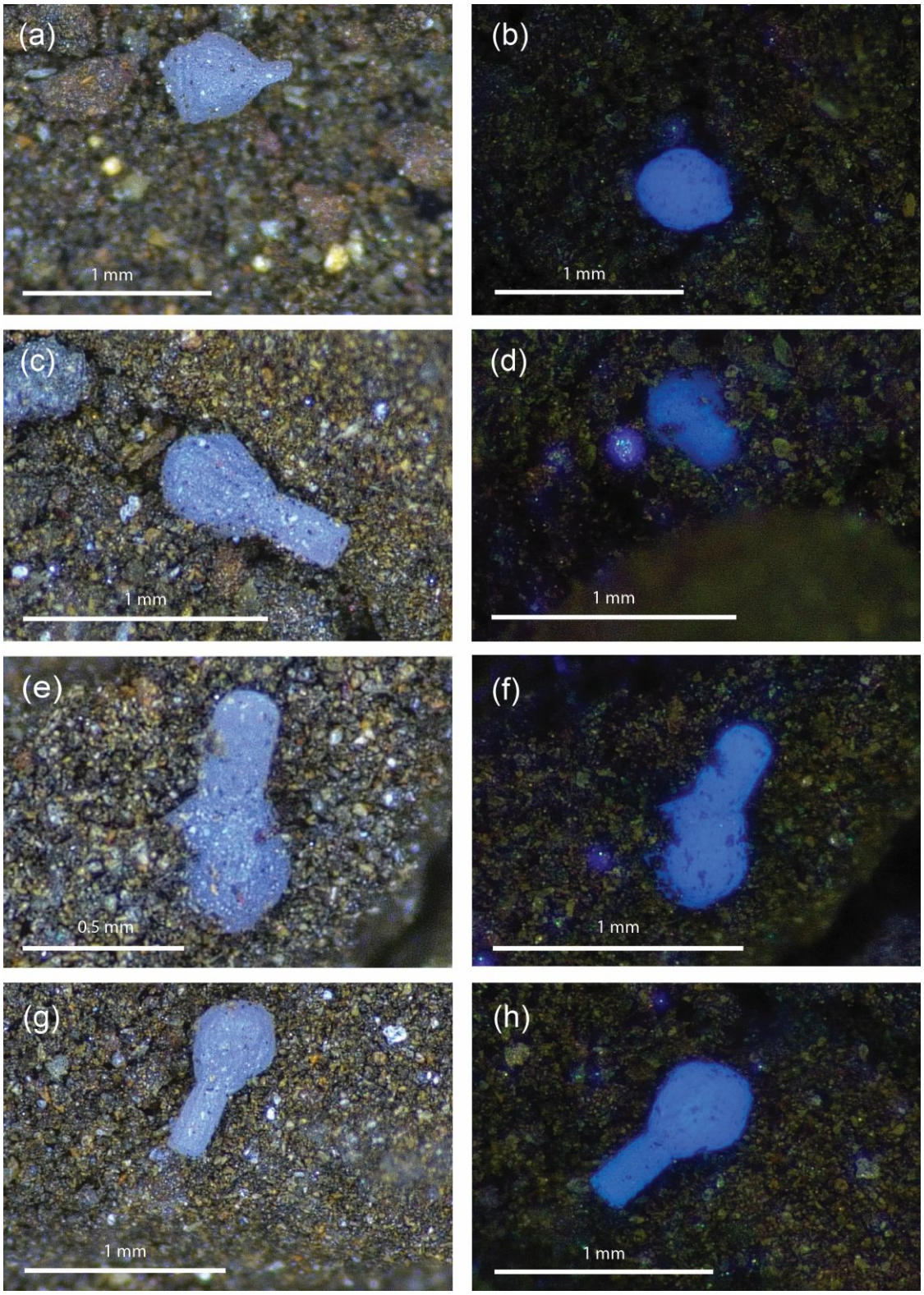

Figure III-5. TPG01 tracer particles in nickel concentrate (origin B) following the short-term low humidity artificial climate ageing tests. Following ageing at 45°C over a 48-h period under (a) natural light and (b) ultraviolet (UV) excitation light; subsequently at 55°C over a 48-h period under (c) natural light and (d) UV excitation light; at 65°C over a 48-h period under (e) natural light and (f) UV excitation light; subsequently at 75°C over a 48-h period under (g) natural light and (h) UV excitation light. Tests were conducted at a humidity of <20% RH.

Funded by the European Union

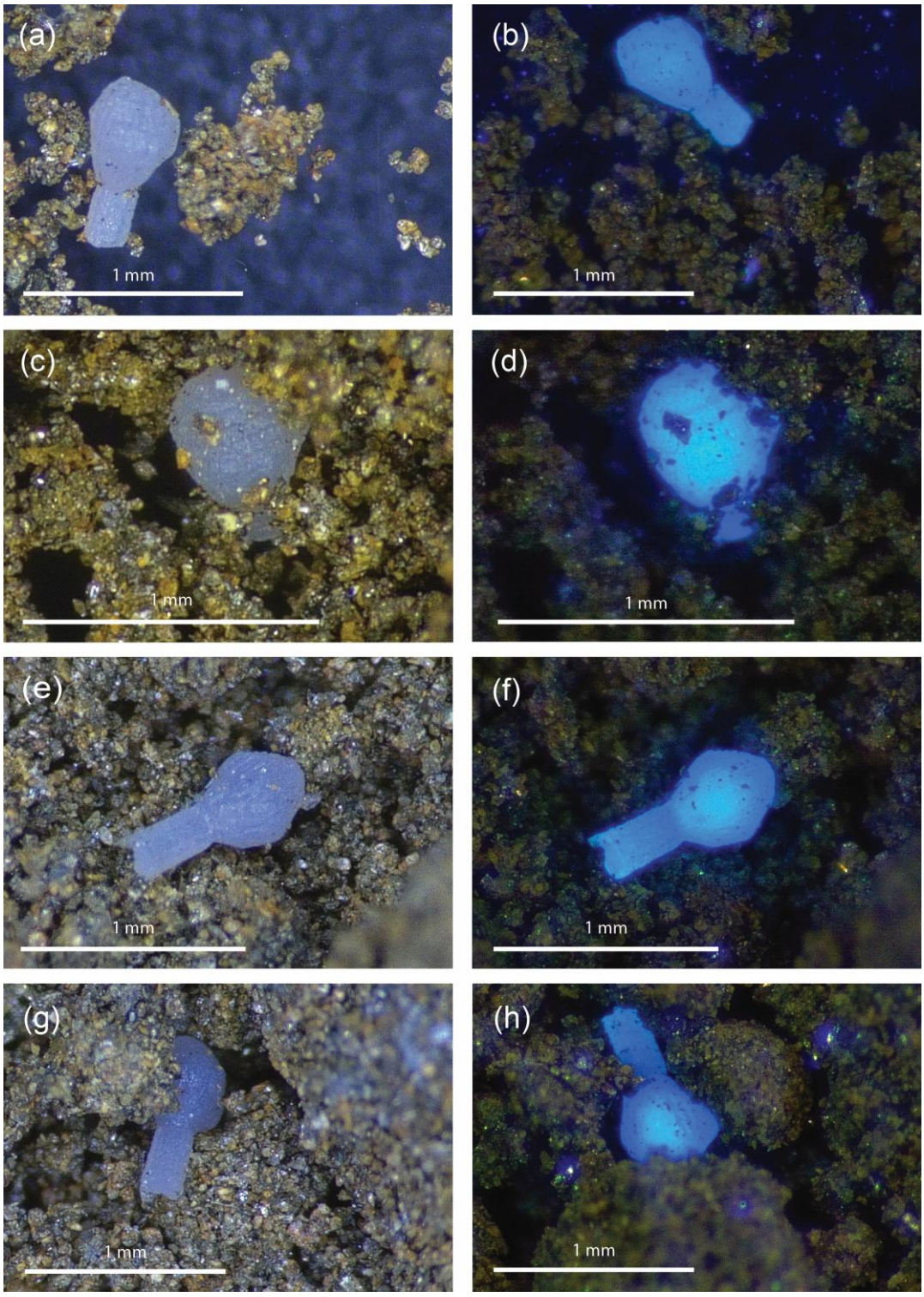

Figure III-6. TPG01 tracer particles in nickel concentrate (origin A) following the short-term low humidity artificial climate ageing tests. Following ageing at 45°C over a 48-h period under (a) natural light and (b) ultraviolet (UV) excitation light; subsequently at 55°C over a 48-h period under (c) natural light and (d) UV excitation light; at 65°C over a 48-h period under (e) natural light and (f) UV excitation light; subsequently at 75°C over a 48-h period under (g) natural light and (h) UV excitation light. Tests were conducted at a humidity of <20% RH.

Funded by the European Union

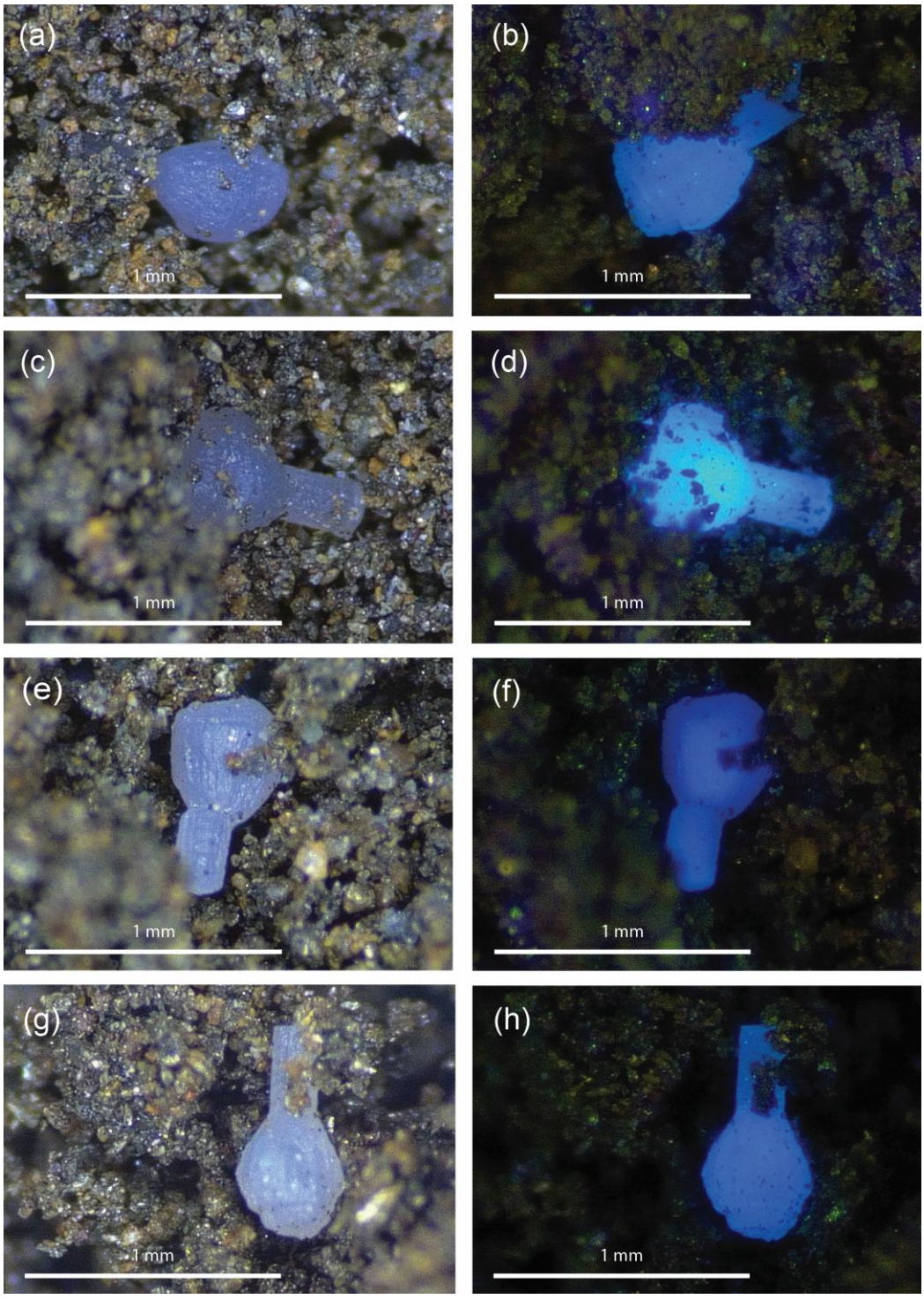

Figure III-7. Effect of short-term high humidity artificial ageing test on TPG01 in nickel concentrate (origin A). Following ageing at 45°C over a 48-h period under (a) natural light and (b) ultraviolet (UV) excitation light; subsequently at 55°C over a 48-h period under (c) natural light and (d) UV excitation light; at 65°C over a 48-h period under (e) natural light and (f) UV excitation light; subsequently at 75°C over a 48-h period under (g) natural light and (h) UV excitation light. Tests were conducted at a humidity of 85% RH.

Funded by the European Union

13.3.4 Transportation Test

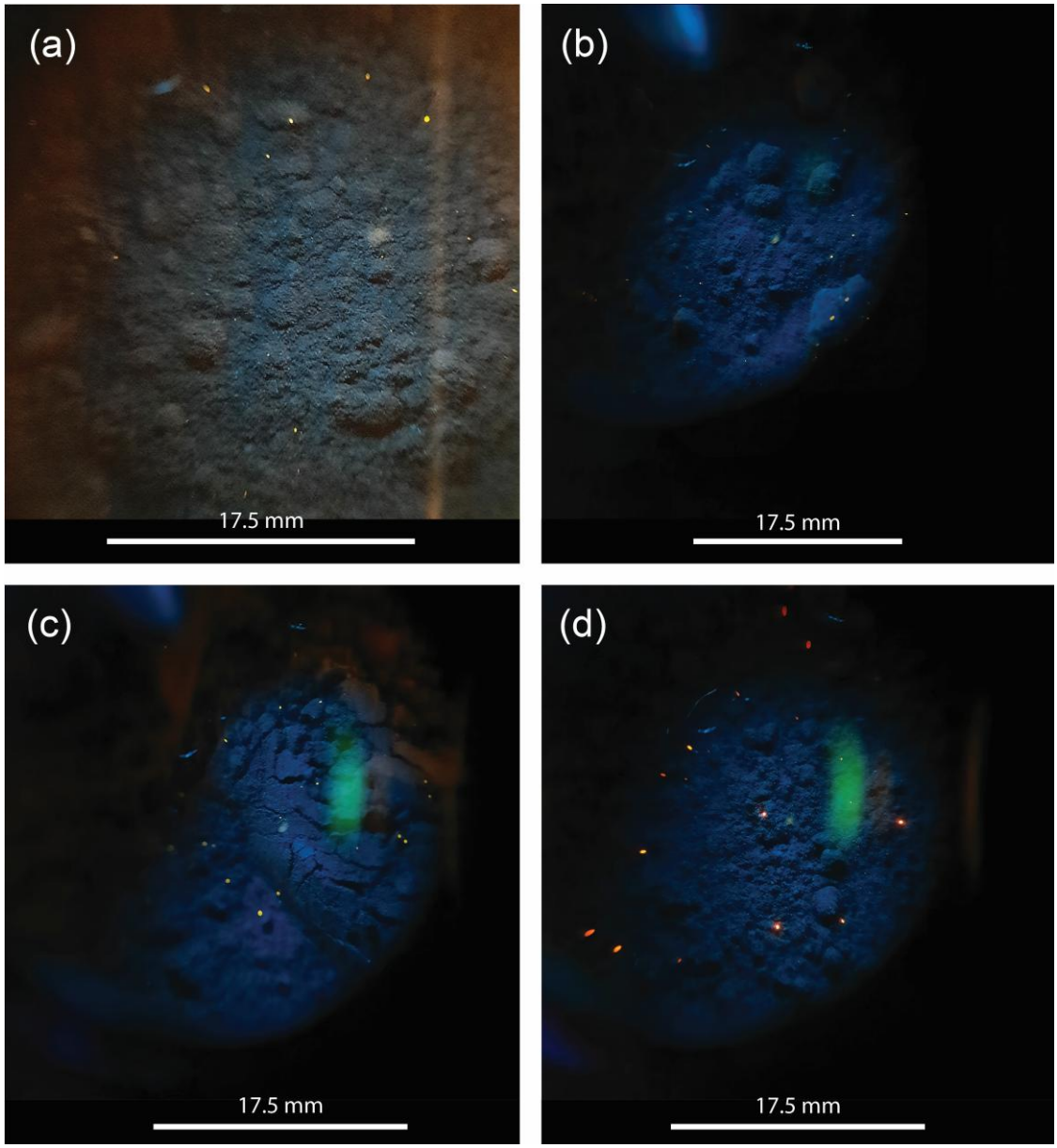

Figure III-8. Distribution of TraceTag's tracer particles in black mass following the transportation test. (a) TPA01, (b) TPA02, (c) TPA03 and (d) TPA04 in black mass as observed through TraceTag's ValiScan S3 detector.

Funded by the European Union

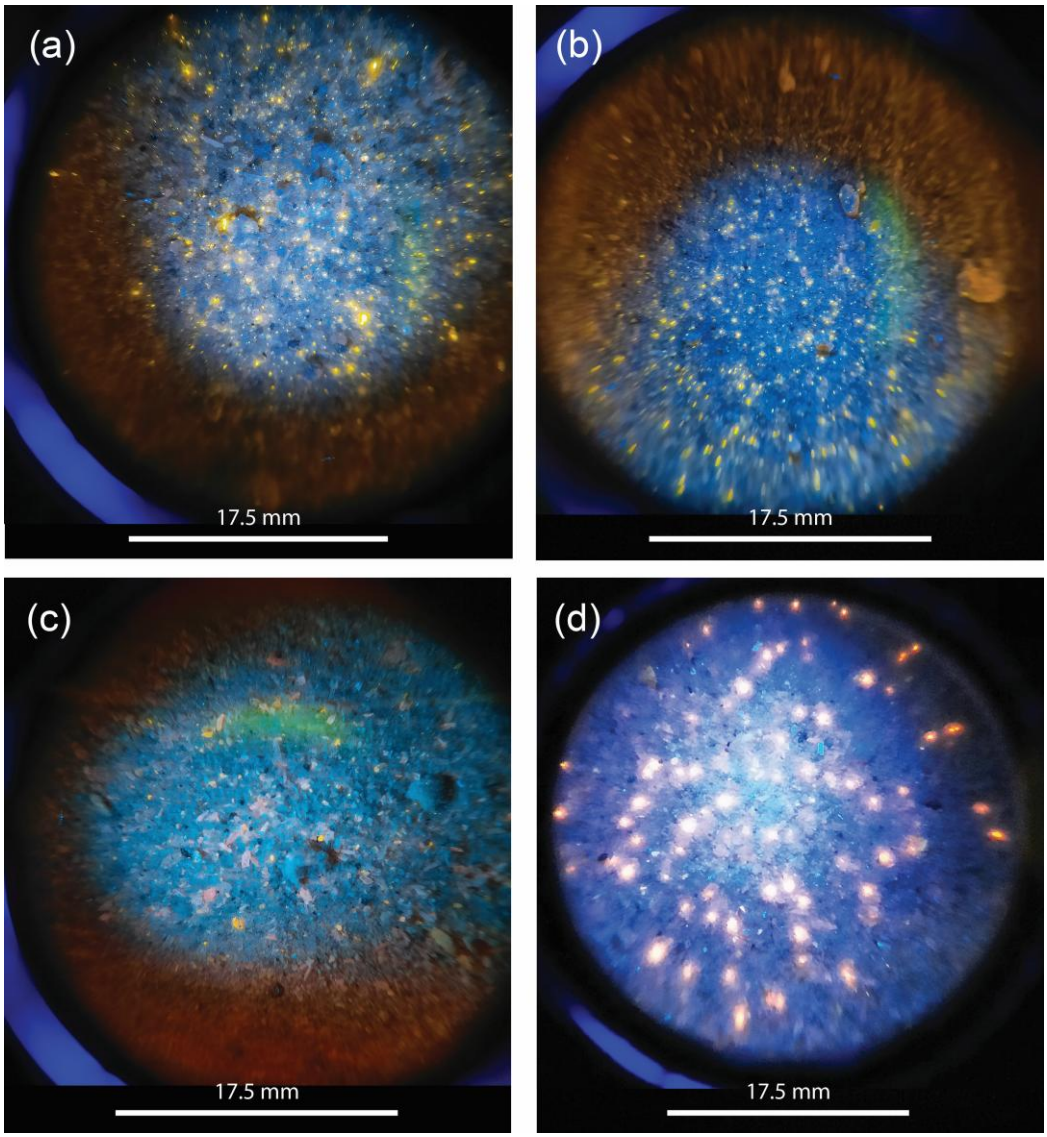

Figure III-9. Distribution of TraceTag's tracer particles in spodumene concentrate following the transportation test. Distribution of (a) TPA01, (b) TPA02, (c) TPA03 and (d) TPA04 in spodumene concentrate as observed through TraceTag's ValiScan S3 detector.

Funded by
the European Union

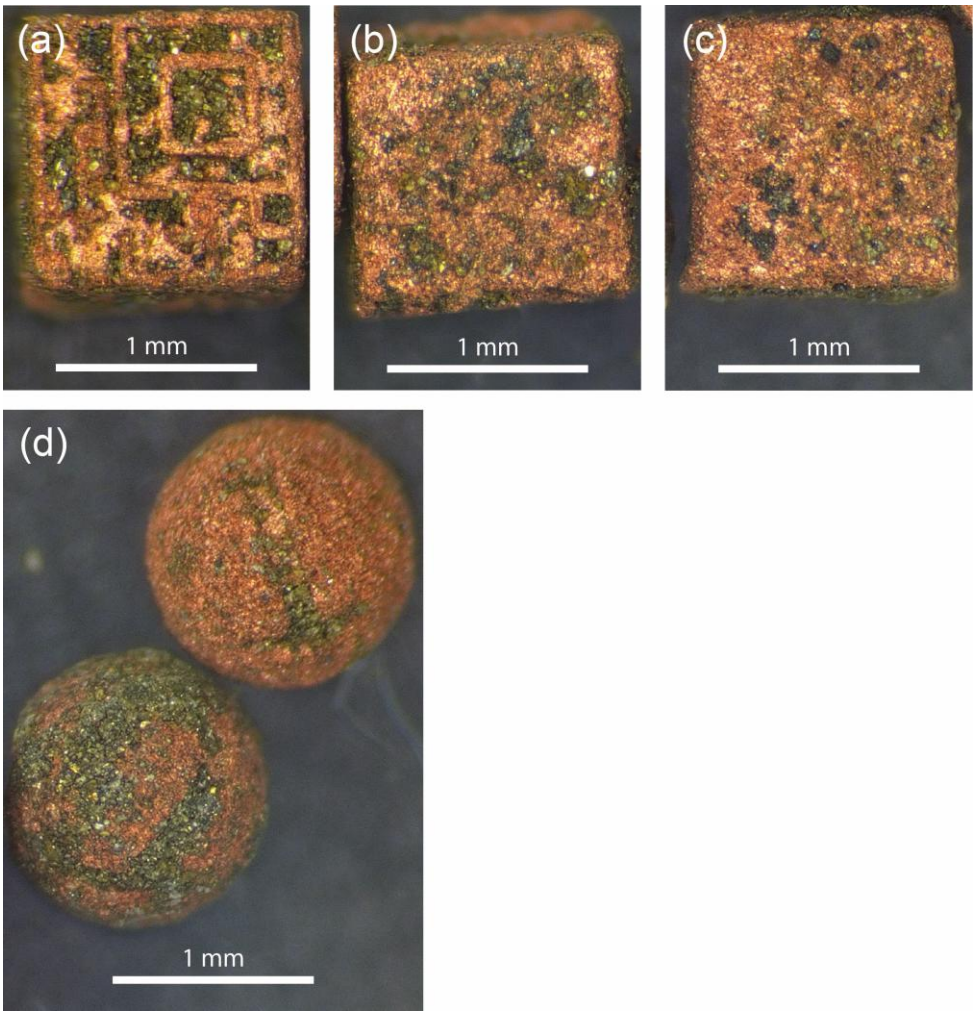

Figure III-10. 3D MicroPrint's TPM01 and TPM02 removed from vacuum-sealed aluminium foil packs containing nickel concentrate (origin A) following the transportation test. (a) TPM01 showing micro QR code. (b) and (c) show other faces of additional TPM01 recovered from the bag. (d) TPM02 with the letters "G" and "T". Note the limited change in colouration and adhesion of host material particles to the tracer particle surfaces.

Funded by
the European Union

13.4 Appendix IV: Cost Evaluation Data

Table IV-1. Manufacturing or retail tracer particle costs (on a 1 g and 0.1 g basis) and average March 2026 commodity prices.

Commodity	Commodity Price per Tonne (March 2026 Average)	TPG Cost		TPH Cost		TPM01 Cost		TPM02 Cost		TPM03 Cost		TPM04 Cost	
		1 g	0. 1 g	1 g	0. 1 g	1 g	0. 1 g	1 g	0. 1 g	1 g	0. 1 g	1 g	0. 1 g
Cobalt Hydroxide	€49,964.27	€78.91	€37.05	€612.00	€61.20	€195.00	€19.50	€340.00	€34.00	€205.00	€20.50	€330.00	€33.00
Cobalt Mixed Hydroxide Precipitate	€7,215.90												
Lithium Carbonate	€17,411.39												
Lithium Hydroxide	€12,175.80												
Natural Graphite	€459.20												
Natural Graphite Spherical Uncoated	€1,435.01												
Rare Earth Oxides	€15,721.27												
Nickel Mixed Hydroxide Precipitate	€7,304.61												
Spodumene Concentrate	€1,858.55												
Black Mass (NMC)	€6,604.49												
LFP Scrap (Gate Fee)	€2,000.00												

Note: NMC = nickel manganese cobalt; LFP = lithium iron phosphate; TP = tracer particle; TPG = GTK TPs; TPH = TPH01, TPH02 and TPH03. GTK TP costs are based on the manufacturing costs of 1 g and 0.1 g, respectively. TPH (Horizon Microtechnologies) and TPM (3D MicroPrint) costs are based on the lowest per-gram price provided by or estimated from outsourcing partner quotations (i.e. derived from the costs associated with the production of 1,000 g of each TP).

Commodity prices in United States Dollar (USD) were converted to Euros (EUR) using a conversion rate of USD 1 = EUR 0.8697; Chinese Yuan (CNY) was converted to Euros using a conversion rate of CNY 1 = EUR 0.1260.

Commodity prices and gate fee costs were determined by averaging the commodity prices/gate fee costs from March 2026. Prices were provided by Benchmark Minerals Intelligence (2026):

- Cobalt Hydroxide: Cobalt; Cobalt Hydroxide; Min 20%; CIF Asia; Price Daily; USD; Tonne.
- Cobalt Mixed Hydroxide Precipitate: Cobalt; Mixed Hydroxide Precipitate Aggregate; 1%<Co<4.5%; CIF Asia; Price; USD; Tonne.
- Lithium Carbonate: Lithium Carbonate; Min 99.5%; CIF Asia (spot); Price Daily; USD; Tonne.
- Lithium Hydroxide: Lithium Hydroxide; Min 55.0%; CIF Europe (contract); Price; USD; Tonne.
- Natural Graphite (94–95% C; -100 mesh): Natural Graphite; Flake; 94-95% C; -100 mesh; FOB East Africa; USD; Tonne.
- Natural Graphite Spherical Uncoated: Natural Graphite; Spherical Uncoated; 99.95%; 15 microns; FOB China; USD; Tonne.
- Rare Earth Oxides: Rare Earths; Oxide; DDP China; CNY; Tonne.
- Nickel Mixed Hydroxide Precipitate: Nickel; Mixed Hydroxide Precipitate Aggregate; 35%<Ni<55%; CIF Asia; USD; Tonne.
- Spodumene Concentrate: Spodumene; 6%; FOB Australia; Price; USD; Tonne.
- NCM Black Mass: Recycling; Black Mass; NCM feedstock; EXW Europe; USD; Tonne.
- LFP Gate Fee: Recycling; Scrap; LFP feedstock; EXW Europe; EUR; Tonne.

Funded by
the European Union

Table IV-2. Price Premium per commodity and per tracer particle at an applied tracer particle dosage of 1 g and 0.1 g.

Commodity	Commodity Price per Tonne (March 2026 Average)	TPG		TPH		TPM01		TPM02		TPM03		TPM04	
		1 g	0. 1 g	1 g	0. 1 g	1 g	0. 1 g	1 g	0. 1 g	1 g	0. 1 g	1 g	0. 1 g
Cobalt Hydroxide	€49,964.27	0.16%	0.07%	1.22%	0.12%	0.39%	0.04%	0.68%	0.07%	0.41%	0.04%	0.66%	0.07%
Cobalt Mixed Hydroxide Precipitate	€7,215.90	1.09%	0.51%	8.48%	0.85%	2.70%	0.27%	4.71%	0.47%	2.84%	0.28%	4.57%	0.46%
Lithium Carbonate	€17,411.39	0.45%	0.21%	3.51%	0.35%	1.12%	0.11%	1.95%	0.20%	1.18%	0.12%	1.90%	0.19%
Lithium Hydroxide	€12,175.80	0.65%	0.30%	5.03%	0.50%	1.60%	0.16%	2.79%	0.28%	1.68%	0.17%	2.71%	0.27%
Natural Graphite	€459.20	17.18%	8.07%	133.27%	13.33%	42.47%	4.25%	74.04%	7.40%	44.64%	4.46%	71.86%	7.19%
Natural Graphite Spherical Uncoated	€1,435.01	5.50%	2.58%	42.65%	4.26%	13.59%	1.36%	23.69%	2.37%	14.29%	1.43%	23.00%	2.30%
Rare Earth Oxides	€15,721.27	0.50%	0.24%	3.89%	0.39%	1.24%	0.12%	2.16%	0.22%	1.30%	0.13%	2.10%	0.21%
Nickel Mixed Hydroxide Precipitate	€7,304.61	1.08%	0.51%	8.38%	0.84%	2.67%	0.27%	4.65%	0.47%	2.81%	0.28%	4.52%	0.45%
Spodumene Concentrate	€1,858.55	4.25%	1.99%	32.93%	3.29%	10.49%	1.05%	18.29%	1.83%	11.03%	1.10%	17.76%	1.78%
Black Mass (NMC)	€6,604.49	1.19%	0.56%	9.27%	0.93%	2.95%	0.30%	5.15%	0.51%	3.10%	0.31%	5.00%	0.50%
LFP Scrap (Gate Fee)	€2,000.00	3.95%	1.85%	30.60%	3.06%	9.75%	0.98%	17.00%	1.70%	10.25%	1.03%	16.50%	1.65%

Note: NMC = nickel manganese cobalt; LFP = lithium iron phosphate; TPG = GTK TPs; TPH = TPH01, TPH02 and TPH03. GTK TP costs are based on the manufacturing costs of 1 g and 0.1 g, respectively. TPH (Horizon Microtechnologies) and TPM (3D MicroPrint) costs are based on the lowest per-gram price provided by or estimated from outsourcing partner quotations (i.e. derived from the costs associated with the production of 1,000 g of each TP).

Commodity prices in United States Dollar (USD) were converted to Euros (EUR) using a conversion rate of USD 1 = EUR 0.8697; Chinese Yuan (CNY) was converted to Euros using a conversion rate of CNY 1 = EUR 0.1260.

Commodity prices and gate fee costs were determined by averaging the commodity prices/gate fee costs from March 2026. Prices were provided by Benchmark Minerals Intelligence (2026):

- Cobalt Hydroxide: Cobalt; Cobalt Hydroxide; Min 20%; CIF Asia; Price Daily; USD; Tonne.
- Cobalt Mixed Hydroxide Precipitate: Cobalt; Mixed Hydroxide Precipitate Aggregate; 1%<Co<4.5%; CIF Asia; Price; USD; Tonne.

Funded by the European Union

- Lithium Carbonate: Lithium Carbonate; Min 99.5%; CIF Asia (spot); Price Daily; USD; Tonne.
- Lithium Hydroxide: Lithium Hydroxide; Min 55.0%; CIF Europe (contract); Price; USD; Tonne.
- Natural Graphite (94–95% C; -100 mesh): Natural Graphite; Flake; 94-95% C; -100 mesh; FOB East Africa; USD; Tonne.
- Natural Graphite Spherical Uncoated: Natural Graphite; Spherical Uncoated; 99.95%; 15 microns; FOB China; USD; Tonne.
- Rare Earth Oxides: Rare Earths; Oxide; DDP China; CNY; Tonne.
- Nickel Mixed Hydroxide Precipitate: Nickel; Mixed Hydroxide Precipitate Aggregate; 35%<Ni<55%; CIF Asia; USD; Tonne.
- Spodumene Concentrate: Spodumene; 6%; FOB Australia; Price; USD; Tonne.
- NCM Black Mass: Recycling; Black Mass; NCM feedstock; EXW Europe; USD; Tonne.
- LFP Gate Fee: Recycling; Scrap; LFP feedstock; EXW Europe; EUR; Tonne.

Funded by
the European Union